Design neuer rotlichtaktivierter Enzyme zur Kontrolle von zyklischen Mononukleotiden

DISSERTATION

zur Erlangung des akademischen Grades eines
Doktors der Naturwissenschaften (Dr. rer. nat.)
an der Fakultät für Biologie, Chemie und Geowissenschaften
der Universität Bayreuth

vorgelegt von

Robert Stabel
aus Duisburg
Bayreuth, 2019

Die vorliegende Arbeit wurde in der Zeit von März/2015 bis Juli/2019 in Bayreuth am Lehrstuhl Biochemie unter Betreuung von Herrn Professor Dr. Andreas Möglich angefertigt.

Vollständiger Abdruck der von der Fakultät für Biologie, Chemie und Geowissenschaften der Universität Bayreuth genehmigten Dissertation zur Erlangung des akademischen Grades eines Doktors der Naturwissenschaften (Dr. rer. nat.)

Dissertation eingereicht am: 10.07.2019

Zulassung durch die Promotionskommission: 17.07.2019

Wissenschaftliches Kolloquium: 17.12.2019

Amtierender Dekan: Prof. Dr. Matthias Breuning

Prüfungsausschuss:

Prof. Dr. Andreas Möglich (Gutachter)
Prof. Dr. Thomas Scheibel (Gutachter)
Prof. Dr. Frank Hahn (Vorsitz)
Prof. Dr. Dirk Schüler

1. Abstract

Sensory photoreceptor proteins mediate diverse light responses across organisms from all domains of life. Like other signal receptors, they feature modular architecture and comprise photosensor and effectors. The sensor module incorporates a chromophore to absorb light of distinct wavelength; conformational signals are then propagated via a linker to the effector to trigger a specific biological response. The modular composition enables the engineering of novel photoreceptors via rewiring of the sensor and effector modules. A particular challenge lies in the coupling of the modules such that productive signal propagation is maintained. Photoreceptors underpin the field of optogenetics where they enable the minimally invasive control of diverse processes in cells and organisms with high spatiotemporal resolution and exquisite molecular specificity.

This thesis covers the engineering of synthetic photoreceptors for optogenetic deployment. To systematically probe the linker between sensor and effector modules, the PATCHY method is applied to two derivatives of the histidine kinase YF1. In the original light-repressed YF1, linker lengths of $7n$ (n = 1, 2, 3, ...) and $7\times n+1$ are associated with light-repressed and light-activated responses, respectively. For the two YF1 variants, light-regulated activity is also concentrated in discrete length registers, albeit with inverted signal response and to lesser extent. Linker length evidently governs output activity of the receptor and hence provides an efficient means for its rational modification.

The main chapters of the thesis focus on the engineering of novel photoreceptors for the optogenetic control of cyclic mononucleotide metabolism. In the cell, phosphodiesterases (PDE) and nucleotidyl cyclases (ACs or GCs) control the level of cyclic mononucleotides which serve as second messengers in many important responses in eukaryotes and prokaryotes alike. This thesis expands the range of optogenetic tools by novel red/far-red-(R/FR) light-regulated cyclases and phosphodiesterases, thus allowing to study cellular metabolism with enhanced control. To this end, the light-inert sensor module of a cyclase is exchanged for different R/FR-switchable bacteriophytochrome (BphP) sensor modules to create novel photoactivated adenylyl cyclases (PACs). A fluorescence-based reporter assay enables the characterization and optimization of the PACs. The variant *Dd*PAC, based on the *Deinococcus desertii* BphP, shows a 9.8 fold activity increase under red light and complete shutting off via far-red light. Likewise, the light-activated PDE LAPD is improved in terms of hydrolysis activity, regulatory efficiency and basal activity. To this end, the BphP and the PDE modules of LAPD are substituted for homologues photosensor and effectors. The variant *Dr-Bt*PDE2A, based on the *Deinococcus radiodurans* BphP and the *Bos taurus*

PDE2A, exhibits the best performance with an 8-fold increased activity upon red light and an improved off-switching upon far red-light illumination. For use in optogenetics, LAPD variants can be used alone or in tandem with PACs to manipulate cyclic mononucleotides levels and downstream processes in living cells like the gating of certain ion channels. The new PAC and LAPD variants, generated throughout this thesis, generally inform the engineering of synthetic R/FR-sensitive photoreceptors. Intermolecular interactions between sensor and effector modules play important functional roles but also complicate receptor engineering. This work identifies the homologous exchange of sensor and effector modules as a valid strategy for the creation of novel R/FR-sensitive photoreceptors.

2. Zusammenfassung

Sensorische Photorezeptor-Proteine vermitteln, in Abhängigkeit von Licht, vielfältige organismische Anpassungen in allen Reichen des Lebens. Wie auch andere Signalproteine weisen sie einen modularen Aufbau auf und bestehen aus einem (Photo-) Sensor- und einem Effektor-Modul. Das Sensor-Modul detektiert mit Hilfe eines Chromophors Licht und leitet das Signal über ein Verbindungsstück, der Linker, in das Effektor-Modul weiter, welches eine spezifische biologische Aktivität vermittelt. Der modulare Aufbau ermöglicht die Rekombination des Sensor-Moduls mit einem Effektor-Modul einer anderen Aktivität. Die Herausforderung ist hierbei, die Signalweiterleitung zwischen Sensor- und Effektor-Modul aufrechtzuerhalten.

In der Optogenetik werden Photorezeptoren zur minimalinvasiven Kontrolle diverser Prozesse in Zellen und Lebewesen durch Licht, eingesetzt. Der größte Vorteil der Optogenetik ist die hohe räumliche und zeitliche Auflösung und die molekulare Spezifität der Methode.

In dieser Arbeit werden verschiedene Aspekte für das Design von synthetischen Photorezeptoren behandelt. Zum einen wird auf die Rolle des verknüpfenden Linker zwischen Sensor und Effektor-Domäne eingegangen, und zum anderen werden neue Hybridproteine als Werkzeug für die optogenetische Kontrolle der Bildung und des Abbaus zyklischer Mononukleotide erschaffen.

Mit Hilfe der PATCHY-Methode wurde der Einfluss des Linkers auf die Aktivität von lichtaktivierten Varianten D21V und H22P der Histidinkinase YF1 untersucht. In YF1 zeigen Varianten mit einer Linkerlänge von 7*n* Aminosäuren lichtreprimiertes und Varianten mit einer Länge von 7*n*+1 lichtaktiviertes Verhalten. Für die Varianten D21V und H22P wurden lichtregulierte Konstrukte ebenfalls nur in bestimmten Registern gefunden, allerdings mit sehr schwach ausgeprägter Periodizität. Dennoch wurden wichtige Erkenntnisse bezüglich der Abhängigkeit der Aktivität von der Linkerlänge gewonnen.

Zyklische Mononukleotide spielen eine wichtige Rolle als Botenstoffe in der Signaltransduktion von Eu- und Prokaryonten. In Zellen erfolgt die Regulation zyklischer Mononukleotide durch Phosphodiesterasen (PDEs) und Zyklasen. Im Bereich der Optogenetik finden bereits photoaktivierbare Adenylylzyklasen (PACs) und die rotlichtaktivierte Phosphodiesterase (LAPD) Anwendung. Die in dieser Arbeit vorgenommene Erschaffung neuer Rot/Fernrot- (R/FR) schaltbarer Zyklasen und Phosphodiesterasen erweitert die Palette der optogenetischen Werkzeuge und ermöglicht so die Adressierung neuer Fragestellungen. Dazu werden, neben anderen Photosensoren, die

(R/FR)-schaltbaren Bakteriophytochrome (BphP) für die Erschaffung von synthetischen Photorezeptoren genutzt.

Für die Erzeugung R/FR schaltbarer Zyklasen wurden das Sensor-Modul einer Zyklase durch verschiedene Bakteriophytochrom Sensor-Module ersetzt.

Mittels eines fluoreszenzbasierten Testsystems konnten die verschiedenen Varianten hinsichtlich ihrer Lichtschaltbarkeit charakterisiert werden. Das beste Konstrukt auf Basis des *Deinococcus dersertii* BphP (*Dd*PAC) zeigte eine 9,8-fache Aktivierung mittels Rotlichtbeleuchtung, die mittels Fernrotlicht aufgehoben werden konnte.

LAPD wurde hinsichtlich ihrer Hydrolyseaktivität, Lichtschaltbarkeit und Dunkelaktivität verbessert. Dazu wurde zum einen das Sensor-Modul, das BphP aus *Deinococcus radiodurans*, gegen homologe Bakteriophytochrome und zum anderen das Effektor-Modul gegen homologe PDEs ausgetauscht. Von den erzeugten LAPD Varianten zeigte die sogenannte *Dr-Bt*PDE2A, auf Basis der *Bos taurus* PDE2A, eine ~8fach höhere Rotlichtaktivität und ebenfalls eine verbesserte Reversibilität der Schaltung. Für die optogenetische Anwendungen können die Konstrukte alleine oder als Antagonisten zu PACs verwendet werden, um die Konzentration von zyklischen Mononukleotiden zu steuern. Erste Versuche in HEK-Zellen zeigten bereits die lichtregulierte Steuerung eines CNG-Kanals mittels LAPD Varianten.

Sowohl die erzeugten PACs, als auch die erzeugten LAPD Varianten, erbringen Einblicke in die Erschaffung synthetischer R/FR-Photorezeptoren. So spielen die intermolekularen Wechselwirkungen zwischen den Sensor- und Effektor-Modulen eine wichtige Rolle und können den Austausch dieser Module verkomplizieren. Der homologe Austausch des Sensor- oder Effektor-Moduls, erweist sich als probate Strategie für die Erzeugung neuer R/FR-Photorezeptoren.

2.1. Einleitung

2.2. Sensorische Photorezeptoren

Licht ist eine Form elektromagnetischer Strahlung. Sichtbares Licht beschreibt den Bereich des elektromagnetischen Spektrums, welcher sich zwischen dem nahen Ultraviolett (UV, 380 nm) und dem nahen Infrarot (IR, 780 nm) Bereich erstreckt.

Die Fähigkeit, Licht wahrzunehmen und darauf zu reagieren, ist ein essentieller Bestandteil für das Leben, wie wir es kennen (Presti and Delbrück, 1978). Für viele Organismen fungiert Licht als ein Träger von Energie oder Information. Die Photosynthese, betrieben von Pflanzen, Bakterien und Algen, ist das bekannteste Beispiel der Umwandlung von Lichtenergie zu chemischer Energie und ist damit der primäre Energielieferant auf unserem Planeten (Arnon 1959). Um Information aus einem Lichtsignal in eine biologische Reaktion umzuwandeln, werden in Organismen sensorische Photorezeptoren genutzt, welche zumeist einen modularen Aufbau besitzen (Möglich et al. 2010). Beispiele für lichtvermittelte Prozesse sind Phototaxis in Mikroalgen (Nagel 2002), Phototropismus in Pflanzen (Christie 1998) und der Sehprozess im Auge (Gehring 2005).

Vereinfacht dargestellt, besteht der Photorezeptor aus zwei funktionalen Modulen, dem Sensor und dem Effektor. Häufig entsprechen Sensor und Effektor separaten, globulär gefalteten Protein-Domänen. Bei den meisten in der Natur vorkommenden Photorezeptoren liegt das Sensor-Modul N-terminal und die Effektor-Modul C-terminal vor (Schultz and Natarajan 2013). Es gibt allerdings auch Rezeptoren mit umgekehrter Architektur (A. Losi and Gärtner 2008). Im Sensor-Modul ist ein Chromophor gebunden, welcher zur Lichtdetektion befähigt.

Der Chromophor absorbiert in seinem dunkeladaptierten Zustand Licht spezifischer Wellenlänge und durchläuft einen sogenannten Photozyklus, welcher die Bildung des (meta)stabilen lichtadaptierten Zustand zur Folge hat (Nathan C. Rockwell and Lagarias 2010). Das Durchlaufen des Zyklus beinhaltet eine photochemische Reaktion und löst konformelle Änderungen im Protein aus (Möglich and Moffat 2010). Als Folge dessen kommt es zur Signalweiterleitung, die zur Aktivierung des Effektor-Moduls führt (Abb.1).

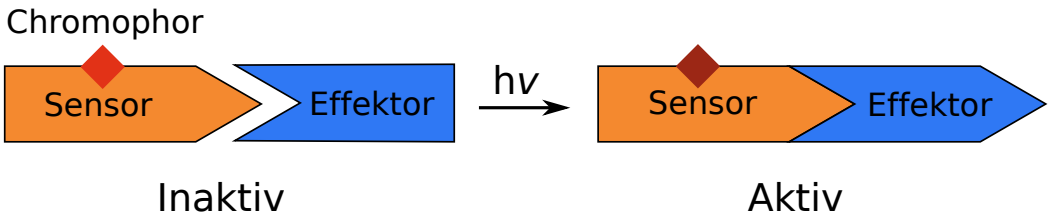

Abbildung 1: Sensorische Photorezeptoren bestehen aus einem N-terminalen Sensor- (orange) und einem C-terminalen Effektor-Modul. Der an die Sensor-Domäne gebundene Chromophor (rot/dunkelrot) absorbiert Licht einer bestimmten Wellenlänge. Licht löst konformelle Änderungen im Photorezeptor aus und geht dann von seinem inaktiven in den aktiven Zustand über.

Die Klassifizierung und Zuordnung der Photorezeptoren ist anhand der verschiedenen Chromophore und ihrer Photochemie möglich (Abb. 2) (Ziegler and Möglich 2015). Die Klasse der UV B (280-315 nm) detektierenden Rezeptoren, welche nur einen bekannten Vertreter, den pflanzlichen *ultraviolet-B receptor* (UVR8) aus *A. thaliana,* beinhaltet (Heijde and Ulm 2012), nutzt Tryptophan-Seitenketten, um Licht im nahen UV-Bereich zu detektieren (Wu et al. 2015, 8).

Die CRY- (*Cryptochrome*), LOV- (*light oxygen voltage*) und BLUF- (*blue light sensors using flavin adenine nucleotide*) Rezeptoren nutzen Flavin Nukleotide als Chromophor und detektieren vorrangig nah-UV bis blaues (350-490 nm) Licht (Aba Losi, Gardner, and Möglich 2018). Die Klasse der Xanthopsine detektiert ebenfalls Licht im blauen Spektralbereich, nutzt jedoch 4-Hydroxyzimtsäure als Kofaktor (Aba Losi, Gardner, and Möglich 2018). Die Opsine bilden eine eigenständige Klasse und binden Retinal als Chromophor und detektieren Licht vom blauen bis hin zum roten Spektralbereich. Sie sind unter anderem bei Vertebraten für das Sehen verantwortlich (Ernst et al. 2014).

Phytochrome sind eine Klasse von Rot/Fernrot (R/FR)-Rezeptoren und binden lineare Tetrapyrrole, auch bekannt als Biline oder. Gallenfarbstoffe. In dieser Familie wird hauptsächlich zwischen den R/FR-absorbierenden Bakterio- und Pflanzenphytochromen, sowie den Cyano- und Algenphytochromen unterschieden, die verschiedene spektrale Eigenschaften aufweisen.

Zusätzlich zu den bereits genannten Klassen existieren noch weitere, erst vor kurzem entdeckte Photorezeptoren. Dazu zählt das *orange carotenoid protein*, (OCP), welches β-Carotin bindet und eine wichtige Rolle in der Photoprotektion in Cyanobakterien spielt. Durch Absorption von Licht im blaugrünen Spektrum kommt es zu einer Translokation des Chromophors, welches einen Farbwechsel von orange nach rot verursacht und photoprotektive Energielöschung ermöglicht (Dominguez-Martin and Kerfeld 2019).

Der erst vor kurzem charakterisierte Photosensor CarH ist ein in Bakterien vorkommender, cytosolischer Transkriptionsfaktor und bindet als Chromophor Vitamin B_{12} in der Form von

5‘-Deoxyadenosylcobalamin (AdoCbl). CarH ist in der Lage, UV-B bis hin zu Grünlicht (280-570 nm) zu detektieren (Padmanabhan, Pérez-Castaño, and Elías-Arnanz 2019).

Eine weitere Klasse sind vom grün fluoreszierenden Protein (*green fluorescent protein*, GFP) abgeleitete Photorezeptoren. Zu dieser Klasse gehört das photoaktivierbare Fluoreszenzprotein Dronpa. Es bildet autokatalytisch den Chomophorkomplex aus drei Aminosäureresten und wechselt durch Absorption von blauen Licht von der inaktiven *trans*- in die fluoreszierende *cis*-Konformation. Diese kann durch Bestrahlung mit UV-Licht wieder in die *trans*-Konformation überführt werden (Habuchi et al. 2005). Der inaktive Zustand bildet Dimere, deren Dissoziation mittels Licht einer Wellenlänge von 488 nm ausgelöst werden kann (Jöhr et al. 2019). Ein anderer Vertreter dieser Klasse ist das photospaltbare Protein (*photocleavable protein*, PhoCl), welches durch violettes Licht (400 nm) in zwei Fragmente gespaltet wird (Zhang et al. 2017).

Im Folgenden wird im Detail auf die, im Mittelpunkt dieser Arbeit stehenden Phytochrome eingegangen.

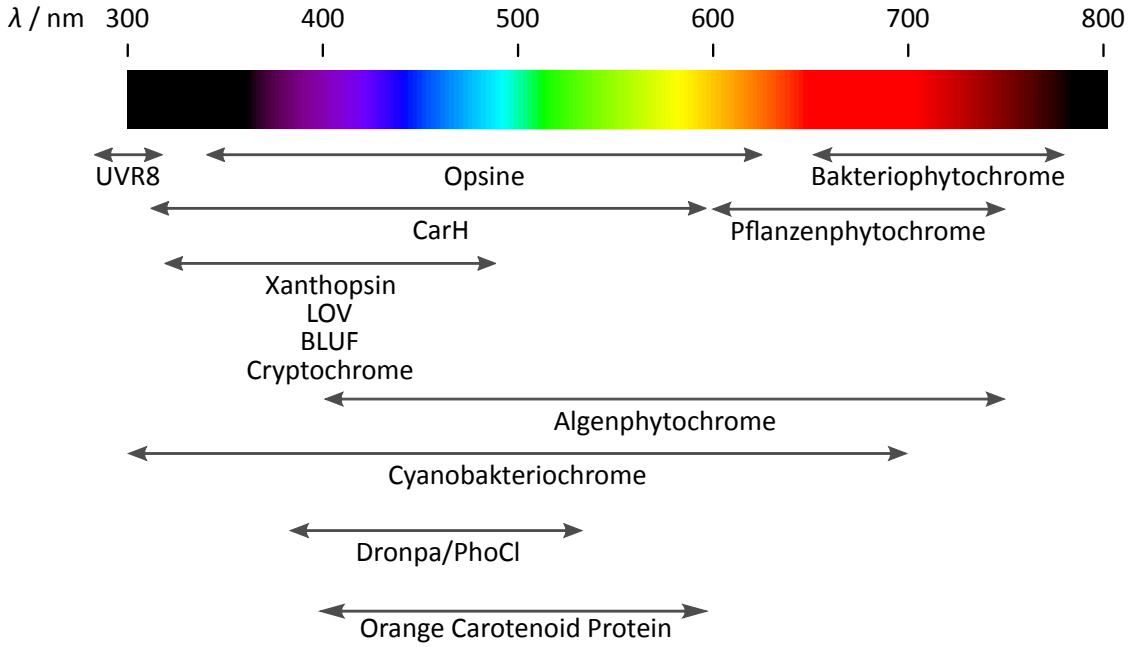

Abbildung 2: Photorezeptoren decken die gesamte Bandbreite des sichtbaren Spektrums ab. Sie können anhand ihrer Chromophore und Photochemie in verschiedene Klassen unterteilt werden. (Ziegler and Möglich 2015)

2.3. Phytochrome

Das Word Phytochrom leitet sich aus dem Griechischen ab und bedeutet Pflanzenfarbe. Der Name wurde vor fast 100 Jahren für einen damals noch unbekannten Bestandteil in Pflanzen verwendet, welcher es ermöglicht, auf Änderungen im Tageslicht zu reagieren (Garner and

Allard 1920). Das dafür verantwortliche Protein Phytochrom wurde erst 1952 in Pflanzen entdeckt (Borthwick et al., 1952). Erst gut fünf Jahre später wurde das photoaktive Pigment mittels Spektroskopie nachgewiesen (Butler et al. 1959). Seitdem wurden Phytochrome in Pilzen, Cyanobakterien und Bakterien nachgewiesen (Blumenstein et al. 2005; Davis 1999; Hughes et al. 1997; Kehoe and Grossman 1996).

Generell werden bilinbindende F/FR-Photosensoren als Phytochrome (Phy) bezeichnet (E. S. Burgie et al. 2014). Das Sensor-Modul setzt sich meist aus einem PAS- (*Per-ARNT-Sim*) GAF- (*cGMP phosphodoesterase/adenylyl cyclase/FhlA*) PHY- (*phytochrome*) Tandem zusammen, und bildet zusammen mit dem Chromophor eine Einheit, photosensorisches Kern-Modul (*photosensory core modul*, PCM) genannt (Nathan C. Rockwell and Lagarias 2010).

Phytochrome aus Cyanobakterien, Pilzen oder Kieselalgen werden entsprechend als Cyanobakterielle- (Cph), Pilz- (Fph) bzw. Algen- (Dph) Phytochrome bezeichnet. Phytochrome aus Bakterien werden Bakteriophytochrome (BphP) genannt und binden ausschließlich das Bilinderivat Biliverdin.

2.3.1. Pflanzliche Phytochrome

Das erste Pflanzenphytochrom wurde aus *Avena sativa* isoliert (Litts, Kelly, and Lagarias 1983; Vierstra and Quail 1983). Phytochrom ist von essentieller Bedeutung für sehr viele Prozesse in der Entwicklung, aber auch der Physiologie von Pflanzen, wie zum Beispiel der Samenkeimung, der Photomorphogenese, der Schattenvermeidung und der Detektion der Lichtperiode (Leivar and Quail 2011; Kendrick and Kronenberg 1994). N-Terminal befindet sich die Sensor-Domäne in Form des PCM, welche mit dem C-terminalen Effektor-Modul verknüpft ist. Das C-terminale Effektor-Modul ist eine Histidinkinase-ähnliche, aber katalytisch inaktive, Domäne (*histidine kinase related* domain, HKRD), welche durch ein weiteres PAS-Tandem an die PHY-Domäne verknüpft ist (siehe Abb. 3) (Sharrock 2008).

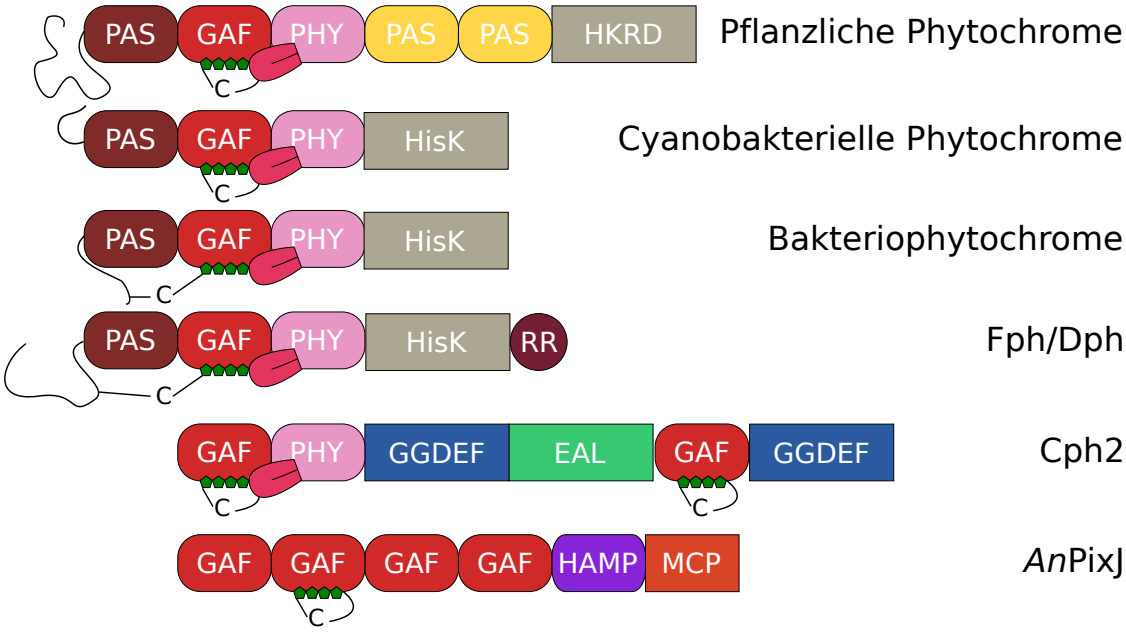

Abbildung 3: Schematische Darstellung der Domänenarchitektur von Phytochromen. In Phytochromen (Phy) besteht das PCM aus einem PAS-GAF-PHY Tandem mit dem in der GAF-Domäne gebundenen linearen Tetrapyrrol. Interaktion der PHY-Domäne mit dem Chromophor und der GAF-Domäne wird durch die PHY-Zunge vermittelt. (Nathan C. Rockwell and Lagarias 2010). Cyanobakteriochrome (CBCR) binden das lineare Tetrapyrrol ebenfalls in einer GAF-Domäne, allerdings fehlen sowohl PAS- als auch PHY-Domänen. Als Effektor-Module kommen in Pflanzen Histidinkinase-ähnliche Domänen (*histidin kinase related domain*, HKRD), in Bakterien Kieselalgen und Pilzen Histidinkinasen (*histidin kinase*, HisK) und in Cyanobakterien GGDEF- und MCP-Domänen vor.

Die in der Natur inkorporierten Kofaktoren sind Biliverdin IXa (BV), Phycocyanobilin (PCB), Phytochromobilin (PΦB), Phycoviolobilin (PVB) und Phycoerythrobilin (PEB) (siehe Abb. 4), welche Bestandteil des Stoffwechselwegs der Porphyrine sind (Briggs and Spudich 2005). Sie haben alle gemein, dass sie eine lichtabhängige *Z*/*E*-Isomerisierung durchlaufen können.

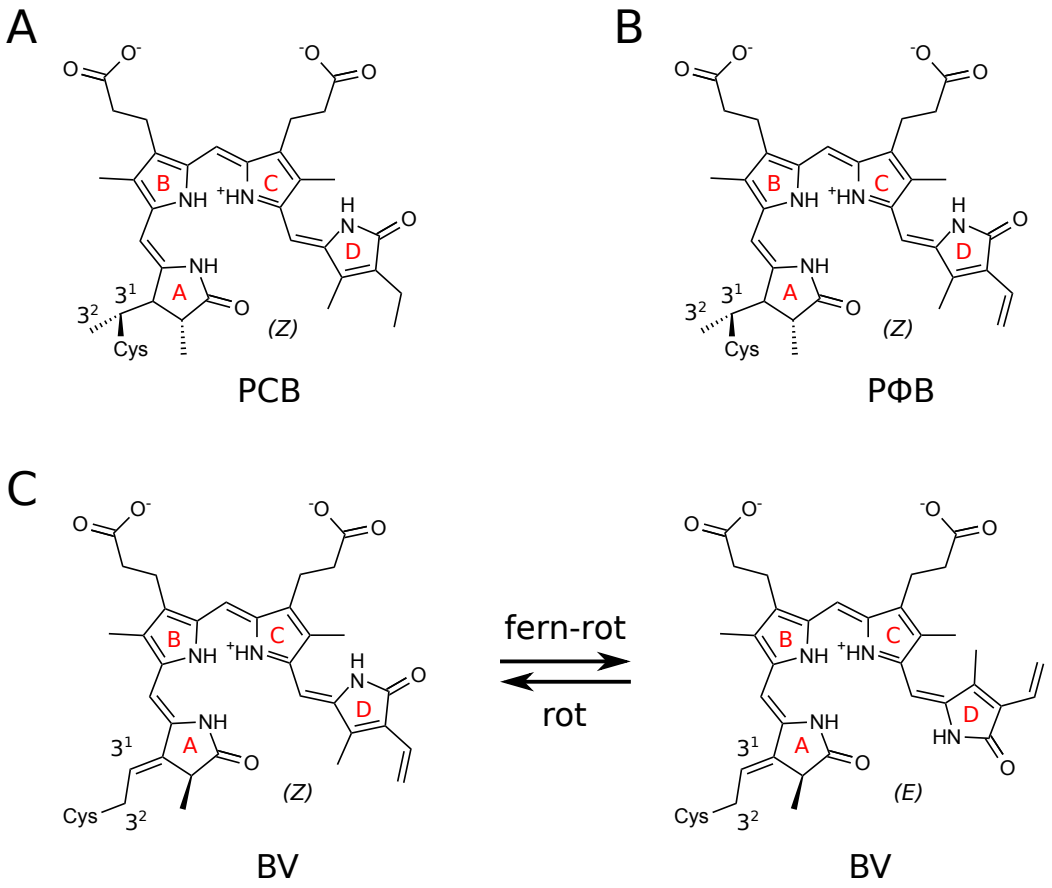

Abbildung 4: Übersicht linearer Tetrapyrrol Chromphore. A) Phycocycanobilin (PCB) B) Phytochromobilin (PΦB) C) Am Beispiel von Biliverdin (BV) ist die lichtabhängige *Z/E*-Isomerisierung gezeigt (Mroginski, Murgida, and Hildebrandt 2007).

Sie sind Abbauprodukte des Haems welches mit Hilfe des Enzyms Haemoxygenase (HO) zunächst zu Biliverdin reduziert wird. In Pflanzen wird BV durch die Phytochromobilin-Reduktase zu PΦB reduziert, welches anschließend als Chromophor eingebaut wird (Briggs and Spudich 2005).

Der genaue Mechanismus des Chromophoreinbaus in Phytochromen ist bislang nicht vollständig geklärt. Es deutet vieles darauf hin, dass die Inkorporation über zwei aufeinander folgende Schritte abläuft. Zunächst kommt es zu einer nicht-kovalenten Bindung an die GAF-Domäne gefolgt von der Ausbildung einer Thioether-Bindung zwischen der Vinylgruppe des Porphyrinrings A mit einem konservierten Cystein, welches sich bei Pflanzenphytochromen in der GAF-Domäne befindet und immer von einem Histidin gefolgt ist (Briggs and Spudich 2005). In Pflanzen kommt es zu einer Bindung des Cysteins an das $C3^1$ Atom der Seitenkette des A-Rings des PΦB bzw. PCB (Briggs and Spudich 2005).

Am besten untersucht ist das Pflanzenphytochrom B (PhyB) aus *Arabidopsis thaliana,* welches ebenfalls ein R/FR Photorezeptor ist (D. Wagner, Tepperman, and Quail 1991). Die durch Rotlicht gesteuerte Aktivität wird durch die direkte Interaktion mit Phytochrom

interagierenden Faktoren (PIF) vermittelt, welche für den Wechsel zwischen Skotomorphogenese und Photomorphogenese verantwortlich sind (Pham, Kathare, and Huq 2018). PIFs gehören zu der Superfamilie der Helix-Schleife-Helix (*basic helix-loop-helix*, bHLH) Transkriptionsfaktoren (Leivar and Quail 2011). Durch Lichtaktivierung der Phytochrome wird die Fähigkeit der PIFs, transkriptionale Reprogrammierung zu induzieren, gestört, indem PIFs zunächst phosphoryliert, ubiquitiniert und anschließend mit Hilfe von Proteasomen degradiert werden (Leivar and Quail 2011; Pham, Kathare, and Huq 2018).

2.3.2. Bakterielle Phytochrome

Die Vertreter der Bakteriophytochrom-Familie binden, wie cyanobakterielle Phytochrome (Cph) und die in Pflanzen- und in Cyanobakterien vorkommende Phytochrome, lineare Tetrapyrrole und sind R/FR-Rezeptoren (Lamparter et al., 2002 Karniol and Vierstra, 2003). Die meisten bekannten Mitglieder der BphPs kommen in nicht-photosynthetischen Eubakterien und photosynthetischen Purpurbakterien vor (Davis et al., 1999; Bhoo et al., 2001; Giraud et al., 2002). Allerdings gibt es ebenfalls Vertreter unter den Actinobakterien und Cyanobakterien (Herdman et al., 2000, Bhoo et al., 2001; Karinop und Vierstra, 2005); letztere nutzen Vertreter der BphP- und der Cph-Familie parallel (Jorissen et al., 2002).

Was die BphPs von anderen Phytochromen maßgeblich unterscheidet, ist der gebundene Kofaktor. So wird in BphPs Biliverdin IXa (BV) anstelle von Phycocyanobilin (PCB) oder Phytochromobilin (PΦB) integriert. Dieser Chromophor wird wiederum in Cyanobakterio bzw. Pflanzenphytochromen nur schlecht bis gar nicht gebunden. Die Bindung des Biliverdin erfolgt an ein konserviertes Cystein, welches sich in der PAS-Domäne befindet und mit dem $C3^2$ Atom des A-Rings interagiert (Tilman Lamparter et al. 2004; Karniol et al. 2005).

Im Genom von Bakterien, die mindestens ein BphP-Gen besitzen, findet sich ebenfalls ein Gen, welches für eine Haemoxygenase (HO) kodiert und im Gegensatz zu pflanzlichen Phys keines für die BV-Reduktase (Frankenberg-Dinkel 2004). Besonders auffällig ist die Operon-Organisation in den Bakterien *Deinococcus radiodurans, Pseudomonas aeruginosa Pseudomonas syringae* und *Rhizobium leguminosarium*. Diese haben das HO und BphP Gen bicistronisch organisiert, was für die Bereitstellung des Chromophors und dessen Einbau von Vorteil ist (Katalin Barkovits et al. 2008; K. Barkovits et al. 2011; Bhoo et al. 2001).

Die in Cyanobakterien vorkommenden Phytochrome sind eine sehr kleine Gruppe von Phys. Sie sind mit den Pflanzenphytochromen verwandt, nutzen aber Phycocyanobilin (PCB)

anstelle von Phytochromobilin (PΦB) (Tilman Lamparter et al. 1997). PCB bindet kovalent an ein konserviertes Cystein in der GAF-Domäne analog zum Chromophoreinbau in Phys. Der bekannteste Vertreter Cph1 aus *Synechocystis sp.* zeigt die R/FR Lichtschaltbarkeit, welche auch in BphPs beobachtet werden kann (Tilman Lamparter, Esteban, and Hughes 2001, 1). Des Weiteren besitzen Cyanobakterien Cyanobakteriochrome (CBCR), welche mit den Phytochromen verwandte sind und ebenfalls lineare Tetrapyrrole in einer GAF-Domäne binden (N. C. Rockwell, Ohlendorf, and Moglich 2013). In einigen CBCRs ist in der GAF-Domäne ein zweites Cystein konserviert, welches die Lichtsensitivität von F/FR zu blau/grün (B/G) verschiebt (N. C. Rockwell et al. 2011). Der Photosensor Cph2 weist neben einem Cyanobakteriophytochrom-Modul ebenfalls ein Cyanobacteriochrom auf (Nathan C. Rockwell and Lagarias 2010).

Sequenzalignments der PCM verschiedener Phytochrome zeigen eine Besonderheit der BphPs. Das konservierte Cystein und Histidin in der GAF-Domäne, welche für die kovalente Bindung des Chromophor in pflanzlichen Phys notwendig sind, fehlen. Stattdessen findet sich ein konserviertes Cystein in der PAS-Domäne (siehe Abb.3) (T. Lamparter et al. 2003). Beim Einbau gibt es einige Ausnahmen, so ist das BphP aus *D. radiodurans* in der Lage, neben BV auch PCB kovalent zu binden (Bhoo et al. 2001). Für CphB aus *Calothrix* und AgP1 aus *Agrobacterium tumerfaciens* wurde nachgewiesen, dass PCB kovalent gebundenes BV verdrängen kann und beide Phytochrome sowohl PCB als auch PΦB einbauen, wenngleich eine nicht-kovalente Bindung eingegangen wird (Jorissen et al. 2002; Borucki et al. 2009). Der Mechanismus der Assemblierung des Chromophors mit dem Apoprotein wurde bislang nur Anhand des Cph1, welches PCB bindet, gezeigt. Im ersten, sehr schnellen, Schritt lagert sich der Chomophor an das Apoprotein an. Im zweiten Schritt kommt es zu einer Konformationsänderung des Chromophors von *ZZZ*sss nach *ZZZ*ssa, sowie Protonierung des Pyrrolstickstoffes. Der dritte Schritt beinhaltet die Ausbildung der kovalenten Bindung (Heyne et al. 2002; van Thor, Ronayne, and Towrie 2007).

2.3.3. Photozyklus der Phytochrome

Bei kanonischen Phytochromen bildet der rotlichtabsorbierende Zustand (Pr) des Chromophors den thermodynamisch stabileren dunkeladaptierten Zustand und wechselt nach Rotlichteinstrahlung in den fernrotlichtabsorbierenden Zustand Pfr. Dabei kommt es im Chromophor zu einer Isomerisierung um die C15=C16 Doppelbindung zwischen den Pyrrol-Ringen C und D von (15*Z*)-anti im Pr zu (15*E*)-anti im Pfr-Zustand (Heyne et al. 2002; van Thor, Ronayne, and Towrie 2007). Durch die Photoisomerisierung ausgelöst,

kommt es im gesamten Protein zu konformellen Änderungen, welche für die Signaltransduktion unerlässlich sind. Auf dem Weg vom Pr- in den metastabilen Pfr-Zustand, durchläuft der Chromophor mehrere Intermediate, die nur wenige Piko- bis Millisekunden stabil sind, die im Folgenden anhand des *Deinococcus radidurans* BphP gezeigt werden (Abb.5). Zunächst kommt es durch Anregung von Rotlicht innerhalb von einigen Pikosekunden zu einer Photoisomerisierung und dadurch zu Bildung des Lumi-R-Zustands. Durch thermische Relaxation wird dieser innerhalb von Mikrosekunden in den Meta-R_a-Zustand überführt, welcher getrieben durch eine Deprotonierung in den Meta-R_c-Zustand übergeht. Nach erneuter Aufnahme eines Protons wird der metastabile Pfr-Zustand erreicht (Borucki et al. 2005). Dieser kann durch thermische Reversion sehr langsam in Pr zurückkehren oder durch Absorption von Fernrotlicht eine deutlich schnellere Photokonversion in den Pr-Zustand durchlaufen. Dabei werden ähnliche Zustände wie bei der Konversion von Pr → Pfr, zum Beispiel die De- und Reprotonierung des Kofaktors, durchlaufen (Braslavsky, Gärtner, and Schaffner 1997; Sineshchekov 2005).

Phytochrome, bei denen der dunkeladaptierte Zustand vom Pfr gebildet wird, werden Bathyphytochrome genannt z.B. das BphP aus *Pseudomonas aeruginosa* (*Pa*BphP).

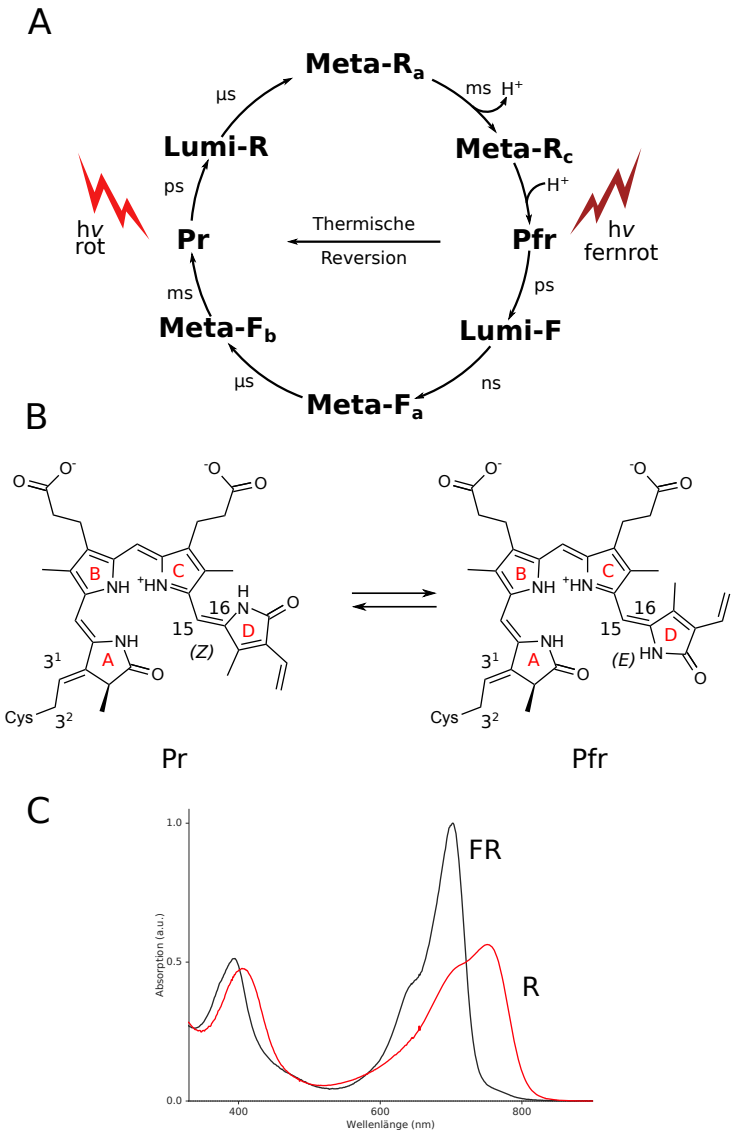

Abbildung 5: Photozyklus vom kanonischen Bakteriophytochrom Deinococcus radiodurans Bakteriophytochrom (DrBphP) A) Der Phytochrom-Photozyklus startet im dunkeladaptierten Zustand Pr. Nach Anregung mit Rotlicht kommt es zu innerhalb von Pikosekunden, durch eine Z-E Isomerisierung der C15-C16 Bindung, zur Entstehung des Lumi-R-Zustandes. Innerhalb von Mikrosekunden relaxiert dieser thermisch zum Meta-Ra-Zustand und durch Deprotonierung in Millisekunden zum Meta-Rc-Zustand. Dieser wiederum reprotoniert in Millisekunden zum metastabilen lichtadaptierten Zustand Pfr. Pfr kann mittels thermischer Reversion langsam in den Pr-Zustand zurückkehren oder mittels Fernrotlicht eine schnelle Konversion über ähnliche Intermediate wie die Rot->Fernrot Konversion wieder in den Pr zurückkehren. Abbildung modifiziert nach (Jeremiah R. Wagner et al. 2008) B) Mittels Rotlicht wird die dunkeladaptierte Pr-Form des Biliverdin in die Pfr-Form und durch Fernrotlicht zurück überführt. Dabei kommt es zu einer Photoisomerisierung von 15Z nach 15E und damit verbunden zu einer Rotation des Pyrrolrings D. Abbildung modifiziert nach (Nathan C. Rockwell and Lagarias 2010) C) Absorptionspektren des *Dr*BPhP PCM im dunkeladaptierten Zustand (schwarz) und nach Rotlicht-Bestrahlung (rot). Zu beachten ist, dass in beiden Fällen Mischzustände vorliegen.

2.3.4. Struktur von Phytochromen

Das N-terminale Sensor-Modul, auch PCM genannt, setzt sich in Phys aus dem PAS-GAF-PHY-Domänentandem zusammen und nimmt in BphPs die Form eines Kopf-an-Kopf Homodimers an (Essen, Mailliet, and Hughes 2008; Yang, Kuk, and Moffat 2008) (siehe Abb. 6).

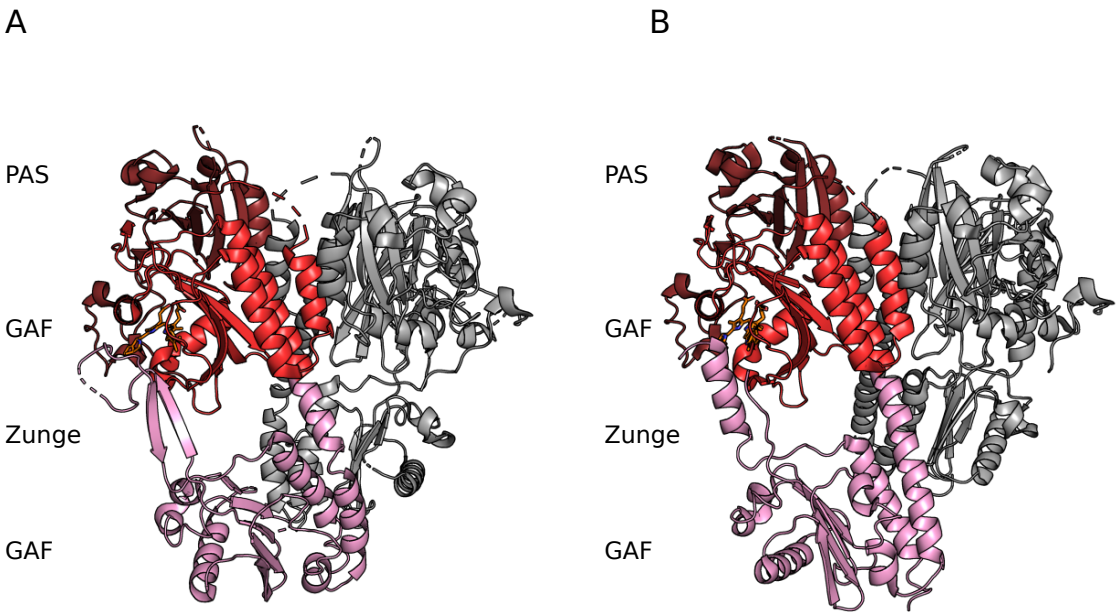

Abbildung 6: Struktur des PCM des *Deinococcus radiodurans* Bakteriphytochroms (*Dr*BphP) im dunkel- (PDB-Eintrag 4o0p) und lichtadaptierten Zustand (PDE-Eintrag 4o01) Die generelle Struktur von BphP entspricht einem Kopf-an-Kopf Homodimer. A) Die PHY-Zunge ist im Pr-Zustand des *Dr*BphP als β-Faltblatt ausgebildet. B) Durch Rotlicht wechselt *Dr*BphP in den Pfr-Zustand und die Phy-Zunge nimmt die Form einer α-Helix an.

Die PAS-Domäne besteht aus ca. 110 Aminosäuren und nimmt die räumliche Struktur eines β-Faltblatt flankiert von α-Helices ein. In allen kanonischen Phys wird eine sogenannte Knotenstruktur ausgebildet, bei der der N-Terminus der PAS-Domäne durch eine Schleife der GAF-Domäne geführt wird (Jeremiah R. Wagner et al. 2005).

Die GAF-Domäne bindet den Chromophor in einer Tasche zwischen einem β-Faltblatt und drei α-Helices und zeigt eine ähnliche Faltung wie die PAS-Domäne. Die an der Bindung des Chromophors beteiligten Aminosäuren sind hoch konserviert (Jeremiah R. Wagner et al. 2008). Anhand von Kristallstrukturen des Bakteriophytochrom PCM aus *Deinococcus radiodurans* im Pr-und Pfr-Zustand ist die Koordination des Kofaktors Biliverdin gut erforscht. Die an der Bindung beteiligten Aminosäuren interagieren über ein Netzwerk aus Salzbrücken bzw. hydrophoben Interaktionen mit dem Kofaktor (Jeremiah R. Wagner et al. 2005).

Beim Wechsel von Pr zu Pfr kommt es zu einer Photoisomerisierung entlang C15=C16 und somit zu einer Drehung des D-Rings. Durch die amphipathische Natur des D-Rings und der

direkten Umgebung in der Bindetasche entsteht ein Zustand mit hoher Bindungsenergie. Dadurch verursacht kommt es zu einer Verschiebung und Drehung des Bilverdin um die Thioetherbindung zwischen dem Cystein 24 (C24) aus der PAS-Domäne und dem $C3^2$ Kohlenstoff. Die Verschiebung hat die Lösung und Neubildung verschiedener Wasserstoffbrücken zur Folge.

Die Reste Aspartat 207 (D207) und Histidin 260 (H260), welche in der gesamten Phytochrom- Superfamilie konserviert sind, interagieren mit den Pyrrolringen A, B und C und mit einem Wassermolekül in der Bindetasche, welches Pyrrolwasser genannt wird (J. R. Wagner et al. 2007). Das Pyrrolwasser wird durch D207 verankert und fungiert mutmaßlich als Protonen- Donor und Akzeptor während der De- und Reprotonierung des Biliverdins (Jeremiah R. Wagner et al. 2008). D207 interagiert darüber hinaus in beiden Zuständen mit der PHY-Domäne. Im Pr-Zustand sind zwischen D207 und Arginin 466 (R466) zwei Salzbrücken ausgebildet, im Pfr hingegen bilden D207 und Phenylalanin 203 (F203) je eine Wasserstoffbrücke mit Serin 468 (S468) aus. D207 bleibt sowohl im Pr-als auch Pfr-Zustand mit dem B-Ring des Kofaktors verbunden (Jeremiah R. Wagner et al. 2008).

Im Pr-Zustand bildet der Pyrrolring B Wasserstoffbrücken mit Arginin 254 (R254) und Tyrosin 216 (T216) Pyrrolring C bildet Wasserstoffbrücken mit Serin 272 und 274. Im Pfr wechselt Ring B zu Arginin 222 (R222) und Ring C zu S272, Histidin 290 (H290) und Tyrosin 176 (T176) (E. Sethe Burgie, Zhang, and Vierstra 2016).

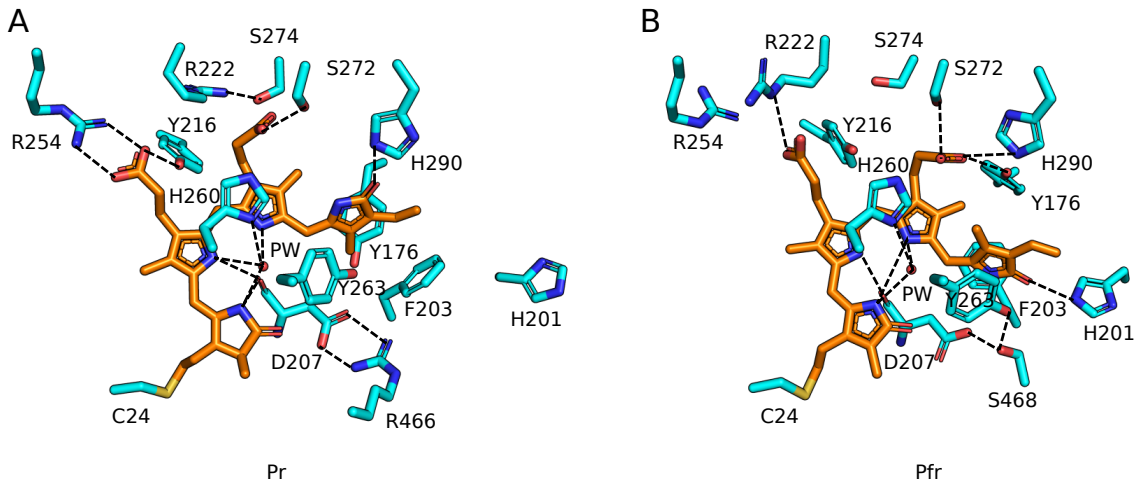

Abbildung 7: Koordination des an Cystein 24 gebundenen Chromophors Biliverdin im *Deinococcus radiodurans* Bakteriophytochrom (*Dr*BphP). A) Koordination im dunkeladaptierten Zustand Pr: Pyrrolring B bildet Wasserstoffbrücken mit Arginin 254 (R254) und Tyrosin 216 (T216) aus, während Pyrrolring C Wasserstoffbrücken mit Serin 272 und 274 ausbildet. Der Chromophor liegt als 15*Z*-Isomer vor. B) Koordination im lichtadaptierten Zustand Pfr: Ring B bildet zu Arginin 222 (R222) und Ring C zu S272, Histidin 290 (H290) und Tyrosin 176 (T176) Wasserstoffbrücken

aus. Der Chromophor liegt als 15*E*-Isomer vor. (E. Sethe Burgie, Zhang, and Vierstra 2016; Jeremiah R. Wagner et al. 2008).

Die PHY-Domäne, welche durch ein langes α-helikales Bündel mit der PAS- und GAF-Domäne verknüpft ist, zeigt ein weiteres, wichtiges Strukturmotiv (Essen, Mailliet, and Hughes 2008; Yang, Kuk, and Moffat 2008). Die sogenannte PHY-Zunge ist eine konservierte Haarnadelstruktur, die im direkten Kontakt mit dem Chromophor steht. Im Pr-Zustand bildet diese ein β-Faltblatt aus und durch Wechsel in den Pfr-Zustand kommt es zu einer Umfaltung zu einer α-Helix. Die PHY-Zunge spielt somit eine wichtige Rolle in der Signalpropagation des Phytochroms (Essen, Mailliet, and Hughes 2008; Takala et al. 2014; Yang, Kuk, and Moffat 2008).

2.4. Stoffwechsel der zyklischen Mononukleotide

Sowohl zyklisches 3‘,5‘-Adenosinmonophosphat (cAMP) als auch zyklisches 3‘-5‘-Guanosinmonophosphat (cGMP) sind wichtige Botenstoffe und regulieren als sogenannte *second messenger* eine Vielzahl an physiologischen Prozessen in Prokaryonten und Eukaryonten (Steiner, Antunes-Rodrigues, and Branco 2002).

Die zyklischen Mononukleotide (cNMP) werden mit Hilfe von Zyklasen (siehe 3.3.2) aus ihren jeweiligen Stoffwechselvorläufern Adenosintriphosphat (ATP) bzw. Guanosintriphosphat (GTP) synthetisiert. Dem entgegen wirken die Phosphodiesterasen (PDE, siehe 3.3.1), welche cNMPs in ihre jeweiligen Abbauprodukte Adenosinmonophosphat (AMP) bzw. Guanosinmonophosphat (GMP) spalten.

In Eukaryonten regulieren zyklische Nukleosidmonophosphate verschiedene Zielproteine, welche eine wichtige Rolle in diversen Signalwegen spielen und deren Störung für viele Krankheiten verantwortlich ist (Gold, Gonen, and Scott 2013).

So binden cAMP und cGMP spezifisch an Proteinkinase A bzw. G (PKA und PKG), welche gezielt spezifische Signalproteine phosphorylieren und an der Regulation des Energiestoffwechsel beteiligt sind (Gold, Gonen, and Scott 2013). Zyklische Nukleotid-gesteuerte (*cyclic nucleotide* gated, CNG) Ionenkanäle werden durch Bindung zyklischer Mononukleotide aktiviert. Dies ermöglicht den Fluss von Kalzium-, Kalium- und Natrium-Ionen (Kaupp and Seifert 2002) . Mitglieder der Popeye-Domäne enthaltenes Protein (*popeye domain-containing protein*, POPDC)- Familie binden cAMP und sind an vielen verschiedenen Prozessen beteiligt. Sie interagieren unter anderem mit Ionenkanälen, sind am vesikulären Transport beteiligt und spielen eine Rolle bei Krebs (Schindler and Brand 2016).

Austauschprotein durch cAMP-direktaktiviert (*exchange protein directly activated by cAMP*, Epac) aktiviert das Proto-Onkogen der Ratten sarcoma (Ras)-Familie, indem sie den GDP zu GTP Austausch nach cAMP Bindung katalysieren (de Rooij et al. 1998; Kawasaki et al. 1998; Madaule and Axel 1985). Ras wiederum aktiviert Mitogen-aktiviertes-Protein (*mitogen-activated protein*, MAP)-Kinasen, welche unter anderem Apoptose, Zelldifferenzierung und Zellwachstum kontrollieren (Santarpia, Lippman, and El-Naggar 2012).

Die meisten Bakterien verwenden cAMP als Signalmolekül. Zur Regulation kann ein aus cAMP und cAMP-Rezeptorprotein (*cAMP-receptor protein,* CRP), auch bekannt als Katabolit Aktivator Protein (*catabolite activator protein*, CAP), geformter Komplex an die Promotorregion verschiedener Zielgene binden und dadurch die Expression inhibieren oder aktivieren (Busby and Ebright 1999; Lawson et al. 2004). Eine Ausnahme bildet mindestens ein Vertreter der Proteobakterien, *Rhodospirillum centenum,* welches eine cGMP spezifische Variante des CAP besitzt (Marden et al. 2011; Dong, Bauer, and Roychowdhury 2015). Neben cNMPs werden zyklische di-Nukleotide, zum Beispiel, zyklisches Diguanylylmonophosphat (c-di-GMP), in Bakterien als *second messenger* genutzt und regulieren verschiedenste Prozesse, wie den Zellzyklus und die Biofilmbildung (Gomelsky 2011; Jenal, Reinders, and Lori 2017).

2.4.1. cNMP spezifische Phosphodiesterasen

Als Phosphodiesterasen (PDE) wird allgemein eine Gruppe von Enzymen, welche Phosphodiester-Bindungen spaltet, bezeichnet (van der Rest et al. 2002). Im Folgenden wird genauer auf die, für diese Arbeit wichtigen, PDEs eingegangen, welche zyklische Mononukleotide zu Nukleosidmonophosphaten abbauen (Bender 2006).

Im Menschen und anderen Säugetieren wird zwischen elf verschiedenen Familien unterschieden, die sich in verschiedene Isoformen aufteilen (Bender 2006; Conti and Beavo 2007). Anhand ihrer Substratspezifität können sie klassifiziert werden. PDE4, 7 und 8 hydrolisieren spezifisch cAMP, PDE 5, 6 und 9 hingegen cGMP. Die PDEs der Klassen 1, 2, 3, 10 und 11 können beide Substrate umsetzen (Francis, Blount, and Corbin 2011). Ein bekannter Vertreter ist die PDE5, welche für erektile Dysfunktion verantwortlich ist und spezifisch durch Sildenafil gehemmt werden kann (Goldstein et al. 1998). Ein weiterer, sehr bekannter, unspezifischer PDE-Hemmer ist das Koffein (Tesarik, Mendoza, and Carreras 1992).

In allen humanen PDEs ist die C-terminale katalytische Domäne konserviert. Jedoch unterscheiden sie sich in ihren N-terminalen Domänen. PDE2, 5, 6, 10 und 11 weisen ein GAF-A-GAF-B-Tandem auf, welches durch Bindung von cAMP, (PDE10) oder cGMP (PDE2, 5, 6, 11) zur allosterischen Regulation der katalytischen Domäne beiträgt. PDE1 besitzt stattdessen zwei Calmodulinbindende-Domänen (CaM), PDE3 zwei neuronale homologe Wiederholungen (*neuronal homology repeat*, NHR) Transmembran-Domänen, PDE4 zwei aufwärts konservierte Regionen (*upstream conserved region*, UCR) Domänen, PDE8 eine einzige PAS-Domäne und PDE7 und PDE9 keine N-terminale Domäne. (Conti and Beavo 2007) (siehe Abb. 8A).

Anhand der Kristallstruktur der humanen PDE2A wurde ein Aktivierungsmechanismus der katalytischen Domäne postuliert. Die Struktur zeigt einen dimeren Aufbau der GAF-A und GAF-B sowie der katalytischen Domäne. Die Dimerisierungsfläche erstreckt sich über das gesamte Protein. An der Stelle zwischen GAF-B- und PDE-Domäne überkreuzen sich die beiden Monomere, ähnlich zu den Messern einer Schere. Beide Untereinheiten haben ein eigenes katalytisches Zentrum welches im inaktiven Zustand durch die sogenannte H-Schleifenstruktur blockiert wird. Durch Bindung von cGMP an die GAF-B Untereinheit kommt es zu einer Umlagerung im Proteinrückgrat, welche eine Lockerung der Dimerisierungsfläche zur Folge hat, die katalytischen Domänen voneinander löst und die H-Schleifen aus dem aktiven Zentrum ausklappt (siehe Abb. 8B). Durch die hohe Konservierung der H-Schleifen Struktur innerhalb der Säugetier PDEs, wird von einem allgemein gültigen Mechanismus ausgegangen (Pandit et al. 2009).

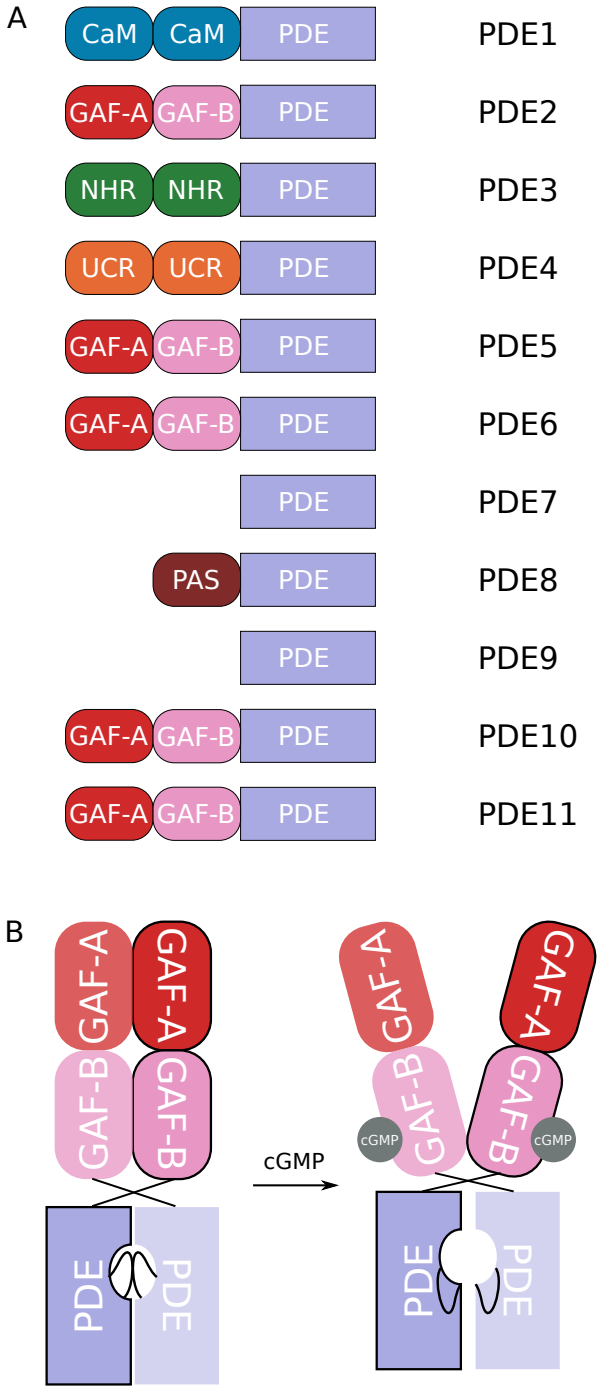

Abbildung 8: Domänenarchitektur der elf PDE-Familien und Aktivierungsmechanismus der katalytischen PDE-Domäne. A) Alle PDE besitzen eine konservierte katalytische Domäne. PDE2, 5, 6, 10 und 11 tragen N-terminal ein GAF-A-GAF-B-Tandem als Sensor-Modul. PDE1 besitzt stattdessen zwei Calmodulinbindende-Domänen (CaM), PDE3 zwei *neuronal homology repeat* (NHR) Transmembrandomänen, PDE 4 zwei *upstream conserved region* (UCR) Domänen, PDE8 eine einzige PAS-Domäne und PDE7 und 9 keine N-terminale Domäne. B) Die inaktive Form der PDE2A zeigt eine große, sich über das gesamte Protein erstreckende, Dimerschnittstelle und das katalytische Zentrum ist darüber hinaus durch H-Schleifen blockiert. Durch Bindung von cGMP an die GAF-B-Domäne kommt es zu einer Lockerung der Dimerschnittstelle, was in einem Auseinanderrücken des katalytischen Zentrums und dem Ausklappen der H-Schleifen resultiert. Die Abbildung wurde modifiziert nach (DeNinno 2012)

2.4.2. cNMP spezifische Zyklasen

Bei cNMP-spezifischen Zyklasen wird im generellen zwischen den Adenylyl- und Guanylyl-Zyklasen (AC und GC) unterschieden. Diese sind auch bekannt als Adenyl oder Adenylat, und Guanyl oder Guanylat. Die ACs werden in sechs verschiedene Klassen aufgeteilt, welche zueinander keine Homologie auf sequenzieller oder struktureller Ebene aufzeigen und zu unterschiedlichen Genfamilien gehören, obwohl sie alle dieselbe Reaktion katalysieren.

Klasse I AC kommen im Cytosol von gramnegativen Bakterien wie *Escherichia coli* vor (Danchin 1993). Die Klasse II Zyklasen werden von pathogenen Bakterien wie *Bacillus anthracis* oder *Pseudomonas aeruginosa* als Toxine in die Zielzelle eingeschleust (Danchin 1993).

Zu den Mitgliedern der Klasse III gehören neben ACs auch alle bekannten GCs und sie zählen aufgrund ihrer wichtigen Rolle für die menschliche Gesundheit zu den am besten untersuchten Zyklasen. Sie kommen hauptsächlich in Säugetieren und in einigen Bakterien vor. Von den zehn im Menschen vorkommenden ACIII Enzymen sind neun membranständig und eine kommt löslich im Cytosol vor (Danchin 1993; Linder 2006).

Für die Klassen IV-VI sind bislang nur wenige Vertreter charakterisiert, die alle aus Bakterien stammen (Tang and Gilman 1992; Cann et al. 2003). Der kleinste Vertreter der Zyklasen, CyaB aus *Yersinia*, ein Dimer von 19kDA Größe gehört zur Klasse IV (Smith et al. 2006).

Eine Besonderheit stellen die photoaktivierbaren Adenylylzyklasen (*photoactivated adenylylcyclase*, PAC) dar, welche in Algen und Bakterien vorgekommen (Briggs and Spudich 2005). Sie sind Vertreter der Klasse III. Der erste charakterisierte Vertreter wurde in der Alge *Euglena gracilis* (EuPAC) entdeckt. *Eu*PAC besteht aus einem Heterotetramer, welches sich aus je zwei Kopien der Kette α und β besteht. Sowohl *Eu*PACα als auch β besteht aus zwei BLUF Photosensoren und zwei Klasse III Adenylylzyklasen. Die beiden Ketten funktionieren unabhängig voneinander, und Kette α zeigt eine 100fach höhere Zyklaseaktivierung durch Blaulicht als Kette β, bei ebenfalls höherer Dunkelaktivität (Schröder-Lang et al. 2007).

Ein weiterer Vertreter der PACs wurde im Bakterium *Beggiatoa sp.* (bPAC) gefunden und besteht aus nur einem BLUF Photorezeptor, der ebenfalls an eine Klasse III Zyklase gekoppelt ist (Ryu et al. 2010; Stierl et al. 2011). Der Vorteil von bPAC gegenüber *Eu*PAC ist zum einen die geringere Größe und zum anderen die stärkere und länger andauernde Aktivierung durch Blaulicht. Beide PACs sind wichtige Entdeckungen für das Feld der

Optogenetik. Weitere lichtregulierte Zyklasen sind die photoaktiverte Adenylylzyklase aus *Microcoleus* (*Microcoleus photoactivated adenylate cyclase*, mPAC), die Rhodopsin Guanylylzyklase (*rhodopsin guanylyl cyclase*, RhoGC) und die auf Cyanobakteriochrom basierende lichtschaltbare Adenylylzyklase (*Cyanobateriochrome-based photoswitchable adenylyl* cyclase, cPAC) (Raffelberg et al. 2013; Trieu et al. 2017; Blain-Hartung et al. 2018).

2.5. Optogenetik

Optogenetik bezeichnet die Kombination von optischen und genetischen Methoden, um mittels Licht spezifische Ereignisse in Zellen und Organismen zu beobachten oder zu manipulieren (Deisseroth 2010). Mittels heterologer Expression von genetisch kodierten Photorezeptoren können zelluläre Prozesse kontrolliert werden. Die Vorteile der Optogenetik liegen in der hohen zeitlichen und räumlichen Auflösung, sowie der gezielten, nicht-invasiven, reversiblen Art der Methode. Das erste eingesetzte optogenetische Werkzeug ist der blaulichtgesteuerte Ionenkanal Kanalrhodopsin 2 (ChR2) aus *Chlomydomonas reinhardtii*. ChR2 ist in der Lage lichtabhängige Depolarisation auszulösen (Boyden et al. 2005). Zusammen mit der gelblichtaktivierbaren Chloridpumpe Halorhodopsin bildete es den Grundstein für die neuronale Optogenetik (Gradinaru, Thompson, and Deisseroth 2008). Seitdem wurden große Fortschritte gemacht und gezielt neue optogenetische Werkzeuge aus natürlich vorkommenden, aber auch synthetischen Photorezeptoren erschaffen. Diese dienen zur optogenetischen Regulation diverser zellulärer Prozesse.

2.5.1. Synthetische Photorezeptoren

Für die Erzeugung von synthetischen Photorezeptoren gibt es verschiedene rationale Ansätze. Zum einen können mittels gezielter oder zufälliger Punktmutationen spektrale, aber auch kinetische Eigenschaften bereits existierender Werkzeuge verändert werden. Eine andere Möglichkeit ist die Erschaffung von neuartigen Hybridproteinen. Dabei werden gezielt Sensor- oder Effektor-Domäne gegen andere Komponenten, welche gewünschte Eigenschaften aufweisen, ausgetauscht (Aba Losi, Gardner, and Möglich 2018; Shcherbakova et al. 2015).

Eines der früheren Beispiele für synthetische Photorezeptoren ist die lichtreprimierte HisK YF1. Bei der Erschaffung dieses Proteins wurde die Sauerstoff detektierende PAS-B Sensordomäne der Sensorhistidinkinase FixL aus *Bradyrhyzobium japonicum* (*Bj*FixL)

durch die LOV-Domäne des *Bacillus subtilis* YtvA (*Bs*YtvA) ersetzt (Möglich, Ayers, and Moffat 2009)(Abb.9).

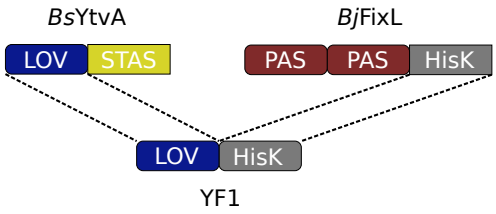

Abbildung 9: Modell der Domänenarchitektur der für den synthetischen Photorezeptor YF1 benutzten Proteine. Das Sensor-Modul wird aus der LOV-Domäne des *Bacillus subtilis* YtvA (*Bs*YtvA) gebildet und die Effektor-Domäne ist die Histidinkinase aus *Bradyrhyzobium japonicum* (*Bj*FixL).

Dabei machte man sich die strukturelle Homologie der beiden Sensor-Domänen zu nutze. Durch Blaulicht konnte die Netto- Phosphorylierungsrate der Effektor-Domäne um mehr als 1000-fach reprimiert werden (Möglich, Ayers, and Moffat 2009). Weitere Untersuchungen von YF1 Varianten zeigten, dass die katalytische Aktivität stark von der Linkerlänge zwischen dem Sensor und Effektor-Modul abhängig ist. (Möglich, Ayers, and Moffat 2009). Mittels der Methode, Primer-gestützte Kürzung für die Erschaffung von Hybridproteinen (*primer aided truncation for the creation of hybrid proteins*, PATCHY), konnte eine Genbibliothek aus *Bs*YtvA-*Bj*FixL Hybridproteinen erzeugt werden, in der sämtliche Linkerlängen zwischen den Domänen enthalten waren. Aktivitätsuntersuchungen zeigten, dass lichtreprimiert Varianten bei einer Linkerlänge von 7*n* und 7*n*+5 und lichtaktivierte Varianten bei einer Linkerlänge von 7n+1 Aminosäuren auftraten. (Ohlendorf et al. 2016). Eine Umkehrung der YF1 Aktivität kann ebenfalls durch das Einbringen von Mutationen erreicht werden. So sind die Varianten D21V und H22P beide lichtaktivierte YF1 Konstrukte (Gleichmann, Diensthuber, and Moglich 2013; Diensthuber et al. 2013).

Einer der ersten synthetischen R/FR-Photorezeptoren ist die Infrarotlicht aktivierte Adenylylzyklase (*infrared-light-activated adenylate cylase*, IlaC). Sie ist eine Chimäre aus dem PCM des nicht-kanonischen Phytochroms BphPG1 aus *Rhodobacter sphaeroides* fusioniert mit der Adenylylzyklase CyaB1 aus *Nostoc sp.*. Das Protein BphG1 kontrolliert normalerweise den zyklischen Diguanosinmonophosphat Umsatz in Bakterien, welches durch die AC ersetzt wurde (siehe Abb. 10). Für eine funktionale Chimäre mussten verschiedene Linkerlängenvariationen zwischen der PHY- und AC-Domäne getestet werden. Mittels Beleuchtung mit Licht einer Wellenlänge von 700 nm konnten cAMP Konzentrationen um den Faktor sechs erhöht werden. In Neuronen von *C. elegans* exprimiert konnte IlaC dazu genutzt werden das intrazelluläre cAMP-Niveau lichtabhängig zu erhöhen was in beschleunigter Fortbewegung resultierte (Ryu et al. 2014).

Basierend auf dem IlaC Designansatz wurde, während der Anfertigung dieser Doktorarbeit, die rotlichtregulierte Phytochrom-aktivierte Guanylylzyklase (PagC) erschaffen. In diesem Fall wurde die Sensor-Domäne CHASE2 der Guanylylzklase Cya2 aus *Synechocystis sp.* durch das PCM aus *Dr*BphP ersetzt (siehe Abb. 10). Auch hier war die Länge des Linkers zwischen PHY und GC von entscheidender Bedeutung für die Aktivität. Die Veränderung von PagC in eine Phytochrom-aktivierte Adenylylzyklase (PaaC) konnte durch eine Punktmutation in der katalytischen Domäne erreicht werden (Etzl et al. 2018a).

Ein weiteres Werkzeug, welches bereits Anwendung in Eukaryonten gefunden hat ist die lichtaktivierte Phosphodiesterase LAPD, auf welche im folgenden Kapitel (3.5) genauer eingegangen wird. Anwendung von LAPD wurde sowohl in Säugetierzellen als auch Zebrafisch Embryonen gezeigt (Gasser et al. 2014).

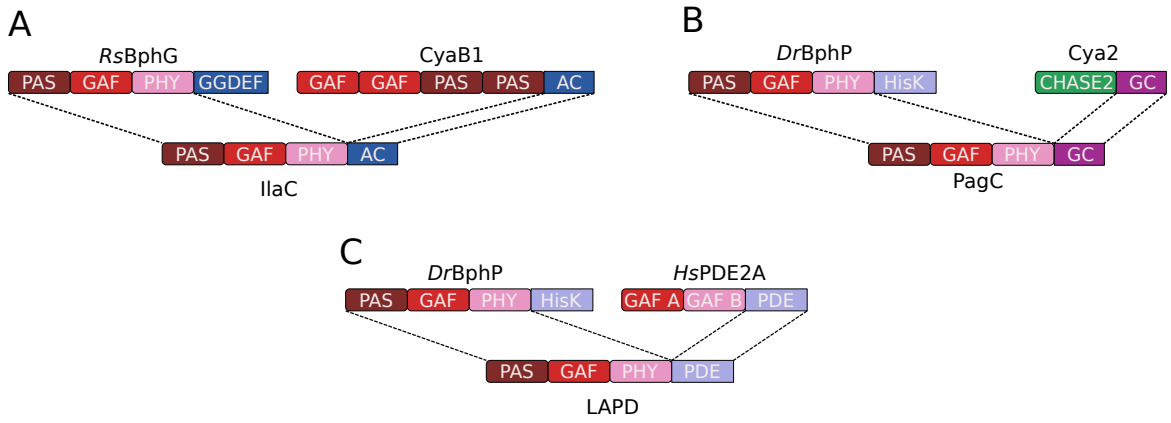

Abbildung 10: Modell der Domänenarchitektur der synthetischen R/FR Photorezeptoren LAPD, IlaC und PagC. A) Die rotlichtabhängige Phosphodiesterase LAPD stzt sich aus dem PCM des *Deinococcus radioduran* Bakteriophytochroms (*Dr*BphP) und dem Effektor-Modul der humanen Phosphodiesterase (*Hs*PDE2A) zusammen. B) Die fernrotlichtabhängige Zyklase IlaC nutzt das PCM des nichtkanonischen *Rhodobacter sphaeroides* Bathyphytochroms (*Rs*BphG) als Sensor und die Adenylylzklase aus *Nostoc sp.* (CyaB1) als Effektor-Modul. C) Die rotlicht-abhängige Zyklase PagC nutzt, wie auch LAPD, das *Dr*BphP PCM als Sensor- und die Guanylylzklase aus *Synechocystis sp.* Cya2 als Effektor-Modul.

Der größte Vorteil von Phytochromen gegenüber anderen natürlichen Photorezeptoren ist ihr durch Licht schaltbarer R/FR-Photozyklus. Mittels Rot- bzw. Fernrotlicht kann zwischen dem Pr- und Pfr-Zustand hin und her geschaltet werden. Außerdem dringt rotes bzw. fernrotes Licht tiefer in Gewebe ein, als Licht kürzerer Wellenlängen, und zum anderen ist es weniger toxisch für lebende Zellen (Mahmoud et al. 2008; Shcherbakova et al. 2015). Daher sind Phys von großem Interesse für die Entwicklung optogenetischer Werkzeuge.

2.6. Die lichtaktivierbare Phosphodiesterase LAPD

Der Erstellung von LAPD liegt die strukturelle Homologie des Phytochrom PAS-GAF-PHY-Tandems mit der N-terminalen GAF-A-GAF-B Sensoreinheit der PDE zugrunde. Hierbei wurde das kanonische BphP aus *Deinococcus radiodurans* (*Dr*BphP) mit der katalytischen Domäne der humanen Phosphodiesterase 2A fusioniert (Gasser et al. 2014). Zu dem damaligen Zeitpunkt war die einzige Kristallstruktur eines vollständigen PAS-GAF-PHY-Tandems die des *Pseudomonas aeruginosa* Phytochroms (*Pa*BphP, PDB 3C2W) und für PDE die Volllängenstruktur der Humanen Phosphodiesterase 2A (*Hs*PDE2A, PDB 3IBJ) (Yang, Kuk, and Moffat 2008; Pandit et al. 2009). Bei der strukturellen Überlagerung zeigte sich, dass die C-terminale Helix der PHY-Domäne sehr gut mit der N-terminalen Helix der PDE-Domäne überlappt und somit wurde dieser Bereich für die Fusionsschnittstelle gewählt (Abbildung 11).

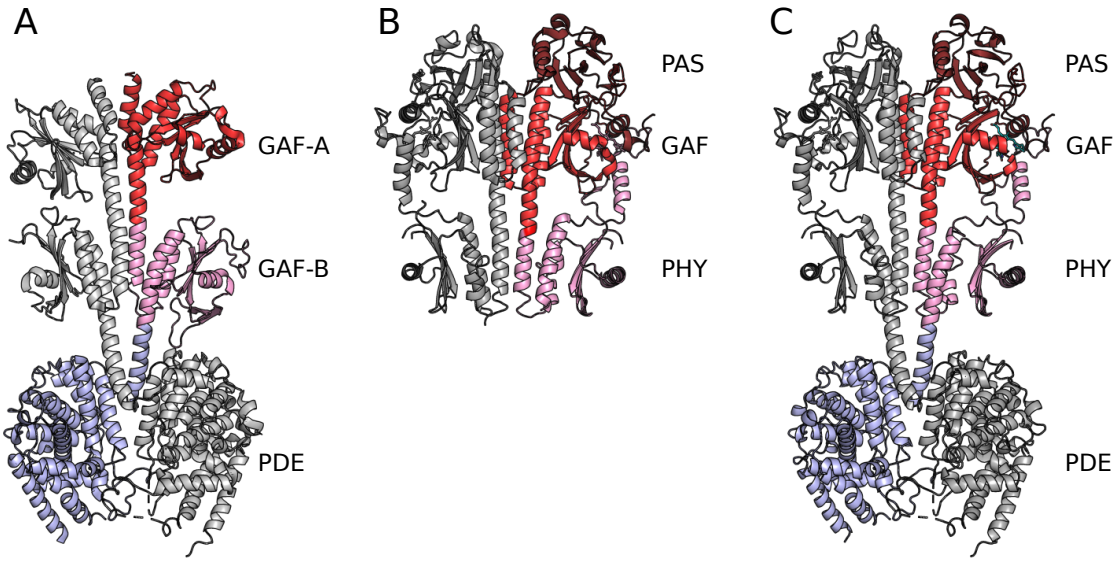

Abbildung 11: Übersicht der zugrundeliegenden Designidee für LAPD. Homologes Strukturmodell basierend auf den Kristallstrukturen des *Pa*BphP (3C2W, (Yang, Kuk, and Moffat 2008)) und *Hs*PDE2A (3IBJ, (Pandit et al. 2009)), modifiziert nach (Gasser et al. 2014).

Das erste Konstrukt, ein *Pa*BphP-*Hs*PDE2A-Hybrid, konnte nicht löslich exprimiert werden. Daher wurde das *Pa*BphP gegen das *Dr*BphP, von dem, zum damaligen Zeitpunkt, die Struktur der PAS-GAF-Domänen gelöst war, ausgetauscht (Jeremiah R. Wagner et al. 2005). Der finale LAPD Entwurf beinhaltete die Aminosäurereste 1-506 des *Dr*BphP, fusioniert an die Reste 555-941 der *Hs*PDE2A. Um Aufschluss über den Einfluss des Linkers auf die Aktivität zu erlangen wurden vier Deletionsvarianten (LAPD-1 bis LAPD-4) und sieben Insertionsvarianten (LAPD+1 bis LAPD+7) erstellt (siehe Abbildung 12).

A

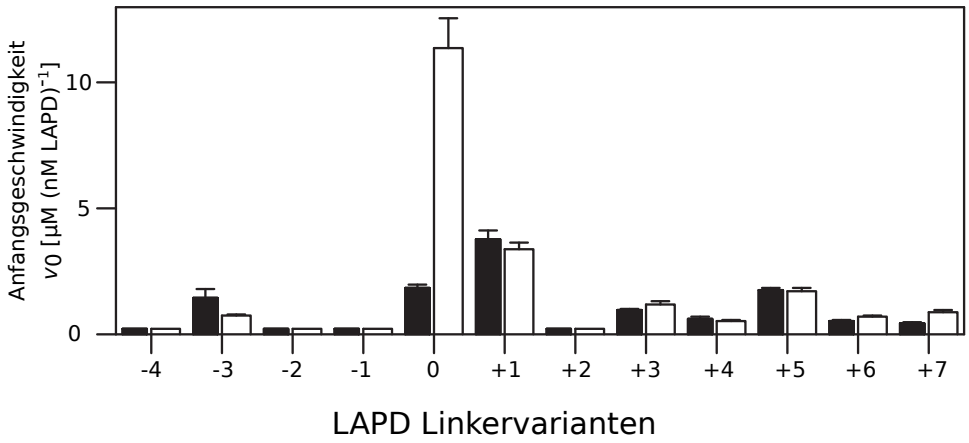

B

LAPD-4	WHPGEIEEAQDLRDTLTGALGERL----------EAQYRSHLANEMMMYHMKVSDDEY
LAPD-3	WHPGEIEEAQDLRDTLTGALGERL----------NEAQYRSHLANEMMMYHMKVSDDEY
LAPD-2	WHPGEIEEAQDLRDTLTGALGERL---------VNEAQYRSHLANEMMMYHMKVSDDEY
LAPD-1	WHPGEIEEAQDLRDTLTGALGERL--------KVNEAQYRSHLANEMMMYHMKVSDDEY
LAPD	WHPGEIEEAQDLRDTLTGALGERL-------KKVNEAQYRSHLANEMMMYHMKVSDDEY
LAPD+1	WHPGEIEEAQDLRDTLTGALGERL------YKKVNEAQYRSHLANEMMMYHMKVSDDEY
LAPD+2	WHPGEIEEAQDLRDTLTGALGERL-----LYKKVNEAQYRSHLANEMMMYHMKVSDDEY
LAPD+3	WHPGEIEEAQDLRDTLTGALGERLS----LYKKVNEAQYRSHLANEMMMYHMKVSDDEY
LAPD+4	WHPGEIEEAQDLRDTLTGALGERLSV---LYKKVNEAQYRSHLANEMMMYHMKVSDDEY
LAPD+5	WHPGEIEEAQDLRDTLTGALGERLSVI--LYKKVNEAQYRSHLANEMMMYHMKVSDDEY
LAPD+6	WHPGEIEEAQDLRDTLTGALGERLSVIR-LYKKVNEAQYRSHLANEMMMYHMKVSDDEY
LAPD+7	WHPGEIEEAQDLRDTLTGALGERLSVIRDLYKKVNEAQYRSHLANEMMMYHMKVSDDEY

Abbildung 12: A) Abhängigkeit der katalytischen Aktivität und Lichtregulation von der Länge des Linkers. Anfangsgeschwindigkeiten wurden für LAPD-Varianten im Dunkeln (schwarz) und nach Illumination mit 690 nm Licht (weiß) bei 1mM cGMP ermittelt. B) Linkerzusammensetzung der Varianten. Abbildung modifiziert nach (Gasser et al. 2014).

Dabei zeigten die wenigsten Konstrukte (lichtschaltbare) Aktivität und eine zu erwartende Heptadenperiodizität einer *coiled-coil* Struktur zeigte sich nicht.

Die katalytische Aktivität wurde sowohl für cGMP als auch cAMP im dunkel- und lichtadaptierten Zustand bestimmt. Dabei diente Rotlicht zur Aktivierung und Fernrotlicht zur Inaktivierung von LAPD. Es wurde eine 6-fache Aktivierung der cGMP-Hydrolyse durch Rotlicht und eine 4-fache für cAMP mittels HPLC-Messungen gezeigt. Allerdings zeigte sich, dass die Schaltung der enzymatischen Aktivität nicht vollständig reversibel ist. Diese geht einher mit einem unvollständigen Übergang des Chromophors von Pfr nach Pr nach Fernrot Beleuchtung (Gasser et al. 2014).

Zusammenfassend bildet LAPD eine neues optogenetisches Werkzeug und bietet Ansatzpunkte für die Erzeugung von R/FR-aktivierbaren Photorezeptorproteinen.

2.7. Ziele der Arbeit

Bei der Erzeugung von synthetischen Photorezeptoren ist die Länge und Komposition des verknüpfenden Linkers zwischen Sensor- und Effektor-Modul von großer Bedeutung, wie die Erschaffung der lichtabhängigen Histidinkinase YF1 zeigte. So kann durch Variation der Linkerlänge in YF1 die Aktivität durch Licht aktiviert, anstatt reprimiert werden.
Durch Mutationen in YF1 kann die Lichtschaltbarkeit ebenfalls umgekehrt werden.
In dieser Arbeit soll PATCHY auf diese YF1 Varianten angewendet werden, um zu überprüfen ob diese Konstrukte ebenfalls, durch Modulation der Linkerlänge, ihre lichtabhängige Aktivität umkehren können und um ein besseres Verständnis der Signaltransduktion zu erhalten.
Ein weiteres Ziel ist die Erweiterung der synthetischen Photorezeptoren für die optogenetische Kontrolle von zyklischen Nukleotidkonzentrationen in Zellen. Da im Bereich der Optogenetik bereits die photoaktivierbare Adenylylzyklasen (PACs) und die rotlichtaktivierte Phosphodiesterase (LAPD) Anwendung finden, sollen neue Varianten mit verbesserten Eigenschaften erzeugt werden.
Für die Erzeugung neuer R/FR-schaltbarer PACS soll das Sensor-Modul der Adenylylzyklase Cya2 aus *Synechocystis* durch Sensor-Module aus Bakteriophytochromen ersetzt werden.
Um PACs schnell und einfach hinsichtlich ihrer lichtabhängigen Aktivität zu testen soll, basierend auf dem pCyclR Plasmid, ein Reportersystem etabliert werden. So gefundene, funktionale Konstrukte, sollen anschließend genauer hinsichtlich ihrer photochemischen und enzymatischen Eigenschaften charakterisiert werden.
Basierend auf LAPD sollen weitere Varianten mit veränderten spektralen, photochemischen und enzymatischen Eigenschaften generiert werden. Dies soll zum einen durch Austausch des Sensor-Moduls mit homologen BphPs oder durch Austausch des Effektor-Moduls durch homologe PDEs erfolgen. Funktionale Varianten sollen *in vitro* photochemisch und enzymatisch charakterisiert werden. Des Weiteren sollen funktionale Konstrukte ebenfalls miteinander kombiniert und charakterisiert werden. Durch die multiplen Austausche soll Aufschluss über erfolgsversprechende Kombinationsmöglichkeiten gewonnen werden.
Anschließend soll die Eignung von funktionalen LAPD Varianten für die optogenetische Anwendung *in vivo* in menschlichen embryonalen Nierenzellen (*human embryonic kidney*, HEK) untersucht werden.

3. Synopsis

Die vorliegende kumulative Dissertation umfasst vier, bereits veröffentlichte oder zur Publikation angenommene, wissenschaftliche Publikationen und einen Übersichtsartikel (Kapitel 2.5. Die Arbeiten behandeln zum einen generelle Designprinzipien für die Erschaffung von synthetischen Photorezeptoren, (Kapitel 2.1) und zum anderen deren Anwendung bei der Konstruktion neuer, synthetischer R/FR Photorezeptoren, um zyklische Nukleotidkonzentrationen in Zellen zu Kontrollieren und deren Anwendung als optogenetisches Werkzeug (Kapitel 2.2-2.4).

3.1. Einfluss des Linkers zwischen Sensor-und Effektor-Modul in Hybridproteinen

Die erste Veröffentlichung behandelt den Einfluss des Linkers zwischen Sensor- und Effektor-Modul auf die Signalweiterleitung und somit auf die Aktivität von Hybridproteinen. Dazu wurde die Methode der Primer-gestützten Kürzung für die Erschaffung von Hybridproteinen (*primer-aided truncation for the creation of hybrid proteins,* PATCHY (Ohlendorf et al. 2016) auf Varianten des synthetischen Photorezeptor YF1 (Möglich, Ayers, and Moffat 2009) angewendet, um Länge und Zusammensetzung des Linker zwischen der *Bs*Ytva LOV Sensor-Domäne und dem *Bj*FixL Histidinkinase Effektor-Modul zu verändern (siehe Abb. 13).

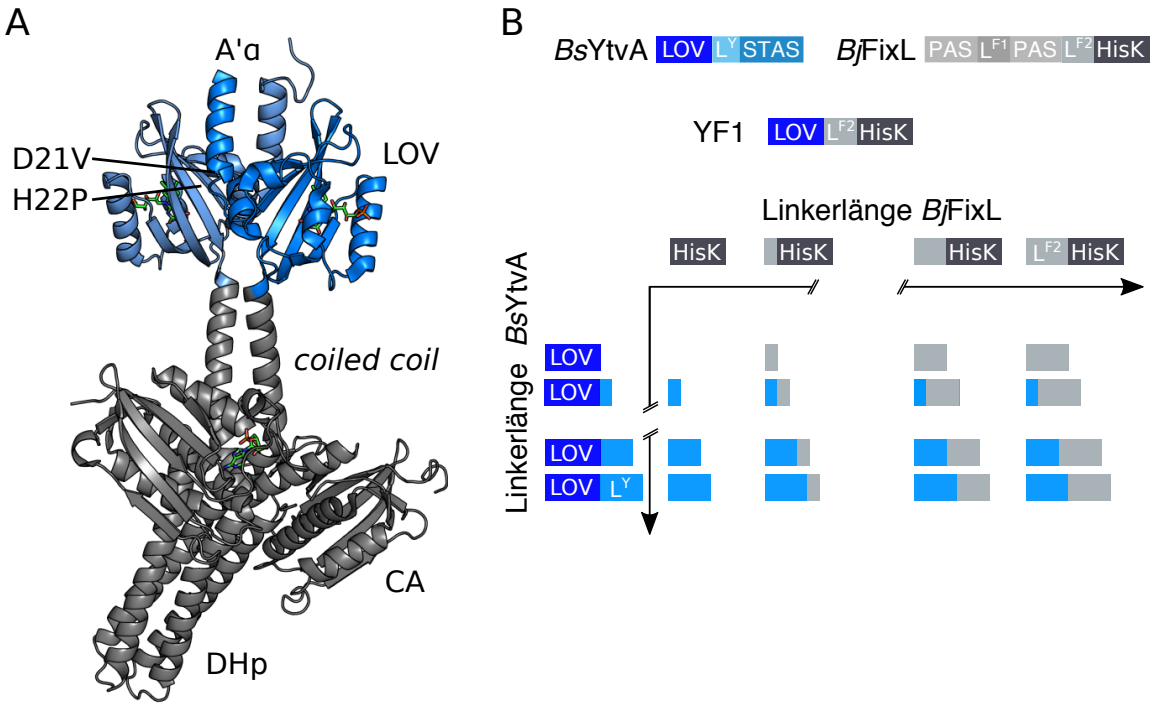

Abbildung 13: A) Kristallstruktur (PDB 4GCZ) des homodimerischen YF1 im dunkeladaptierten Zustand zeigt den *coiled coil* Linker zwischen Photosensor- und Effektor-Modul. B) Schematische Darstellung möglicher Linkerkombinationen für Hybridproteine aus *Bs*YtvA Photosensor- und *Bj*FixL Effektor-Modul. In YF1 entstammt der verbindende Linker fas vollständig aus *Bj*FixL.

Es handelte sich dabei um YF1 Konstrukte, welche die Mutation D21V (Gleichmann, Diensthuber, and Moglich 2013) oder H22P (Diensthuber et al. 2013) trugen, die eine invertierte Lichtregulation zur Folge haben. Beide Positionen befinden sich, in der N-terminalen A`α *coiled coil* Helix nahe der Dimerisierungsfläche, und bilden wichtige intra- bzw. intermolekulare Wasserstoffbrücken aus.

Ziel war es, festzustellen, welchen Einfluss die Linkerzusammensetzung, analog zu YF1, auf die Aktivität der Varianten D21V und H22P hat. Um das Testen der Konstrukte zu vereinfachen wurde das pDusk-*Ds*Red Reporterplasmidsystem verwendet (siehe Abb.14) (Ohlendorf et al. 2012). Für YF1 wurden zuvor licht-reprimierte Konstrukte bei Linkerlängen von 7*n* und 7*n*+5 (n=1, 2, 3, ...) Aminosäureresten gefunden, Varianten mit invertierten Schaltung zeigten sich hingegen bei einer Länge von 7*n*+1 Resten (Ohlendorf et al. 2016).

Für YF1 D21V kommen lichtaktivierte Varianten bei Linkerlängen von 7*n* und 7*n*+1 Aminosäureresten und lichtreprimierte bei Längen von 7*n* und 7*n*+3 vor. Für H22P wurden für lichtaktivierte Konstrukte hauptsächlich Linkerlängen von 7*n* Aminosäuren und keine lichtreprimierten Konstrukte gefunden.

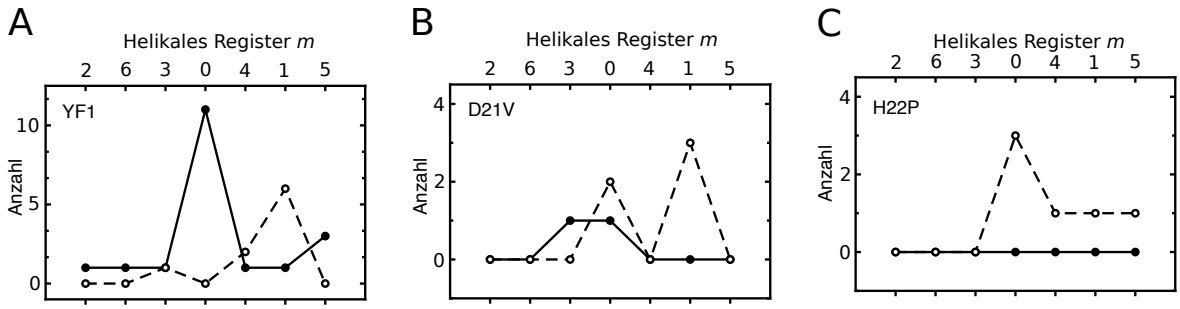

Abbildung 14: Analyse der Linkerlängen von lichtregulierten *Bs*YtvA-*Bj*FixL Hybridproteinen. A) Für YF1 wurden lichtreprimierte Varianten (schwarz) vorranging bei einer Periodizität der Linkerlänge von 7*n* oder 7*n*+5 Aminosäureresten gefunden, lichtaktivierte Varianten (weiß) hingegen bei einer Linkerlänge von 7*n*+1 Resten. B) Lichtaktivierte D21V Varianten hatten eine Linkerlänge von 7*n* oder 7*n*+1 Aminosäureresten. Zwei Varianten mit Linkerlängen von 7*n* und 7*n*+3 Resten zeigten invertiertes also lichtreprimiertes Verhalten. C) H22P Varianten zeigten lichtaktivierte Konstrukte hauptsächlich bei Linkerlängen von 7*n* Aminosäuren und keine lichtreprimierten Konstrukte.

Im Vergleich zu YF1 wurden insgesamt weniger lichtabhängige Konstrukte gefunden und auch die Heptadenperiodizität ist schwächer ausgeprägt oder fast nicht erkennbar. Dennoch wurde deutlich, dass die Länge des Linkers starke Auswirkungen auf die Aktivität hat und für ein erfolgreiches Design das richtige Register gefunden werden muss.

3.2. Erzeugung & Charakterisierung neuer lichtregulierter Zyklasen

Die zweite Veröffentlichung behandelt die Etablierung eines Testsystems für lichtaktivierte Zyklasen (PACs) zur Erschaffung von R/FR-gesteuerten Zyklasen. Ein Reportergen System wurde im zyklasedefizienten *E. coli* Stamm CmpX13 ΔcyaA etabliert. Dazu wurde ein Plasmid, welches die zu untersuchende Zyklase codiert, mit dem Reporterplasmid pCyclR, welches unter anderem die Expression des Fluoreszenzprotein *Ds*Red kontrolliert, kombiniert (siehe Abbildung 16A) (Ohlendorf et al. 2012). Das System wurde mit Hilfe der bereits charakterisierten Zyklase bPAC genauer charakterisiert und etabliert (Abbildung 16B-D).

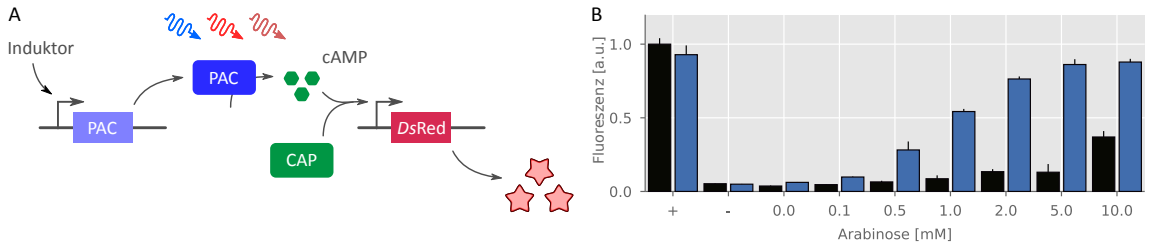

Abbildung 15: A) pCyclR Testsystem für lichtaktivierte Adenylylzyklasen (PACs). B) Reportergen Aktivität für Kulturen, welche bPAC abhängig von verschiedenen Konzentrationen des Induktion L-Arabinose exprimieren. In schwarz sind im Dunkeln exprimierte und in blau sind permanent mit 40 µW cm^{-2} 470-nm Licht beleuchtete Kulturen gezeigt.

Die von Winkler *et al.* veröffentlichen PAC PagC (Etzl et al. 2018b) ermöglicht einen genaueren Einblick in die Linkerregion zwischen Sensor- und Effektor-Modul und liefert somit wichtige Informationen für die Verknüpfung der beiden Domänen. Darauf basierend entwarfen wir drei PACs mit dem PCM aus homologen Bakteriophytochromen und untersuchten sie mit Hilfe des Reportersystems. Für alle drei PACs konnten wir Lichtregulation feststellen und sie mit unserem System hinsichtlich ihrer Lichtsensitivität untersuchen. Die enzymatische Aktivität des besten Konstrukts *Dd*PAC, basierend auf dem PCM von *Deinococcus dersertii* BphP, wurde mit Hilfe eines HPLC basierten Assay genauer charakterisiert (Abb. 17).

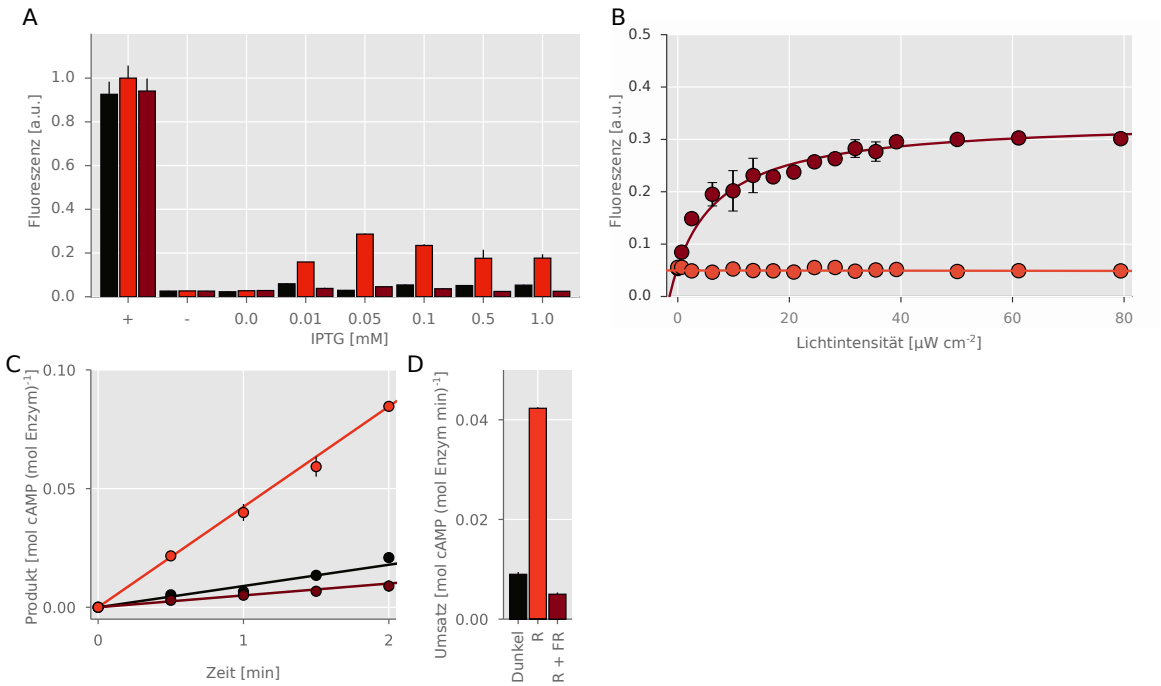

Abbildung 16: Reportergen Aktivität für *Dd*PAC im pCyclR. A) Expression von *Dd*PAC bei verschiedenen Konzentrationen des Induktors IPTG. Kulturen wurden entweder im Dunkeln (schwarz) oder unter konstanter Beleuchtung mit 655 nm (rot) bzw. 850 nm (braun) Licht einer Intensität von 40 µW cm^{-2} gehalten. B) Reportergen Aktivität für bei Expression von *Dd*PAC mit 0,05 mM IPTG unter konstanter Beleuchtung von 655 nm und 850 nm Licht bei verschiedenen Intensitäten.C) Reportergen Aktivität bei Expression von *Dd*PAC mit einer Induktorkonzentration von 0,05 mM IPTG und gepulster Beleuchtung von 40 µW cm^{-2} 655-nm Licht. D) HPLC Messungen der Adenylylzyklaseaktivität für *Dd*PAC. E) Anfangsgeschwindigkeiten der Aktivität aus D).

Der große Vorteil von *Dd*PAC gegenüber bereits beschriebenen PACs ist, dass die Zyklase gezielt und vollständig mittels Fernrotlicht ausgeschaltet werden kann. Für die Anwendung ist ebenfalls von Vorteil, dass bereits geringe Lichtdosen zur Regulierung ausreichen. Somit ist *Dd*PAC eine sehr gute Erweiterung der optogenetischen Werkzeuge für die Manipulation von zyklischen Mononukleotiden.

3.3. Anwendungen gepulster Beleuchtung zur Charakterisierung optogenetischer Systeme

Die dritte Publikation beschreibt die Anwendung von gepulster Beleuchtung im Bereich der Photobiologie und Optogenetik. Bei der Anwendung von optogenetischen Werkzeugen zur präzisen Kontrolle von Prozessen in Zellen und lebenden Organismen, spielen synthetische Photorezeptoren eine wichtige Rolle. Da Beleuchtung mit hoher Intensität auf Dauer, abhängig von der benutzen Wellenlänge, Schaden in Gewebe und Lebewesen anrichtet, ist es von Vorteil, die intrinsische Kinetik, mit der ein System nach Anregung wieder in seinen dunkeladaptierten Zustand zurückkehrt, genauer zu untersuchen, um die Beleuchtungsdauer

und -dosis möglichst gering zu halten. Mittels gepulster Illumination kann genau dies erreicht werden. Anhand von zwei Anwendungsbeispielen, YF1 und *Dd*PAC zeigen wir, dass mit Hilfe unseres System, auf einfache und kostengünstige Art und Weise, zum Beispiel durch die Nutzung von Leuchtdioden (*light-emitting diodes*, LEDs) als Lichtquelle, verschiedene Systeme hinsichtlich Lichtsensitivität und Dauer untersucht werden können. Des Weiteren können mittels gepulster Beleuchtung Photorezeptoren, welche dieselbe Lichtart absorbieren, getrennt voneinander adressiert werden, solange sie sich hinsichtlich ihrer Rückkehrkinetik unterscheiden.
Damit zeigen die beschriebenen Methoden die breite Anwendbarkeit von gepulster Beleuchtung im Bereich der Optogenetik und der Photobiologie.

3.4. Erzeugung und Charakterisierung R/FR-abhängige Phosphodiesterasen

Die vierte Publikation behandelt Designansätze zur Erschaffung R/FR schaltbarer PDEs und deren Anwendung zur Kontrolle zyklischer Mononukleotide. Basierend auf einem aktualisierten Strukturmodell von LAPD wurden homologe Austausche der Sensor- und Effektor-Domäne durchgeführt, welche mit Hilfe eines fluoreszenzbasierten Testsystems in *E. coli* Lysat untersucht wurden. Zunächst wurde im Sensor-Modul das gesamte PAS-GAF-PHY-Modul, aber auch nur das PAS-GAF-Domänenpaar gegen homologe Bakteriophytochrome ausgetauscht, mit dem Ziel, die Lichtschaltbarkeit und Aktivität zu verbessern (Abb. 18). Das Effektor-Modul wurde gegen Teile homologer PDE2A Varianten ausgetauscht, um ebenfalls die Aktivität aber auch Spezifität zu verändern. Während der Austausch des Effektor-Moduls aufgrund der hohen Sequenzhomologie viele aktive Konstrukte hervorbrachte, zeigten viele Sensoraustausche keine lichtabhängige oder gar keine Aktivität. Aufgrund dessen wurden in LAPD Aminosäurereste in der Linkerregion ausgetauscht, um ein tiefergehendes Verständnis für die Signalweiterleitung zu erhalten. Basierend auf diesen Ergebnissen konnten wir zeigen, dass die Linkerregion sehr empfindlich selbst gegenüber konservativen Mutationen ist und die Originalsequenz des Linkers von LAPD am besten funktionierte. Das Einbringen dieses Sequenzmotivs an die Fusionsstelle von homologen PAS-GAF-PHY Austauschen ermöglichte es (lichtabhängige) Aktivität wiederherzustellen.

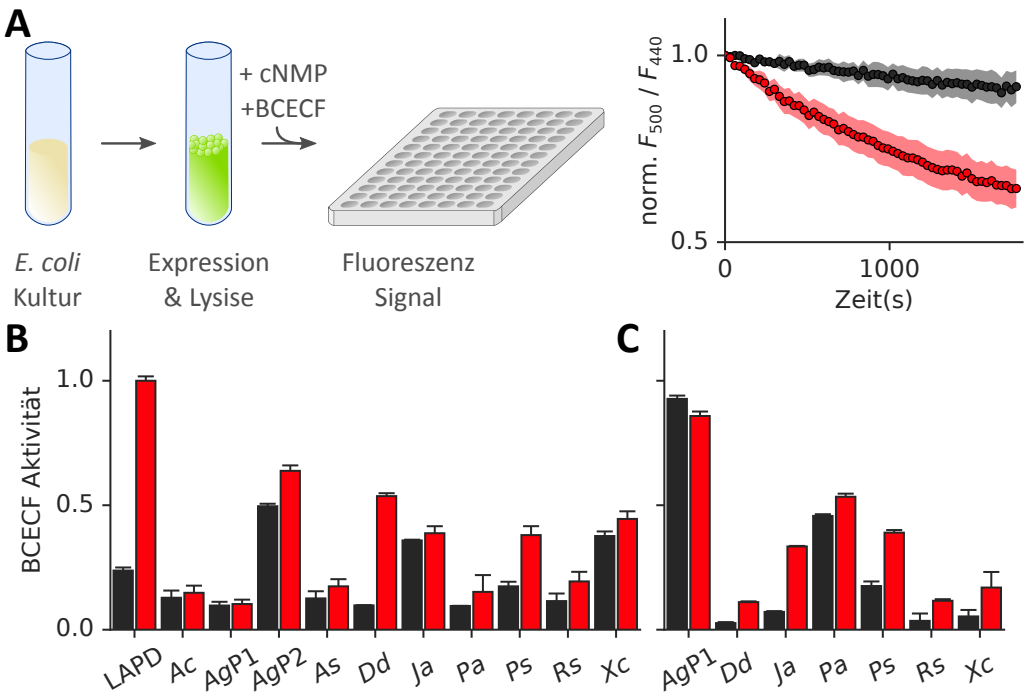

Abbildung 17: Testsystem für lichtregulierte PDE Varianten. A) Konstrukte werden in *E. coli* exprimiert und das Lysat auf lichtregulierte Aktivität untersucht. Mit Hilfe des pH-Sensitiven Fluoreszenzfarbstoff BCECF kann die cNMP Hydrolyserate über die Zeit verfolgt werden. B) Die PAS-GAF-Domänen wurden durch entsprechende Domänen aus anderen Bakteriophytochromen ersetzt. C) Durch Veränderungen in der Fusionsschnittstelle konnten inaktive Varianten lichtreguliert werden. Die Abkürzungen bezeichnen verschiedene BphPs (siehe Stabel *et al*., 2019).

Die Konstrukte mit der besten Lichtregulation wurden exprimiert und die cAMP und cGMP Hydrolyseaktivität von dunkeladaptierten und mit Rot bzw. Fernrotlicht beleuchteten Proben verglichen. Dabei zeigte sich in HPLC Messungen, dass die Variante *Dr-Bt*PDE2A nicht nur eine höhere Aktivität, sondern auch eine verbesserte Reversibilität gegenüber LAPD aufweist (siehe Abb. 19).

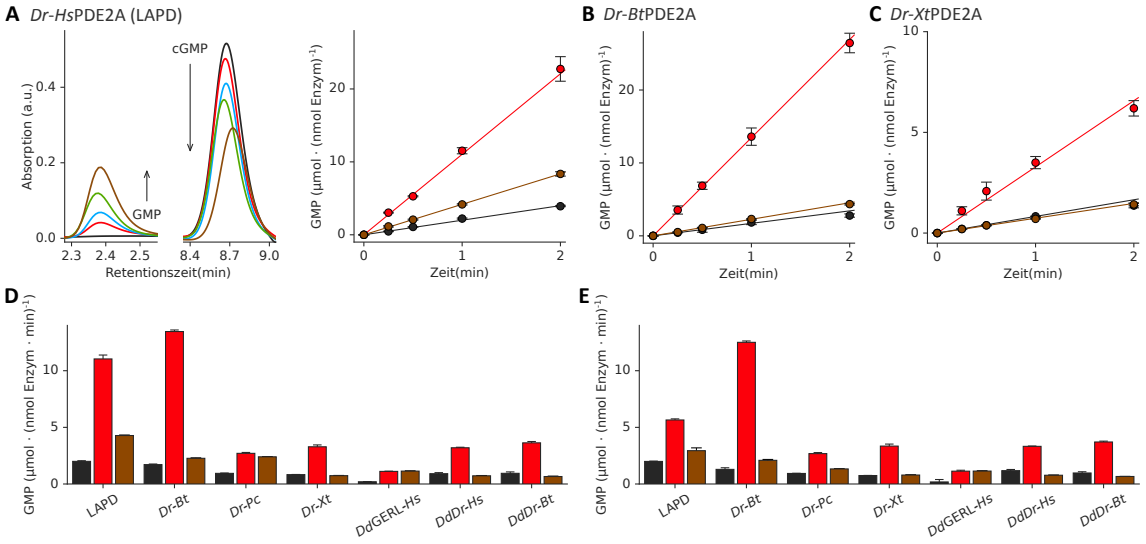

Abbildung 18: A-C) HPLC Analyse der cGMP Hydrolyse für LAPD und davon abgeleitete, lichtregulierte PDEs im Dunkeln (schwarz) und nach Bestrahlung mit Rotlicht (rot) bzw. Fernrotlicht (braun). D) Übersicht des cGMP Umsatzes des Varianten im Dunkeln (schwarz) und nach Bestrahlung mit Rotlicht (rot) bzw. Fernrotlicht (braun) E) Übersicht des cAMP Umsatzes

Für optogenetische Anwendung in HEK-TM Zellen wurden LAPD-Varianten in Zellen, welche den zyklische Mononukleotid gesteuerten Ionenkanal (*cyclic nucleotide-gated ino channel*, CNG) CNGA2 stabil exprimierten, transfiziert. Zellen, welche sowohl CNG als auch LAPD-Varianten stabil exprimierten, wurden für Aktivitätsversuche genutzt. Dabei zeigte sich, dass einige Konstrukte *in vivo* von den *in vitro* Messungen abwichen. So konnte für die meisten Konstrukte lichtabhängige Aktivität festgestellt werden, allerdings mit geringeren Licht/Dunkel Unterschieden.

In der Summe konnten neue, verbesserte R/FR-PDEs als Werkzeuge für die Optogenetik erstellt werden. Die mögliche Anwendung ist im folgenden Kapitel näher aufgeführt.

3.5. Kontrolle zyklischer Mononukleotide mittels Licht

Der fünfte Artikel behandelt die optogenetische Anwendung von Werkzeugen zur Kontrolle von zyklischen Mononukleotiden in Zellen. Der Fokus liegt auf der rotlicht-aktivierten Phosphodiesterase LAPD und deren Zusammenspiel mit (blau)licht-aktivierten Zyklasen (PACs). Die simultane Anwendung in eukaryontischen Zellen würde eine genaue Kontrolle de cNMP Konzentrationen ermöglichen. Dadurch könnten verschiedene cNMP-abhängiger Prozesse optogenetisch kontrolliert werden. Zum Beispiel könnten CNG Kanäle oder PKA bzw. PKG, sowie andere cNMP gesteuerte Prozesse aktiviert und inaktiviert werden.

Neben den möglichen neuen Einblicken durch eine Kombination der Werkzeuge, liegt das besondere Augenmerk auf dem Potential von neuartigen R/FR Photorezeptoren, welche

durch die Kombination aus Phytochrom PCM mit verschiedenen Effektor-Modulen erschaffen werden.

3.6. Fazit

Die Konstruktion und Charakterisierung von synthetischen Photosensoren liefert Erkenntnisse hinsichtlich der Verknüpfung von Sensor- und Effektor-Domäne. Damit kann ein genaueres Verständnis der Signaltransduktion gewonnen werden.

Aufgrund dieser Ergebnisse ist es für die Anwendung optogenetischer Werkzeuge von großem Interesse, eine große Diversität an Konstrukten mit leicht unterschiedlichen Parametern hinsichtlich Aktivität und Lichtschaltbarkeit zu besitzen. So ist für manche Fragestellungen eine niedrige Basalaktivität von größerem Interesse, als eine großer Licht/Dunkel Unterschied, oder eine hohe Lichtaktivität. Alles in allem kann mit den durchgeführten Arbeiten gezeigt werden, dass die grundlegenden Designprinzipien für die Erschaffung von Phytochrom basierten R/FR Photorezeptoren auf verschiedene Systeme mit unterschiedlichen Effektor-Domänen übertragen werden kann. Insbesondere konnten verbesserte optogenetische Werkzeuge für die Manipulation von zyklischen Mononukleotiden erzeugt und ihre Funktionalität *in vivo* gezeigt werden.

4. Abkürzungsverzeichnis

AC	Adenylyl-Zyklasen
AMP	Adenosinmonophosphat
ATP	Adenosintriphosphat
BLUF	*blue light sensors using flavin adenine nucleotide*
bHLH	*basic helix-loop-helix*
bPAC	*Beggiatoa sp* PAC
BphP	Bakteriophytochrome
Bt	*Bos taurus*
BV	Biliverdin
c-di-GMP	zyklisches Diguanylylmonophosphat
CaM	Calmodulinbindende-Domänen
cAMP	zyklisches 3‘,5‘-Adenosinmonophosphat
CAP	*catabolite activator protein*
CBCR	Cyanobakteriochrom
cGMP	zyklisches 3‘,5‘-Guanosinmonophosphat
cNMP	zyklischen Mononukleotide
ChR2	Kanalrhodopsin 2
Cph	cyanobakterielle Phytochrome
CRP	*cAMP-receptor protein*
CRY	*Cryptochrom*e
Dd	*Deinococcus desertii*
Dph	Algenphytochrome
Dr	*Deinococcus radiodurans*
Eu	*Euglena gracilis*
Fph	Pilzphytochrome
GAF	*cGMP phosphodoesterase/adenylyl cyclase/FhlA*
GC	Guanylyl-Zyklasen
GMP	Guanosinmonophosphat
GTP	Guanosintriphosphat
HisK	Histidinkinase
HKRD	*histidine kinase related*
HO	Haemoxygenase
HPLC	Hochleistungsflüssigkeitschromatographie

IlaC	*infrared-light-activated adenylate cylase*
IR	Infrarot
LAPD	lichtaktivierte Phosphodiesterase
LOV	*light oxygen voltage*
MAP	*mitogen-activated protein*
mPAC	*Microcoleus photoactivated adenylate cyclase*
NHR	*neuronal homology repeat*
OCP	*orange carotenoid protein*
PΦB	Phytochromobilin
PAC	photoaktivierte Zyklasen
PATCHY	*primer aided truncation for the creation of hybrid proteins*
PAS	*Per-ARNT-Sim*
PCM	*photosensory core module*
PDE	Phosphodiesterase
P_{fr}	Fernrotlichtadaptiert
RhoGC	*rhodopsin guanylyl cyclase*
P_r	Rotlichtadaptiert
Phy	Phytochrom
PEB	Phycoerythrobilin
PVB	Phycoviolobilin
UCR	*upstream conserved region*
UV	Ultraviolett
UVR8	*ultraviolet-B receptor* 8
Z/*E*	*zusammen/entgegen*

5. Literaturverzeichnis

Arnon, D. I. 1959. “Conversion of Light into Chemical Energy in Photosynthesis.” *Nature* 184 (4679): 10–21. https://doi.org/10.1038/184010a0.

Barkovits, K., B. Schubert, S. Heine, M. Scheer, and N. Frankenberg-Dinkel. 2011. “Function of the Bacteriophytochrome BphP in the RpoS/Las Quorum-Sensing Network of Pseudomonas Aeruginosa.” *Microbiology* 157 (6): 1651–64. https://doi.org/10.1099/mic.0.049007-0.

Barkovits, K., A. Harms, C. Benkartek, J. L. Smart, and N. Frankenberg-Dinkel. 2008. “Expression of the Phytochrome Operon in Pseudomonas Aeruginosa Is Dependent on the Alternative Sigma Factor RpoS: Phytochrome Operon Regulation.” *FEMS Microbiology Letters* 280 (2): 160–68. https://doi.org/10.1111/j.1574-6968.2007.01058.x.

Bender, A. T. 2006. “Cyclic Nucleotide Phosphodiesterases: Molecular Regulation to Clinical Use.” *Pharmacological Reviews* 58 (3): 488–520. https://doi.org/10.1124/pr.58.3.5.

Bhoo, S.-H., S. J. Davis, J. Walker, B. Karniol, and R. D. Vierstra. 2001. “Bacteriophytochromes Are Photochromic Histidine Kinases Using a Biliverdin Chromophore.” *Nature* 414 (6865): 776–779.

Blain-Hartung, M., N. C. Rockwell, M. V. Moreno, S. S. Martin, F. Gan, D. A. Bryant, and J. C. Lagarias. 2018. “Cyanobacteriochrome-Based Photoswitchable Adenylyl Cyclases (CPACs) for Broad Spectrum Light Regulation of CAMP Levels in Cells.” *Journal of Biological Chemistry* 293 (22): 8473–83. https://doi.org/10.1074/jbc.RA118.002258.

Blumenstein, A., K. Vienken, R. Tasler, J. Purschwitz, D. Veith, N. Frankenberg-Dinkel, and R. Fischer. 2005. “The Aspergillus Nidulans Phytochrome FphA Represses Sexual Development in Red Light.” *Current Biology* 15 (20): 1833–38. https://doi.org/10.1016/j.cub.2005.08.061.

Borucki, B., S. Seibeck, M.P. Heyn, and T. Lamparter. 2009. “Characterization of the Covalent and Noncovalent Adducts of Agp1 Phytochrome Assembled with Biliverdin and Phycocyanobilin by Circular Dichroism and Flash Photolysis.” *Biochemistry* 48 (27): 6305–17. https://doi.org/10.1021/bi900436v.

Borucki, B., D. von Stetten, S. Seibeck, T. Lamparter, N. Michael, M. A. Mroginski, H. Otto, D. H. Murgida, M. P. Heyn, and P. Hildebrandt. 2005. “Light-Induced Proton Release of Phytochrome Is Coupled to the Transient Deprotonation of the Tetrapyrrole Chromophore.” *Journal of Biological Chemistry* 280 (40): 34358–64. https://doi.org/10.1074/jbc.M505493200.

Boyden, E. S., F. Zhang, E. Bamberg, G. Nagel, and K. Deisseroth. 2005. “Millisecond-Timescale, Genetically Targeted Optical Control of Neural Activity.” *Nature Neuroscience* 8 (9): 1263–68. https://doi.org/10.1038/nn1525.

Braslavsky, S. E., W. Gärtner, and K. Schaffner. 1997. “Phytochrome Photoconversion.” *Plant, Cell and Environment* 20 (6): 700–706. https://doi.org/10.1046/j.1365-3040.1997.d01-101.x.

Briggs, W. R., and J. L. Spudich, eds. 2005. *Handbook of Photosensory Receptors*. 1st ed. Wiley. https://doi.org/10.1002/352760510X.

Burgie, E. S., A. N. Bussell, J. M. Walker, K. Dubiel, and R. D. Vierstra. 2014. “Crystal Structure of the Photosensing Module from a Red/Far-Red Light-Absorbing Plant Phytochrome.” *Proceedings of the National Academy of Sciences* 111 (28): 10179–84. https://doi.org/10.1073/pnas.1403096111.

Burgie, E. S., J. Zhang, and R. D. Vierstra. 2016. “Crystal Structure of Deinococcus Phytochrome in the Photoactivated State Reveals a Cascade of Structural

Rearrangements during Photoconversion." *Structure* 24 (3): 448–57. https://doi.org/10.1016/j.str.2016.01.001.

Busby, S., and R. H. Ebright. 1999. "Transcription Activation by Catabolite Activator Protein (CAP)." *Journal of Molecular Biology* 293 (2): 199–213. https://doi.org/10.1006/jmbi.1999.3161.

Butler, W. L., K. H. Norris, H. W. Siegelman, and S. B. Hendricks. 1959. "Detection Assay, and Preliminary Purification of the Prigment Controlling Photoresponsive Development of Plants." *Proceedings of the National Academy of Sciences* 45 (12): 1703–8. https://doi.org/10.1073/pnas.45.12.1703.

Cann, M. J., A. Hammer, J. Zhou, and T. Kanacher. 2003. "A Defined Subset of Adenylyl Cyclases Is Regulated by Bicarbonate Ion." *Journal of Biological Chemistry* 278 (37): 35033–38. https://doi.org/10.1074/jbc.M303025200.

Christie, J. M. 1998. "Arabidopsis NPH1: A Flavoprotein with the Properties of a Photoreceptor for Phototropism." *Science* 282 (5394): 1698–1701. https://doi.org/10.1126/science.282.5394.1698.

Conti, M., and J. Beavo. 2007. "Biochemistry and Physiology of Cyclic Nucleotide Phosphodiesterases: Essential Components in Cyclic Nucleotide Signaling." *Annual Review of Biochemistry* 76 (1): 481–511. https://doi.org/10.1146/annurev.biochem.76.060305.150444.

Danchin, A. 1993. "Phylogeny of Adenylyl Cyclases." *Advances in Second Messenger and Phosphoprotein Research* 27: 109–35.

Davis, S. J. 1999. "Bacteriophytochromes: Phytochrome-Like Photoreceptors from Nonphotosynthetic Eubacteria." *Science* 286 (5449): 2517–20. https://doi.org/10.1126/science.286.5449.2517.

Deisseroth, K. 2010. "Controlling the Brain with Light." *Scientific American*, 8.

DeNinno, M. P. 2012. "Future Directions in Phosphodiesterase Drug Discovery." *Bioorganic & Medicinal Chemistry Letters* 22 (22): 6794–6800. https://doi.org/10.1016/j.bmcl.2012.09.028.

Diensthuber, R. P., M. Bommer, T. Gleichmann, and A. Möglich. 2013. "Full-Length Structure of a Sensor Histidine Kinase Pinpoints Coaxial Coiled Coils as Signal Transducers and Modulators." *Structure* 21 (7): 1127–36. https://doi.org/10.1016/j.str.2013.04.024.

Dominguez-Martin, M. A., and C. A. Kerfeld. 2019. "Engineering the Orange Carotenoid Protein for Applications in Synthetic Biology." *Current Opinion in Structural Biology* 57 (August): 110–17. https://doi.org/10.1016/j.sbi.2019.01.023.

Dong, Q., C. E. Bauer, and S. Roychowdhury. 2015. "DNA-Binding Properties of a CGMP-Binding CRP Homologue That Controls Development of Metabolically Dormant Cysts of Rhodospirillum Centenum." *Microbiology* 161 (11): 2256–64. https://doi.org/10.1099/mic.0.000172.

Ernst, O. P., D. T. Lodowski, M. Elstner, P. Hegemann, L. S. Brown, and H. Kandori. 2014. "Microbial and Animal Rhodopsins: Structures, Functions, and Molecular Mechanisms." *Chemical Reviews* 114 (1): 126–63. https://doi.org/10.1021/cr4003769.

Essen, L.-O., J. Mailliet, and J. Hughes. 2008. "The Structure of a Complete Phytochrome Sensory Module in the Pr Ground State." *Proceedings of the National Academy of Sciences* 105 (38): 14709–14. https://doi.org/10.1073/pnas.0806477105.

Etzl, S., R. Lindner, M. D. Nelson, and A. Winkler. 2018a. "Structure-Guided Design and Functional Characterization of an Artificial Red Light–Regulated Guanylate/Adenylate Cyclase for Optogenetic Applications." *Journal of Biological Chemistry* 293 (23): 9078–89. https://doi.org/10.1074/jbc.RA118.003069.

———. 2018b. “Structure-Guided Design and Functional Characterization of an Artificial Red Light–Regulated Guanylate/Adenylate Cyclase for Optogenetic Applications.” *Journal of Biological Chemistry* 293 (23): 9078–89. https://doi.org/10.1074/jbc.RA118.003069.

Francis, S. H., M. A. Blount, and J. D. Corbin. 2011. “Mammalian Cyclic Nucleotide Phosphodiesterases: Molecular Mechanisms and Physiological Functions.” *Physiological Reviews* 91 (2): 651–90. https://doi.org/10.1152/physrev.00030.2010.

Frankenberg-Dinkel, N. 2004. “Bacterial Heme Oxygenases.” *Antioxidants & Redox Signaling* 6 (5): 13.

Garner, W. W., and H. A. Allard. 1920. “Effect of the Relative Length of Day and Night and Other Factors of the Environment on Growth and Reproduction in Plants.” *Monthly Weather Review* 48 (7): 415–415. https://doi.org/10.1175/1520-0493(1920)48<415b:EOTRLO>2.0.CO;2.

Gasser, C., S. Taiber, C.-M. Yeh, C. H. Wittig, P. Hegemann, S. Ryu, F. Wunder, and A. Moglich. 2014. “Engineering of a Red-Light-Activated Human CAMP/CGMP-Specific Phosphodiesterase.” *Proceedings of the National Academy of Sciences* 111 (24): 8803–8. https://doi.org/10.1073/pnas.1321600111.

Gehring, W. J. 2005. “New Perspectives on Eye Development and the Evolution of Eyes and Photoreceptors.” *Journal of Heredity* 96 (3): 171–84. https://doi.org/10.1093/jhered/esi027.

Gleichmann, T., R. P. Diensthuber, and A. Moglich. 2013. “Charting the Signal Trajectory in a Light-Oxygen-Voltage Photoreceptor by Random Mutagenesis and Covariance Analysis.” *Journal of Biological Chemistry* 288 (41): 29345–55. https://doi.org/10.1074/jbc.M113.506139.

Gold, M. G., T. Gonen, and J. D. Scott. 2013. “Local CAMP Signaling in Disease at a Glance.” *Journal of Cell Science* 126 (20): 4537–43. https://doi.org/10.1242/jcs.133751.

Goldstein, I., T. F. Lue, H. Padma-Nathan, R. C. Rosen, W. D. Steers, and P. A. Wicker. 1998. “Oral Sildenafil in the Treatment of Erectile Dysfunction.” *The New England Journal of Medicine* 338 (20): 8.

Gomelsky, M. 2011. “CAMP, c-Di-GMP, c-Di-AMP and Now CGMP: Bacteria Use Them All!” *Molecular Microbiology* 79 (3): 562–65. https://doi.org/10.1111/j.1365-2958.2010.07514.x.

Gradinaru, V., L. R. Thompson, and K. Deisseroth. 2008. “ENpHR: A Natronomonas Halorhodopsin Enhanced for Optogenetic Applications.” *Brain Cell Biology* 36 (1–4): 129–39. https://doi.org/10.1007/s11068-008-9027-6.

Habuchi, S., R. Ando, P. Dedecker, W. Verheijen, H Mizuno, A. Miyawaki, and J. Hofkens. 2005. “Reversible Single-Molecule Photoswitching in the GFP-like Fluorescent Protein Dronpa.” *PNAS* 102 (27): 9511–16.

Heijde, M., and R. Ulm. 2012. “UV-B Photoreceptor-Mediated Signalling in Plants.” *Trends in Plant Science* 17 (4): 230–37. https://doi.org/10.1016/j.tplants.2012.01.007.

Heyne, K., J. Herbst, D. Stehlik, B. Esteban, T. Lamparter, J. Hughes, and R. Diller. 2002. “Ultrafast Dynamics of Phytochrome from the Cyanobacterium Synechocystis, Reconstituted with Phycocyanobilin and Phycoerythrobilin.” *Biophysical Journal* 82 (2): 1004–16. https://doi.org/10.1016/S0006-3495(02)75460-X.

Hughes, J., T. Lamparter, F. Mittmann, E. Hartmann, W. Gärtner, A. Wilde, and T. Börner. 1997. “A Prokaryotic Phytochrome.” *Nature* 386 (6626): 663–663. https://doi.org/10.1038/386663a0.

Jenal, U., A. Reinders, and C. Lori. 2017. “Cyclic Di-GMP: Second Messenger Extraordinaire.” *Nature Reviews Microbiology* 15 (5): 271–84. https://doi.org/10.1038/nrmicro.2016.190.

Jöhr, R., M. S. Bauer, L. C. S., C. Kluger, and H. E. Gaub. 2019. "Dronpa: A Light-Switchable Fluorescent Protein for Opto-Biomechanics." *Nano Letters* 19 (5): 3176–81. https://doi.org/10.1021/acs.nanolett.9b00639.

Jorissen, H. J. M. M., B. Quest, A. Remberg, T. Coursin, S. E. Braslavsky, K. Schaffner, N. Tandeau de Marsac, and W. Gärtner. 2002. "Two Independent, Light-Sensing Two-Component Systems in a Filamentous Cyanobacterium: Light Sensing Two Component Systems in *Calothrix*." *European Journal of Biochemistry* 269 (11): 2662–71. https://doi.org/10.1046/j.1432-1033.2002.02928.x.

Karniol, B., J. R. Wagner, J. M. Walker, and R. D. Vierstra. 2005. "Phylogenetic Analysis of the Phytochrome Superfamily Reveals Distinct Microbial Subfamilies of Photoreceptors." *Biochemical Journal* 392 (1): 103–16. https://doi.org/10.1042/BJ20050826.

Kaupp, B. U., and R. Seifert. 2002. "Cyclic Nucleotide-Gated Ion Channels." *Physiol Rev* 82: 56.

Kawasaki, H., G. M. Springett, N. Mochizuki, S. Toki, M. Nakaya, M. Matsuda, D. E. Housman, and A. M. Graybiel. 1998. "A Family of CAMP-Binding Proteins That Directly Activate Rap1." *Science* 282 (5397): 2275–79. https://doi.org/10.1126/science.282.5397.2275.

Kehoe, D. M., and A. R. Grossman. 1996. "Similarity of a Chromatic Adaptation Sensor to Phytochrome and Ethylene Receptors." *Science* 273 (5280): 1409–12. https://doi.org/10.1126/science.273.5280.1409.

Kendrick, R. E., and G. H. M. Kronenberg, eds. 1994. *Photomorphogenesis in Plants*. Dordrecht: Springer Netherlands. https://doi.org/10.1007/978-94-011-1884-2.

Lamparter, T., N. Michael, O. Caspani, T. Miyata, K. Shirai, and K. Inomata. 2003. "Biliverdin Binds Covalently to Agrobacterium Phytochrome Agp1 via Its Ring A Vinyl Side Chain." *Journal of Biological Chemistry* 278 (36): 33786–92. https://doi.org/10.1074/jbc.M305563200.

Lamparter, T., M. Carrascal, N. Michael, E. Martinez, G. Rottwinkel, and J. Abian. 2004. "The Biliverdin Chromophore Binds Covalently to a Conserved Cysteine Residue in the N-Terminus of *Agrobacterium* Phytochrome Agp1 †." *Biochemistry* 43 (12): 3659–69. https://doi.org/10.1021/bi0356931.

Lamparter, T., B. Esteban, and J. Hughes. 2001. "Phytochrome Cph1 from the Cyanobacterium *Synechocystis* PCC6803: Purification, Assembly, and Quaternary Structure." *European Journal of Biochemistry* 268 (17): 4720–30. https://doi.org/10.1046/j.1432-1327.2001.02395.x.

Lamparter, T., F. Mittmann, W. Gärtner, T. Börner, E. Hartmann, and J. Hughes. 1997. "Characterization of Recombinant Phytochrome from the Cyanobacterium Synechocystis." *PNAS* 94 (October): 11792–97.

Lawson, C. L., D. Swigon, K. S. Murakami, S. A. Darst, H. M. Berman, and R. H. Ebright. 2004. "Catabolite Activator Protein (CAP): DNA Binding and Transcription Activation." *Current Opinion in Structural Biology* 14 (1): 10–20. https://doi.org/10.1016/j.sbi.2004.01.012.

Leivar, P., and P. H. Quail. 2011. "PIFs: Pivotal Components in a Cellular Signaling Hub." *Trends in Plant Science* 16 (1): 19–28. https://doi.org/10.1016/j.tplants.2010.08.003.

Linder, J. U. 2006. "Class III Adenylyl Cyclases: Molecular Mechanisms of Catalysis and Regulation." *Cellular and Molecular Life Sciences* 63 (15): 1736–51. https://doi.org/10.1007/s00018-006-6072-0.

Litts, J. C., J. M. Kelly, and J. C. Lagarias. 1983. "Structure-Function Studies on Phytochrome PRELIMINARY CHARACTERIZATION OF HIGHLY PURIFIED PHYTOCHROME FROM A VENASATIVA ENRICHEDIN THE 124-

KILODALTON SPECIES." *The Journal of Biological Chemistry* 258 (18): 11025–31.

Losi, A., and W. Gärtner. 2008. "Shedding (Blue) Light on Algal Gene Expression." *Proceedings of the National Academy of Sciences* 105 (1): 7–8. https://doi.org/10.1073/pnas.0710523105.

Losi, A., K. H. Gardner, and A. Möglich. 2018. "Blue-Light Receptors for Optogenetics." *Chemical Reviews* 118 (21): 10659–709. https://doi.org/10.1021/acs.chemrev.8b00163.

Madaule, P., and R. Axel. 1985. "A Novel Ras-Related Gene Family." *Cell* 41 (1): 31–40. https://doi.org/10.1016/0092-8674(85)90058-3.

Mahmoud, B. H., C. L. Hexsel, I. H. Hamzavi, and H. W. Lim. 2008. "Effects of Visible Light on the Skin." *Photochemistry and Photobiology* 84 (2): 450–62. https://doi.org/10.1111/j.1751-1097.2007.00286.x.

Marden, J. N., Q. Dong, S. Roychowdhury, J. E. Berleman, and C. E. Bauer. 2011. "Cyclic GMP Controls Rhodospirillum Centenum Cyst Development: CGMP Control of Encystment." *Molecular Microbiology* 79 (3): 600–615. https://doi.org/10.1111/j.1365-2958.2010.07513.x.

Möglich, A., R. A. Ayers, and K. Moffat. 2009. "Design and Signaling Mechanism of Light-Regulated Histidine Kinases." *Journal of Molecular Biology* 385 (5): 1433–44. https://doi.org/10.1016/j.jmb.2008.12.017.

Möglich, A., and K. Moffat. 2010. "Engineered Photoreceptors as Novel Optogenetic Tools." *Photochemical & Photobiological Sciences* 9 (10): 1286. https://doi.org/10.1039/c0pp00167h.

Möglich, A., X. Yang, R. A. Ayers, and K. Moffat. 2010. "Structure and Function of Plant Photoreceptors." *Annual Review of Plant Biology* 61 (1): 21–47. https://doi.org/10.1146/annurev-arplant-042809-112259.

Mroginski, M. A., D. H. Murgida, and P. Hildebrandt. 2007. "The Chromophore Structural Changes during the Photocycle of Phytochrome: A Combined Resonance Raman and Quantum Chemical Approach." *Accounts of Chemical Research* 40 (4): 258–66. https://doi.org/10.1021/ar6000523.

Nagel, G. 2002. "Channelrhodopsin-1: A Light-Gated Proton Channel in Green Algae." *Science* 296 (5577): 2395–98. https://doi.org/10.1126/science.1072068.

Ohlendorf, R., C. H. Schumacher, F. Richter, and A. Möglich. 2016. "Library-Aided Probing of Linker Determinants in Hybrid Photoreceptors." *ACS Synthetic Biology* 5 (10): 1117–26. https://doi.org/10.1021/acssynbio.6b00028.

Ohlendorf, R., R. R. Vidavski, A. Eldar, K. Moffat, and A. Möglich. 2012. "From Dusk till Dawn: One-Plasmid Systems for Light-Regulated Gene Expression." *Journal of Molecular Biology* 416 (4): 534–42. https://doi.org/10.1016/j.jmb.2012.01.001.

Padmanabhan, S., R. Pérez-Castaño, and M. Elías-Arnanz. 2019. "B12-Based Photoreceptors: From Structure and Function to Applications in Optogenetics and Synthetic Biology." *Current Opinion in Structural Biology* 57 (August): 47–55. https://doi.org/10.1016/j.sbi.2019.01.020.

Pandit, J., M. D. Forman, K. F. Fennell, K. S. Dillman, and F. S. Menniti. 2009. "Mechanism for the Allosteric Regulation of Phosphodiesterase 2A Deduced from the X-Ray Structure of a near Full-Length Construct." *Proceedings of the National Academy of Sciences* 106 (43): 18225–30. https://doi.org/10.1073/pnas.0907635106.

Pham, V. N., P. K. Kathare, and E. Huq. 2018. "Phytochromes and Phytochrome Interacting Factors." *Plant Physiology* 176 (2): 1025–38. https://doi.org/10.1104/pp.17.01384.

Presti, D., and M. Delbruck. 1978. "Photoreceptors for Biosynthesis, Energy Storage and Vision." *Plant, Cell and Environment* 1 (2): 81–100. https://doi.org/10.1111/j.1365-3040.1978.tb00751.x.

Raffelberg, S., L. Wang, S. Gao, A. Losi, W. Gärtner, and G. Nagel. 2013. "A LOV-Domain-Mediated Blue-Light-Activated Adenylate (Adenylyl) Cyclase from the Cyanobacterium *Microcoleus Chthonoplastes* PCC 7420." *Biochemical Journal* 455 (3): 359–65. https://doi.org/10.1042/BJ20130637.

Rest, B. van der, A.-M. Boisson, E. Gout, R. Bligny, and R. Douce. 2002. "Glycerophosphocholine Metabolism in Higher Plant Cells. Evidence of a New Glyceryl-Phosphodiester Phosphodiesterase." *Plant Physiology* 130 (1): 244–55. https://doi.org/10.1104/pp.003392.

Rockwell, N. C., S. S. Martin, K. Feoktistova, and J. C. Lagarias. 2011. "Diverse Two-Cysteine Photocycles in Phytochromes and Cyanobacteriochromes." *Proceedings of the National Academy of Sciences* 108 (29): 11854–59. https://doi.org/10.1073/pnas.1107844108.

Rockwell, N. C., R. Ohlendorf, and A. Moglich. 2013. "Cyanobacteriochromes in Full Color and Three Dimensions." *Proceedings of the National Academy of Sciences* 110 (3): 806–7. https://doi.org/10.1073/pnas.1220690110.

Rockwell, N. C., and J. C. Lagarias. 2010. "A Brief History of Phytochromes." *ChemPhysChem* 11 (6): 1172–80. https://doi.org/10.1002/cphc.200900894.

Rooij, J. de, F. J. T. Zwartkruis, M. H. G. Verheijen, R. H. Cool, S. M. B. Nijman, A. Wittinghofer, and J. L. Bos. 1998. "Epac Is a Rap1 Guanine-Nucleotide-Exchange Factor Directly Activated by Cyclic AMP." *Nature* 396 (6710): 474–77. https://doi.org/10.1038/24884.

Ryu, M.-H., I.-H. Kang, M. D. Nelson, T. M. Jensen, A. I. Lyuksyutova, J. Siltberg-Liberles, D. M. Raizen, and M. Gomelsky. 2014. "Engineering Adenylate Cyclases Regulated by Near-Infrared Window Light." *Proceedings of the National Academy of Sciences* 111 (28): 10167–72. https://doi.org/10.1073/pnas.1324301111.

Ryu, M.-H., O. V. Moskvin, J. Siltberg-Liberles, and M. Gomelsky. 2010. "Natural and Engineered Photoactivated Nucleotidyl Cyclases for Optogenetic Applications." *Journal of Biological Chemistry* 285 (53): 41501–8. https://doi.org/10.1074/jbc.M110.177600.

Santarpia, L., S. M. Lippman, and A. K. El-Naggar. 2012. "Targeting the MAPK–RAS–RAF Signaling Pathway in Cancer Therapy." *Expert Opinion on Therapeutic Targets* 16 (1): 103–19. https://doi.org/10.1517/14728222.2011.645805.

Schindler, R. F.R., and T. Brand. 2016. "The Popeye Domain Containing Protein Family – A Novel Class of CAMP Effectors with Important Functions in Multiple Tissues." *Progress in Biophysics and Molecular Biology* 120 (1–3): 28–36. https://doi.org/10.1016/j.pbiomolbio.2016.01.001.

Schröder-Lang, S., M. Schwärzel, R. Seifert, T. Strünker, S. Kateriya, J. Looser, M. Watanabe, U. B. Kaupp, P. Hegemann, and G. Nagel. 2007. "Fast Manipulation of Cellular CAMP Level by Light in Vivo." *Nature Methods* 4 (1): 39–42. https://doi.org/10.1038/nmeth975.

Schultz, J. E., and J. Natarajan. 2013. "Regulated Unfolding: A Basic Principle of Intraprotein Signaling in Modular Proteins." *Trends in Biochemical Sciences* 38 (11): 538–45. https://doi.org/10.1016/j.tibs.2013.08.005.

Sharrock, R. A. 2008. "The Phytochrome Red/Far-Red Photoreceptor Superfamily." *Genome Biology* 9 (8): 230.

Shcherbakova, D. M., A. A. Shemetov, A. A. Kaberniuk, and V. V. Verkhusha. 2015. "Natural Photoreceptors as a Source of Fluorescent Proteins, Biosensors, and Optogenetic Tools." *Annual Review of Biochemistry* 84 (1): 519–50. https://doi.org/10.1146/annurev-biochem-060614-034411.

Sineshchekov, V. A. 2005. “Polymorphism of Phytochrome A and Its Functional Implications.” In *Light Sensing in Plants*, edited by M. Wada, K. Shimazaki, and M. Iino, 95–102. Tokyo: Springer Japan. https://doi.org/10.1007/4-431-27092-2_10.

Smith, N., S.-K. Kim, P. T. Reddy, and D. T. Gallagher. 2006. “Crystallization of the Class IV Adenylyl Cyclase from *Yersinia Pestis*.” *Acta Crystallographica Section F Structural Biology and Crystallization Communications* 62 (3): 200–204. https://doi.org/10.1107/S1744309106002855.

Steiner, A. A, J. Antunes-Rodrigues, and L. G. S. Branco. 2002. “Role of Preoptic Second Messenger Systems (CAMP and CGMP) in the Febrile Response.” *Brain Research* 944 (1–2): 135–45. https://doi.org/10.1016/S0006-8993(02)02738-5.

Stierl, M., P. Stumpf, D. Udwari, R. Gueta, R. Hagedorn, A. Losi, W. Gärtner, et al. 2011. “Light Modulation of Cellular CAMP by a Small Bacterial Photoactivated Adenylyl Cyclase, BPAC, of the Soil Bacterium Beggiatoa.” *Journal of Biological Chemistry* 286 (2): 1181–88. https://doi.org/10.1074/jbc.M110.185496.

Takala, H., A. Björling, O. Berntsson, H. Lehtivuori, S. Niebling, M. Hoernke, I. Kosheleva, et al. 2014. “Signal Amplification and Transduction in Phytochrome Photosensors.” *Nature* 509 (7499): 245–48. https://doi.org/10.1038/nature13310.

Tang, W.-J., and A. G. Gilman. 1992. “Adenylyl Cyclases.” *Cell* 70 (6): 869–72. https://doi.org/10.1016/0092-8674(92)90236-6.

Tesarik, J., C. Mendoza, and A. Carreras. 1992. “Effects of Phosphodiesterase Inhibitors Caffeine and Pentoxifylline on Spontaneous and Stimulus-Induced Acrosome Reactions in Human Sperm.” *Fertility and Sterility* 58 (6): 1185–90. https://doi.org/10.1016/S0015-0282(16)55567-8.

Thor, J. J. van, K. L. Ronayne, and M. Towrie. 2007. “Formation of the Early Photoproduct Lumi-R of Cyanobacterial Phytochrome Cph1 Observed by Ultrafast Mid-Infrared Spectroscopy.” *Journal of the American Chemical Society* 129 (1): 126–32.

Trieu, M. M., E. L. Devine, L. B. Lamarche, A. E. Ammerman, J. A. Greco, R. R. Birge, D. L. Theobald, and D. D. Oprian. 2017. “Expression, Purification, and Spectral Tuning of RhoGC, a Retinylidene/Guanylyl Cyclase Fusion Protein and Optogenetics Tool from the Aquatic Fungus *Blastocladiella Emersonii*.” *Journal of Biological Chemistry* 292 (25): 10379–89. https://doi.org/10.1074/jbc.M117.789636.

Vierstra, R. D., and P. H. Quail. 1983. “Photochemistry of 124 Kilodalton *Avena* Phytochrome *In Vitro*.” *Plant Physiology* 72 (1): 264–67. https://doi.org/10.1104/pp.72.1.264.

Wagner, D., J. M. Tepperman, and P. H. Quail. 1991. “Overexpression of Phytochrome B Induces a Short Hypocotyl Phnetype in Transgenic Arabidopsis.” *The Plant Cell* 3 (December).

Wagner, J. R., J. Zhang, J. S. Brunzelle, R. D. Vierstra, and K. T. Forest. 2007. “High Resolution Structure of Deinococcus Bacteriophytochrome Yields New Insights into Phytochrome Architecture and Evolution.” *Journal of Biological Chemistry* 282 (16): 12298–309. https://doi.org/10.1074/jbc.M611824200.

Wagner, J. R., J. S. Brunzelle, K. T. Forest, and R. D. Vierstra. 2005. “A Light-Sensing Knot Revealed by the Structure of the Chromophore-Binding Domain of Phytochrome.” *Nature* 438 (7066): 325–31. https://doi.org/10.1038/nature04118.

Wagner, J. R., J. Zhang, D. von Stetten, M. Günther, D. H. Murgida, M. A. Mroginski, J. M. Walker, K. T. Forest, P. Hildebrandt, and R. D. Vierstra. 2008. “Mutational Analysis of *Deinococcus Radiodurans* Bacteriophytochrome Reveals Key Amino Acids Necessary for the Photochromicity and Proton Exchange Cycle of Phytochromes.” *Journal of Biological Chemistry* 283 (18): 12212–26. https://doi.org/10.1074/jbc.M709355200.

Wu, Q., B. Huang, T. A. Niehaus, X. Yang, J. Fan, and R.-Q. Zhang. 2015. “The Role of Tryptophans in the UV-B Absorption of a UVR8 Photoreceptor – a Computational Study.” *Phys. Chem. Chem. Phys.* 17 (16): 10786–94. https://doi.org/10.1039/C4CP06073C.

Yang, X., J. Kuk, and K. Moffat. 2008. “Crystal Structure of Pseudomonas Aeruginosa Bacteriophytochrome: Photoconversion and Signal Transduction.” *Proceedings of the National Academy of Sciences* 105 (38): 14715–14720.

Zhang, W., A. W. Lohman, Y. Zhuravlova, X. Lu, M. D. Wiens, H. Hoi, S. Yaganoglu. 2017. “Optogenetic Control with a Photocleavable Protein, PhoCl.” *Nature Methods* 14 (March): 391.

Ziegler, T., and A. Möglich. 2015. “Photoreceptor Engineering.” *Frontiers in Molecular Biosciences* 2 (June). https://doi.org/10.3389/fmolb.2015.00030.

6. Eigenanteil

6.1. Manuskript I

Titel: "*Primer- Aided Truncation for the Creation of Hybrid Proteins*"
Autoren: **Stabel, R.**; Stüven, B.; Ohlendorf, R.; Möglich, A.
Veröffentlicht in: Methods in Molecular Biology (2017), vol. 1596 pp. 287-304
doi:10.1007/978-1-4939-6940-1_18

Eigenanteil:
Idee & Konzept: 20%, Experimente: 20%, Datenauswertung: 50%, Abbildungen: 100%, Verfassen des Manuskripts: 40%

A. Möglich und R. Ohlendorf hatten die zugrunde liegende Idee. A. Möglich, R. Stabel und B. Stüven planten die Experimente, und R. Stabel und B. Stüven werteten die Daten aus. R. Stabel erstellte die Abbildungen, und R. Stabel und A. Möglich erstellten das Manuskript. R. Stabel, B. Stüven, R. Ohlendorf und A. Möglich bearbeiteten gemeinsam das Manuskript, und korrespondierender Autor ist A. Möglich.

6.2. Manuskript II

Titel: "*Characterization and engineering of photoactivated adenylyl cyclases*"
Autoren: Stüven, B.*; **Stabel, R.***; Ohlendorf, R.; Beck, J.; Schubert, R.; Möglich, A.
Veröffentlicht in: Biological Chemistry (2019), vol. 400, issue 3, pp. 429–441
doi:10.1515/hsz-2018-0375

Eigenanteil:
Idee & Konzept: 33%, Experimente: 60%, Datenauswertung: 50% Abbildungen: 60%, Verfassen des Manuskripts: 40%

A. Möglich, R. Stabel und B. Stüven hatten die zugrunde liegende Idee. A. Möglich, R. Stabel und B. Stüven planten die Experimente, und J. Beck, R. Ohlendorf, R. Schubert, B. Stüven und R. Stabel führten die Experimente durch und werteten sie aus. R. Stabel und A. Möglich erstellten die Abbildungen, und R. Stabel, B. Stüven und A. Möglich erstellten das Manuskript, und bearbeiteten es gemeinsam mit R. Ohlendorf, J. Beck und R. Schubert. Der korrespondierende Autor ist A. Möglich.

6.3. Manuskript III

Titel: "*Pulsatile Illumination for Photobiology and Optogenetics*"
Autoren: Dietler, J.; **Stabel, R.**; Möglich, A.
Veröffentlicht in: Methods in Enzymology (2019) vol. 624 pp. 227-248
doi.org/10.1016/bs.mie.2019.04.005

Eigenanteil:
Idee & Konzept: 33%, Experimente: 50%, Datenauswertung: 40%, Abbildungen: 33%, Verfassen des Manuskripts: 25%

A. Möglich, J. Dietler und R. Stabel hatten die zugrunde liegende Idee. A. Möglich, J. Dietler und R. Stabel planten die Experimente. J. Dietler und R. Stabel führten die Experimente durch. J. Dietler und R. Stabel erstellten die Abbildungen, und J. Dietler und A. Möglich erstellten das Manuskript. J. Dietler, R. Stabel und A. Möglich bearbeiteten das Manuskript, und der korrespondierende Autor ist A. Möglich.

6.4. Manuskript IV

Titel: "*Revisiting and Redesigning Light-activated Cyclic-Mononucleotide Phosphodiesterases*"
Autoren: **Stabel, R.**; Stüven, B.; Hansen, J.N.; Körschen, H.G.; Wachten D.; Möglich, A.
Veröffentlicht in: Journal of Molecular Biology (2019) vol. 431, issue 17, pp. 3029-3045
doi.org/10.1016/j.jmb.2019.07.011

Eigenanteil:
Idee & Konzept: 50%, Experimente: 80%, Datenauswertung: 80% Abbildungen: 80%, Verfassen des Manuskripts: 50%

A. Möglich und R. Stabel hatten die zugrunde liegende Idee. A. Möglich, D. Wachten, R. Stabel und B. Stüven planten die Experimente. R. Stabel, B. Stüven und J.N. Hansen führten die Experimente durch und werteten die Daten aus. R. Stabel und B. Stüven erstellten die Abbildungen, und R. Stabel und A. Möglich erstellten das Manuskript. R. Stabel, B. Stüven, J.N. Hansen, H.G. Körschen, D. Wachten und A. Möglich bearbeiteten das Manuskripts. Der korrespondierende Autor ist A. Möglich.

6.5. Manuskript V

(Übersichtsartikel)

Titel: „Die Kontrolle zyklischer Nukleotide mittels Licht“

Autoren: Stabel, R.; Möglich, A.

Veröffentlicht in: BIOspektrum (2017) vol. 23, issue 4, pp. 384-387

doi:10.1007/s12268-017-0813-5

Eigenanteil: Abbildungen: 100%, Verfassen des Manuskripts: 50 %

R. Stabel erstellte die Abbildungen, und R. Stabel und A. Möglich erstellten und bearbeiteten gemeinsam das Manuskript, der korrespondierende Autor ist A. Möglich.

7. Manuskripte

7.1. Manuskript I

Stabel, R.; Stüven, B.; Ohlendorf, R.; Möglich, A.; *Methods in Molecular Biology* (2017) "*Primer-Aided Truncation for the Creation of Hybrid Proteins*"

Chapter 18

Primer-Aided Truncation for the Creation of Hybrid Proteins

Robert Stabel, Birthe Stüven, Robert Ohlendorf, and Andreas Möglich

Abstract

Proteins frequently display modular architecture with several domains and segments connected by linkers. Proper protein functionality hinges on finely orchestrated interactions among these constituent elements. The underlying modularity lends itself to the engineering of hybrid proteins via modular rewiring; novel properties can thus be obtained, provided the linkers connecting the individual elements are conducive to productive interactions. As a corollary, the process of protein engineering often encompasses the generation and screening of multiple linker variants. To aid these steps, we devised the PATCHY method (primer-aided truncation for the creation of hybrid proteins) to readily generate hybrid gene libraries of predefined composition. We applied PATCHY to the mechanistic characterization of hybrid receptors that possess blue-light-regulated histidine kinase activity. Comprehensive sampling of linker composition revealed that catalytic activity and response to light are primarily functions of linker length. Variants with linkers of $7n$ residues mostly have light-repressed activity but those with $7n + 1$ residues mostly have inverted, light-induced activity. We further probed linker length in the context of single residue exchanges that also lead to an inversion of the signal response. As in the original context, activity is only observed for certain periodic linker lengths. Taken together, these results provide mechanistic insight into signaling strategies employed by sensory photoreceptors and sensor histidine kinases. PATCHY represents an adequate and facile method to efficiently generate and probe hybrid gene libraries and to thereby identify key determinants for proper function.

Key words DNA library, Hybrid gene, Light–oxygen–voltage, Protein engineering, Sensor histidine kinase, Sensory photoreceptor, Signal transduction

1 Introduction

Proteins of diverse biological roles consist of multiple modules, often corresponding to distinct protein domains, that are connected through linker segments [1]. Proper function generally depends on productive and precisely calibrated interactions among these modules, as facilitated by the intervening linkers [2]. Depending upon protein context, linkers differ in a number of parameters including length, sequence, surface charge, structure and flexibility. Given their eminent role in mediating interactions

Viktor Stein (ed.), *Synthetic Protein Switches: Methods and Protocols*, Methods in Molecular Biology, vol. 1596,
DOI 10.1007/978-1-4939-6940-1_18,

between protein modules, linkers are also decisive in the engineering of proteins with novel function. In particular, desired traits can often be obtained by covalently connecting different modules via suitable linkers and by thus generating hybrid (or, chimeric) proteins. Some cases call for flexible linkers that bring modules into spatial proximity, but allow reorientation and relative movements; in other cases, rigid connectors are required to fix modules at discrete distances and defined angular orientations. Additional considerations in linker design include proper folding, intracellular trafficking, chemical and biological stability of resultant hybrid proteins [3]. Structural information, where available, and multiple sequence alignments often provide valuable clues as to which linker suffices for a specific engineering purpose. Nonetheless, *a priori* it is difficult to select among many possible linker variants the one(s) best suited for meeting the above criteria. As a corollary, often multiple linkers are constructed and empirically tested for best performance, which incurs considerable expenditure of time and effort.

These concepts are exemplified in signal receptors and their engineering. In particular, sensory photoreceptors constitute the group of signal receptors that impart sensation of light [4]. Photosensor modules absorb light of appropriate quality and in response modulate the biological activity of effector (or, output) modules. Across different photoreceptor classes, the linkers connecting these modules are often of α-helical or coiled-coil conformation; modifications to the linker as confined as exchange, addition or deletion of single residues can profoundly affect receptor activity and regulation [5–7]. As a case in point, we constructed the photoreceptor YF1 by recombining the blue-light-responsive light–oxygen–voltage (LOV) photosensor module of *Bacillus subtilis* YtvA (*Bs*YtvA) with the *Bradyrhizobium japonicum* FixL (*Bj*FixL) histidine kinase effector [8] (Fig. 1). The crystal structure of homodimeric YF1 in its dark-adapted state showed its two LOV photosensor modules to be connected to the effector module via a parallel coiled-coil linker, denoted Jα [9]. Length variations of Jα revealed heptad (i.e., seven-residue) periodicities of catalytic activity and regulation by light [8]. The original YF1 construct derived almost its entire linker from the parental protein *Bj*FixL, but equally one could have used the corresponding linker of the other parental protein *Bs*YtvA, or hybrids of both linkers. Given that the parental linkers are 23 and 27 residues long, there are (23 + 1)·(27 + 1) = 672 possible combinations for connecting *Bs*YtvA and *Bj*FixL if one restricts hybrid fusions to these linker segments (Fig. 1). Although comprehensive interrogation of all linker combinations could provide invaluable insight into signaling mechanisms and engineering principles, manual construction and separate testing of each individual variant is prohibitively cumbersome. We hence sought to assess all possible linker variants in parallel. To this

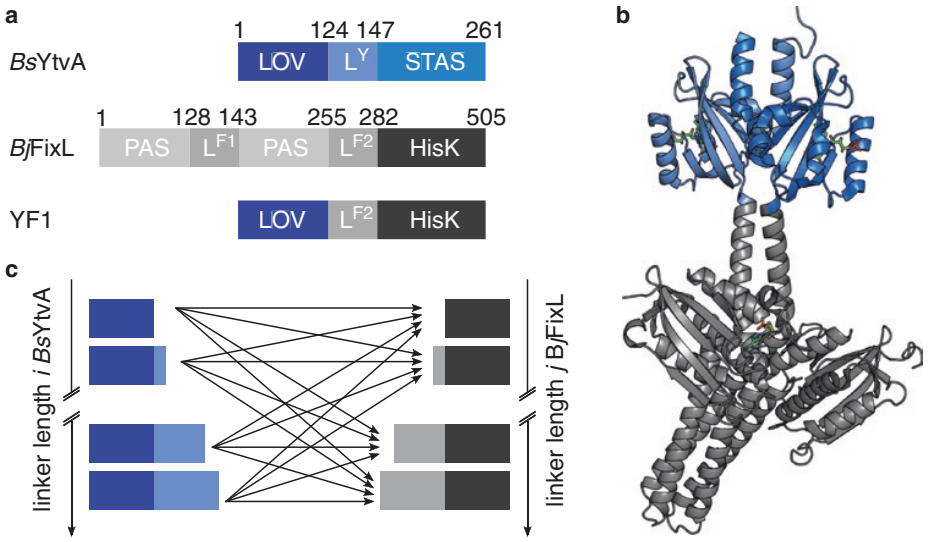

Fig. 1 (**a**) Domain architecture of *Bs*YtvA, *Bj*FixL, and YF1. The hybrid YF1 consists of the *Bs*YtvA LOV domain fused to the *Bj*FixL histidine kinase, where almost the entire linker derives from *Bj*FixL. (**b**) The crystal structure (PDB entry 4GCZ [9]) of homodimeric YF1 in its dark-adapted state shows the coiled-coil linker between the LOV photosensor and histidine kinase effector modules. (**c**) Schematic of the possible linker combinations for hybrids between the *Bs*YtvA photosensor and the *Bj*FixL effector modules

end, we established the PATCHY (primer-aided truncation for the creation of hybrid proteins) method for the efficient generation of hybrid gene libraries with defined composition [10].

Prior to this, alternate strategies for creating hybrid gene libraries had been proposed and successfully applied for the construction of novel signal receptors, in particular the methods SHIPREC (sequence homology-independent protein recombination) and ITCHY (incremental truncation for the creation of hybrid proteins) [11–14]. However, for fragmentation of the parental genes, these methods rely on endonucleolytic or exonucleolytic DNA cleavage, both of which are challenging to titrate. Moreover, it is inherently difficult to confine hybrid fusions to specific regions of the parental genes such as their linker regions. Taken together, these limitations have hampered the wider application of either method [15]. In contrast, PATCHY circumvents problems arising from nucleolytic DNA fragmentation by means of PCR amplification with sets of staggered primers to truncate the parental genes and thus produce linker libraries of defined composition (Fig. 2). As detailed in this chapter (*see* Subheading 3.1), PATCHY starts from a template construct in which two parental gene fragments are concatenated such that they are separated by a nucleotide stretch that introduces a frameshift and a unique restriction site. The template is then amplified in a one-pot PCR reaction with sets of forward and reverse primers. Both primer sets are staggered in

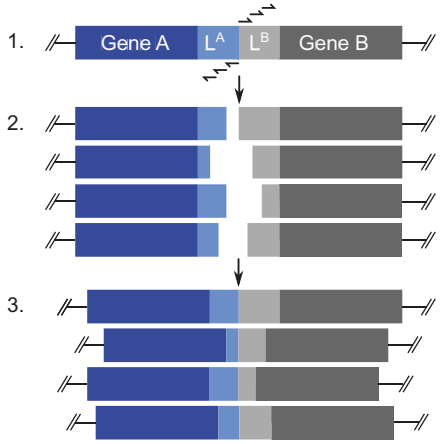

Fig. 2 The PATCHY template construct contains a tandem fusion of the longest desired fragments of genes A and B on a circular plasmid (*step 1*). PATCHY uses staggered primers to create linear DNA molecules bearing versions of genes A and B that are terminally truncated at certain positions corresponding to the primer annealing sites (*step 2*). The PATCHY hybrid gene library is created through phosphorylation and blunt-end ligation to yield circular plasmids (*step 3*)

increments of three nucleotides such as to truncate the template construct in the register of nucleotide triplets which corresponds to single amino acids at the protein level. The resultant linearized plasmid fragments are phosphorylated and religated to produce a library of circular plasmids. Optionally, remnants of the template construct can be depleted from the library by restriction digest. Plasmid libraries are then transformed and screened for favorable phenotypes (*see* Subheading 3.2).

We applied PATCHY to the fusion of the *Bs*YtvA LOV photosensor and the *Bj*FixL effector module that previously yielded the blue-light-repressed histidine kinase YF1 [8], see above. To facilitate library screening, hybrid gene libraries were constructed in the context of the pDusk-*Ds*Red reporter plasmid [16] which encodes YF1, the cognate response regulator *Bj*FixJ and the *Ds*Red fluorescent reporter under control of the *Bj*FixK2 promotor. In the dark, YF1 phosphorylates *Bj*FixJ which in turn binds to the *Bj*FixK2 promotor and thereby ramps up the expression of the reporter gene. Under blue light, YF1 acts as a net phosphatase on *Bj*FixJ which in turn results in about 10–15 fold decreased *Ds*Red expression compared to in the dark (Fig. 3). Fluorescence-based screening (*see* Subheading 3.3.1) of the PATCHY library revealed that photoreceptor activity and regulation by light are by and large determined by linker length with a pronounced heptad (seven-residue) periodicity. Insertion of single residues sufficed to invert the response to blue light. An inversion of the light response of YF1 can not only be effected via linker-length modifications but

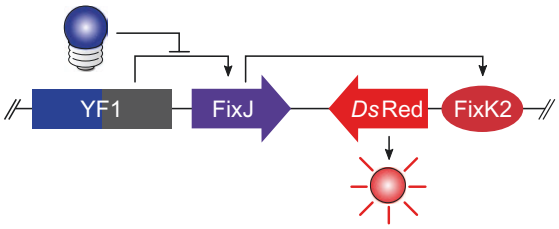

Fig. 3 The pDusk-*Ds*Red reporter plasmid. In the absence of blue light, YF1 phosphorylates the response regulator *Bj*FixJ which binds to the *Bj*FixK2 promotor and thereby upregulates reporter gene expression. Blue light inhibits expression of *Ds*Red by around 10–15-fold as it converts YF1 to a net phosphatase [16]

also via the introduction of the single amino-acid exchanges D21V or H22P within the LOV photosensor module [9, 17]. To obtain a better mechanistic understanding of signal transduction and modulation of the signal response, we applied PATCHY to the systematic interrogation of linker determinants in the background of either residue exchange (*see* Subheading 3.3.2). Similar to the results for YF1, activity was only observed in discrete heptad registers, i.e., $7n$ for H22P, as well as $7n$ and $7n + 1$ for D21V. In one variant, elongation of the linker by three residues counteracted the inversion of the signal response originally caused by the D21V exchange.

2 Materials

2.1 Chemicals and Consumables

1. 5× HF Buffer for PCR.
2. 2 U/µL Phusion High-Fidelity DNA Polymerase.
3. 10 mM dNTPs each.
4. 10 µM total forward primer pool for PATCHY.
5. 10 µM total reverse primer pool for PATCHY.
6. 10 U/µL *Nhe*I restriction enzyme.
7. 10 U/µL *Dpn*I restriction enzyme.
8. 10 U/µL T4 Polynucleotide Kinase.
9. 50% PEG-4000 (w/v).
10. 0.5 mM ATP.
11. 30 U/µL T4 DNA Ligase.
12. 50× TAE buffer: 2 M Tris-Acetate, 50 mM EDTA, pH 8.5.
13. 1% Agarose in 1× TAE Buffer.
14. LB/Kanamycin medium: 10 g peptone, 5 g yeast extract and 10 g NaCl in 1 L dH_2O supplemented with 50 mg/L Kanamycin.

15. LB/Kanamycin agar plates: LB/Kanamycin medium supplemented with 20 g/L agar.
16. Chemically or electrocompetent *Escherichia coli* cells.
17. 50% glycerol (w/v).
18. NucleoSpin Extract Kit for purification of PCR products (Macherey Nagel).
19. 96-deep-well microtiter plates for growth of bacterial clones (e.g., Axygen).
20. Clear 96-well microtiter plates for absorption measurements (e.g., Nunc).
21. Black 96-well microtiter plates for fluorescence measurements (e.g., Nunc).

2.2 Lab Equipment

1. Gradient thermal cycler for PCR amplification (e.g., Thermal Cycler S1000, Bio-Rad).
2. Electrophoresis chamber (e.g., Wide Mini-Sub Cell GT Cell, Bio-Rad).
3. Nanodrop spectrophotometer (e.g., Spark 10 M with Nanoquant plate, Tecan).
4. Microplate reader with absorption and fluorescence optics (e.g., Infinite M200 pro, Tecan).
5. Two incubators (e.g., Incu Line IL10, VWR).
6. Two shakers for microtiter plates (e.g., PMS-1000i, Grant).
7. Blue-light LED array, custom built, 10 × 8 LEDs of 470 ± 10 nm (Winger Electronics).
8. Lamp power meter (model 842-PE, Newport) with silicon photo detector (model 918D–UV-OD3, Newport).
9. Laser safety goggles for fluorescence-based screening on agar plate (Roithner Lasertechnik, 550 nm long pass).
10. *Optional*: Flow cytometer with sort functionality (e.g., S3e, Bio-Rad).

2.3 Software

1. Python script for design of staggered primers: https://github.com/vrylr/PATCHY.git

3 Methods

The generation and analysis of PATCHY hybrid gene libraries are described in Subheadings 3.1 and 3.2, respectively. To illustrate the general method and individual steps, by way of example we repeatedly refer to a recent study in which we applied PATCHY to recombine the *Bs*YtvA photosensor with the *Bj*FixL effector module (*see* Subheading 1) [10]. Key results from these experiments are

summarized as a case study in Subheading 3.3.1. The application of PATCHY to the same two modules but with either the residue exchange D21V or H22P within the photosensor is covered as a second case study in Subheading 3.3.2.

3.1 Generation of PATCHY Libraries

1. Principal considerations: In a one-pot reaction, PATCHY generates defined libraries of hybrid genes with single fusion sites between an upstream gene A and a downstream gene B. Individual library members differ in which fragments of the parental genes A and B they comprise. As a first step, the desired composition of the library is specified by deciding which set of gene fragments of A and B are to be recombined. In the case study, we constructed hybrid variants that connect the entire *Bs*YtvA LOV photosensor module including a variable number i of residues of its C-terminal linker ($i \in \{0, 1, ..., 23\}$) to the entire *Bj*FixL effector module including a variable number j of residues of its N-terminal linker ($j \in \{0, 1,..., 27\}$) (*see* Figs. 1 and 2).
2. PATCHY template construct: PATCHY libraries are obtained by PCR amplification of a template construct with staggered primer sets. The template construct contains a hybrid fusion between the longest desired fragments of each of genes A and B. A spacer sequence that harbors a unique restriction site and deliberately introduces a frameshift is inserted between the two gene fragments. In the case study, the *Bs*YtvA LOV photosensor including its entire C-terminal linker ($i = 23$) was connected to the *Bj*FixL effector including its entire N-terminal linker ($j = 27$). The intervening spacer sequence encoded a frameshift and a unique *Nhe*I restriction site. To facilitate subsequent analysis and screening of PATCHY libraries (*see* Subheading 3.2), the template construct was assembled in the background of the pDusk-*Ds*Red reporter plasmid [16] which affords facile fluorescence readout of receptor activity, *see* Subheading 1 and Fig. 3.
3. Primer design: Sets of forward and reverse oligonucleotide primers are devised such that during the PATCHY PCR reaction they lead to incremental truncations of the template construct at the 3′ end of the upstream gene A and at the 5′ end of the downstream gene B (*see* Fig. 2). For this purpose, both sets are staggered in increments of base triplets, corresponding to single amino acids at the protein level. To facilitate the PATCHY PCR reaction, the primers should be designed with largely uniform melting temperatures (T_m), ideally all within ±1 °C. Primers can either be designed manually or in automated manner with a Python script (*see* **Note 1**). All forward primers are pooled at equimolar ratios, and the total concentration is adjusted to 10 μM; likewise, a pool of all reverse primers at 10 μM total concentration is prepared (*see* **Note 2**).

Table 1
PATCHY PCR reaction mix

Reagent	Quantity
5× HF buffer	10 µL
10 mM dNTP mix	1 µL (0.2 mM each)
DNA template	1 µL (50 pg–1 µg)
10 µM total fwd. primer pool	1.25 µL (0.25 µM)
10 µM total rev. primer pool	1.25 µL (0.25 µM)
2 U/µL Phusion polymerase	1 µL
ddH_2O	Add to 50 µL

Table 2
PATCHY PCR program

Step	Temperature	Time
1	95 °C	30 s
2	95 °C	30 s
3	T_m–5 °C	30 s
4	72 °C	30 s/kb
5	go to step 2	35 cycles
6	72 °C	10 min
7	10 °C	∞

4. PATCHY PCR reaction: The PCR reaction mixture is prepared according to Table 1, and PCR amplification is conducted as described in Table 2 where the annealing temperature is set at T_m–5 °C. Analysis of the reaction products by agarose gel electrophoresis should show one dominant or even a single DNA band of the expected size. For n forward and m reverse primers, the PCR product should theoretically comprise $n \bullet m$ different, incrementally truncated, linear PCR fragments.
5. Workup of PATCHY PCR reaction: The product of the PCR reaction is purified using standard molecular biology kits (e.g., NucleoSpin Gel and PCR clean up, Macherey-Nagel). To achieve high DNA concentration for subsequent steps, the PCR product should be eluted with 30 µL ddH_2O or elution buffer. The concentration is determined spectrophotometrically or by analysis via gel electrophoresis and comparison to a standard of known concentration. Ideally, one should have a total of at least 1–2 µg DNA at this stage (*see* **Note 3**).

Table 3
Phosphorylation of linear DNA fragments

Reagent	Quantity
10× T4 DNA ligase buffer	3.5 µL
Linear PCR fragment	30 µL (50 pg–1 µg)
10 U/µL T4 polynucleotide linase	2 µL

Table 4
Ligation of phosphorylated linear DNA fragments

Reagent	Quantity
Phosphorylation reaction mix	35 µL
50% PEG-4000 (w/v)	4 µL
0.5 mM ATP (optional)	0.5 µL
30 U/µL T4 DNA ligase	1 µL

6. *Optional*: To deplete the template construct from the reaction mixture, the PCR product is alternatively purified via agarose gel extraction. Depending upon the plasmid size, the circular, negatively supercoiled template can show different electrophoretic mobility on agarose gels from the desired linear PCR products. It is hence often possible to separate the original template construct from the PATCHY library (*see* **Note 4**).
7. Phosphorylation of PCR product: The PCR product is phosphorylated at the 5′ end by polynucleotide kinase according to Table 3. The reaction mixture is incubated at 37 °C for 30 min.
8. Circularization of linear PCR product: Ligation of the phosphorylated, linear PCR products yields circular plasmids and is carried out in the same reaction solution as phosphorylation. The reaction mix is allowed to cool to 22 °C before T4 DNA ligase, PEG-4000, and ATP (optional) are added (Table 4). The reaction mix is then incubated at 22 °C for 1 h (*see* **Note 5**).
9. *Optional*—Depletion of template construct from PATCHY library: The original template construct is selectively depleted from the PATCHY library via restriction digest with the enzyme that cuts at the deliberately introduced unique site within the spacer sequence of the template (*see* **step 2**). For the example case of the PATCHY library between the *Bs*YtvA LOV sensor and the *Bj*FixL effector, 1.5 µL *Nhe*I was added, followed by incubation at 37 °C for 30 min. To prevent recircularization, 1.5 µL of the phosphatase FastAP was added and

incubation continued for 15 min at 37 °C. Enzymes were inactivated by incubation at 75 °C for 15 min (*see* **Note 4**).

10. *Optional* – Depletion of template construct from PATCHY library: Alternatively, the template construct can selectively be digested with *Dpn*I which cleaves DNA in methylation-dependent manner (*see* **Note 4**).
11. Transformation of PATCHY library: The PATCHY library can directly be transformed into *Escherichia coli* cells (e.g., DH10b). For example, 5–10 μL of the reaction mix were transformed into chemically competent cells, or up to 1.5 μL were transformed into electrocompetent cells. After plating on LB agar and overnight incubation at 37 °C, the library can either be processed right away (*see* Subheading 3.2) or stored at −80 °C as a glycerol stock.

3.2 Analysis of PATCHY Libraries

1. Sequence analysis of the naïve PATCHY library: To assess the quality of the PATCHY library, a number of individual clones can be analyzed by Sanger sequencing. In case the original template construct is found with significant frequency, extra efforts should be taken to deplete it from the library (*see* Subheading 3.1, **steps 6, 9,** and **10** as well as **Note 4**).
2. *Optional*: Alternatively, the library can be analyzed by next-generation sequencing (NGS). In the case study [10], the entire PATCHY plasmid library was fragmented by ultrasound and sequenced on an Illumina platform with paired-end 150-base-pair reads. Although most reads covered the invariant plasmid backbone, the low cost of NGS still allowed to get good coverage of the variant parts of the plasmids. We obtained approximately 5500 paired-end reads covering the linker region, corresponding to an ~8-fold oversampling of the expected 672 different hybrid genes (Fig. 4). Out of these 672 variants, 578 could be detected by NGS. The data also indicated that each forward and reverse primer had been used in the PATCHY PCR reaction albeit to varying extents.
3. *Optional*: In case the sequence analysis indicates a nonrandom, biased distribution of expected constructs in the PATCHY library, one may rerun the PATCHY PCR reaction with adjusted relative primer concentrations (*see* Subheading 3.1, **steps 3** and **4** as well as **Note 2**).
4. *Optional*: To further diversify the PATCHY library, it can be subjected to an error-prone PCR reaction (*see* **Note 6**).
5. Isolation of hybrid variants from the PATCHY library: The identification of hybrid variants with desirable traits in the PATCHY library is obviously governed by the assays available to read out activity. In principle, individual clones can be isolated and analyzed separately, but ideally functionality can

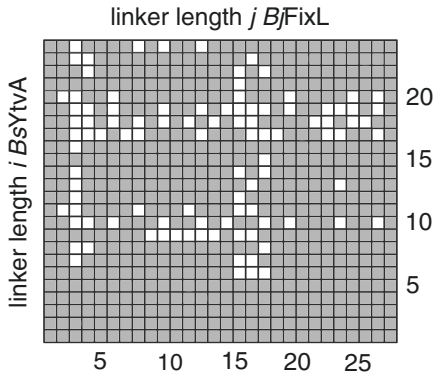

Fig. 4 Next-generation sequencing of the PATCHY library of hybrids between *Bs*YtvA photosensor and *Bj*FixL effector. The *x*- and *y*-axes denote the number of residues *i* and *j* from the linkers of the parental *Bs*YtvA and *Bj*FxL that a given variant contains. *Grey squares* indicate theoretically expected constructs indeed observed in the library. Each primer was used in the PATCHY-PCR reaction

directly be assessed with high throughput and in parallel in vivo, i.e., without laborious intermediate steps such as protein purification. Efficient in vivo assays largely fall into two clades: first, screening assays are based on a readily measurable, often colorimetric readout such as fluorescence; second, selection systems link functionality of the hybrid variants to cell survival or proliferation. In the example case of the chimerae between *Bs*YtvA LOV and the *Bj*FixL histidine kinase, we resorted to the pDusk-*Ds*Red screening system which links hybrid receptor activity to expression of a *Ds*Red fluorescent reporter gene [10, 16]. Transformed cells are cultured at 37 °C on plate in darkness or under constant blue light illumination (470 nm, 40 μW/cm^2). Clones harboring functional hybrid variants that expressed *Ds*Red under the given incubation condition are visually identified via observation of fluorescence through a 550-nm long-pass filter goggle. As detailed in Subheading 3.1 **step 1**, the template construct is incapacitated by a deliberate frameshift between the two gene fragments recombined via PATCHY. Screening for function is thus well suited to further discriminate against the template construct (*see* **Note 4**).

6. *Optional*: As an alternative screening method, fluorescence-activated cell sorting can be used, provided function of hybrids is linked to a fluorescent readout [16] (*see* **Note 7**).
7. Storage of isolated hybrid variants: Clones with desirable phenotypes identified in the previous two steps are grown at 37 °C to stationary phase. To this end, single wells of a 96-deep-well microtiter plate are filled with 600 μL LB medium supplemented with the required antibiotic and are inoculated with a

single clone. For long-term storage, 200 µL of the saturated cultures is mixed with 200 µL 50% (w/v) glycerol and frozen at −80 °C.

8. Quantitative characterization of isolated hybrid variants: Using suitable functional assays, the biological activity of the hybrid variants isolated in Subheading 3.2 **step 5** should be characterized in more detail. In the example case, replicates of each clone were inoculated in 5 mL LB/Kanamycin and grown at 37 °C for 16 h in darkness or constant blue light (470 nm, 100 µW/cm^2) (*see* **Note 8**). Saturated cultures were diluted tenfold in ddH_2O, and OD_{600} was measured in clear microtiter plates with a microplate reader. Samples were further diluted fivefold in ddH_2O, and *Ds*Red fluorescence was measured in black microtiter plates with settings of 554 ± 9 nm for excitation and 591 ± 20 nm for emission, respectively. Fluorescence readings were normalized to the OD_{600} of the corresponding sample.
9. Sequence analysis of isolated hybrid variants: Clones that showed desirable properties in the previous step are analyzed by Sanger DNA sequencing (*see* **Note 9**).

3.3 PATCHY Case Studies

3.3.1 Linker Libraries of YF1

We applied PATCHY to better characterize the underlying design principles and signal-transduction mechanisms in the chimeric photoreceptor YF1 [8]. The original YF1 receptor originated from the fusion of the blue light-sensitive light–oxygen–voltage photosensor module of *Bs*YtvA to the effector module of the *Bj*FixL histidine kinase. Notably, in YF1 the linker between these modules essentially derived from the *Bj*FixL parental protein, i.e., $i = 3$ and $j = 25$ (*see* Subheading 3.1 **step 1**). Sparse sampling of linker composition had earlier identified linker length as the main determinant for activity and regulation of the hybrid receptors [8]. A seven-residue periodicity of the dependence of activity and regulatory properties on linker length resulted from the coiled-coil conformation of the linker, as later evidenced in the high-resolution structure of dark-adapted YF1 [9]. Notably, only a tiny fraction of many conceivable hybrid variants were studied at this point [8].

Despite these biochemical and structural data, the mechanism by which signals are transduced from the LOV photosenor to the histidine kinase effector remained unclear. We reasoned that comprehensive interrogation of linker sequence space could yield additional mechanistic insight. The linkers between the respective sensor and effector modules in the parental receptors *Bs*YtvA and *Bj*FixL comprise 23 and 27 residues, respectively. Provided that fusions between the parental proteins are restricted to these linker regions, there are $(23 + 1) \bullet (27 + 1) = 672$ different ways to recombine the *Bs*YtvA LOV photosensor with the *Bj*FixL effector (*see* Figs. 1 and 2). Using PATCHY as described in Subheading 3.1, we generated a construct library that theoretically contains

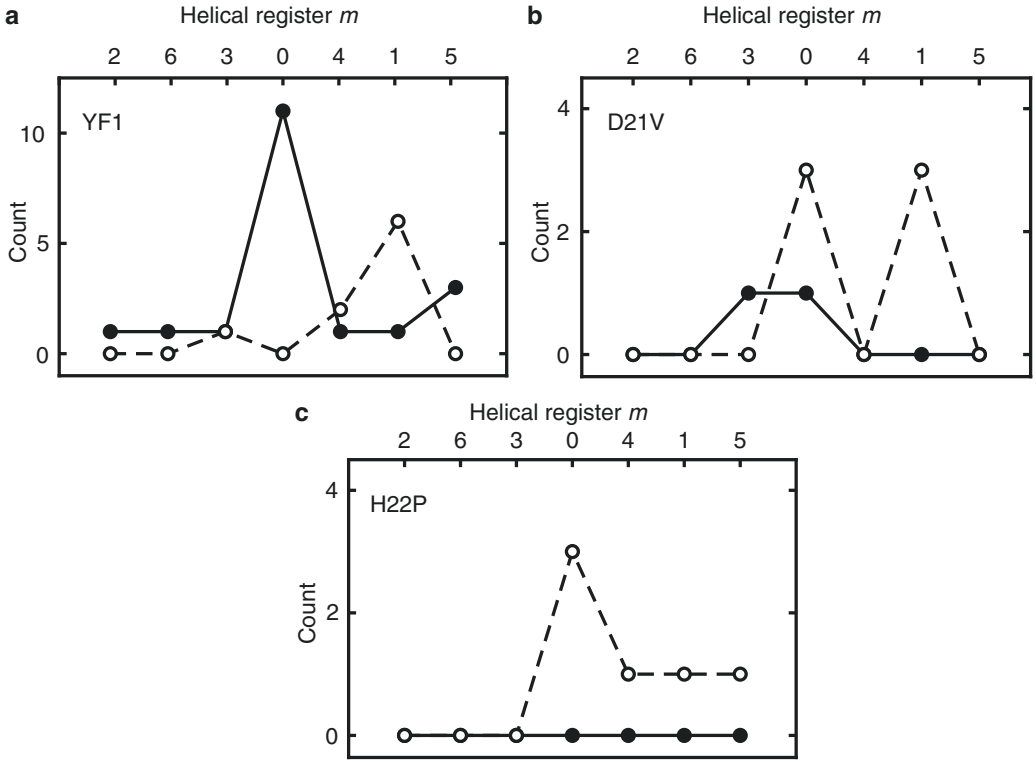

Fig. 5 Linker-length analysis of light-regulated *Bs*YtvA-*Bj*FixL hybrid variants. (**a**) For YF1, light-repressed variants (*filled circles*) showed periodic linker lengths of 7*n* or 7*n* + 5 residues but light-activated variants (open circles) mostly occurred at linker lengths of 7*n* + 1 residues. (**b**) Light-activated D21V variants had linkers of 7*n* or 7*n* + 1 residues. Two variants with linkers belonging to the 7*n* and 7*n* + 3 classes showed inverted, light-repressed response. (**c**) For H22P, only light-activated variants were identified that predominantly possessed linkers of 7*n* residues

these 672 linker variants. Library construction was performed in the context of the pDusk-*Ds*Red reporter plasmid [16] that affords rapid screening for functional hybrid variants as described in Subheading 3.2 (*see* Fig. 3).

Key results from the analysis of the PATCHY library are summarized in the following and in Fig. 5a. Strikingly, light-regulated activity in *Bs*YtvA-*Bj*FixL hybrids is supported by quite different linker lengths ranging from 4 to 50 residues, whereas the original YF1 possesses a linker of 28 residues. Assuming a continuous α-helical coiled-coil structure of the linker elements, this translates into distances of separation of ~6–75 Å between LOV photosensor and effector modules. In addition to hybrids with light-repressed activity as in YF1, several variants showed an inverse response to light, i.e., they had light-induced activity. Hybrid variants with alike responses to light usually displayed a pronounced

heptad periodicity in their linker lengths. Whereas light-repressed hybrid variants predominantly possessed linkers of $7n$ and $7n + 5$ residues, those with light-induced activity mostly had linkers of $7n + 1$ residues ($n \in \{1, \ldots, 7\}$). The heptad dependence on linker length can be accounted for by the coiled-coil nature of the linker. Sequence analysis of a large group of related, natural sensor histidine kinases revealed their sensor and effector modules to be mainly connected by coiled-coil linkers of length $7n$ and $7n + 5$ residues [10].

The difference in the preferred linker lengths for light-repressed and light-activated hybrid variants provides clues as to the mechanistic bases for signal transduction in YF1. Notably, the registers $7n$ and $7n + 1$ differ by insertion of a single residue; within a canonical coiled coil such an insertion induces an angular shift of around 100° [18]. We thus propose that signal transduction in YF1 is predicated on angular reorientation of the LOV photosensor relative to the histidine kinase effector modules [8, 9, 19, 20]. This type of angular reorientation could also be brought about by a change in the degree of supercoiling of the linker. We recently investigated light-dependent signal transduction in YF1 by electron paramagnetic resonance (EPR) spectroscopy and X-ray solution scattering [19, 20]. Indeed, the two independent and complementary approaches identify light-induced left-handed supercoiling as the mode for signal transduction and thereby provide a structural rationale for the PATCHY data.

3.3.2 Linker Libraries of Signal-Inverted YF1

The inversion of the response to light in YF1 cannot only be achieved by linker variations but also by the replacement of certain residues within the LOV photosensor units [9, 17]. To investigate the basis for this profound effect on signal transduction, we repeated the PATCHY analysis of the *Bs*YtvA-*Bj*FixL chimerae in the background of either the D21V or H22P exchange, both of which induce inversion of the light response in YF1.

In case of D21V, hybrid variants with the same qualitative signal response as the original YF1 D21V, i.e., with an increase in activity upon blue-light exposure, fell into two distinct classes with linkers of $7n$ and $7n + 1$ residues, respectively (Fig. 5b). The preference for these classes is indicative of the coiled-coil structure of the linker in the D21V variants. Interestingly, in the YF1 context the clades $7n$ and $7n + 1$ were associated with light-repressed and light-induced activity, respectively, whereas in case of D21V they both predominantly gave rise to light activation. However, two D21V variants with linkers of 31 ($= 7 \cdot 4 + 3$) and 42 ($= 7 \cdot 6$) residues displayed light-repressed activity; in particular, in the former construct, *Ds*Red reporter fluorescence was enhanced by around 9-fold in darkness versus blue light. Intriguingly, the signal inversion introduced by the D21V exchange could thus be reverted in a

construct with a linker that is elongated by three residues. Currently, only two D21V variants with distinctly light-repressed activity could be identified, and a more detailed analysis of the underlying linker lengths is therefore precluded. Exhaustive sampling of linker variants in the D21V context by PATCHY might yield additional light-repressed variants and allow this type of analysis.

For the H22P background, only hybrid variants with light-induced activity as the original YF1 H22P were found but none with light-repressed activity (Fig. 5c). Consistent with a coiled-coil conformation, the linkers of these variants predominantly comprised $7n$ residues. A recent EPR investigation [19] revealed that introduction of the H22P exchange leads to a complete rearrangement of the dimer interface; two N-terminal α helices that in YF1 are tucked in between the LOV photosensor domains (*see* Fig. 1) are displaced and probably unfolded in H22P. Given this drastic change of the dimer interface, it is perplexing that the H22P variant transduces signals, let alone in inverted manner. Despite these differences, signal transduction in H22P apparently employs a highly similar structural mode as YF1, albeit with inverted sign [19]. In support of this view, we now find that the linkers of variants with signal response corresponding to that of YF1 H22P mostly conformed to $7n$ residues. By that token, one would also expect to find H22P linker variants with inverted, i.e., light-repressed activity. Our inability to do so may stem from insufficient sampling of linker sequence space or from an inherent difference in the signal mechanism of H22P. The above finding that the light response of the D21V variant could be inverted for certain linker lengths implies that the former is true and that signal inversion by linker-length variations also applies to the H22P context.

3.4 Conclusion

The PATCHY method offers an efficient route toward libraries of hybrid genes with a single fusion between defined fragments of two parental genes A and B. In contrast to related approaches for the construction of hybrid gene libraries [11–15], PATCHY uses a simpler protocol and obviates incremental nucleolytic digest of the parental genes which is difficult to precisely adjust. Rather, PCR amplification with sets of staggered primers exactly delineates which fragments of A and B are generated and recombined. The analysis of PATCHY hybrid libraries benefits from efficient activity assays, in particular cell-based screening and selection approaches.

We demonstrate the utility of PATCHY for the test case of hybrid blue light photoreceptors. Catalytic activity and response to light are largely governed by the length of the linker intervening the constituent photosensor and effector modules of the receptors. A striking seven-residue dependence of receptor function on linker length is explained by the continuous coiled-coil

structure of said linker. Insertion of single residues in the linker can lead to inversion of the receptor response to blue light [10]. Recent mechanistic investigations [19, 20] reveal light-induced left-handed supercoiling of the linker and thus provide the structural rationale for signal inversion via linker-length variations. In the context of the residue exchanges D21V and H22P, each of which induces signal inversion in YF1, light-regulated function is only sustained by linkers of discrete lengths.

As a method, PATCHY is generally suitable for the construction and mechanistic interrogation of hybrid gene libraries. In addition to the engineering of signal receptors, PATCHY also appears well suited to the construction of fluorescent reporters.

4 Notes

1. The computer script is available from Github at https://github.com/vrylr/PATCHY.git. To execute it, a Python interpreter is required which can be obtained free of charge from http://www.python.org or https://winpython.github.io.
2. We recommend to initially pool all forward primers at equimolar ratio and use them at a total concentration of 10 μM. The reverse primers should be prepared accordingly. Given that the individual primers differ in their sequences, they may well possess different annealing and amplification efficiencies which would result in a biased distribution of hybrid genes. Adjustment of the relative primer concentrations may be a remedy for this problem. In principle, one can employ non-equal concentrations within each primer pool to deliberately predispose the PATCHY PCR reaction toward the generation of certain sets of hybrid variants. Alternatively, the PATCHY protocol can be rerun with subsets of the forward and reverse pools that entirely lack certain primers.
3. One can carry on with the subsequent steps, even if less DNA has been obtained at this stage.
4. We found it useful to implement several steps for removal of the initial template construct from the PATCHY library. (a) In many cases, the linear PATCHY PCR products can effectively be separated from the circular template via gel extraction (*see* Subheading 3.1 **step 6**). (b) Following phosphorylation and circularization of the PATCHY PCR products, the template can selectively be degraded via restriction digest with *Dpn*I or the specific endonuclease chosen in the template design (*see* Subheading 3.1 **steps 9** and **10**). (c) Lastly, a deliberate frameshift can be introduced into the template construct to disable it. Functional analysis of the PATCHY library, in particular by

efficient screening or selection procedures, provides a ready means for discrimination against the template construct (*see* Subheading 3.2 **step 5**). In case the resultant PATCHY library still contains an exceedingly high fraction of the initial template construct, steps (a) and (b) can be repeated.

5. The ligation reaction can alternatively be carried out at 16 °C over night.
6. A particular strength of PATCHY is the generation of hybrid genes of defined composition. Although this usually is the wanted outcome, in certain scenarios the desired traits may not manifest in any of the hybrid gene variants within the PATCHY libraries. In these cases, the PATCHY libraries can further be diversified via error-prone PCR [21]. Introduction of random residue exchanges, in particular within the linker region between protein modules, may well yield variants with the desired functional properties.
7. The screening of PATCHY libraries can be expedited with fluorescence-activated cell sorting. This is especially useful in case of protein switches that are supposed to show differential activity in response to a signal. PATCHY hybrid libraries can alternately be screened in the absence and presence of this signal, and stringently responding variants can thus be enriched, identified and isolated.
8. Alternatively, the activity of the PATCHY variants can be assessed in microtiter format. Within a 96-deep-well plate, aliquots of 600 μL LB/Kanamycin medium are inoculated with individual variants and incubated for 16 h in darkness or under constant blue light (470 nm, 40 μW/cm^2). All subsequent steps are conducted as described in Subheading 3.2 **steps 8** and **9**.
9. Many companies offer plasmid preparation and Sanger sequencing in microtiter format. For larger number of hybrid variants, this approach usually is more economic in terms of time and money.

Acknowledgments

Discussions with C. Engelhard and R. Bittl (Freie Universität Berlin) are appreciated. Financial support through Deutsche Forschungsgemeinschaft grant MO2192/4-1 (A.M.), through a Sofja-Kovalevskaya Award by the Alexander-von-Humboldt Foundation (A.M.), and through Boehringer-Ingelheim Fonds (R.O.) is gratefully acknowledged.

References

1. Pawson T, Nash P (2003) Assembly of cell regulatory systems through protein interaction domains. Science 300:445–452
2. Gokhale RS, Khosla C (2000) Role of linkers in communication between protein modules. Curr Opin Chem Biol 4:22–27
3. Amet N, Lee H-F, Shen W-C (2009) Insertion of the designed helical linker led to increased expression of Tf-based fusion proteins. Pharm Res 26:523–528
4. Möglich A, Yang X, Ayers RA, Moffat K (2010) Structure and function of plant photoreceptors. Annu Rev Plant Biol 61:21–47
5. Ziegler T, Möglich A (2015) Photoreceptor engineering. Front Mol Biosci 2:30
6. Ryu M-H, Gomelsky M (2014) Near-infrared light responsive synthetic c-di-GMP module for optogenetic applications. ACS Synth Biol 3:802–810
7. Wu YI, Frey D, Lungu OI, Jaehrig A, Schlichting I, Kuhlman B, Hahn KM (2009) A genetically encoded photoactivatable Rac controls the motility of living cells. Nature 461: 104–108
8. Möglich A, Ayers RA, Moffat K (2009) Design and signaling mechanism of light-regulated histidine kinases. J Mol Biol 385:1433–1444
9. Diensthuber RP, Bommer M, Gleichmann T, Möglich A (2013) Full-length structure of a sensor histidine kinase pinpoints coaxial coiled coils as signal transducers and modulators. Structure 21:1127–1136
10. Ohlendorf R, Schumacher CH, Richter F, Möglich A (2016) Library-aided probing of linker determinants in hybrid photoreceptors. ACS Synth Biol 5(10):1117–26. doi:10.1021/acssynbio.6b00028.
11. Ostermeier M, Shim JH, Benkovic SJ (1999) A combinatorial approach to hybrid enzymes independent of DNA homology. Nat Biotechnol 17:1205–1209
12. Ostermeier M, Nixon AE, Shim JH, Benkovic SJ (1999) Combinatorial protein engineering by incremental truncation. Proc Natl Acad Sci 96:3562–3567
13. Lutz S, Ostermeier M (2003). Preparation of SCRATCHY hybrid protein libraries. Directed Evolution Library Creation: Methods and Protocols 143–151
14. Arnold FH, Georgiou G (2003) Methods in molecular biology, vol. 231. Directed evolution library creation methods and protocols. Humana Press, Totowa, NJ
15. Ostermeier M (2003) Theoretical distribution of truncation lengths in incremental truncation libraries. Biotechnol Bioeng 82:564–577
16. Ohlendorf R, Vidavski RR, Eldar A, Moffat K, Möglich A (2012) From dusk till dawn: one-plasmid systems for light-regulated gene expression. J Mol Biol 416:534–542
17. Gleichmann T, Diensthuber RP, Möglich A (2013) Charting the signal trajectory in a light-oxygen-voltage photoreceptor by random mutagenesis and covariance analysis. J Biol Chem 288:29345–29355
18. Lupas AN, Gruber M (2005) The structure of alpha-helical coiled coils. Adv Protein Chem 70:37–78
19. Engelhard C, Diensthuber RP, Möglich A, Bittl R (2016) Blue-light reception through quaternary transitions. Submitted
20. Berntsson O, Diensthuber RP, Panman MR, et al (2016) Conformational photoactivation of a light-oxygen-voltage photosensor. Submitted
21. Leung DW, Chen E, Goeddel DV (1989) A method for random mutagenesis of a defined DNA segment using a modified polymerase chain reaction. Technique 1:11–15

7.2. Manuskript II

Stüven, B.*; Stabel, R.*; Ohlendorf, R.; Beck, J.; Schubert, R.; Möglich, A.; *Biological Chemistry* (2019) "*Characterization and engineering of photoactivated adenylyl cyclases*"

Birthe Stüven[a], Robert Stabel[a], Robert Ohlendorf[b], Julian Beck, Roman Schubert and Andreas Möglich*

Characterization and engineering of photoactivated adenylyl cyclases

https://doi.org/10.1515/hsz-2018-0375
Received September 15, 2018; accepted December 7, 2018; previously published online December 14, 2018

Abstract: Cyclic nucleoside monophosphates (cNMP) serve as universal second messengers in signal transduction across prokaryotes and eukaryotes. As signaling often relies on transiently formed microdomains of elevated second messenger concentration, means to precisely perturb the spatiotemporal dynamics of cNMPs are uniquely poised for the interrogation of the underlying physiological processes. Optogenetics appears particularly suited as it affords light-dependent, accurate control in time and space of diverse cellular processes. Several sensory photoreceptors function as photoactivated adenylyl cyclases (PAC) and hence serve as light-regulated actuators for the control of intracellular levels of 3′, 5′-cyclic adenosine monophosphate. To characterize PACs and to refine their properties, we devised a test bed for the facile analysis of these photoreceptors. Cyclase activity is monitored in bacterial cells via expression of a fluorescent reporter, and programmable illumination allows the rapid exploration of multiple lighting regimes. We thus probed two PACs responding to blue and red light, respectively, and observed significant dark activity for both. We next engineered derivatives of the red-light-sensitive PAC with altered responses to light, with one variant, denoted *Dd*PAC, showing enhanced response to light. These PAC variants stand to enrich the optogenetic toolkit and thus facilitate the detailed analysis of cNMP metabolism and signaling.

Keywords: adenylyl cyclase; BLUF; optogenetics; phytochrome; sensory photoreceptor; synthetic biology.

[a]**Birthe Stüven and Robert Stabel:** These authors contributed equally to this work.
[b]Present address: Department of Biological Engineering, Massachusetts Institute of Technology, Cambridge, MA 02139, USA.
***Corresponding author: Andreas Möglich,** Lehrstuhl für Biochemie, Universität Bayreuth, D-95447 Bayreuth, Germany; Institut für Biologie, Humboldt-Universität zu Berlin, D-10115 Berlin, Germany; Research Center for Bio-Macromolecules, Universität Bayreuth, D-95447 Bayreuth, Germany; Bayreuth Center for Biochemistry and Molecular Biology, Universität Bayreuth, D-95447 Bayreuth, Germany; and North-Bavarian NMR Center, Universität Bayreuth, D-95447 Bayreuth, Germany,
e-mail: andreas.moeglich@uni-bayreuth.de.
https://orcid.org/0000-0002-7382-2772
Birthe Stüven, Robert Stabel and Julian Beck: Lehrstuhl für Biochemie, Universität Bayreuth, D-95447 Bayreuth, Germany
Robert Ohlendorf and Roman Schubert: Institut für Biologie, Humboldt-Universität zu Berlin, D-10115 Berlin, Germany

Introduction

Second messenger molecules are integral to signal-transduction networks across most organisms. As intracellular, diffusible agents, they amplify and relay signals in time and space within cells (Krauss, 2014). As one class of universal second messengers, 3′, 5′-cyclic nucleoside monophosphates (cNMP) are engaged in regulating manifold physiological processes in prokaryotes and eukaryotes alike. cNMPs are generally produced from the corresponding 5′-nucleoside triphosphates by nucleotidyl cyclases and are degraded to the non-cyclic 5′-nucleoside monophosphates by phosphodiesterases (PDE). In eukaryotic cells, the two predominant cNMPs, 3′, 5′-cyclic adenosine monophosphate (cAMP) and 3′, 5′-cyclic guanosine monophosphate (cGMP) (Rall et al., 1957; Ashman et al., 1963), bind to and thereby modulate the activity of multiple targets, including protein kinases A and G (Walsh et al., 1968; Kuo and Greengard, 1970), cyclic-nucleotide-gated (CNG) ion channels (Fesenko et al., 1985), Epac (exchange protein directly activated by cAMP) (de Rooij et al., 1998), and popeye-domain-containing proteins (Andrée et al., 2000). As these cyclic nucleotides play crucial roles in diverse signaling pathways, misregulation of their metabolism can be causative for disease (Gold et al., 2013). In bacteria, cAMP mediates various responses via binding to proteins of the cAMP-receptor protein family (McDonough and Rodriguez, 2012). A particularly well-studied example is the carbon catabolite repression present in most bacteria (Görke and Stülke, 2008). In the presence of their preferred carbon sources, bacteria grow rapidly, and the activity of the endogenous adenylyl cyclase (AC) is inhibited. Once the preferred carbon source is depleted, AC activity ramps up, and intracellular cAMP accumulates. In *Escherichia coli* and related bacteria, cAMP forms a complex with the

catabolite activator protein [CAP, also known as cAMP receptor protein (CRP)] which then binds to the promoter region of numerous target genes and thereby either activates or represses their expression (Shimada et al., 2011). By contrast, cGMP signaling is absent from most bacteria but occurs in certain species (Gomelsky, 2011). As a case in point, the α-proteobacterium *Rhodospirillum centenum* employs a CAP variant that responds to cGMP rather than cAMP (Marden et al., 2011; Roychowdhury et al., 2015). In addition to cNMPs, bacteria also use cyclic dinucleotides as second messengers as exemplified by cyclic diguanylate that is involved in the regulation of manifold processes including cell cycle, biofilm formation and virulence (Jenal et al., 2017).

Signaling pathways relying on cNMPs frequently involve the formation of spatiotemporal microdomains of elevated second messenger concentration. Hence, implements that allow to monitor and alter intracellular cNMP levels with precision in time and space are uniquely suited to investigate and control such pathways. Optogenetics represents a particularly versatile approach as it enables the noninvasive, spatiotemporally precise and reversible perturbation of cellular events by light (Deisseroth et al., 2006). Originating in the neurosciences, optogenetics now extends to manifold cellular processes and parameters including cNMP signaling (Losi et al., 2018). Sensory photoreceptor proteins underpin optogenetics as genetically encodable, light-regulated actuators (Möglich et al., 2010). Several photoreceptors found in nature function as photoactivated adenylyl cyclases (PAC) or guanylyl cyclases that increase production of the respective cNMP upon light exposure. The first discovered PAC from the protist *Euglena gracilis* (Iseki et al., 2002), denoted *Eu*PAC, responds to blue light through a flavin-binding BLUF photosensor module (Gomelsky and Klug, 2002). Although *Eu*PAC has seen optogenetic use (Schröder-Lang et al., 2007), it has been largely superseded by bPAC from the γ-proteobacterium *Beggiatoa* sp. which offers smaller and simpler protein architecture combined with more pronounced blue-light-dependent regulation of AC activity compared to *Eu*PAC (Ryu et al., 2010; Stierl et al., 2011). bPAC has thus become a tool of choice in optogenetics (Jansen et al., 2017), and variants have been engineered that possess guanylyl cyclase (GC) activity (Ryu et al., 2010; Kim et al., 2015). Other naturally occurring photoactivated nucleotidyl cyclases resort to light-oxygen-voltage, rhodopsin and cyanobacteriochrome photosensor units (Raffelberg et al., 2013; Avelar et al., 2014; Blain-Hartung et al., 2018). Striving to extend the light sensitivity of PACs to the long-wavelength spectral range, Gomelsky and colleagues engineered the red-light-regulated AC IlaC by fusing the photosensory core module (PCM), comprising PAS, GAF and PHY domains, of the *Rhodobacter sphaeroides* bacteriophytochrome (BPhy) BPhG1 to the catalytic effector module of the *Nostoc* sp. AC CyaB1 (Ryu et al., 2014). Notably, BPhys utilize the linear tetrapyrrole biliverdin as chromophore and adopt two (meta)stable states, denoted Pr and Pfr. Absorption of red and far-red light drive the Pr→Pfr and Pfr→Pr transitions, respectively (Rockwell and Lagarias, 2010). Recently, Winkler and colleagues refined this engineering approach and fused the *Deinococcus radiodurans* BPhy (*Dr*BPhy) PCM to the effector module of *Synechocystis* PCC6803 Cya2 (Etzl et al., 2018) to obtain the red-light-regulated GC PaaG. Via introduction of a previously described single-residue substitution within the effector module (Rauch et al., 2008), PaaG was converted to a PAC named PaaC (Etzl et al., 2018). In a similar vein, we generated the red-light-activated cAMP- and cGMP-specific PDE LAPD by recombining the *Dr*BPhy PCM with the effector module of *Homo sapiens* PDE2A (Gasser et al., 2014).

The mechanistic characterization and optimization of photoactivated cyclases and phosphodiesterases require efficient assays that probe enzymatic activity under different lighting conditions. Formation and breakdown of cNMPs can be routinely quantified by high-performance liquid chromatography (HPLC). While highly precise and well suited for recording complete Michaelis-Menten kinetics, HPLC-based assays usually necessitate prior purification of the enzymes which may prove limiting when studying large numbers of variants, e.g. en route to the development of optimized light-regulated enzymes. Several assays overcome this limitation by doing away with protein purification. Enzyme-linked immunosorbent assays (ELISAs) are capable of precisely determining cNMP quantities even within heterogenous mixtures like cell lysates. Similarly, we developed a fluorescence-based readout that exploits that both the making and the breaking of cNMPs entail acidification of the solution (Schumacher et al., 2016). Cyclase and PDE turnover can hence be detected via the pH-sensitive fluorophore 2′,7′-bis-(2-carboxyethyl)-5-(and-6)-carboxyfluorescein (BCECF) (Rink et al., 1982), and this assay applies to either purified protein or crude cell lysates, thus allowing enhanced throughput. Finally, approaches exist that permit the detection of light-regulated cyclase activity inside of bacterial cells. One of the targets in *E. coli* upregulated via action of CAP:cAMP is the *lac* operon which encodes genes engaged in metabolizing lactose. Intracellular cAMP levels can hence be indirectly detected by monitoring the activity of gene products of this operon, in particular of β-galactosidase (LacZ) which is essential for hydrolytic

breakdown of lactose and subsequent metabolization. In one approach, bacterial growth on minimal medium containing lactose as sole carbon source is monitored, often combined with a pH-indicator dye (so-called MacConkey agar) (Ryu et al., 2010). Alternatively, the enzymatic activity of LacZ is assessed via lactose analogs, such as X-gal, that upon hydrolysis yield colored output (Ryu et al., 2014, 2015; Etzl et al., 2018). For tests in eukaryotic cells, PACs were combined with CNG channels, thus allowing readout of activity via electrophysiology or ion-sensitive fluorophores (Stierl et al., 2011; Jansen et al., 2015).

In the present work, we strove to analyze and optimize the performance of PACs. To this end, we devised a bacterial assay that reports on intracellular AC activity and affords sensitive fluorescent readout. The reporter assay seamlessly integrates with a setup for the programmable illumination of microtiter plates (MTP), thus affording the facile, parallelized interrogation of multiple experimental conditions and lighting regimes. The resulting test bed readily recorded light-dependent readout for both bPAC and PaaC. Thus equipped, we engineered PaaC derivatives that differ in their activation profiles, with one variant offering the advantage of reduced sensitivity to far-red light compared to PaaC.

Results

A test bed for photoactivated adenylyl cyclases

To streamline the characterization and optimization of photoactivated adenylyl cyclases, we devised an efficient screening platform. We reasoned that an ideal platform would possess key desirable traits: (i) the readout of catalytic activity should be specific and sensitive; (ii) the readout should be facile, ideally obviating laborious purification of candidate cyclases; (iii) the readout should be compatible with various illumination regimes and should avoid undue photoactivation of the system under study; (iv) the platform should be scalable and parallelizable

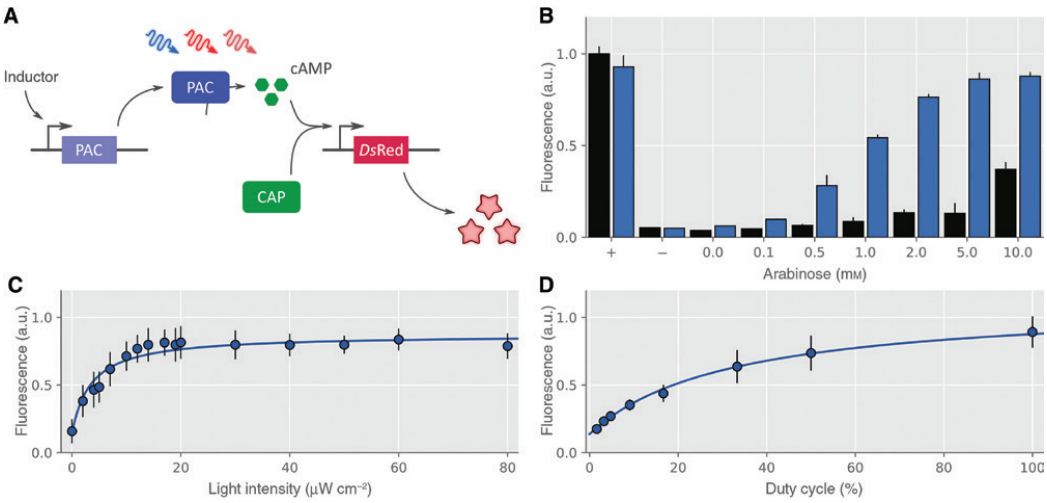

Figure 1: Test bed for photoactivated adenylyl cyclases (PAC) as applied to bPAC.
(A) A reporter-gene assay for PACs was realized in the *E. coli* strain CmpX13 Δ*cyaA* on two plasmids. The first plasmid harbors a PAC gene cassette, the expression of which is controlled by inductor addition. Once functionally expressed, the PAC enzyme catalyzes the production of intracellular 3′, 5′-cyclic adenosine monophosphate (cAMP) depending upon illumination. cAMP binds to the endogenous catabolite activator protein (CAP) and the resultant CAP:cAMP complex induces expression of the red-fluorescent reporter *Ds*Red from the second plasmid denoted pCyclR. (B) *Ds*Red reporter-gene activity for cultures expressing bPAC at different strength as controlled by L-arabinose addition. Readings for cultures incubated in darkness or under 40 μW cm^{-2} 470-nm light are shown in black and blue, respectively. Cultures expressing CyaA instead of bPAC or carrying an empty expression vector serve as a positive and negative controls (indicated by the + and – signs). Fluorescence data were normalized to optical density of cultures and represent mean ± SD of four biological replicates. (C) Expression of bPAC was induced with 5 mM L-arabinose, and reporter-gene activity recorded at different intensities of continuous 470-nm illumination. (D) The response of bPAC, induced by 5 mM L-arabinose, to pulsed illumination of 470 nm and 40 μW cm^{-2} intensity was assessed.

to afford the interrogation of manifold cyclase variants and lighting regimes (color, intensity, duration, pulsed light). To meet these criteria, we envisioned a bacterial reporter assay based on the cAMP-dependent expression of a red-fluorescent reporter (Figure 1A). Intracellular, light-dependent cyclase activity could hence be linked to a stable readout which can be recorded in intact cells and is both sensitive and specific (criteria i and ii). Provided the fluorescence reporter persists over time, illumination of the system and readout can be temporally separated, and cross-talk thereby largely minimized (criterion iii). Lastly, fluorescence readout is compatible with many assay formats and can be detected with even single-cell sensitivity (criterion iv). To implement this system, we opted for the *E. coli lac* promoter which is intrinsically weak but comprises a binding site for the catabolite activator protein (Malan and McClure, 1984). Binding of the CAP:cAMP complex to this operator site strongly upregulates expression of downstream genes. We constructed the plasmid pCyclR in which this promoter controls expression of the *Ds*Red Express2 reporter (Strack et al., 2008), a stable, well-tolerated fluorescent protein suitable for whole-cell labeling (Ohlendorf et al., 2012; Richter et al., 2016). We first assessed the performance of this reporter system in the *E. coli* strain CmpX13 (Mathes et al., 2009) which is a BL21 derivative stably expressing a riboflavin transporter. Upon over-night cultivation at 37°C, CmpX13 cultures harboring pCyclR exhibited intense *Ds*Red fluorescence, indicative of strong promoter activity even in the absence of any photoactivated adenylyl cyclase. To reduce background activation of the *lac* promoter, we generated a knockout strain in which the endogenous *E. coli* adenylyl cyclase CyaA is disrupted. In the resultant CmpX13 Δ*cyaA* strain, the pCyclR reporter only yielded ~50-fold reduced, low fluorescence (Figure 1B; negative control). When CyaA was ectopically expressed from an additional medium-copy pBAD plasmid with pBR322 origin of replication, high fluorescence readout was restored, thus confirming principal functionality of the cAMP reporter assay. All subsequent experiments were carried out in the CmpX13 Δ*cyaA* strain.

To calibrate the system, we next replaced the CyaA cyclase in the pBAD plasmid with the photoactivated adenylyl cyclase bPAC that is sensitive to blue light. Upon introduction of this plasmid into the CmpX13 Δ*cyaA* pCyclR context, reporter fluorescence increased depending upon bPAC expression strength which was adjusted via addition of up to 10 mM of the inductor L-arabinose (Figure 1B). In the regime of strong expression, elevated reporter fluorescence developed even when cultures were incubated in darkness which is consistent with the substantial dark-state activity reported for bPAC (Ryu et al., 2010; Stierl et al., 2011) that exceeds that found in certain rhodopsin-coupled cyclases (Avelar et al., 2014; Gao et al., 2015; Scheib et al., 2015). To facilitate characterization of the system response to blue light, the cAMP reporter assay was implemented in 96-well microtiter-plate format. We could thus resort to a programmable matrix of light-emitting diodes (LED) for the illumination of MTPs that we recently reported (Hennemann et al., 2018). Briefly, this setup uses an Arduino open-electronics circuit board to individually control an eight-by-eight array of three-color LEDs with peak wavelengths of 470, 525, and 620 nm. We deployed this setup to assess the response of bPAC within the reporter context to constant illumination at 40 $\mu W\ cm^{-2}$ blue light (470 nm) at different concentrations of the inductor L-arabinose. For all inductor amounts greater than zero, *Ds*Red reporter fluorescence was elevated under blue light relative to darkness, with the most pronounced difference of ~4.4-fold observed for 5 mM L-arabinose. We note that considerably larger light:dark differences in activity above 100-fold were reported for bPAC when analyzed by high-performance liquid chromatography (HPLC) (Ryu et al., 2010; Stierl et al., 2011). The comparatively diminished difference in our reporter assay is likely due to leakiness of the *lac* promoter, background fluorescence and potentially to non-linearities in the system response, e.g. caused by cooperative reaction steps. That notwithstanding, the cAMP reporter assay qualitatively replicates previous findings for bPAC and hence is suited to characterize the performance of this photoreceptor inside bacterial cells. We repeated the experiment at 5 mM arabinose for different intensities of constant blue-light illumination (Figure 1C). The *Ds*Red reporter fluorescence increased hyperbolically with intensity, and a half-maximal dose of $(3.8 \pm 0.8)\ \mu W\ cm^{-2}$ was obtained. Notably, a much higher half-maximal dose of $(3.7 \pm 0.4)\ \mu W\ mm^{-2}$ was determined for the light-induced activation of purified bPAC protein (Stierl et al., 2011). Likewise, in our own measurements, the half-maximal dose for bPAC activation in a coupled reporter assay within mammalian cells amounted to $(5.8 \pm 0.1)\ \mu W\ mm^{-2}$ (Richter et al., 2015). We note that both these earlier measurements reported on acute bPAC activity whereas our current assay integrates bPAC activity over an extended period. Although the underlying reasons remain unclear, these differences between the assays may underpin the observed discrepancy in half-maximal dose for bPAC activation. We next assessed the effect of intermittently applied illumination which can enable multiplexing of several light-responsive circuits and reduce overall required light dose (Hennemann et al., 2018) (Figure 1D). To this end, bacterial cultures were periodically illuminated by blue-light pulses of 40 $\mu W\ cm^{-2}$

intensity and 1 min duration followed by dark periods of 0–60 min. Reporter fluorescence increased as a function of duty cycle (defined as the fraction of time during which illumination was applied) with a half-maximal duty cycle of (32 ± 6)%.

Characterization of red-light-regulated adenylyl cyclases

Having established an efficient test bed for photoactivated adenylyl cyclases, we sought to extend our analysis to other PACs. Variants deriving from the fusion of bacteriophytochrome photosensors with cyclase effector domains (Ryu et al., 2014; Etzl et al., 2018) are regulated by red and far-red light and are of prime interest for at least two principal reasons. First, BPhys are photochromic in that red and far-red light drive the bidirectional transition between the two (meta)stable states Pr and Pfr, thus potentially enabling enhanced precision in space and time (Ziegler and Möglich, 2015). Second, light of longer wavelengths exhibits deeper penetration in tissue which is of particular relevance for *in vivo* optogenetics (Shu et al., 2009). Although our original programmable LED setup can also emit red light (at ~620 nm), a far-red option is missing (Hennemann et al., 2018). We hence designed a new programmable, dual-color LED matrix that allows the use of custom LEDs, including such that emit in the red and far-red spectral range. As illustrated in Figure 2, we outfitted the matrix with two sets of 64 LEDs with emission wavelengths of (655 ± 10) and (850 ± 21) nm, respectively, the intensity and timing of which can be programmed. Thus equipped, we analyzed the red-light-regulated PAC PaaC in the pCyclR reporter-gene setup. To this end, we cloned the *PaaC* gene into a medium-copy pCDF plasmid that also harbors an expression cassette for *Synechocystis* sp. heme oxygenase 1 (*Ss*HO1), an enzyme which provides the biliverdin chromophore via oxidative cleavage of heme. The expression of both PaaC and *Ss*HO1 from this plasmid can be adjusted via addition of the inductor isopropyl β-D-1-thiogalactopyranoside (IPTG). We introduced the plasmid into the CmpX13 Δ*cyaA* pCyclR context and measured reporter readout after incubation in darkness or under constant illumination with 655 or 850 nm at 40 μW cm^{-2} intensity (Figure 3A). For samples incubated in darkness, low *Ds*Red fluorescence was obtained that only slightly increased with inductor concentration. For the cultures grown under 655-nm light, *Ds*Red fluorescence was elevated relative to the dark-incubated samples, with a maximally 9-fold upregulation at 1 mM IPTG. Unexpectedly, illumination with 850 nm also prompted an increase in reporter fluorescence to around 40% of the values observed for illumination with 655 nm. Although the peak wavelength of the LED at 850 nm is well separated from the absorption spectrum of the Pr state of the *Dr*BPhy photosensor (Figure 4A), evidently the short-wavelength tail of the emission spectrum suffices for actuating PaaC. To arrive at a better understanding of this effect, we reran the experiment at a constant inductor concentration of 1 mM but varying intensities of constant illumination with either 655 nm or 850 nm (Figure 3B). For both light qualities, *Ds*Red reporter fluorescence hyperbolically increased with intensity and displayed half-maximal

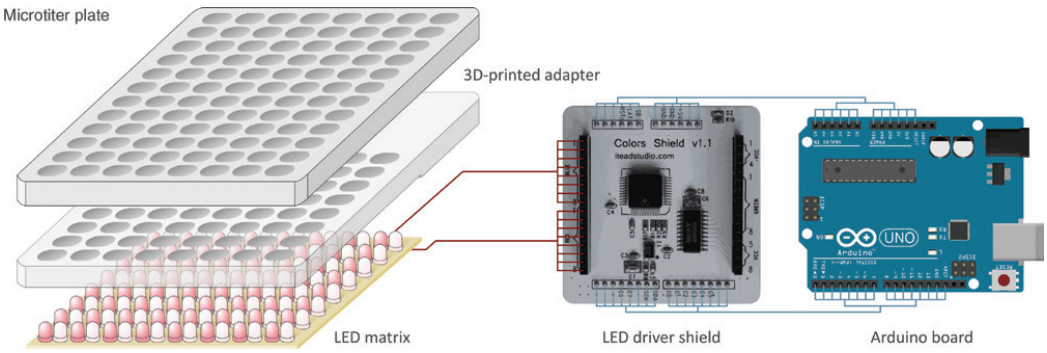

Figure 2: Schematic of a programmable matrix of light-emitting diodes (LED) for the illumination of microtiter plates (MTP).
A circuit board was outfitted with two sets of 64 LEDs with peak emission wavelengths of 655 and 850 nm. A 3D-printed adapter encases this board and enables the illumination from below of 64 wells of an MTP with one 655-nm and one 850-nm LED per well. Timing and intensity of the LEDs can be individually configured via a driver shield that is controlled by a conventional Arduino board. Programming of the LED matrix is facilitated by a graphical user interface implemented in Python.

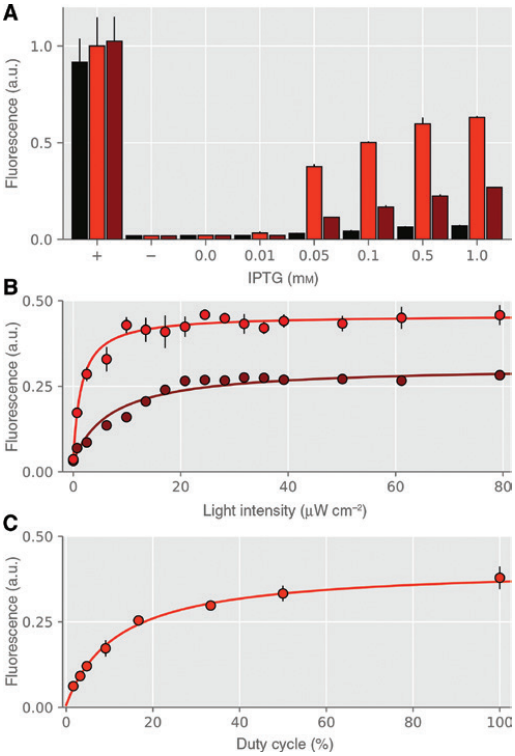

Figure 3: Reporter-gene assay for PaaC.
(A) Expression of PaaC was induced by IPTG addition and *Ds*Red reporter readout recorded for cultures grown in darkness (black) or under constant illumination with 655 nm (red) or 850 nm (brown). CyaA positive and empty-vector negative controls are denoted by + and – signs. (B) Reporter-gene activity for PaaC, induced with 0.05 mM IPTG, under constant illumination with 655-and 850-nm light of different intensities. (C) Reporter readout for application of intermittent 655-nm light at 40 μW cm^{-2} intensity.

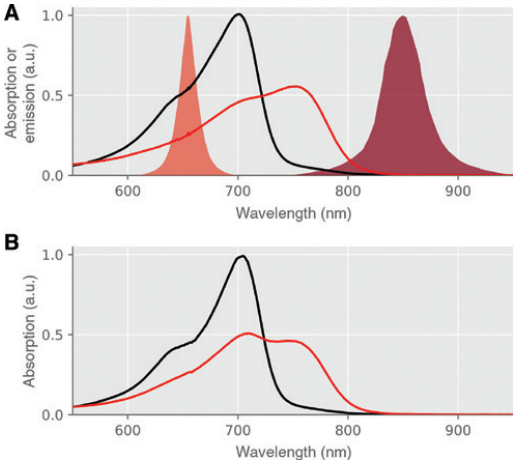

Figure 4: Absorption spectra of bacteriophytochrome proteins and emission spectra of LEDs used in programmable matrix.
(A) The absorption spectra of the PAS-GAF-PHY PCM from *D. radiodurans* following saturating illumination with red and far-red light, respectively, are drawn as red and black lines. The emission spectra of the 655-nm and 855-nm LEDs are shown as shaded areas in red and brown. (B) The absorption spectra of the PCM from *D. deserti* following saturating illumination with red and far-red light, respectively, are drawn as red and black lines.

doses of (2.0 ± 0.4) and (7.0 ± 1.6) μW cm^{-2}, respectively. The observation that near-infrared light activates PaaC to considerable extent is reminiscent of the red-light-activated phosphodiesterase LAPD which is also based on the *Dr*BPhy photosensor (Gasser et al., 2014). In this system, red light prompted an increase of catalytic activity that could only be partially reverted by near-infrared light. In marked contrast to the present findings for PaaC, illumination of dark-adapted LAPD with 850 nm did not upregulate catalytic activity. We also subjected the PaaC-expressing cultures to intermittent illumination with 655 nm at 40 μW cm^{-2} and found that *Ds*Red reporter fluorescence increased with a half-maximal duty cycle of (12 ± 2)% (Figure 3C).

Engineering red-light-regulated adenylyl cyclases

We next addressed whether the design blueprint underpinning PaaC developed by the Winkler group (Etzl et al., 2018) and based on pioneering work by the Gomelsky laboratory (Ryu et al., 2014) extends to other BPhy photosensors. Put another way, is it possible to construct additional red-light-sensitive PACs according to the same rationale, and if so, do the resultant photoreceptors differ in their properties? In addressing these questions, we capitalized on the test bed that we implemented for light-regulated adenylyl cyclases. We replaced the *Dr*Bphy photosensor module in PaaC by the homologous PCM segments of the BPhys from *Deinococcus deserti* (*Dd*BPhy), *Pseudomonas aeruginosa* (*Pa*BPhy) and *Janthinobacter* CG23_2 (*Ja*BPhy). As the length of the linker between photosensor and effector moieties can greatly alter activity and regulation by light of photoreceptors (Möglich et al., 2009; Gasser et al., 2014; Ryu et al., 2014; Etzl et al., 2018), we retained the linker length used in PaaC (Figure 5). The choice of the specific BPhys was motivated by the close homology between *Dd*BPhy and *Dr*BPhy, and by *Pa*BPhy being a bathy-bacteriophytochrome (Yang et al., 2008)

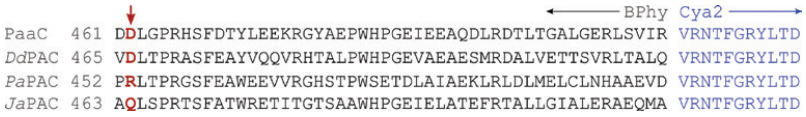

Figure 5: Sequence alignment of engineered BPhy-cyclases.
The design blueprint PaaC (Etzl et al., 2018) informs the construction of *Dd*PAC, *Pa*PAC and *Ja*PAC. Note that all these BPhy-cyclases are constructed in the same residue register and thus have linkers of the same length between the BPhy photosensor and the adenylyl-cyclase effector modules. The red arrow denotes a residue position that usually is occupied by an aspartate in canonical BPhys (Escobar et al., 2017).

which assumes in its dark-adapted state the Pfr form rather than Pr (Rockwell and Lagarias, 2010). The *Ja*BPhy had not been previously characterized in depth but sequence comparisons tentatively assign it as a bathy-BPhy as well; in particular, an aspartate residue within the PHY tongue region prevalent in canonical BPhys is absent from *Ja*BPhy (Escobar et al., 2017) (cf. Figure 5, red arrow). As before, we assessed light-regulated cyclase activity in the CmpX13 Δ*cyaA* pCyclR system in either darkness or under illumination with 40 µW cm^{-2} 655-nm and 850-nm light. In case of the *Dd*BPhy-based variant denoted *Dd*PAC, *Ds*Red reporter fluorescence for samples incubated under 655-nm light increased with inductor concentration but stayed essentially constant for samples incubated in darkness (Figure 6A). In marked contrast to PaaC, *Dd*PAC showed no upregulation of reporter fluorescence with 850-nm light but a slight reduction compared to darkness. The maximum differences between the readout for dark and 655-nm incubation amounted to 9.8-fold, and that between 655-nm and 850-nm illumination to 9.1-fold (Figure 6B). The absorption spectra of the isolated *Dd*Bphy PAS-GAF-PHY PCM prior and after red-light illumination closely resembled those obtained for *Dr*Bphy (Figure 4B). The variants *Pa*PAC and *Ja*PAC based on the *bona fide* and putative bathy-BPhys *Pa*Bphy and *Ja*BPhy showed similar behavior in that reporter readout increased with inductor concentration for all lighting conditions (Figures 7A and 8A). Interestingly, illumination with 655 and 850 nm upregulated *Ds*Red fluorescence to the same extent and with similar sensitivity (Figures 7B, C and 8B, C). Taken together, all three PaaC derivatives are genuine PACs with activity that is enhanced by light. The absence of activation by 850-nm light in the *Dd*PAC variant might be of advantage for eventual applications in optogenetics, and we thus characterized this protein in more detail. We analyzed cultures, which harbored *Dd*PAC and were incubated under varying intensities of 655-nm light and found that *Ds*Red fluorescence hyperbolically increased with a half-maximal intensity of (8.8 ± 1.6) µW cm^{-2}, comparable to the value for PaaC. By contrast, no increase in reporter readout was observed with 855-nm light, even at intensities of up to 80 µW cm^{-2} (Figure 6B). Pulsed illumination with 655-nm light enhanced reporter readout with a half-maximal duty cycle of (26 ± 4)% (Figure 6C). To determine specific enzymatic activities, we expressed and purified *Dd*PAC, and conducted multiple-turnover measurements (Figure 6D). The specific activity for *Dd*PAC incubated in darkness or under red light amounted to (8.8 ± 0.1) and (61.0 ± 2.8) · 10^{-3} mol cAMP (mol enzyme · min)$^{-1}$, respectively, corresponding to a ~6.9-fold difference (Figure 6E). When *Dd*PAC was incubated under red light followed by far-red illumination, turnover was decreased to (8.5 ± 0.1) · 10^{-3} mol cAMP (mol enzyme · min)$^{-1}$, which is around 7.2-fold less than under red light. For comparison, PaaC showed similar overall adenylyl cyclase activity with a 3.8-fold difference between dark-adapted and red-light-exposed enzyme; the influence of subsequent illumination with far-red light was not investigated (Etzl et al., 2018).

Discussion

As evidenced by measurements on two different PAC classes, the reporter setup established in this work provides an efficient test environment for the analysis and optimization of these photoreceptors. By linking light-dependent cyclase activity to bacterial expression of the fluorescent reporter *Ds*Red, we achieve sensitive readout that should be compatible with various assay formats and illumination protocols. In contrast to measurements by HPLC, ELISA or BCECF fluorescence (cf. Introduction), our assay reports on AC activity only indirectly, and hence specific enzyme activities cannot be determined. Moreover, as reporter fluorescence is usually evaluated at the end of prolonged incubation and illumination periods, a value that reflects AC activity integrated over time is obtained rather than acute activity readings. In addition, measurements with the cAMP reporter-gene assay will be influenced by the cellular environment and constituents of *E. coli*, not least by the endogenous cAMP-specific PDE CpdA. Notwithstanding these inherent limitations, which

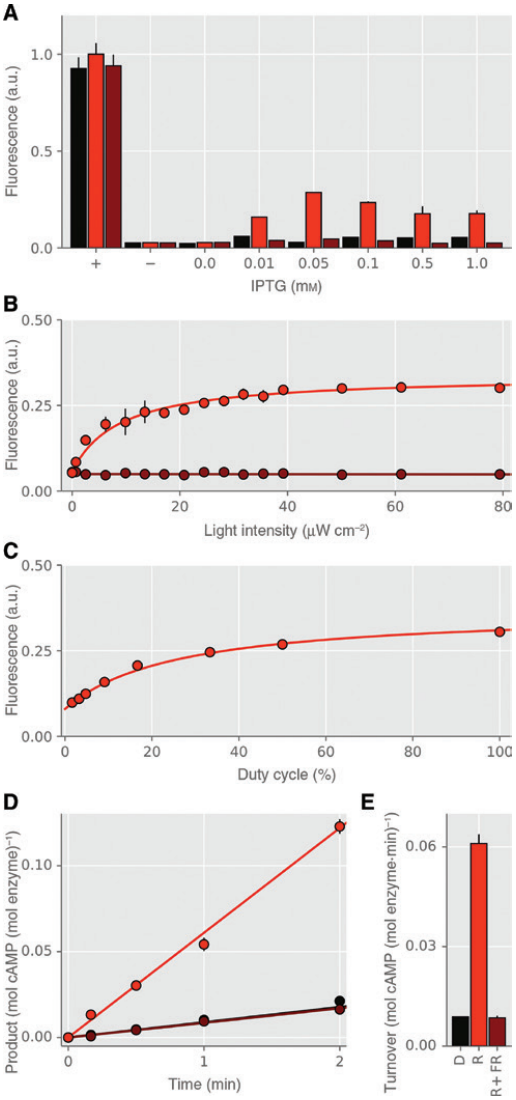

Figure 6: Reporter-gene assay for *Dd*PAC.
(A) Expression of *Dd*PAC was induced by IPTG addition and *Ds*Red reporter readout recorded for cultures grown in darkness (black) or under constant illumination with 655 nm (red) or 850 nm (brown). CyaA positive and empty-vector negative controls are denoted by + and – signs, as described in Figure 3. (B) Reporter-gene activity for *Dd*PAC, induced with 0.05 mM IPTG, under constant illumination with 655-and 850-nm light of different intensities. (C) Reporter readout for application of intermittent 655-nm light at 40 µW cm^{-2} intensity. (D) Adenylyl cyclase activity measured by HPLC for *Dd*PAC incubated in darkness (black), under red light (red), or under red light followed by far-red light (brown). (E) Initial reaction velocities from (D).

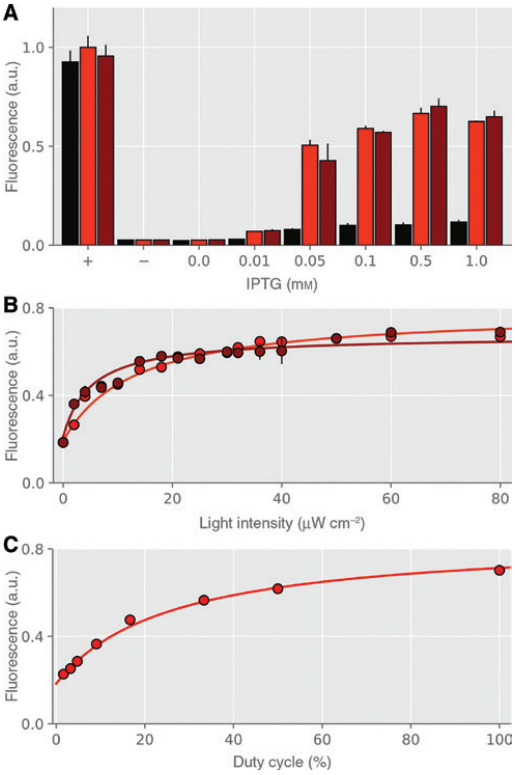

Figure 7: Reporter-gene assay for *Pa*PAC.
(A) Expression of *Pa*PAC was induced by IPTG addition and *Ds*Red reporter readout recorded for cultures grown in darkness (black) or under constant illumination with 655 nm (red) or 850 nm (brown). CyaA positive and empty-vector negative controls are denoted by + and – signs, as described in Figure 3. (B) Reporter-gene activity for *Pa*PAC, induced with 0.5 mM IPTG, under constant illumination with 655-and 850-nm light of different intensities. (C) Reporter readout for application of intermittent 655-nm light at 40 µW cm^{-2} intensity.

also apply to other bacterial assays, e.g. detection via X-gal, the pCyclR setup enables the qualitative characterization of PACs within a cellular setting. The reporter assay lends itself to parallelization and hence to the screening of novel and improved PAC variants. In particular, the fluorescence readout of AC activity enables analysis by flow cytometry and thus facilitates the engineering of enhanced PAC variants via directed evolution and related approaches (Gleichmann et al., 2013).

We combined the facile activity readout afforded by the pCyclR system with custom-built setups for the controllable and parallelizable illumination of samples. Both our previous matrix of light-emitting diodes

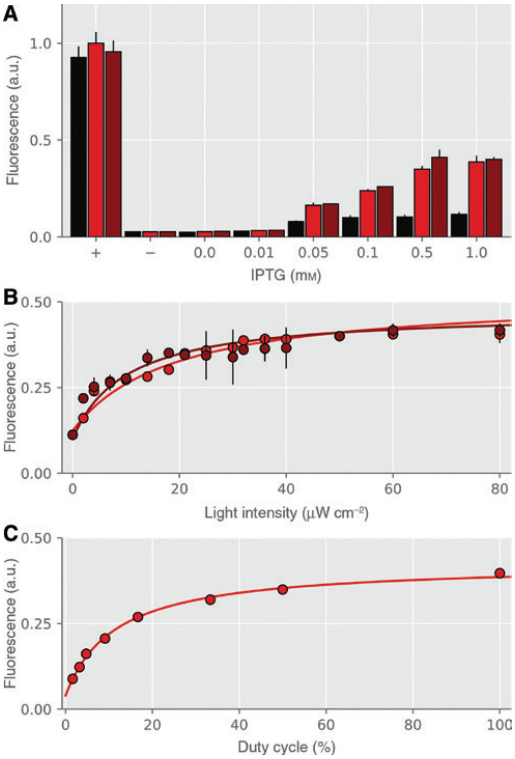

Figure 8: Reporter-gene assay for *Ja*PAC.
(A) Expression of *Ja*PAC was induced by IPTG addition and *Ds*Red reporter readout recorded for cultures grown in darkness (black) or under constant illumination with 655 nm (red) or 850 nm (brown). CyaA positive and empty-vector negative controls are denoted by + and – signs, as described in Figure 3. (B) Reporter-gene activity for *Ja*PAC, induced with 0.5 mM IPTG, under constant illumination with 655-and 850-nm light of different intensities. (C) Reporter readout for application of intermittent 655-nm light at 40 µW cm^{-2} intensity.

(Hennemann et al., 2018) and the present one are based on open electronics and commercially available, inexpensive parts. Thus, these setups can be readily implemented in most laboratories. The availability of LED matrices of different light color stands to also enable the analysis and optimization of PACs other than bPAC and IlaC. In particular, the new setup can be equipped with custom LEDs of the required wavelength. An obvious requirement for applying our test bed to other PACs is that they can be functionally expressed in *E. coli* which may for instance prove challenging for the transmembrane rhodopsin-based nucleotidyl cyclases. Currently, our system is restricted to the analysis of AC activity but an extension to measurements of GC activity is conceivable. As remarked above, certain bacteria possess cGMP-specific CAP variants which might be integrated into our reporter assay. Alternatively, the test environment may be expanded to efficiently screen the activity of cNMP-specific PDEs. More generally, related test and screening platforms could also be established for other second messengers. In particular, bacteriophytochrome photosensors are known to regulate the activity of GGDEF enzymes which catalyze the production of cyclic diguanylate (Ryu and Gomelsky, 2014). Provided a pertinent reporter-gene assay can be built, these enzymes might also be analyzed in efficient manner.

The analysis of bPAC and PaaC in our test environment revealed residual background activity in darkness, especially in the regime of strong PAC expression. These findings are in line with previous reports on these PACs and indicate scope for improvement. Unexpectedly, PaaC was also activated by 850-nm illumination to around half-maximal extent, presumably due to the short-wavelength flank of the LED emission spectrum. Whereas the activation by 655 nm showed a half-maximal dose of (2.0 ± 0.4) µW cm^{-2}, that by 850 nm yielded a value of (7.0 ± 1.6) µW cm^{-2}. Although PaaC thus appears more sensitive to 655-nm light, activation by 850-nm light is substantial. These findings indicate that the light-driven Pfr→Pr transition in PaaC is inefficient compared to the Pr→Pfr transition that entails increase of AC activity. Related observations were made for LAPD which shares with PaaC the *Dr*BPhy PCM; following prior activation of LAPD with red light, far-red light could not fully shut off PDE activity (Gasser et al., 2014). It is currently unclear whether these traits of PaaC and LAPD have the same origin, whether they are rooted in the *Dr*BPhy PCM, or whether they are due to the fusion with a heterologous effector module. Detailed biochemical, enzymatic and photochemical analyses will be required to resolve this question.

In the meantime, we have applied our test bed to engineer PaaC derivatives that are directly based on the blueprint developed by the Winkler group (Etzl et al., 2018). Strikingly, we succeeded in engineering novel PACs for all three BPhy PCMs we tried, suggesting that the design rationale is robust and portable to other photosensors and, by extension, possibly to other effectors. All three PACs presently generated showed light responses that markedly differ from that of PaaC. The variants *Pa*PAC and *Ja*PAC were activated equally well by 655- and 850-nm light. Although this finding implies impairment of the light-driven Pr↔Pfr transition, cf. above, these PACs may still be interesting for optogenetic deployment as they are efficiently activated by near-infrared light. As mentioned in the introduction, light of these wavelengths

exhibits superior tissue penetration, and hence these PACs may be attractive for applications *in vivo*. Finally, the *Dd*PAC variant differs from PaaC by not showing appreciable activation by 850-nm light despite absorption properties of its photosensor module that closely correspond to that of PaaC (cf. Figure 4). Measurements of the specific activity showed that *Dd*PAC can be effectively switched off by far-red light. Although the underlying reasons for the difference to PaaC are unclear, this behavior may indicate improved Pr↔Pfr photoswitching in *Dd*PAC. By capitalizing on the PAC test bed presently implemented, *Dd*PAC can be readily diversified and thus potentially enhanced. Specifically, the length and composition of the linker between photosensor and effector may be varied. Comparable modifications in the linkers of several engineered, homodimeric photoreceptors modulated activity and regulation by light (Möglich et al., 2009; Gasser et al., 2014; Ryu et al., 2014; Ohlendorf et al., 2016; Etzl et al., 2018). The already existing and upcoming new PAC variants stand to enrich optogenetics and facilitate the precise analysis of manifold processes mediated by cNMPs across diverse organisms.

Materials and methods

Molecular biology

The gene encoding bPAC from *Beggiatoa* sp. was excised from an earlier expression plasmid (Stierl et al., 2011) and cloned into the pBADM-30 vector under control of the arabinose-inducible pBAD promoter by restriction digest with SpeI and HindIII (gift by M. Stierl). Enzymes for molecular biology were obtained from Thermo Fisher Scientific (Dreieich, Germany). As a positive control, the adenylyl cyclase CyaA was amplified by PCR from *E. coli* BL21 genomic DNA and cloned into the pBADM-30 plasmid by restriction digest with SpeI and KpnI (primers 5′-GCA CAG ACT AGT TTG TAC CTC TAT ATT GAG AC-3′ and 5′-CTG TTG GGT ACC TCA CGA AAA ATA TTG CTG-3′; restriction sites underlined); an empty pBADM-30 vector served as negative control in experiments on bPAC. To construct *PaaC* (Etzl et al., 2018), a gene encoding residues 410–756 of Cya2 from *Synechocystis* PCC6803 and bearing the E488K substitution (Rauch et al., 2008) was synthesized with *E. coli*-adapted codon usage (GeneArt, Regensburg, Germany). This fragment was then fused to the 3′ end of a gene encoding the PCM of *D. radiodurans* BPhy (residues 1–510) via Gibson assembly and cloned (Gibson et al., 2009) into the pCDFDuet vector (Novagen, Darmstadt, Germany) under control of a T7 promoter inducible by IPTG. To aid production of the biliverdin chromophore of BPhys, the *Synechocystis* sp. heme oxygenase 1 gene was additionally placed on the same plasmid under control of T7 and IPTG induction. To this end, the corresponding gene was amplified by PCR from pKT270 (Mukougawa et al., 2006), using the primers 5′-GGA GAT ATA CAT ATG AGT G-3′ and 5′-CTA TTC TCG AGC TAG CCT TCG GAG GTG GC-3′, and cloned into pCDFDuet by restriction digest with NdeI/XhoI. A pCDFDuet vector harboring the heme oxygenase but no cyclase gene served as negative control in the experiments. Other BPhy-cyclase variants were cloned by replacing the *Dr*BPhy moiety of PaaC via Gibson assembly. The gene encoding the PCM of *P. aeruginosa* BPhy (residues 1–501) was amplified from a pET-24a-based vector described in (Yang et al., 2008); genes encoding the PCMs of the *D. deserti* (residues 1–514) and *Janthinobacter* CG23_2 BPhys (residues 1–512) were synthesized with *E. coli* codon adaptation. To construct the pCyclR reporter plasmid, the promoter region in the pET-28c-*Ds*Red plasmid (Ohlendorf et al., 2012) was excised with *Bgl*II/*Xba*I and replaced with a promoter fragment of the *lac* operon from *E. coli* BL21 that includes the CAP binding site (nucleotides −84 to +1 relative to the transcription start site).

The Δ*cyaA* knockout variant of the *E. coli* strain CmpX13 (Mathes et al., 2009) was generated according to (Datsenko and Wanner, 2000). Briefly, a kanamycin resistance cassette was amplified by PCR from plasmid pKD4 with the primers 5′-GTT GGC GGA ATC ACA GTC ATG ACG GGT AGC AAA TCA GGC GAT ACG TCT TGG TGT AGG CTG GAG CTG CTT C-3′ and 5′-CGG ATA AGC CTC GCT TTC CGG CAC GTT CAT CAC GAA AAA TAT TGC TGT AAC GGC TGA CAT GGG AAT TAG C-3′, where the flanking regions homologous to the *E. coli cyaA* gene are underlined. The resultant linear PCR fragment was transformed into CmpX13 along with the pKD46 plasmid encoding the λ Red recombinase. Bacteria were selected for genome integration of the cassette by incubation on LB/kanamycin agar. The antibiotic resistance marker was subsequently removed by Flp recombinase encoded on the pCP20 plasmid.

Programmable matrix of light-emitting diodes

For experiments with bPAC, we adapted a previously designed matrix of 8-by-8 individually programmable three-color light-emitting diodes (Hennemann et al., 2018). Briefly, the setup allows the illumination of individual wells of microtiter plates and is realized based on Arduino open electronics and a three-dimensional (3D)-printed housing. A Python/Qt-based graphical user interface allows facile configuration of the LED matrix. In the present revamped design, we adjusted the housing to further minimize light contamination between adjacent wells, and we expanded the Python software to allow the setting of an initial lag period prior to start of illumination. By contrast, the electronics *per se* remained unchanged. Updated versions of the software and template files for the housing are freely available from http://www.moeglich.uni-bayreuth.de/en/software.

To achieve programmable illumination of microtiter plates with diverse, customizable LEDs, e.g. red and far-red ones, particularly applicable for experiments with plant and bacterial phytochromes, we reconstructed the programmable LED matrix from scratch. As illustrated in Figure 2, we combined a regular Arduino Uno board with the 'ITEAD Full Color RGB LED Matrix Driver Shield' (Itead, Shenzhen, China). A circuit layout for individually addressing two sets of 8-by-8 LEDs each was designed and printed by the electrical workshop at the University of Bayreuth. We then equipped the circuit board with 64 3-mm 655-nm LEDs [full width at half maximum (fwhm) 20 nm, Kingbright WP908A8SRD] and 64 3-mm 850-nm LEDs (fwhm 42 nm, Harvatek HE1-120AC-XXXX). To fit the new setup, the 3D-printed housing was adjusted accordingly. To allow ready configuration of the revamped setup, we refactored the Python program and the underlying Arduino code but essentially

retained the graphical user interface. A wiring diagram, templates for the circuit board and the housing, and the Python software can be obtained from the mentioned URL. Via the software interface, the light intensities of the LEDs can be adjusted by pulse-width modulation in increments from 0 to 255. The resulting effective light intensities were calibrated with a power meter (model 842-PE, Newport, Darmstadt, Germany) equipped with a silicon photodetector (model 918D-UV-OD3, Newport).

Cyclase reporter-gene assays

The reporter plasmid pCyclR was transformed into chemically competent CmpX13 Δ*cyaA* cells. Empty control vectors (pBADM-30 and pCDFDuet negative controls, cf. above) or plasmids encoding bPAC, various BPhy-cyclases and *E. coli* CyaA (positive control) were additionally introduced into these cells by chemical transformation. Liquid cultures of 5 ml lysogeny broth (LB) supplemented with 50 μg ml^{-1} kanamycin (for the pCyclR plasmid) and 50 μg ml^{-1} ampicillin (for pBADM-30) or 100 μg ml^{-1} streptomycin (for pCDFDuet) were inoculated and grown for 18 h at 37°C. Cultures were then diluted 100-fold in LB (supplemented with antibiotics) and transferred to black-wall clear-bottom 96-well microtiter plates (Greiner BioOne, Frickenhausen, Germany) in a volume of 200 μl per well. MTPs were sealed with gas-permeable sealing film (BF-400-S, Corning, New York, NY, USA) and incubated for 1 h at 37°C (HN-2 Herp Nursery II, Lucky Reptile, Waldkirch, Germany) and 800 rpm (MTP shaker, PMS-1000i, Grant Instruments, Cambridge, UK). Expression of cyclases was then induced by addition of varying amounts of L-arabinose (for bPAC) or IPTG (for BPhy-cyclases); expression of the positive control CyaA was induced by addition of 10 mM L-arabinose. The incubation of cultures continued for 21 h at 37°C with illumination of the MTP from below via programmable LED arrays, after which the optical density at 600 nm (OD_{600}) and *Ds*Red fluorescence of the bacterial cultures were measured in a Tecan Infinite M200 PRO plate reader (Tecan Group Ltd., Männedorf, Switzerland). For fluorescence detection, excitation and emission wavelengths of (554 ± 9) nm and (591 ± 20) nm, respectively, were used. Fluorescence readings were normalized to OD_{600} and are reported as averages of four biological replicates ± standard deviation (SD), where replicates correspond to separate cultures inoculated from individual bacterial clones. Note that introduction of pCyclR into the CmpX13 Δ*cyaA* strain alone increased fluorescence by around 10-fold compared to the empty bacterial strain. Data were evaluated and plotted with the Fit-o-mat software (Möglich, 2018).

Protein purification and high-performance liquid chromatography

The pCDFDuet plasmid encoding the *Synechocystis* sp. heme oxygenase and *Dd*PAC with a C-terminal His_6 tag (cf. above) was transformed into chemically competent *E. coli* LOBSTR cells (Andersen et al., 2013). Bacteria were grown in LB medium supplemented with 100 μg ml^{-1} streptomycin at 37°C and 200 rpm. Upon reaching midlogarithmic phase (optical density at 600 nm of ~0.6), the bacterial cultures were cooled to 16°C, and 1 mM IPTG and 0.5 mM 5-aminolevulinic acid were added. After incubation for 16 h at 16°C and 200 rpm, cells were harvested and resuspended in lysis buffer [50 mM Tris/HCl pH 8.0, 20 mM NaCl, 20 mM imidazole, complemented with protease inhibitor mix (Roche, Darmstadt, Germany)]. Lysis was performed via sonication, and the supernatant was applied to a gravity-flow cobalt-sepharose column (HisPur, Thermo Fisher Scientific). Upon washing, the protein was eluted with 200 mM imidazole and dialyzed overnight into 50 mM Tris/HCl pH 8.0, 20 mM NaCl. The protein was further purified by anion-exchange chromatography on a HiTrap Q HP column (Macherey and Nagel, Düren, Germany). Purified protein was dialyzed against storage buffer [50 mM Tris/HCl pH 8.0, 20 mM NaCl, 20% (w/v) glycerol], concentrated, flash-frozen in liquid nitrogen, and stored at −80°C.

Adenylyl cyclase activity of *Dd*PAC was assessed by HPLC as described by (Etzl et al., 2018). To this end, 20 μM *Dd*PAC was incubated at 20°C in assay buffer (50 mM HEPES pH 7.0, 150 mM NaCl, 50 mM $MgCl_2$) in the presence of 1 mM substrate ATP. Prior to the measurement, *Dd*PAC was either kept in darkness, or exposed to red light (670 nm, 40 μW cm^{-2}, 60 s), or exposed to red light followed by illumination with far-red light (780 nm, 80 μW cm^{-2}, 60 s). Reaction aliquots were taken at discrete times, incubated at 95°C for 1 min to stop the reaction, and then cleared by centrifugation for 5 min at 20 000 *g*. Samples were analyzed on a Kinetex 5u EVO C18 reverse-phase column on a Waters Acquity UPLC using isocratic conditions [20 mM ammonium acetate pH 4.5, 3% (v/v) acetonitrile]. Peak areas were integrated with the Waters Empower software and calibrated against cAMP and ATP standards. All measurements were performed in triplicate.

Acknowledgments: We thank members of the Möglich laboratory for discussions, Dr. Manuela Stierl for providing the pBADM-30-bPAC plasmid, Dr. Tilo Mathes for advice on generating the CmpX13 Δ*cyaA* knockout strain, Norbert Grillenbeck for technical support, and Dr. Markus Lippitz for advice on the design of the LED matrix. We are indebted to the electrical workshop at the University of Bayreuth for circuit-board design and overall stellar support. Funding through Boehringer-Ingelheim Fonds (R.O.), funder id: 10.13039/100005156, a Sofja-Kovalevskaya Award (to A.M.) by the Alexander-von-Humboldt Foundation, and Deutsche Forschungsgemeinschaft (funder id: 10.13039/501100001659, grant MO21921/4-1) is gratefully acknowledged.

References

Andersen, K.R., Leksa, N.C., and Schwartz, T.U. (2013). Optimized *E. coli* expression strain LOBSTR eliminates common contaminants from His-tag purification. Proteins Struct. Funct. Bioinform. *81*, 1857–1861.

Andrée, B., Hillemann, T., Kessler-Icekson, G., Schmitt-John, T., Jockusch, H., Arnold, H.-H., and Brand, T. (2000). Isolation and characterization of the novel Popeye gene family expressed in skeletal muscle and heart. Dev. Biol. *223*, 371–382.

Ashman, D.F., Lipton, R., Melicow, M.M., and Price, T.D. (1963). Isolation of adenosine 3′, 5′-monophosphate and guanosine 3′, 5′-monophosphate from rat urine. Biochem. Biophys. Res. Commun. *11*, 330–334.

Avelar, G.M., Schumacher, R.I., Zaini, P.A., Leonard, G., Richards, T.A., and Gomes, S.L. (2014). A rhodopsin-guanylyl cyclase gene fusion functions in visual perception in a fungus. Curr. Biol. *24*, 1234–1240.

Blain-Hartung, M., Rockwell, N.C., Moreno, M.V., Martin, S.S., Gan, F., Bryant, D.A., and Lagarias, J.C. (2018). Cyanobacteriochrome-based photoswitchable adenylyl cyclases (cPACs) for broad spectrum light regulation of cAMP levels in cells. J. Biol. Chem. *293*, 8473–8483.

Datsenko, K.A. and Wanner, B.L. (2000). One-step inactivation of chromosomal genes in *Escherichia coli* K-12 using PCR products. Proc. Natl. Acad. Sci. USA *97*, 6640–6645.

de Rooij, J., Zwartkruis, F.J.T., Verheijen, M.H.G., Cool, R.H., Nijman, S.M.B., Wittinghofer, A., and Bos, J.L. (1998). Epac is a Rap1 guanine-nucleotide-exchange factor directly activated by cyclic AMP. Nature *396*, 474–477.

Deisseroth, K., Feng, G., Majewska, A.K., Miesenböck, G., Ting, A., and Schnitzer, M.J. (2006). Next-generation optical technologies for illuminating genetically targeted brain circuits. J. Neurosci. *26*, 10380–10386.

Escobar, F.V., Buhrke, D., Michael, N., Sauthof, L., Wilkening, S., Tavraz, N.N., Salewski, J., Frankenberg-Dinkel, N., Mroginski, M.A., Scheerer, P., et al. (2017). Common structural elements in the chromophore binding pocket of the Pfr state of bathy phytochromes. Photochem. Photobiol. *93*, 724–732.

Etzl, S., Lindner, R., Nelson, M.D., and Winkler, A. (2018). Structure-guided design and functional characterization of an artificial red light–regulated guanylate/adenylate cyclase for optogenetic applications. J. Biol. Chem. *293*, 9078–9089.

Fesenko, E.E., Kolesnikov, S.S., and Lyubarsky, A.L. (1985). Induction by cyclic GMP of cationic conductance in plasma membrane of retinal rod outer segment. Nature *313*, 310–313.

Gao, S., Nagpal, J., Schneider, M.W., Kozjak-Pavlovic, V., Nagel, G., and Gottschalk, A. (2015). Optogenetic manipulation of cGMP in cells and animals by the tightly light-regulated guanylyl-cyclase opsin CyclOp. Nat. Commun. *6*, 8046.

Gasser, C., Taiber, S., Yeh, C.-M., Wittig, C.H., Hegemann, P., Ryu, S., Wunder, F., and Möglich, A. (2014). Engineering of a red-light-activated human cAMP/cGMP-specific phosphodiesterase. Proc. Natl. Acad. Sci. USA *111*, 8803–8808.

Gibson, D.G., Young, L., Chuang, R.-Y., Venter, J.C., Hutchison, C.A., and Smith, H.O. (2009). Enzymatic assembly of DNA molecules up to several hundred kilobases. Nat. Methods *6*, 343–345.

Gleichmann, T., Diensthuber, R.P., and Möglich, A. (2013). Charting the signal trajectory in a light-oxygen-voltage photoreceptor by random mutagenesis and covariance analysis. J. Biol. Chem. *288*, 29345–29355.

Gold, M.G., Gonen, T., and Scott, J.D. (2013). Local cAMP signaling in disease at a glance. J. Cell Sci. *126*, 4537–4543.

Gomelsky, M. (2011). cAMP, c-di-GMP, c-di-AMP and now cGMP: bacteria use them all! Mol. Microbiol. *79*, 562–565.

Gomelsky, M. and Klug, G. (2002). BLUF: a novel FAD-binding domain involved in sensory transduction in microorganisms. Trends Biochem. Sci. *27*, 497–500.

Görke, B. and Stülke, J. (2008). Carbon catabolite repression in bacteria: many ways to make the most out of nutrients. Nat. Rev. Microbiol. *6*, 613–624.

Hennemann, J., Iwasaki, R.S., Grund, T.N., Diensthuber, R.P., Richter, F., and Möglich, A. (2018). Optogenetic control by pulsed illumination. ChemBioChem *19*, 1296–1304.

Iseki, M., Matsunaga, S., Murakami, A., Ohno, K., Shiga, K., Yoshida, K., Sugai, M., Takahashi, T., Hori, T., and Watanabe, M. (2002). A blue-light-activated adenylyl cyclase mediates photoavoidance in *Euglena gracilis*. Nature *415*, 1047–1051.

Jansen, V., Alvarez, L., Balbach, M., Strünker, T., Hegemann, P., Kaupp, U.B., and Wachten, D. (2015). Controlling fertilization and cAMP signaling in sperm by optogenetics. eLife *4*, e05161.

Jansen, V., Jikeli, J.F., and Wachten, D. (2017). How to control cyclic nucleotide signaling by light. Curr. Opin. Biotechnol. *48*, 15–20.

Jenal, U., Reinders, A., and Lori, C. (2017). Cyclic di-GMP: second messenger extraordinaire. Nat. Rev. Microbiol. *15*, 271–284.

Kim, T., Folcher, M., Baba, M.D.-E., and Fussenegger, M. (2015). A synthetic erectile optogenetic stimulator enabling blue-light-inducible penile erection. Angew. Chem. Int. Ed. *54*, 5933–5938.

Krauss, G. (2014). Biochemistry of Signal Transduction and Regulation (Weinheim, Germany: Wiley-VCH).

Kuo, J.F. and Greengard, P. (1970). Cyclic nucleotide-dependent protein kinases. VI. Isolation and partial purification of a protein kinase activated by guanosine 3′,5′-monophosphate. J. Biol. Chem. *245*, 2493–2498.

Losi, A., Gardner, K.H., and Möglich, A. (2018). Blue-light receptors for optogenetics. Chem. Rev. *118*, 10659–10709.

Malan, T.P. and McClure, W.R. (1984). Dual promoter control of the *Escherichia coli* lactose operon. Cell *39*, 173–180.

Marden, J.N., Dong, Q., Roychowdhury, S., Berleman, J.E., and Bauer, C.E. (2011). Cyclic GMP controls *Rhodospirillum centenum* cyst development. Mol. Microbiol. *79*, 600–615.

Mathes, T., Vogl, C., Stolz, J., and Hegemann, P. (2009). *In vivo* generation of flavoproteins with modified cofactors. J. Mol. Biol. *385*, 1511–1518.

McDonough, K.A. and Rodriguez, A. (2012). The myriad roles of cyclic AMP in microbial pathogens: from signal to sword. Nat. Rev. Microbiol. *10*, 27–38.

Möglich, A. (2018). An open-source, cross-platform resource for nonlinear least-squares curve fitting. J. Chem. Educ. *95*, 2273–2278.

Möglich, A., Ayers, R.A., and Moffat, K. (2009). Design and signaling mechanism of light-regulated histidine kinases. J. Mol. Biol. *385*, 1433–1444.

Möglich, A., Yang, X., Ayers, R.A., and Moffat, K. (2010). Structure and function of plant photoreceptors. Annu. Rev. Plant Biol. *61*, 21–47.

Mukougawa, K., Kanamoto, H., Kobayashi, T., Yokota, A., and Kohchi, T. (2006). Metabolic engineering to produce phytochromes with phytochromobilin, phycocyanobilin, or phycoerythrobilin chromophore in *Escherichia coli*. FEBS Lett. *580*, 1333–1338.

Ohlendorf, R., Vidavski, R.R., Eldar, A., Moffat, K., and Möglich, A. (2012). From dusk till dawn: one-plasmid systems for light-regulated gene expression. J. Mol. Biol. *416*, 534–542.

Ohlendorf, R., Schumacher, C.H., Richter, F., and Möglich, A. (2016). Library-aided probing of linker determinants in hybrid photoreceptors. ACS Synth. Biol. *5*, 1117–1126.

Raffelberg, S., Wang, L., Gao, S., Losi, A., Gärtner, W., and Nagel, G. (2013). A LOV-domain-mediated blue-light-activated adenylate (adenylyl) cyclase from the cyanobacterium *Microcoleus chthonoplastes* PCC 7420. Biochem. J. *455*, 359–365.

Rall, T.W., Sutherland, E.W., and Berthet, J. (1957). The relationship of epinephrine and glucagon to liver phosphorylase Iv. Effect of epinephrine and glucagon on the reactivation of phosphorylase in liver homogenates. J. Biol. Chem. *224*, 463–475.

Rauch, A., Leipelt, M., Russwurm, M., and Steegborn, C. (2008). Crystal structure of the guanylyl cyclase Cya2. Proc. Natl. Acad. Sci. USA *105*, 15720–15725.

Richter, F., Scheib, U.S., Mehlhorn, J., Schubert, R., Wietek, J., Gernetzki, O., Hegemann, P., Mathes, T., and Möglich, A. (2015). Upgrading a microplate reader for photobiology and all-optical experiments. Photochem. Photobiol. Sci. *14*, 270–279.

Richter, F., Fonfara, I., Bouazza, B., Schumacher, C.H., Bratovič, M., Charpentier, E., and Möglich, A. (2016). Engineering of temperature- and light-switchable Cas9 variants. Nucleic Acids Res. *44*, 10003–10014.

Rink, T.J., Tsien, R.Y., and Pozzan, T. (1982). Cytoplasmic pH and free Mg^{2+} in lymphocytes. J. Cell Biol. *95*, 189–196.

Rockwell, N.C. and Lagarias, J.C. (2010). A brief history of phytochromes. Chemphyschem Eur. J. Chem. Phys. Phys. Chem. *11*, 1172–1180.

Roychowdhury, S., Dong, Q., and Bauer, C.E. (2015). DNA-binding properties of a cGMP-binding CRP homologue that controls development of metabolically dormant cysts of Rhodospirillum centenum. Microbiology *161*, 2256–2264.

Ryu, M.-H. and Gomelsky, M. (2014). Near-infrared light responsive synthetic c-di-GMP module for optogenetic applications. ACS Synth. Biol. *3*, 802–810.

Ryu, M.-H., Moskvin, O.V., Siltberg-Liberles, J., and Gomelsky, M. (2010). Natural and engineered photoactivated nucleotidyl cyclases for optogenetic applications. J. Biol. Chem. *285*, 41501–41508.

Ryu, M.-H., Kang, I.-H., Nelson, M.D., Jensen, T.M., Lyuksyutova, A.I., Siltberg-Liberles, J., Raizen, D.M., and Gomelsky, M. (2014). Engineering adenylate cyclases regulated by near-infrared window light. Proc. Natl. Acad. Sci. USA *111*, 10167–10172.

Ryu, M.-H., Youn, H., Kang, I.-H., and Gomelsky, M. (2015). Identification of bacterial guanylate cyclases. Proteins *83*, 799–804.

Scheib, U., Stehfest, K., Gee, C.E., Körschen, H.G., Fudim, R., Oertner, T.G., and Hegemann, P. (2015). The rhodopsin–guanylyl cyclase of the aquatic fungus *Blastocladiella emersonii* enables fast optical control of cGMP signaling. Sci. Signal *8*, rs8.

Schröder-Lang, S., Schwärzel, M., Seifert, R., Strünker, T., Kateriya, S., Looser, J., Watanabe, M., Kaupp, U.B., Hegemann, P., and Nagel, G. (2007). Fast manipulation of cellular cAMP level by light *in vivo*. Nat. Methods *4*, 39–42.

Schumacher, C.H., Körschen, H.G., Nicol, C., Gasser, C., Seifert, R., Schwärzel, M., and Möglich, A. (2016). A fluorometric activity assay for light-regulated cyclic-nucleotide-monophosphate actuators. Methods Mol. Biol. *1408*, 93–105.

Shimada, T., Fujita, N., Yamamoto, K., and Ishihama, A. (2011). Novel Roles of cAMP Receptor Protein (CRP) in Regulation of Transport and Metabolism of Carbon Sources. PLoS One *6*, e20081.

Shu, X., Royant, A., Lin, M.Z., Aguilera, T.A., Lev-Ram, V., Steinbach, P.A., and Tsien, R.Y. (2009). Mammalian expression of infrared fluorescent proteins engineered from a bacterial phytochrome. Science *324*, 804–807.

Stierl, M., Stumpf, P., Udwari, D., Gueta, R., Hagedorn, R., Losi, A., Gärtner, W., Petereit, L., Efetova, M., Schwarzel, M., et al. (2011). Light-modulation of cellular cAMP by a small bacterial photoactivated adenylyl cyclase, bPAC, of the soil bacterium beggiatoa. J. Biol. Chem. *286*, 1181–1188.

Strack, R.L., Strongin, D.E., Bhattacharyya, D., Tao, W., Berman, A., Broxmeyer, H.E., Keenan, R.J., and Glick, B.S. (2008). A noncytotoxic DsRed variant for whole-cell labeling. Nat. Methods *5*, 955–957.

Walsh, D.A., Perkins, J.P., and Krebs, E.G. (1968). An adenosine 3′,5′-monophosphate-dependant protein kinase from rabbit skeletal muscle. J. Biol. Chem. *243*, 3763–3765.

Yang, X., Kuk, J., and Moffat, K. (2008). Crystal structure of *Pseudomonas aeruginosa* bacteriophytochrome: Photoconversion and signal transduction. Proc. Natl. Acad. Sci. USA *105*, 14715–14720.

Ziegler, T. and Möglich, A. (2015). Photoreceptor engineering. Front. Mol. Biosci. *2*, 30.

7.3. Manuskript III

Dietler, J.; Stabel, R.; Möglich, A.; *Methods in Enzymology* (2019) "*Pulsatile Illumination for Photobiology and Optogenetics*"

Pulsatile illumination for photobiology and optogenetics

Julia Dietler[a,†], **Robert Stabel**[a,†], **Andreas Möglich**[a,b,c,d,*,†]
[a]Lehrstuhl für Biochemie, Universität Bayreuth, Bayreuth, Germany
[b]Research Center for Bio-Macromolecules, Universität Bayreuth, Bayreuth, Germany
[c]Bayreuth Center for Biochemistry & Molecular Biology, Universität Bayreuth, Bayreuth, Germany
[d]North-Bavarian NMR Center, Universität Bayreuth, Bayreuth, Germany
*Corresponding author: e-mail address: andreas.moeglich@uni-bayreuth.de

Contents

Abstract

Living organisms exhibit a wide range of intrinsic adaptive responses to incident light. Likewise, in optogenetics, biological systems are tailored to initiate predetermined cellular processes upon light exposure. As genetically encoded, light-gated actuators, sensory photoreceptors are at the heart of these responses in both the natural and engineered scenarios. Upon light absorption, photoreceptors enter a series of generally rapid photochemical reactions leading to population of the light-adapted signaling

† ORCID identifiers: J.D. 0000-0002-0418-0796; R.S. 0000-0002-9159-0004; A.M. 0000-0002-7382-2772.

Methods in Enzymology
ISSN 0076-6879
https://doi.org/10.1016/bs.mie.2019.04.005

state of the receptor. Notably, this state persists for a while before thermally reverting to the original dark-adapted resting state. As a corollary, the inactivation of photosensitive biological circuits upon light withdrawal can exhibit substantial inertia. Intermittent illumination of suitable pulse frequency can hence maintain the photoreceptor in its light-adapted state while greatly reducing overall light dose, thereby mitigating adverse side effects. Moreover, several photoreceptor systems may be actuated sequentially with a single light color if they sufficiently differ in their inactivation kinetics. Here, we detail the construction of programmable illumination devices for the rapid and parallelized testing of biological responses to diverse lighting regimes. As the technology is based on open electronics and readily available, inexpensive components, it can be adopted by most laboratories at moderate expenditure. As we exemplify for two use cases, the programmable devices enable the facile interrogation of diverse illumination paradigms and their application in optogenetics and photobiology.

1. Introduction

Numerous organisms employ sensory photoreceptor proteins to derive spatial and temporal cues from incident light for the adjustment of physiology, behavior and lifestyle (Hegemann, 2008; Möglich, Yang, Ayers, & Moffat, 2010). Photoreceptors double as genetically encoded, light-gated actuators in optogenetics (Deisseroth et al., 2006) to enable the non-invasive optical manipulation of diverse cellular processes with exquisite spatiotemporal resolution (Losi, Gardner, & Möglich, 2018). In the absence of light, sensory photoreceptors assume their thermodynamically most stable, dark-adapted state, denoted D in the following; absorption of light initiates a cyclic series of photochemical reactions, denoted photocycle, as part of which the light-adapted signaling state L is populated (Ziegler & Möglich, 2015). This photocycle is generally reversible, and the metastable state L persists for a while before passively, i.e., thermally, decaying to D in a process called dark recovery over the course of seconds to days, depending on photoreceptor. Based on the chromophore used for light absorption and the photochemistry exhibited, sensory photoreceptors divide into around 10 families. As one family, light-oxygen-voltage (LOV) receptors bind flavin-nucleotide chromophores and respond to blue light (Christie et al., 1998; Salomon et al., 2001; Yee et al., 2015). Of note, the light-adapted state L of LOV receptors reverts to D in a strongly temperature-dependent, base-catalyzed reaction (Alexandre, Arents, van Grondelle, Hellingwerf, & Kennis, 2007), the kinetics of which can be deliberately varied over several orders of magnitude via modification of certain amino acids adjacent to the flavin chromophore (Pudasaini, El-Arab, &

Zoltowski, 2015). Phytochromes (Phys) constitute a large receptor family sensitive to red and far-red light that occur in plants, (cyano)bacteria and fungi (Rockwell & Lagarias, 2010). In conventional Phys, red light drives the transition of D to the light-adapted state L which returns to D either thermally or through absorption of a second light quantum of far-red color.

Experiments in the neurosciences aside, optogenetic applications often take place on comparatively long time scales and frequently involve the prolonged exposure to light of the system under study. The underlying photoreceptors hence repeatedly transition between their dark-adapted and light-adapted states D and L, and under constant illumination a photostationary state is assumed. Rather than continuously illuminating throughout the experiment, light may also be applied intermittently in pulsatile manner. By reducing the overall light dose (cf. below), this approach can mitigate phototoxicity, photobleaching and sample heating. In addition, pulsed illumination can enable the multiplexing of several light-sensitive systems and their selective activation (Hennemann et al., 2018). We illustrate these aspects by means of two numerical simulations (Fig. 1). In the first and conceptually simplest scenario, a given photoreceptor be monomeric and assume either the D or L state. The forward transition $D \rightarrow L$ proceed with a unimolecular rate constant k_1, dependent on the applied light intensity, and the backward reaction $L \rightarrow D$, i.e., the dark recovery, with a light-independent unimolecular rate constant k_{-1}. As shown in Fig. 1B, during a train of light pulses the system repeatedly cycles between the D and L states as determined by the relative magnitudes of the microscopic rate constants k_1 and k_{-1} and of the applied pulse frequency. At least two points are of note: first, lighting schemes with the same overall light dose may activate the photoreceptor to rather different average levels, depending upon the timing of successive light pulses (left and right panels in Fig. 1B); second, two photoreceptor systems may be discriminated in the pulse-frequency domain, albeit to limited extent, given the single-exponential recovery kinetics. A second, more complex scenario considers a homodimeric photoreceptor subjected to the same light-pulse sequence as before (Fig. 1C). For simplicity, we assume that the two subunits of the receptor undergo the $D \leftrightarrow L$ transition independently of another with microscopic rate constants of k_1 and k_{-1}. As a consequence, the reaction from the fully dark-adapted state DD to the fully light-adapted state LL, and vice versa, proceeds via the mixed-state intermediates DL and LD, therefore giving rise to sigmoidal reaction kinetics instead of single-exponential ones. For the present scope, we further assume that the receptor be cooperative (Monod,

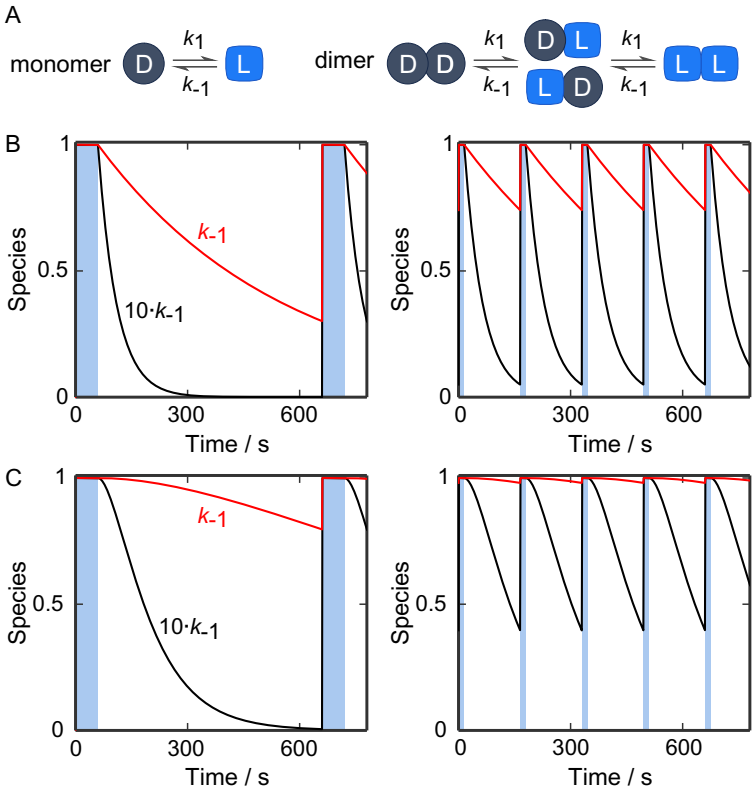

Fig. 1 The response of light-sensitive systems to pulsed illumination. (A) In the simplest scenario, light drives the transition of a monomeric photoreceptor from its dark-adapted state (D) to its light-adapted signaling state (L) with a unimolecular rate constant k_1 that depends on illumination intensity. Once in the signaling state, the receptor thermally reverts to state D with a unimolecular rate constant k_{-1}. In a somewhat more complex scenario, the photoreceptor be dimeric and capable of populating an intermediate state with one protomer in the D, and the other in the L state. For simplicity, the protomers are assumed to transition between the two photochemical states D and L independently of another with the rate constants k_1 and k_{-1}, respectively. (B) The kinetic scheme for the monomer scenario was numerically solved in time for the indicated regime of periodic illumination. Blue bars mark periods where light is applied and the D→L transition is hence promoted; at other times, light is off, and the mono-exponential L→D reversion predominates. The ordinate denotes the fraction of the receptor in the L state. Two simulations for slow and fast dark recovery with rate constants $k_{-1} = 0.01\,s^{-1}$ and $10{\cdot}k_{-1}$ are shown as red and black lines, respectively. Compared to the left panel, in the righthand one the frequency of pulsing is increased fourfold and the duration of each light period reduced by the same factor, thus retaining the same overall light dose. (C) The two panels report corresponding simulations for the dimer scenario, where the ordinate shows the sum of the species DL, LD and LL. In contrast to (B), the recovery reaction is of sigmoidal functionality.

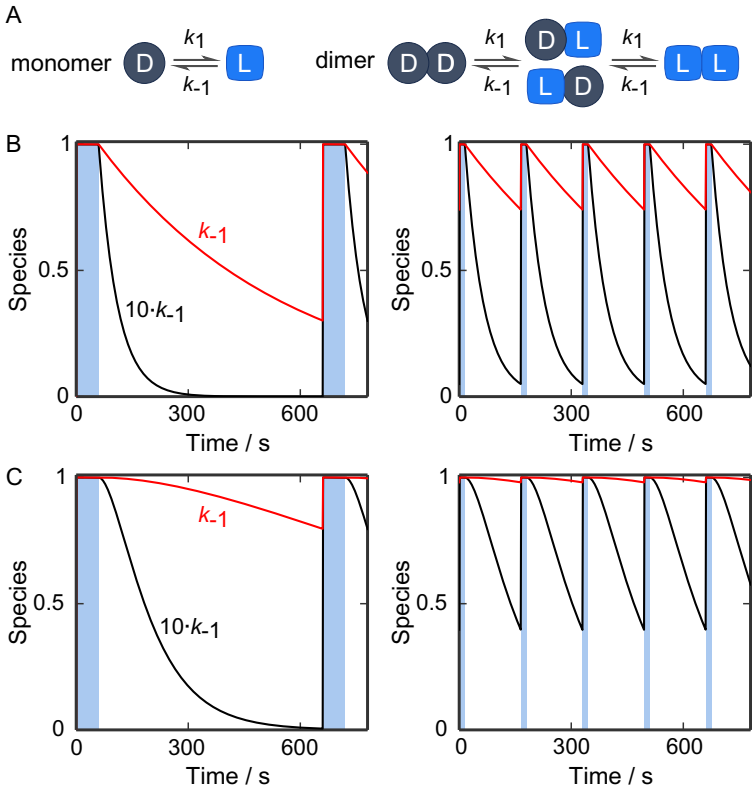

Fig. 1 The response of light-sensitive systems to pulsed illumination. (A) In the simplest scenario, light drives the transition of a monomeric photoreceptor from its dark-adapted state (D) to its light-adapted signaling state (L) with a unimolecular rate constant k_1 that depends on illumination intensity. Once in the signaling state, the receptor thermally reverts to state D with a unimolecular rate constant k_{-1}. In a somewhat more complex scenario, the photoreceptor be dimeric and capable of populating an intermediate state with one protomer in the D, and the other in the L state. For simplicity, the protomers are assumed to transition between the two photochemical states D and L independently of another with the rate constants k_1 and k_{-1}, respectively. (B) The kinetic scheme for the monomer scenario was numerically solved in time for the indicated regime of periodic illumination. Blue bars mark periods where light is applied and the D→L transition is hence promoted; at other times, light is off, and the mono-exponential L→D reversion predominates. The ordinate denotes the fraction of the receptor in the L state. Two simulations for slow and fast dark recovery with rate constants $k_{-1} = 0.01\,s^{-1}$ and $10{\cdot}k_{-1}$ are shown as red and black lines, respectively. Compared to the left panel, in the righthand one the frequency of pulsing is increased fourfold and the duration of each light period reduced by the same factor, thus retaining the same overall light dose. (C) The two panels report corresponding simulations for the dimer scenario, where the ordinate shows the sum of the species DL, LD and LL. In contrast to (B), the recovery reaction is of sigmoidal functionality.

Wyman, & Changeux, 1965) in that the LL, DL and LD states have the same output activity, a situation that has been experimentally demonstrated for at least one photoreceptor system (Möglich, Ayers, & Moffat, 2009). As illustrated in Fig. 1C, the homodimeric scenario also exhibits higher average extents of light activation if a given light dose is spread over several shorter pulses rather than concentrated in infrequent but longer pulses. In addition, the simulations show that the sigmoidal reaction course enables a much better discrimination between two systems with different recovery kinetics, thus allowing the sequential addressing of these systems by light of varying pulse frequency and intensity (Hennemann et al., 2018). While, evidently, other and more complex photoreceptor reaction schemes are conceivable, even the simple simulations compellingly show that the response to light may drastically differ between systems. We note that during optogenetic deployment, reaction steps downstream of photoreceptor activation, often nonlinear and cooperative, may additionally contribute to complex recovery kinetics and response dynamics to pulsatile light (Ziegler & Möglich, 2015).

To efficiently probe and subsequently exploit the response of optogenetic systems to intermittently applied light, we built programmable arrays of light-emitting diodes (LEDs) that allow the testing and application of multiple lighting regimes in parallel (Hennemann et al., 2018; Stüven et al., 2019). Here, we recapitulate the construction of these arrays (Section 2) and their deployment to two photoreceptor systems (Sections 3 and 4).

2. Programmable arrays of light-emitting diodes

2.1 Arrays with red/green/blue-emitting diodes

In this section, we detail the assembly of a programmable matrix of red/green/blue (RGB) three-color LEDs based on an open-source Arduino microcontroller and commercially available electronics (Hennemann et al., 2018). The setup allows the illumination from below of 64 wells of a standard 96-well microtiter plate (MTP) with programmable light signals of adjustable intensity, timing and color (peak wavelengths of 470, 525 and 620 nm) (Fig. 2). The wiring scheme (Fritzing file) of the three-color LED setup can be obtained at http://www.moeglich.uni-bayreuth.de/en/software.

2.1.1 Materials

- Arduino Uno microcontroller (Arduino, Turin, Italy)

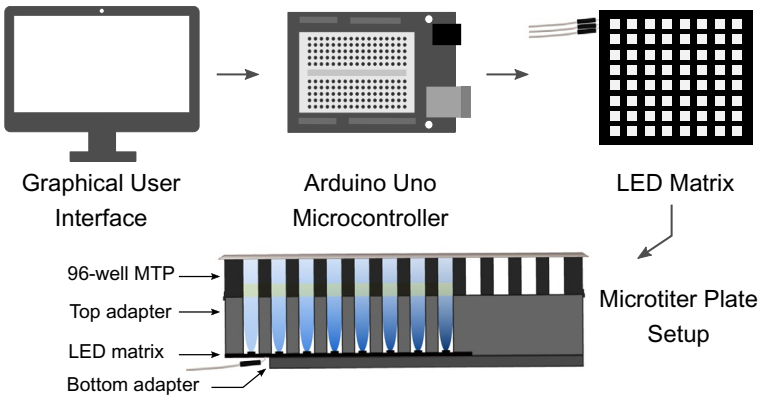

Fig. 2 Schematic illustrating the application of programmable lighting in microtiter-plate (MTP) format. A graphical user interface, implemented in Python/Qt, facilitates the configuration of the programmable array of 64 light-emitting diodes (LED). The configuration file is uploaded to an Arduino circuit board which controls the timing and intensity of the single LEDs in the array. The array is encased in a 3D-printed housing and an MTP mounted on top to allow illumination of individual wells from below (Hennemann et al., 2018; Stüven et al., 2019).

- Adafruit NeoPixel NeoMatrix 8 × 8 (Adafruit Industries, New York, USA)
- jumper wires (EXP GmbH, Saarbrücken, Germany)
- resistor 470 Ω (EXP GmbH)
- electrolytic capacitor 4700 µF, 10 V (EXP GmbH)
- breadboard (EXP GmbH)
- solder and soldering iron
- AC power supply 5 V, 4 A (EXP GmbH)
- *optional:* real-time clock DS3221 (Adafruit Industries)

2.1.2 Protocol

i. Optionally, a real-time clock (RTC) for enhanced temporal precision can be used. If so, place the RTC on the breadboard and connect it to the 5 V power (5 V) and ground (GND) pins of the Arduino board using jumper wires. Further, connect the SCL (serial clock line) and SDA (serial data line) pins of the RTC to the analog inputs 4 and 5, respectively, of the Arduino board.

ii. Connect the 5 V and GND pins of the Arduino board to the "+" and "−" rows of the breadboard. Now, any pin/wire inserted into these rows will also be connected to power or ground, respectively.

iii. Connect the electrolytic capacitor by attaching its cathode (short leg) to the "−" row and its anode (long leg) to the "+" row of the board.

iv. Place the 470 Ω resistor on the breadboard and connect it to the digital pin 6 of the Arduino microcontroller.
v. Connect the 5 V and GND pins of the NeoPixel LED matrix to "+"/"−" on the breadboard; connect the DIN pin to the resistor. To secure the connections, the jumper wires can be soldered in place.

2.2 Arrays with custom light-emitting diodes

Here, we describe a dual-color array that uses custom LEDs (Stüven et al., 2019). The setup allows the illumination from below of 64 wells of a standard 96-well MTP with programmable light signals of adjustable intensity, timing and two custom colors. In the example detailed here, LEDs with peak wavelengths of 655 and 850 nm are used, but the design also applies to other LEDs of diverse colors.

2.2.1 Materials

- Arduino Uno microcontroller (Arduino)
- ITEAD Full Color RGB LED Matrix Driver Shield (Itead, Shenzhen, China)
- jumper wires (EXP GmbH)
- resistor 470 Ω (EXP GmbH)
- electrolytic capacitor 4700 μF, 10 V (EXP GmbH)
- breadboard (EXP GmbH)
- solder and soldering iron
- AC power supply 5 V, 4 A (EXP GmbH)
- 64 × 3-mm LED color #1 [e.g., Kingbright WP908A8SRD, (655 ± 20) nm, Mouser Electronics, Munich, Germany]
- 64 × 3-mm LED color #2 [e.g., Harvatek HE1-120AC-XXXX (850 ± 42) nm, Conrad Electronic SE, Hirschau, Germany]
- printed circuit board (PCB) [Eagle template file (.brd) and wiring scheme (.sch) are available at http://www.moeglich.uni-bayreuth.de/en/software]
- *optional:* real-time clock DS3221 (Adafruit Industries)

2.2.2 Protocol

i. Print the custom circuit board according to the Eagle template file (.brd). Electronics shops or dedicated companies, such as PCBA-Store (http://www.pcbastore.com), EasyEDA (http://easyeda.com), Pad2pad (http://www.pad2pad.com), or ExpressPCB (http://www.expresspcb.com), can routinely do this for a small fee.

ii. Position the two sets of 64 LEDs on the PCB according to the wiring scheme (.sch) and solder them in place.
iii. Connect the LED driver shield to the Arduino microcontroller such that the pins on both elements line up.
iv. Use jumper wires to connect the assembled PCB and the LED driver shield according to the wiring scheme.

2.3 Housing and adapters for the LED arrays

The above LED arrays need to be embedded in a custom-made mounting adapter that reduces light contamination between adjacent LEDs and allows positioning of an MTP on top such that it can be illuminated from below. As one option, the required adapter pieces may be obtained by subtractive manufacturing, which is offered by various companies. As described below, alternatively the pieces can be obtained by 3D printing.

2.3.1 Materials

- template files for the base plate and mounting adapter (.stl files available at http://www.moeglich.uni-bayreuth.de/en/software)
- 3D printer, e.g., Anycubic I3 MEGA (GearBest, China)
- polylactic acid (PLA) print filament, ideally in black (available from diverse suppliers)

2.3.2 Protocol

i. There are separate versions of the adapter pieces for the RGB (cf. Section 2.1) and the custom LED arrays (cf. Section 2.2); ensure to use the correct one. Prior to printing, the template file for the adapter pieces can be further adjusted to accommodate individual needs (e.g., different MTPs, incubator platforms, etc.). To this end, free software for computer-aided design, e.g., TinkerCAD (http://www.tinkercad.com) can be used.
ii. Print bottom and top piece of the adapter using PLA filament, a fill factor between 25% and 50%, and a precision of 100 μm. Use of ABS filament is not recommended as it is prone to warping. We found that the print precision of consumer-grade printers is fully sufficient for the task. Alternatively, printing can be done by 3D-printing services, such as Proto Labs (http://www.protolabs.com), i.materialise (http://all3dp.com) or 3D Hubs (http://www.3dhubs.com).
iii. Remove residual filament from the printed pieces using pliers and scissors.

iv. Place LED array on bottom adapter piece, then cover with top piece.

2.4 Configuration and calibration of the LED arrays

To facilitate the configuration of the programmable LED matrices, we supply a Python-based graphical user interface (GUI). As output, the interface generates an Arduino sketch file (.ino) that needs to be compiled and uploaded to the Arduino board. Optionally, a light power meter may be used to calibrate the intensity of the programmable LED arrays.

2.4.1 Materials

- USB-A to USB-B cable
- Python-based LED controller interface (available at http://www.moeglich.uni-bayreuth.de/en/software)
- Arduino Integrated Development Environment (IDE) (available at http://www.arduino.cc)
- *optional:* light power meter (model 842-PE, Newport, Darmstadt, Germany)
- *optional:* silicon photodetector (model 918D-UV-OD3, Newport)

2.4.2 Protocol

i. Identify the version of the GUI applicable to the LED matrix you are using (RGB, cf. Section 2.1; or custom LEDs, cf. Section 2.2) and download the corresponding Python file. The program can be executed with Python version 3 on Windows, Linux and OS X platforms. Alternatively, for Windows platforms, we supply a stand-alone binary file.

ii. Use the GUI to configure the timing scheme and brightness of each LED individually. Note that the brightness of the LEDs is set by pulse-width modulation (PWM) on an 8-bit scale.

iii. *optional*: To enhance the temporal accuracy of the Arduino board (which can be quite modest), an RTC module (cf. above) may be included. If so, a checkbox in the GUI should be activated.

iv. Once the configuration is completed, the current settings can be saved as a configuration file (.cfg). Export the configuration as an Arduino sketch file (.ino), close the GUI.

v. Start the Arduino IDE and open the (.ino) file generated in the previous step. At first use, Arduino driver libraries for the RTC and, in case of the RGB LED matrix (cf. Section 2.1), the NeoPixel matrix need to be installed. To this end, select "Manage Libraries" from

the "Sketch → Include Library" pull-down menu. Locate the "RTClib" and "Adafruit NeoMatrix" entries and install the libraries as required.

vi. Advanced users may optionally wish to directly modify the Arduino sketch file rather than use the GUI. Connect the Arduino board to the computer via the USB cable, compile the program code and upload it to the board.

vii. Provided no errors occurred, the LED array should now start lighting up as configured.

viii. *optional*: The actual light output of the LED matrix for given intensity settings may be calibrated with a lamp power meter. To this end, place the detector of the lamp power meter directly atop the upper piece of the LED assembly and measure the emitted light output for several software intensity settings. Owing to the use of PWM, we found the set and actual light intensities to be linearly correlated. Variations between different LEDs of the matrix were found to be negligible. Note that the light output may depend on the power supply attached to the LED matrix; hence, the calibration should be done for the power supply to be used in the actual experiment.

3. Control of bacterial gene expression by varying light intensity and pulse frequency

We deployed the programmable RGB LED matrix (cf. Section 2.1) to systematically chart the response of the YF1/*Bj*FixJ two-component system (TCS) (Hennemann et al., 2018), as implemented on the pDusk plasmid (Ohlendorf, Vidavski, Eldar, Moffat, & Möglich, 2012), to intermittently applied blue light of varying intensity (Fig. 3A). Briefly, the LOV receptor YF1 derives from the fusion of the photosensor module of *Bacillus subtilis* YtvA and the effector module of the *Bradyrhizobium japonicum Bj*FixL histidine kinase (Möglich et al., 2009). Provided both LOV sensors of the homodimeric YF1 reside in their dark-adapted states (denoted DD), the receptor readily phosphorylates the so-called response regulator (RR) *Bj*FixJ. In its phosphorylated form, the RR drives the expression from cognate promoters, e.g., of the red-fluorescent reporter *Ds*Red (Strack et al., 2008). Upon blue-light absorption by the LOV modules, YF1 assumes the photochemically mixed states DL and LD or the fully light-adapted state LL, all of which act as a phosphatase on phospho-*Bj*FixJ (Möglich et al.,

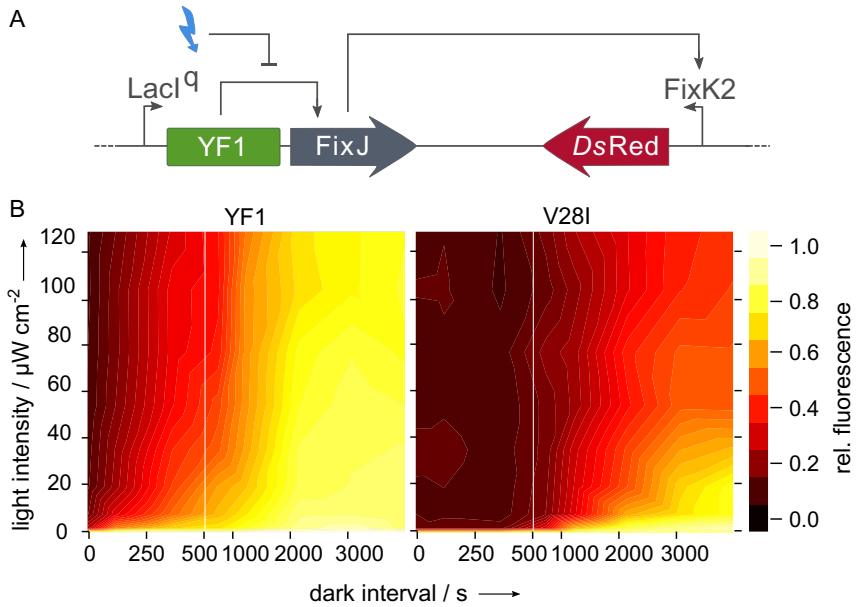

Fig. 3 Optogenetic control of the pDusk system by pulsed blue light. (A) The pDusk-*Ds*Red plasmid wires the blue-light-inhibited two-component system YF1/*Bj*FixJ to the expression of the red-fluorescent reporter *Ds*Red (Möglich et al., 2009; Ohlendorf et al., 2012). (B) *Escherichia coli* bacteria harboring pDusk-*Ds*Red were cultivated under different lighting regimes as controlled by the programmable LED array. In periodic manner, illumination for 30 s at different intensities (denoted on the ordinate) was followed by dark intervals of variable duration (abscissa). For each parameter setting, the reporter fluorescence of three replicate bacterial cultures was averaged and is plotted as color code. Data for the original pDusk system (left) are juxtaposed to data for a derivative pDusk system (right) which employs the V28I variant of YF1 that features much decelerated recovery kinetics and is hence effectively more light-sensitive (Hennemann et al., 2018).

2009). As for other LOV receptors, the light-adapted state thermally returns to the dark-adapted state in the dark recovery reaction. Certain residue exchanges placed near the flavin chromophore of the LOV sensor can strongly modulate the kinetics of dark recovery (Pudasaini et al., 2015). Specifically, within the pDusk context, we replaced valine 28 of YF1 by isoleucine which resulted in greatly decelerated recovery kinetics (Hennemann et al., 2018; Kawano, Aono, Suzuki, & Sato, 2013). As explained in the below protocol, we assessed the impact of different blue-light regimes on *Ds*Red reporter expression from pDusk plasmids encoding the original YF1 receptor or its V28I variant.

3.1 Materials

- plasmid pDusk encoding a fluorescent reporter such as *Ds*Red (plasmid pDusk available from Addgene, plasmid 43795)
- *Escherichia coli* expression strain, e.g., BL21 or CmpX13 (Mathes, Vogl, Stolz, & Hegemann, 2009)
- lysogeny broth medium supplemented with 50 μg mL^{-1} kanamycin (LB/Kan)
- programmable RGB LED matrix (cf. Sections 2.1 and 2.3)
- black-wall clear-bottom 96-well MTPs (Greiner BioOne, Frickenhausen, Germany)
- black 96-well MTPs (e.g., Greiner)
- transparent 96-well MTPs (e.g., Greiner)
- gas-permeable sealing film (BF-410400-S, Corning, New York, USA)
- incubator, e.g., HN-2 Herp Nursery II (Lucky Reptile, Waldkirch, Germany)
- MTP shaker, e.g., PMS-1000i (Grant Instruments, Cambridge, UK)
- multimode MTP reader, e.g., Tecan Infinite M200 PRO (Tecan Group Ltd., Männedorf, Switzerland)

3.2 Protocol

i. Transform between 10 pg and 100 ng of the pDusk-*Ds*Red plasmid into *E. coli* CmpX13 cells, plate on LB/Kan agar and incubate over night at 37 °C. (Note that here and in the following experimental steps, we assume that the *Ds*Red reporter and *E. coli* CmpX13 cells are used. However, other fluorescent proteins and *E. coli* BL21 strains may be used instead.)

ii. Inoculate a 5-mL LB/Kan starter culture with a single clone from a freshly transformed plate and incubate at 37 °C until an optical density at 600 nm (OD_{600}) of 0.3 is reached.

iii. Take 10 μL of the starter culture and inoculate 15 mL of pre-warmed LB/Kan medium.

iv. Mix thoroughly and dispense 200 μL each to 64 wells (use rows A–H and columns 1–8) of a black-wall, clear-bottom 96-well MTP using a multichannel pipette.

v. Seal the MTP with a gas-permeable film to allow sufficient air circulation during subsequent incubation.

vi. Configure the LED matrix according to Section 2. For the study of light-dependent gene expression in pDusk, we varied the intensity of blue light (470 nm) between 0 and 130 $\mu W\,cm^{-2}$ and used a periodic illumination scheme where individual wells were exposed to light for 30 s before incubation in the dark for periods between 0 and 65 min. The alternating dark/light cycles continued until the end of the incubation (Hennemann et al., 2018).

vii. Place the sealed MTP plate on top of the configured LED-array setup. If necessary, fix the plate in position with duct tape.

viii. Mount the assembly on an MTP shaker, place inside a suitable incubator and incubate at 37 °C and 600 rpm for 16 h. Continuous shaking throughout the entire experiment promotes aeration of the cultures and ensures their homogenous mixing and illumination. Ensure that the incubator is tightly sealed against stray light from the outside and stays closed for the entire experiment.

ix. Remove the sealing film. Using a multi-channel pipette, transfer 40 µL of each culture to a transparent MTP and add 210 µL H_2O. Measure OD_{600} of each well in an MTP reader. If absorbance falls outside the interval 0.1–1.0, prepare another solution of the bacterial cultures at an appropriate dilution factor.

x. Using a multi-channel pipette, transfer 40 µL of the diluted solutions from the previous step to a black MTP and add 210 µL H_2O. Measure reporter fluorescence of each well in an MTP reader. To monitor *Ds*Red fluorescence, we used excitation and emission wavelengths of (554 ± 9) and (591 ± 20) nm, respectively. For optimal results, adjust the gain and focal height of the MTP reader. To allow comparison between experiments on different days, these settings must be left unchanged.

xi. Normalize fluorescence data to OD_{600} and plot as 2D contours plots as a function of the duration of the dark period and the intensity of pulsed illumination (Fig. 3B).

xii. As the expected result, the *Ds*Red reporter-gene output for either YF1 or V28I should decrease monotonically with light intensity (ordinate in Fig. 3B) but increase monotonically with the length of the dark period (abscissa). In comparison to the original YF1, the V28I variant with slower dark-recovery kinetics is toggled by lower overall light doses, i.e., it is more light-sensitive.

4. Engineering and characterization of photoactivated adenylyl cyclases

We originally developed the programmable arrays with custom LEDs (cf. Section 2.2) to probe the response of certain photoactivated adenylyl cyclases (PAC) to red/far-red light regimes of varying intensity and timing (Stüven et al., 2019). Briefly, PACs mediate the production of the versatile second messenger 3′, 5′ cyclic adenosine monophosphate (cAMP) in a light-stimulated manner. Several naturally occurring, mostly blue-light-sensitive PACs (Blain-Hartung et al., 2018; Iseki et al., 2002; Raffelberg et al., 2013; Ryu, Moskvin, Siltberg-Liberles, & Gomelsky, 2010; Schröder-Lang et al., 2007; Stierl et al., 2011) have been supplemented by engineered PACs that respond to red and far-red light (Etzl, Lindner, Nelson, & Winkler, 2018; Ryu et al., 2014; Stüven et al., 2019). These PACs are based on bacteriophytochrome (BPhy) sensor units and can be bidirectionally toggled between two functional states by red and far-red light, respectively, thus potentially enhancing the precision in time and space of optogenetic applications (Ziegler & Möglich, 2015). Moreover, red and far-red light exhibit deeper penetration of biological tissue than blue light (Weissleder, 2001), thus rendering BPhy-based PACs attractive for optogenetics in vivo. To rapidly assess the light-dependent activity of PACs, we established the pCyclR reporter-gene assay in *E. coli*, as illustrated in Fig. 4A (Stüven et al., 2019). In this assay, the functional expression of PACs, followed by stimulation with light of suitable quality and quantity, prompts the intracellular production of cAMP. In turn, the endogenous *E. coli* catabolite activator protein binds cAMP and activates the expression of the red-fluorescent reporter *Ds*Red. By resorting to this assay, we engineered the photoreceptor *Dd*PAC which displays cAMP production that is elevated and diminished by exposure to red and far-red light, respectively. The two protocols below illustrate the application of the pCyclR reporter system to record the response of *Dd*PAC to red and far-red light of varying intensity (protocol A, Fig. 4B) and timing (protocol B, Fig. 4C).

4.1 Materials

- pCyclR reporter plasmid (kanamycin resistance marker; available from the authors)
- pCDF plasmid harboring expression cassettes for *Dd*PAC and *Synechocystis* sp. heme oxygenase (streptomycin resistance marker; available from the authors)

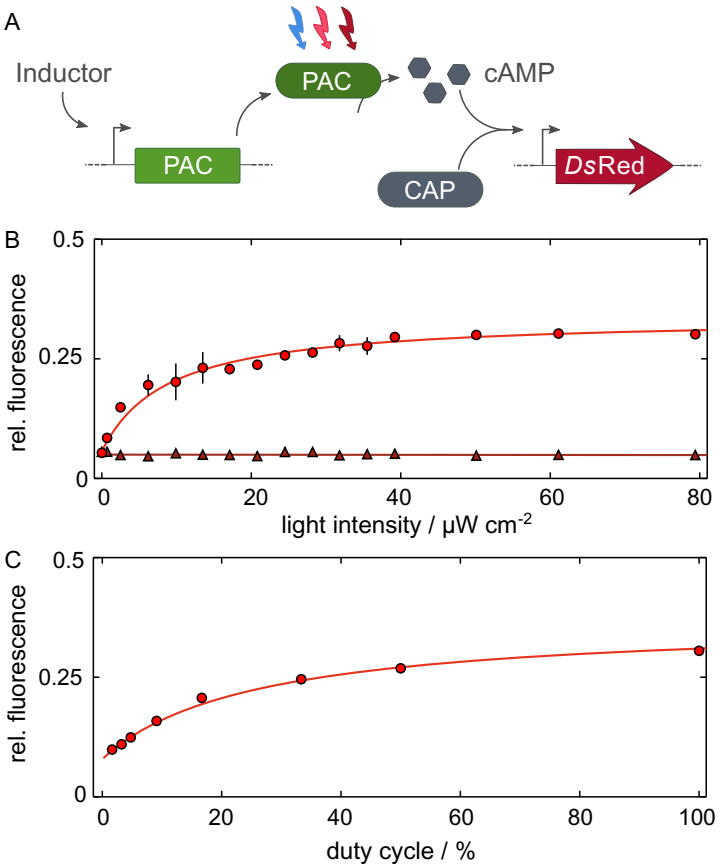

Fig. 4 Characterization of the red-light-responsive adenylyl cyclase *Dd*PAC (Stüven et al., 2019). (A) The pCyclR test bed for photoactivated adenylyl cyclases (PAC) relies on the inducible expression of PACs in *Escherichia coli*. Upon stimulation with light, PACs ramp up the production of the second messenger 3′, 5′ cyclic adenosine monophosphate (cAMP) which associates with the endogenous catabolite activator protein (CAP) to enable upregulation of the expression of a *Ds*Red reporter gene. (B) Using the pCyclR system and programmable lighting, we probed the response of *Dd*PAC to constant illumination of varying intensity and wavelengths of 655 (circles) and 850 nm (triangles), respectively. *E. coli* cultures harboring pCyclR and *Dd*PAC were grown at the different light settings, and *Ds*Red fluorescence of four biological replicates ± standard deviation is reported. (C) As in (B), but cultures were intermittently illuminated with 655-nm light at 40 µW cm^{-2}. The abscissa denotes the fraction of time for which light was applied.

- adenylyl-cyclase-deficient *E. coli* strain CmpX13 Δ*cyaA* (available from the authors)
- lysogeny broth medium supplemented with 50 µg mL^{-1} kanamycin and 100 µg mL^{-1} streptomycin (LB/Kan + Strep)
- isopropyl β-D-1-thiogalactopyranoside (IPTG; 1 M stock solution)
- programmable matrix with 655 and 850-nm LEDs (cf. Sections 2.2 and 2.3)

- black-wall clear-bottom 96-well MTPs (Greiner)
- black 96-well MTPs (e.g., Greiner)
- transparent 96-well MTPs (e.g., Greiner)
- gas-permeable sealing film (BF-410400-S, Corning)
- incubator, e.g., HN-2 Herp Nursery II (Lucky Reptile)
- MTP shaker, e.g., PMS-1000i (Grant Instruments)
- multimode MTP reader, e.g., Tecan Infinite M200 PRO (Tecan Group Ltd.)

4.2 Protocol A

i. Transform between 10 pg and 100 ng each of the pCyclR reporter and the pCDF expression plasmids into *E. coli* CmpX13 *ΔcyaA* cells, plate on LB/Kan + Strep agar and incubate over night at 37 °C. If efficiency is insufficient, transform the two plasmids sequentially. (Note that here and in the following experimental steps, we assume that the pCDF *Dd*PAC expression plasmid and *E. coli* CmpX13 *ΔcyaA* cells are used. However, other PAC proteins and cyclase-deficient *E. coli* BL21 strains may be used instead.)

ii. Inoculate a 5-mL LB/Kan + Strep starter culture with a single clone from a freshly transformed plate and incubate over night at 37 °C.

iii. Dispense 180 µL LB/Kan + Strep each to 64 wells (use rows A–H and columns 1–8) of a black-wall, clear-bottom 96-well MTP using a multichannel pipette. Inoculate each well with 2 µL of the over-night culture.

iv. Seal the MTP with a gas-permeable film to allow sufficient air circulation during subsequent incubation.

v. Place the MTP on a shaker and incubate at 37 °C and 800 rpm for 1 h in darkness.

vi. Add 60 µL of 0.2 mM IPTG in LB/Kan + Strep to each well. The resultant final IPTG concentration of 50 µM proved ideal for *Dd*PAC; however, other PACs may require different inductor concentrations.

vii. Configure the LED matrix according to Section 2. For the study of *Dd*PAC activation by constant illumination, we varied the intensity of red (peak emission 655 nm) and far-red light (850 nm) between 0 and 80 µW cm^{-2} (Stüven et al., 2019).

viii. Place the sealed MTP plate on top of the configured LED-array setup. If necessary, fix the plate in position with duct tape.

ix. Mount the assembly on an MTP shaker, place inside a suitable incubator and incubate at 37 °C and 800 rpm for 22 h. Ensure that the incubator is tightly sealed against stray light from the outside and stays closed for the entire experiment.

x. Remove the sealing film. Using a multi-channel pipette, transfer 25 µL of each culture to a transparent MTP and add 225 µL H_2O. Measure OD_{600} of each well in an MTP reader. If absorbance falls outside the interval 0.1–1.0, prepare another solution of the bacterial cultures at an appropriate dilution factor.

xi. Using a multi-channel pipette, transfer 50 µL of the diluted solutions from the previous step to a black MTP and add 200 µL H_2O. Measure reporter fluorescence of each well in an MTP reader. To monitor *Ds*Red fluorescence, we used excitation and emission wavelengths of (554 ± 9) and (591 ± 20) nm, respectively. For optimal results, adjust the gain and focal height of the MTP reader. To allow comparison between experiments on different days, these settings must be left unchanged.

xii. Normalize fluorescence data to OD_{600} and plot as a function of the intensity of red/far-red illumination, e.g., using the open-source Fit-o-mat software (Möglich, 2018) (Fig. 4B).

xiii. As the expected result, the *Ds*Red reporter-gene output should increase hyperbolically with red-light intensity but should stay constant at a basal level for far-red illumination.

4.3 Protocol B

i. Follow steps i–vi as described for protocol A.

ii. Configure the LED matrix according to Section 2. For the study of *Dd*PAC activation by pulsed illumination, we used a red-light (peak emission 655 nm) intensity of 40 µW cm^{-2}. In periodic manner, illumination for 60 s was followed by incubation in darkness for between 0 and 3600 s. The alternating dark/light cycles continued until the end of the incubation (Stüven et al., 2019).

iii. Follow steps viii–xii as described for protocol A.

iv. As the expected result, the *Ds*Red reporter-gene output should increase hyperbolically with the duty cycle of red-light exposure (Fig. 4C), where the duty cycle denotes the fraction of time during which light was applied.

5. Summary and conclusion

Beyond variation of light quantity (intensity) and quality (color), the timing of intermittently applied light affords an additional input dial for adjusting the output of optogenetic systems. Pulsatile illumination offers at least two principal advantages (Hennemann et al., 2018): first, carefully chosen lighting sequences can significantly lower the required overall light dose, thus reducing phototoxicity, photobleaching and heat input, but retaining the desired optogenetic output. Second, intermittent light facilitates the parallel deployment of several light-regulated circuits even when they are sensitive to the same light quality (i.e., wavelength), as long as they differ in their response to pulsatile light. As exemplified for the pDusk variants YF1 and V28I (cf. Section 3), a single light color suffices for successively actuating two systems, thus freeing up optical input channels that may be used for other optogenetic actuators and fluorescent reporters. The exact response to pulsed illumination is primarily governed by the reversal kinetics of the system in question, i.e., how fast is the dark-adapted state regained after prior light exposure, but other aspects matter as well. Whereas in simple scenarios these kinetics are of single-exponential form (cf. Fig. 1B), the output of other systems may be governed by oligomeric species and cooperative effects, thus giving rise to non-exponential and more complex reversal kinetics (cf. Fig. 1C). This type of cooperativity has indeed been observed for certain homodimeric photoreceptors (Möglich et al., 2009) and is generally expected to at least some extent for light-mediated reactions that involve two or more light-responsive entities. As a case in point, the plant cryptochrome 2 is known to undergo light-dependent homo-oligomerization which has been amply exploited for optogenetic intervention in different cellular processes (Bugaj, Choksi, Mesuda, Kane, & Schaffer, 2013; Bugaj et al., 2015; Losi et al., 2018; Taslimi et al., 2014). Moreover, reaction sequences downstream of the photoreceptor and en route to the eventual optogenetic output may entail nonlinear and thresholding effects, thus further altering the response dynamics of the system to (pulsed) illumination. Taken together, the relevant response kinetics may be challenging to gauge upfront and should ideally be assessed on a case-by-case basis for each optogenetic system.

Against this backdrop, the advent of affordable, customizable, parallelizable and programmable illumination devices appears particularly relevant. Numerous light intensities and timing schemes can be interrogated

in parallel and facile manner, thus allowing the response characteristics of a given light-sensitive system to be precisely mapped. Provided two such systems sufficiently differ in that regard, they can be sequentially activated by a single light color (cf. Fig. 3; Hennemann et al., 2018). To fully capitalize on the enhanced throughput for light-mediated actuation, the recording of the system response should support commensurate throughput. On the one hand, reporter-gene assays, as demonstrated here (cf. Sections 3 and 4), apply as they efficiently report on the activity of the light-responsible system, even if only in indirect manner. On the other hand, one may directly monitor the desired optogenetic response of the system under study if it gives rise to a readily recordable phenotype.

The programmable arrays of light-emitting diodes used here are entirely based on open electronics and commercially available parts. Hence, most laboratories will be able to assemble them at moderate expenditure of time and cost. Our setups (Hennemann et al., 2018; Stüven et al., 2019) and a host of related ones for programmable illumination (Chen, Mertiri, Holland, & Basu, 2012; Davidson, Basu, & Bayer, 2013; Gerhardt et al., 2016; Heo, Cho, Ramanan, Oh, & Kim, 2015; Lee, Lee, Kim, & Lee, 2013; Olson, Hartsough, Landry, Shroff, & Tabor, 2014; Pilizota & Yang, 2018; Richter et al., 2015; Szymula et al., 2018) now allow the routine testing of multiple lighting settings and efficient exploration of the accessible parameter space. As discussed above, this methodology particularly benefits optogenetics but it also extends to other light-dependent biological and even chemical phenomena, with pertinent examples being the growth dynamics of photoautotrophic organisms (Reimers, Knoop, Bockmayr, & Steuer, 2017), the activity of light-driven enzymes (Sorigué et al., 2017), and the photocatalysis of diverse chemical conversions (König, 2013; Romero & Nicewicz, 2016).

Acknowledgments

We thank our colleagues in the Möglich laboratory for discussion; Dr. Markus Lippitz for advice on the design of the programmable LED arrays; and the electronics shop at the University of Bayreuth for help with the assembly. This work was supported by Grant MO2192/4-1 (to A.M.) by the Deutsche Forschungsgemeinschaft.

References

Alexandre, M. T. A., Arents, J. C., van Grondelle, R., Hellingwerf, K. J., & Kennis, J. T. M. (2007). A base-catalyzed mechanism for dark state recovery in the Avena sativa phototropin-1 LOV2 domain. *Biochemistry*, *46*(11), 3129–3137. https://doi.org/10.1021/bi062074e.

Blain-Hartung, M., Rockwell, N. C., Moreno, M. V., Martin, S. S., Gan, F., Bryant, D. A., et al. (2018). Cyanobacteriochrome-based photoswitchable adenylyl cyclases (cPACs)

for broad spectrum light regulation of cAMP levels in cells. *Journal of Biological Chemistry*, *293*(22), 8473–8483. https://doi.org/10.1074/jbc.RA118.002258.

Bugaj, L. J., Choksi, A. T., Mesuda, C. K., Kane, R. S., & Schaffer, D. V. (2013). Optogenetic protein clustering and signaling activation in mammalian cells. *Nature Methods*, *10*(3), 249–252. https://doi.org/10.1038/nmeth.2360.

Bugaj, L. J., Spelke, D. P., Mesuda, C. K., Varedi, M., Kane, R. S., & Schaffer, D. V. (2015). Regulation of endogenous transmembrane receptors through optogenetic Cry2 clustering. *Nature Communications*, *6*, 6898. https://doi.org/10.1038/ncomms7898.

Chen, M., Mertiri, T., Holland, T., & Basu, A. S. (2012). Optical microplates for high-throughput screening of photosynthesis in lipid-producing algae. *Lab on a Chip*, *12*(20), 3870–3874. https://doi.org/10.1039/c2lc40478h.

Christie, J. M., Reymond, P., Powell, G. K., Bernasconi, P., Raibekas, A. A., Liscum, E., et al. (1998). Arabidopsis NPH1: A flavoprotein with the properties of a photoreceptor for phototropism. *Science*, *282*(5394), 1698–1701.

Davidson, E. A., Basu, A. S., & Bayer, T. S. (2013). Programming microbes using pulse width modulation of optical signals. *Journal of Molecular Biology*, *425*(22), 4161–4166. https://doi.org/10.1016/j.jmb.2013.07.036.

Deisseroth, K., Feng, G., Majewska, A. K., Miesenböck, G., Ting, A., & Schnitzer, M. J. (2006). Next-generation optical technologies for illuminating genetically targeted brain circuits. *Journal of Neuroscience*, *26*(41), 10380–10386. https://doi.org/10.1523/JNEUROSCI.3863-06.2006.

Etzl, S., Lindner, R., Nelson, M. D., & Winkler, A. (2018). Structure-guided design and functional characterization of an artificial red light–regulated guanylate/adenylate cyclase for optogenetic applications. *Journal of Biological Chemistry*, *293*(23), 9078–9089. https://doi.org/10.1074/jbc.RA118.003069.

Gerhardt, K. P., Olson, E. J., Castillo-Hair, S. M., Hartsough, L. A., Landry, B. P., Ekness, F., et al. (2016). An open-hardware platform for optogenetics and photobiology. *Scientific Reports, 6*, 35363. https://doi.org/10.1038/srep35363.

Hegemann, P. (2008). Algal sensory photoreceptors. *Annual Review of Plant Biology*, *59*, 167–189. https://doi.org/10.1146/annurev.arplant.59.032607.092847.

Hennemann, J., Iwasaki, R. S., Grund, T. N., Diensthuber, R. P., Richter, F., & Möglich, A. (2018). Optogenetic control by pulsed illumination. *Chembiochem*, *19*(12), 1296–1304. https://doi.org/10.1002/cbic.201800030.

Heo, J., Cho, D.-H., Ramanan, R., Oh, H.-M., & Kim, H.-S. (2015). PhotoBiobox: A tablet sized, low-cost, high throughput photobioreactor for microalgal screening and culture optimization for growth, lipid content and CO2 sequestration. *Biochemical Engineering Journal*, *103*, 193–197. https://doi.org/10.1016/j.bej.2015.07.013.

Iseki, M., Matsunaga, S., Murakami, A., Ohno, K., Shiga, K., Yoshida, K., et al. (2002). A blue-light-activated adenylyl cyclase mediates photoavoidance in *Euglena gracilis*. *Nature*, *415*(6875), 1047–1051. https://doi.org/10.1038/4151047a.

Kawano, F., Aono, Y., Suzuki, H., & Sato, M. (2013). Fluorescence imaging-based high-throughput screening of fast- and slow-cycling LOV proteins. *PLoS One*, *8*(12). e82693. https://doi.org/10.1371/journal.pone.0082693.

König, B. (2013). *Chemical photocatalysis*. Berlin, Boston: De Gruyterhttps://doi.org/10.1515/9783110269246.

Lee, J. M., Lee, J., Kim, T., & Lee, S. K. (2013). Switchable gene expression in Escherichia coli using a miniaturized photobioreactor. *PLoS One*, *8*(1), e52382. https://doi.org/10.1371/journal.pone.0052382.

Losi, A., Gardner, K. H., & Möglich, A. (2018). Blue-light receptors for optogenetics. *Chemical Reviews*, *118*(21), 10659–10709. https://doi.org/10.1021/acs.chemrev.8b00163.

Mathes, T., Vogl, C., Stolz, J., & Hegemann, P. (2009). In vivo generation of flavoproteins with modified cofactors. *Journal of Molecular Biology*, *385*(5), 1511–1518. https://doi.org/10.1016/j.jmb.2008.11.001.

Möglich, A. (2018). An open-source, cross-platform resource for nonlinear least-squares curve fitting. *Journal of Chemical Education*, *95*(12), 2273–2278. https://doi.org/10.1021/acs.jchemed.8b00649.

Möglich, A., Ayers, R. A., & Moffat, K. (2009). Design and signaling mechanism of light-regulated histidine kinases. *Journal of Molecular Biology*, *385*(5), 1433–1444. https://doi.org/10.1016/j.jmb.2008.12.017.

Möglich, A., Yang, X., Ayers, R. A., & Moffat, K. (2010). Structure and function of plant photoreceptors. *Annual Review of Plant Biology*, *61*, 21–47. https://doi.org/10.1146/annurev-arplant-042809-112259.

Monod, J., Wyman, J., & Changeux, J. P. (1965). On the nature of allosteric transitions: A plausible model. *Journal of Molecular Biology*, *12*, 88–118. https://doi.org/10.1016/S0022-2836(65)80285-6.

Ohlendorf, R., Vidavski, R. R., Eldar, A., Moffat, K., & Möglich, A. (2012). From dusk till dawn: One-plasmid systems for light-regulated gene expression. *Journal of Molecular Biology*, *416*(4), 534–542. https://doi.org/10.1016/j.jmb.2012.01.001.

Olson, E. J., Hartsough, L. A., Landry, B. P., Shroff, R., & Tabor, J. J. (2014). Characterizing bacterial gene circuit dynamics with optically programmed gene expression signals. *Nature Methods*, *11*(4), 449–455. https://doi.org/10.1038/nmeth.2884.

Pilizota, T., & Yang, Y.-T. (2018). "Do it yourself" microbial cultivation techniques for synthetic and systems biology: Cheap, fun, and flexible. *Frontiers in Microbiology*, *9*, https://doi.org/10.3389/fmicb.2018.01666.

Pudasaini, A., El-Arab, K. K., & Zoltowski, B. D. (2015). LOV-based optogenetic devices: Light-driven modules to impart photoregulated control of cellular signaling. *Frontiers in Molecular Biosciences, 2*, 18. https://doi.org/10.3389/fmolb.2015.00018.

Raffelberg, S., Wang, L., Gao, S., Losi, A., Gärtner, W., & Nagel, G. (2013). A LOV-domain-mediated blue-light-activated adenylate (adenylyl) cyclase from the cyanobacterium Microcoleus chthonoplastes PCC 7420. *Biochemical Journal*, *455*(3), 359–365. https://doi.org/10.1042/BJ20130637.

Reimers, A.-M., Knoop, H., Bockmayr, A., & Steuer, R. (2017). Cellular trade-offs and optimal resource allocation during cyanobacterial diurnal growth. *Proceedings of the National Academy of Sciences of the United States of America*, *114*, E6457–E6465. https://doi.org/10.1073/pnas.1617508114.

Richter, F., Scheib, U. S., Mehlhorn, J., Schubert, R., Wietek, J., Gernetzki, O., et al. (2015). Upgrading a microplate reader for photobiology and all-optical experiments. *Photochemical & Photobiological Sciences*, *14*(2), 270–279. https://doi.org/10.1039/c4pp00361f.

Rockwell, N. C., & Lagarias, J. C. (2010). A brief history of phytochromes. *Chemphyschem*, *11*(6), 1172–1180. https://doi.org/10.1002/cphc.200900894.

Romero, N. A., & Nicewicz, D. A. (2016). Organic photoredox catalysis. *Chemical Reviews*, *116*(17), 10075–10166. https://doi.org/10.1021/acs.chemrev.6b00057.

Ryu, M.-H., Kang, I.-H., Nelson, M. D., Jensen, T. M., Lyuksyutova, A. I., Siltberg-Liberles, J., et al. (2014). Engineering adenylate cyclases regulated by near-infrared window light. *Proceedings of the National Academy of Sciences of the United States of America*, *111*(28), 10167–10172. https://doi.org/10.1073/pnas.1324301111.

Ryu, M.-H., Moskvin, O. V., Siltberg-Liberles, J., & Gomelsky, M. (2010). Natural and engineered photoactivated nucleotidyl cyclases for optogenetic applications. *Journal of Biological Chemistry*, *285*(53), 41501–41508. https://doi.org/10.1074/jbc.M110.177600.

Salomon, M., Eisenreich, W., Dürr, H., Schleicher, E., Knieb, E., Massey, V., et al. (2001). An optomechanical transducer in the blue light receptor phototropin from Avena sativa. *Proceedings of the National Academy of Sciences of the United States of America*, *98*(22), 12357–12361. https://doi.org/10.1073/pnas.221455298.

Schröder-Lang, S., Schwärzel, M., Seifert, R., Strünker, T., Kateriya, S., Looser, J., et al. (2007). Fast manipulation of cellular cAMP level by light in vivo. *Nature Methods*, *4*(1), 39–42. https://doi.org/10.1038/nmeth975.

Sorigué, D., Légeret, B., Cuiné, S., Blangy, S., Moulin, S., Billon, E., et al. (2017). An algal photoenzyme converts fatty acids to hydrocarbons. *Science*, *357*(6354), 903–907. https://doi.org/10.1126/science.aan6349.

Stierl, M., Stumpf, P., Udwari, D., Gueta, R., Hagedorn, R., Losi, A., et al. (2011). Light-modulation of cellular cAMP by a small bacterial photoactivated adenylyl cyclase, bPAC, of the soil bacterium beggiatoa. *Journal of Biological Chemistry*, *286*(2), 1181–1188. https://doi.org/10.1074/jbc.M110.185496.

Strack, R. L., Strongin, D. E., Bhattacharyya, D., Tao, W., Berman, A., Broxmeyer, H. E., et al. (2008). A noncytotoxic DsRed variant for whole-cell labeling. *Nature Methods*, *5*(11), 955–957. https://doi.org/10.1038/nmeth.1264.

Stüven, B., Stabel, R., Ohlendorf, R., Beck, J., Schubert, R., & Möglich, A. (2019). Characterization and engineering of photoactivated adenylyl cyclases. *Biological Chemistry*, *400*, 429–441. https://doi.org/10.1515/hsz-2018-0375.

Szymula, K. P., Magaraci, M. S., Patterson, M., Clark, A., Mannickarottu, S. G., & Chow, B. Y. (2018). An open-source plate reader. *Biochemistry*, *58*, 468–473. https://doi.org/10.1021/acs.biochem.8b00952.

Taslimi, A., Vrana, J. D., Chen, D., Borinskaya, S., Mayer, B. J., Kennedy, M. J., et al. (2014). An optimized optogenetic clustering tool for probing protein interaction and function. *Nature Communications, 5*, 4925. https://doi.org/10.1038/ncomms5925.

Weissleder, R. (2001). A clearer vision for *in vivo* imaging. *Nature Biotechnology*, *19*, 316–317. https://doi.org/10.1038/86684.

Yee, E. F., Diensthuber, R. P., Vaidya, A. T., Borbat, P. P., Engelhard, C., Freed, J. H., et al. (2015). Signal transduction in light-oxygen-voltage receptors lacking the adduct-forming cysteine residue. *Nature Communications*, *6*, 10079. https://doi.org/10.1038/ncomms10079.

Ziegler, T., & Möglich, A. (2015). Photoreceptor engineering. *Frontiers in Molecular Biosciences*, *2*, 30. https://doi.org/10.3389/fmolb.2015.00030.

7.4. Manuskript IV:

Stabel, R.; Stüven, B.; Hansen, J.N.; Körschen, H.G.; Wachten D.; Möglich, A.; *Journal of Molecular Biology* (2019) "*Revisiting and Redesigning Light-activated Cyclic-Mononucleotide Phosphodiesterases*"

Revisiting and Redesigning Light-Activated Cyclic-Mononucleotide Phosphodiesterases

Robert Stabel [1], Birthe Stüven [1,2], Jan Niklas Hansen [2], Heinz G. Körschen [3], Dagmar Wachten [2,3] and Andreas Möglich [1,4,5,6]

*1 - **Lehrstuhl für Biochemie,** Universität Bayreuth, 95447 Bayreuth, Germany*
*2 - **Institute of Innate Immunity,** Universität Bonn, 53127 Bonn, Germany*
*3 - **Center of Advanced European Studies and Research (caesar),** 53175 Bonn, Germany*
*4 - **Research Center for Bio-Macromolecules,** Universität Bayreuth, Bayreuth, Germany*
*5 - **Bayreuth Center for Biochemistry & Molecular Biology,** Universität Bayreuth, 95447 Bayreuth, Germany*
*6 - **North-Bavarian NMR Center,** Universität Bayreuth, 95447 Bayreuth, Germany*

***Correspondence to Andreas Möglich:** Lehrstuhl für Biochemie, Universität Bayreuth, 95447 Bayreuth, Germany.*
andreas.moeglich@uni-bayreuth.de.
https://doi.org/10.1016/j.jmb.2019.07.011

Abstract

As diffusible second messengers, cyclic nucleoside monophosphates (cNMPs) relay and amplify molecular signals in myriad cellular pathways. The triggering of downstream physiological responses often requires defined cNMP gradients in time and space, generated through the concerted action of nucleotidyl cyclases and phosphodiesterases (PDEs). In an approach denoted optogenetics, sensory photoreceptors serve as genetically encoded, light-responsive actuators to enable the noninvasive, reversible, and spatiotemporally precise control of manifold cellular processes, including cNMP metabolism. Although nature provides efficient photoactivated nucleotidyl cyclases, light-responsive PDEs are scarce. Through modular recombination of a bacteriophytochrome photosensor and the effector of human PDE2A, we previously generated the light-activated, cNMP-specific PDE LAPD. By pursuing parallel design strategies, we here report a suite of derivative PDEs with enhanced amplitude and reversibility of photoactivation. Opposite to LAPD, far-red light completely reverts prior activation by red light in several PDEs. These improved PDEs thus complement photoactivated nucleotidyl cyclases and extend the sensitivity of optogenetics to red and far-red light. More generally, our study informs future efforts directed at designing bacteriophytochrome photoreceptors.

Introduction

Various cellular pathways in both prokaryotes and eukaryotes harness diffusible second messengers to amplify and relay molecular signals in time and space [1]. Cyclic nucleotides represent a widespread class of second messengers that underpin a cohort of physiological responses. In eukaryotes, the two predominant cyclic mononucleotides, 3′, 5′-cyclic adenosine and guanosine monophosphate (cAMP and cGMP) [2–4], bind to the protein kinases A and G [5,6], cyclic nucleotide-gated (CNG) ion channels [7], Epac (exchange protein directly activated by cAMP) [8] and popeye-domain-containing proteins [9], and thereby allosterically regulate the activity of these entities. With but few exceptions [10,11], prokaryotes lack cGMP signaling but widely employ cAMP to regulate gene expression, prominently so in the context of catabolite repression [12,13]. The cyclic nucleoside monophosphates (cNMPs) cAMP and cGMP are generally produced by nucleotidyl cyclases from adenosine and guanosine triphosphate (ATP and GTP). Phosphodiesterases (PDE) mediate the hydrolytic breakdown of cNMPs to the (non-cyclic) 5′-adenosine and 5′-guanosine monophosphates (AMP and GMP), respectively. Mammals possess 11 different PDE families, which subdivide into several isoforms [15,16]. Depending

0022-2836/

on family, these PDEs are specific for either cAMP, cGMP or both. Although the precise protein architecture differs between families, the mammalian PDEs generally comprise N-terminal domains that process signal input and C-terminal catalytically active effector domains. As a case in point, the cAMP/cGMP-specific PDE2A adopts a homodimeric structure, in which two regulatory GAF domains (denoted GAF-A and GAF-B), connect to the C-terminal PDE domain via a parallel α-helical coiled-coil linker [17] (Fig. S1a). cGMP binding to GAF-B prompts an about 4-fold increase in catalytic turnover by displacing an autoinhibitory protein loop (termed H loop) from the PDE active site [17].

Inside the cell, the activities of nucleotidyl cyclases and PDEs are tightly orchestrated to allow generation of complex spatiotemporal cNMP gradients that underpin downstream physiological responses. Implements that modulate the intracellular amounts of cNMPs with precision in space and time are hence particularly applicable for probing and elucidating pertinent signal processes. Optogenetics [18], referring to the monitoring and control by light of cellular events via genetically encoded agents, has contributed versatile tools for the study of cNMP signal transduction [19,20]. In specific, certain sensory photoreceptors occurring in nature act as photoactivated adenylyl cyclases (PAC) and ramp up cAMP production upon light application [21–26]. While most of these cyclases respond to blue light, a group of PACs sensitive to red/far-red light were engineered by recombining cyclase effector modules with the so-called photosensory core modules (PCMs) of bacterial phytochrome (BphP) receptors [27–30]. The phytochrome PCM comprises tandem PAS, GAF, and PHY domains and harbors a linear tetrapyrrole (bilin) chromophore, biliverdin (BV) in case of BphPs [31]. In darkness, conventional BphPs assume the red-light-absorbing Pr state with their BV cofactor in its 15*Z* conformation. Red light drives the photoisomerization of BV to the 15*E* state, giving rise to the far-red-light-absorbing Pfr form; the reversion to the Pr state occurs in a slow thermal reaction or can be actively driven by far-red light. By contrast, in bathyphytochromes, the Pfr state is the thermodynamically stable state assumed in darkness [31]. Structures of the isolated PCM of the conventional BphP from *Deinococcus radiodurans* (*Dr*BphP) revealed that the chromophore isomerization induces refolding of a protrusion of the PHY domain, denoted tongue, from a β-sheet conformation in Pr to an α-helical conformation in Pfr, which in turn promotes quaternary structural rearrangements in the dimeric receptor [32,33]. BphP-based actuators are attractive as optogenetic tools for at least three principal reasons: first, long-wavelength light penetrates biological tissue more deeply than light of shorter wavelengths [34]; second, BphPs can be bimodally switched by red and far-red light, thus affording enhanced spatiotemporal resolution in optogenetics [35]; and third, BV widely occurs in mammalian tissue as a heme degradation product, thus obviating exogenous chromophore addition and greatly facilitating optogenetic applications [27,36,37]. In addition to PACs, a number of photoactivated guanylyl cyclases are available in nature or by protein engineering [24,38–42]. By contrast, there has been a relative dearth of light-regulated actuators that would mediate the hydrolytic breakdown of cNMPs. To fill this gap, we previously constructed the light-activated PDE LAPD via recombination of the *Dr*BphP PCM and the effector module of *Homo sapiens* PDE2A (*Hs*PDE2A) [36] (Fig. 1a). Similar to the parental *Hs*PDE2A, LAPD hydrolyzed both cAMP and cGMP with comparable rates and affinities; red light elevated the maximum catalytic turnover of LAPD by around 6-fold. However, although far-red light partially reverted this increase in turnover, the reaction was incomplete, hinting at inefficient Pfr → Pr photoconversion [36]. Since, a PDE covalently linked to a microbial rhodopsin photosensor unit has been discovered in the choanoflagellate *Salpingoeca rosetta* [43,44]. Biochemical analyses revealed a preference for cGMP over cAMP, and an around 7-fold increase in cGMP affinity upon light absorption [45].

Against this backdrop, we here report the engineering of cNMP-specific PDEs that respond to red/far-red light and improve on LAPD regarding extent and reversibility of switching. The analysis of multiple PDE variants identifies sequence motifs underpinning efficient regulation by light and thus establishes refined design rules for constructing light-activated PDEs. As we showcase for the gating of CNG channels in mammalian cells, the novel LAPD variants can be deployed to probe and control cNMP-associated cellular processes. Light-regulated PDEs thus complement the diverse set of PACs and enrich the arsenal of optogenetics [19,46].

Results

Modular construction of cyclic-mononucleotide Phosphodiesterases

To engineer derivative red-/far-red-light-responsive PDEs, we revisited the original LAPD design, which was informed by the structural homology between the sensor modules of BphPs and certain mammalian PDEs [36]. Despite vastly different phylogenetic origin, both entities share a parallel homodimeric architecture, structurally homologous N-terminal sensor domains and central α-

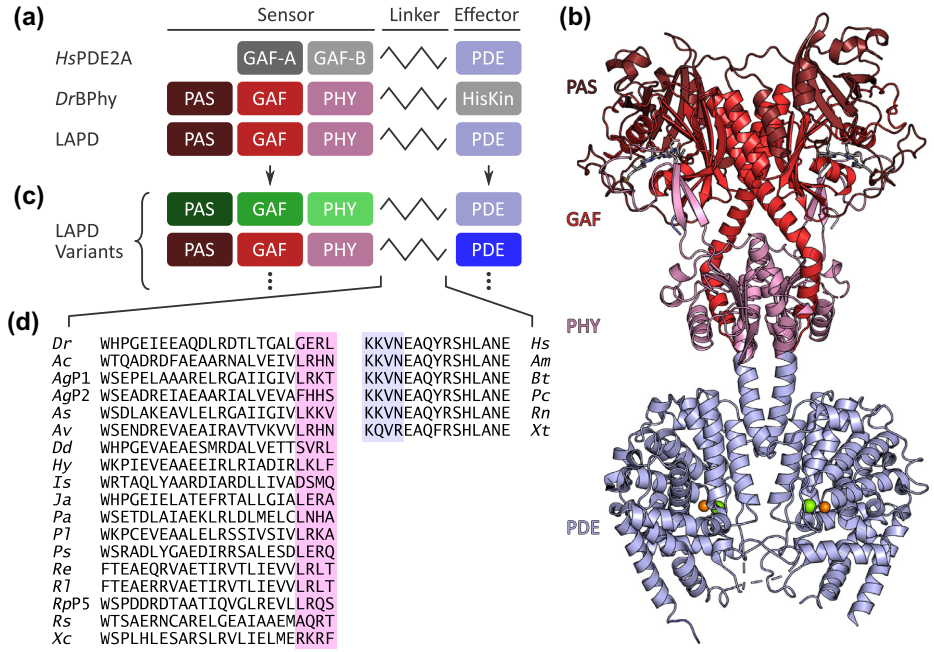

Fig. 1. Engineering of light-regulated cNMP-specific PDEs. (a) The prototype LAPD originated from the modular recombination of the *Deinococcus radiodurans* bacteriophytochrome (*Dr*BphP) photosensor, comprising PAS-GAF-PHY domains, and the *Homo sapiens* PDE2A (*Hs*PDE2A) effector domain [36]. (b) Structural model of LAPD based on the structures of the engineered BphP PagC (PDB code 6FHT) [28] and *Hs*PDE2A (3IBJ) [17]. The PAS, GAF, PHY and PDE domains are colored in dark red, red, pink and light blue, respectively; the green and orange spheres in the PDE domain denote magnesium and zinc ions. (c) To generate derivative light-regulated PDEs, the photosensor and/or the effector moieties of LAPD were exchanged for modules from homologous BphPs and PDEs. (d) Partial sequence alignment of the linker region of BphPs and PDEs used in the construction of LAPD derivatives. The top line denotes the fusion between *Dr*BphP and *Hs*PDE2A and corresponds to the prototypical LAPD. Residues near the fusion site are highlighted by pink and blue shading. Species abbreviations for the BphP PCMs are *Ag*P1, *Agrobacterium tumefaciens* BphP P1; *Ag*P2, *A. tumefaciens* BphP P2; *Ac*, *Azorhizobium caulinodans*; *As*, *Acaryochloris* sp. CCMEE 5410; Av, *Agrobacterium vitis*; *Dd*, *Deinococcus deserti*; *Dr*, *Deinococcus radiodurans*; *Hy*, *Hymenobacter swuensis*; *Is*, *Idiomarina* sp. A28L; *Ja*, *Janthinobacterium* sp. CG23_2; *Pa*, *Pseudomonas aeruginosa*; *Pl*, *Pleurocapsa* sp. PCC7319; *Ps*, *Pseudomonas syringae*; *Re*, *Rhizobium etli*; *Rl*, *Rhizobium leguminosarum*; *Rp*P5, *Rhodopseudomonas palustris* BphP P5; *Rs*, *Rhodobacter sphaeroides*; and *Xc*, *Xanthomonas campestris*. PDE modules derive from *Am*, *Alligator mississippiensis*; *Bt*, *Bos taurus*; *Hs*, *Homo sapiens*; *Pc*, *Phascolarctos cinereus*; *Rn*, *Rattus norvegicus*; and *Xt*, *Xenopus tropicalis*.

helical spines, which coincide with the C_2-symmetry axes and feed into coiled-coil linkers connecting to the respective effector modules (Fig. S1). At the time, structural information on the complete *D. radiodurans* PCM was lacking, and the LAPD design relied on the PCM structure of *Pseudomonas aeruginosa* BphP (*Pa*BphP) in its Pfr state [47]. Although eventually fruitful, this design blueprint suffered from several shortcomings: first, in the actual LAPD, the *Hs*PDE2A effector is fused to the *Dr*BphP PCM, rather than to the *Pa*BphP PCM (Fig. 1a); second, unlike *Dr*BphP, *Pa*BphP is a bathyphytochrome; third, the coiled-coil linker was not resolved in the *Pa*BphP structure, thus leaving ambiguous the precise molecular arrangement of this structural region in LAPD. Arguably due to these deficits, the design initially favored a chimeric receptor, denoted LAPD+2, with two additional residues in the coiled-coil linker relative to LAPD, but devoid of light-regulated PDE activity [36]; subsequent removal of these two residues gave rise to the light-responsive LAPD. Structures of the complete PCM of *Dr*BphP in both the Pr and Pfr states have since become available [32,33], as has that of the engineered BphP-guanylyl cyclase PagC, which atomically resolves the coiled-coil linker of *Dr*BphP [28]. Informed by these data, we updated our structural model for LAPD (Figs. 1b and S1). Whereas the original model placed the BphP PCM and the PDE effector of one chain on opposite sides

of the α-helical spine traversing the homodimeric receptor, the new model positions them on the same side. Moreover, the revised model enables structural modeling of the fusion site in LAPD with enhanced confidence, see below.

We hypothesized that the limited reversibility of light-dependent activation evidenced in LAPD might be rooted in the *Dr*BphP PCM. This view is borne out in a recently engineered PAC that shares with LAPD the *Dr*BphP PCM and likewise exhibits limited photo reversibility upon prior activation by light [28,29]. By contrast, replacing the PCM of *Dr*BphP with that of *Deinococcus deserti* BphP (*Dd*BphP) yielded a PAC with photoreversible adenylyl cyclase activity [29]. We hence generated LAPD variants by substituting the PCM of *Dr*BphP for those of 17 different BphPs (Fig. 1c), some of which were previously described as conventional and bathyphytochromes, respectively [48]. In choosing so, we sought to cover a wide range of BphP modules with different properties, and to thereby increase the chance of eventually obtaining enhanced LAPD variants. For the facile assessment of PDE activity and response to light, we resorted to an enzymatic assay that can be conducted in crude cell lysate [49]. Briefly, the hydrolysis of cNMP to NMP is accompanied by proton release, thus leading to acidification of weakly buffered solutions, which is readily detectable with the pH-sensitive fluorescein derivative BCECF [50] (Fig. 2a). We thus expressed LAPD in *Escherichia coli* along with *Synechocystis* sp. heme oxygenase 1 (*Ss*HO) [51], that supplies biliverdin, and ascertained production of the holo enzyme by green coloration of the bacterial suspension and zinc-induced fluorescence of the bilin chromophore [52]. Following cell lysis, PDE activity can be directly probed in bacterial lysate. Within this assay, LAPD showed an initial drop in normalized BCECF fluorescence of -3.9×10^{-3} min^{-1} when incubated with saturating amounts of 2 mM cGMP in darkness and of -1.9×10^{-2} min^{-1} when illuminated with 670-nm light. In the following, we report results from this lysate assay as unitless BCECF activity values normalized to the signal of LAPD under red light (arbitrarily set to 1.0). Previous studies on LAPD and related homodimeric receptors had pinpointed the length and, to lesser extent, the sequence of coiled-coil linkers between sensor and effector modules as crucial for overall activity and responsiveness to light [27,28,36,53,54]; even the mere insertion or omission of single residues within this region can utterly alter light-dependent receptor output. When constructing fusions between the various BphP PCMs and the *Hs*PDE2A effector module, we thus retained the same linker register as in LAPD (Fig. 1d). We first ascertained expression in *E. coli* by green coloration and Western blot (Fig. S2), which revealed that almost all BphP-PDE variants were expressed to similar extent as LAPD. Merely, the variant based on

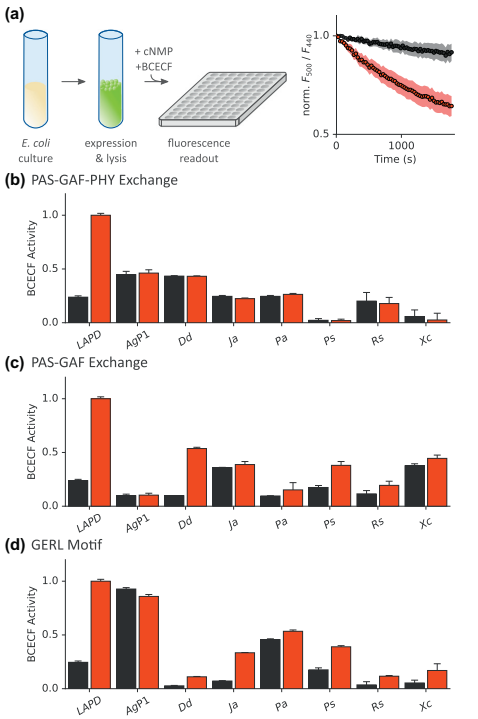

Fig. 2. Screening for light-regulated cNMP-specific PDE variants. (a) Candidate PDEs are expressed in *E. coli* and assessed for light-regulated activity in bacterial lysate. As cNMP hydrolysis entails proton release, the progressive acidification of a weakly buffered solution can be monitored over time via the pH-sensitive fluorophore BCECF [49]. As exemplarily shown for LAPD, the assay provides a facile readout for candidate PDEs in their dark-adapted states (black) and following red-light exposure (red). In panels b through d, the apparent cGMP hydrolysis activities of candidate PDEs are reported as the initial slopes in the BCECF assays, normalized to the signal obtained for LAPD upon red-light stimulation. All data represent mean ± s.d. of four biological replicates. (b) The PAS-GAF-PHY photosensor of LAPD was exchanged for the corresponding modules from homologous bacteriophytochromes (BphP) and cGMP hydrolysis of the resultant PDE variants was measured. Species abbreviations are provided in Fig. 1. (c) The PAS and GAF domains of LAPD were substituted for the corresponding domains of other BphPs (see Fig. S4). (d) The linker regions of select BphP-PDE variants from panel b were modified to resemble the GERL motif found in the light-responsive LAPD prototype (see Figs. 1d and S5). In case of *Rs*-*Hs*PDE2A and *Xc*-*Hs*PDE2A variants, data for the most strongly light-regulated variants with the linker sequences GERT and GERF are shown.

the PCM from *Rhodopseudomonas palustris* BphP P5 exhibited attenuated yet detectable expression. We then assessed the cGMP hydrolysis activity of these variants in bacterial lysate by BCECF fluorescence (Figs. 2b and S3a). All tested BphP-PDE variants exhibited lower PDE activity compared to LAPD, but none showed significant red-light dependence of activity. Likewise, illumination with far-red light did not elicit any activity increase. While the differences in the observable overall activity might be attributable to variations in functional expression and specific activity, we were puzzled by the complete lack of light responsiveness. Evidently, the design template underpinning LAPD is not directly transferrable to homologous BphP PCMs, at least not without further optimization.

Imparting light sensitivity on cyclic-mononucleotide Phosphodiesterases

We tentatively ascribed the consistent lack of light responsiveness in the LAPD variants to deficient allosteric coupling between the bacterial PCM and the eukaryotic PDE module. To enhance this coupling and thus attain light-regulated PDE activity, we pursued two concurrent strategies. In a first approach, we replaced the PAS and GAF domains of the light-responsive LAPD for those of homologous BphPs while retaining the *Dr*PHY and *Hs*PDE2A domains. Although this replacement generates an additional seam between the GAF and PHY domains deriving from different BphPs, it preserves the critical junction between the PHY and PDE domains of LAPD. We selected 10 of the above BphPs and created chimera between their PAS-GAF portions and the PHY-PDE fragment of LAPD (Fig. S4). As before, we coexpressed the resultant BphP-PDE variants with *Ss*HO (Fig. S2) and assessed their cGMP hydrolytic activity in darkness and under 670-nm light by BCECF fluorescence (Figs. 2c and S3b). Out of the 10 variants, 7 showed constitutive hydrolysis activity, but 3 variants, harboring the PAS-GAF fragments of *Dd*BphP, *Pseudomonas syringae* BphP (*Ps*BphP) and *Agrobacterium tumefaciens* P2 (*Ag*P2), significantly increased activity in response to red light relative to darkness. In particular, the variants based on *Dd*BphP and *Ps*BphP, referred to as *DdDr-Hs*PDE2A and *PsDr-Hs*PDE2A, exhibited red-light-induced increases in BCECF activity of around 5.5-fold and 2.2-fold, respectively.

In light of these findings, we reasoned that the configuration of the linker around the junction between the PHY and PDE domains of LAPD might be particularly relevant for efficient coupling between photosensor and effector. Based on amino acid sequence and full-length structures of BphP receptors [28,56–58], the linker of LAPD is expected to adopt a continuous α helix, with the BphP PCM terminating in the four residues Gly-503, Glu-504, Arg-505 and Leu-506 (GERL in single-letter code), and the PDE effector continuing with the residues Lys-507 and Lys-508 (KK). As illustrated by the LAPD homology model (Figs. 1b and 3a), residues E504 and K508 are appropriately spaced to potentially form an *i*, *i* + 4 salt bridge that traverses the seam between the PCM and PDE moieties. In the vicinity, two additional salt bridges are formed between R505 and E426 within the PHY domain, and between K507 and E511 within the PDE part. To probe the relevance of this region of LAPD, we exchanged individual residues of the GERL motif for amino acids found in the corresponding position of the homologous BphPs (Figs. 1d and 3b–e). In summary, almost all substitutions within the GERL motif severely attenuated the light response or entirely abolished it. As exceptions, the exchanges of E504 to alanine or arginine preserved light responsiveness to significant extent, as did the replacement of L506 for isoleucine. To further probe the functional role of the potential E504:K508 and K507:E511 salt bridges running along the linker helix, we also substituted the two lysine residues (Fig. 3f). Replacement of K507 for serine, the corresponding amino acid present in *Dr*BphP [36] (see Fig. S4), resulted in a PDE variant with constitutively low activity and minute light response. By contrast, the exchange of K508 to alanine neither affected PDE activity nor light regulation. Although it is challenging to fully rationalize the various substitutions at a structural and functional level, several general aspects emerge. First, the linker segment of LAPD is highly sensitive to structural perturbations, with most residue exchanges, even those of conservative type, impairing overall activity and light responsiveness. Second, a putative salt bridge between E504 and K508, if present at all in LAPD, is not essential for productive signal transduction. Third, although we probed more than 20 sequence variations of the linker region, the original motif proved the best-suited for robust activity and regulation by light.

Given the pronounced preference for the ^{503}GERL^{506} sequence at the BphP-PDE junction in LAPD, we investigated whether light sensitivity can be bestowed on the above light-inert BphP-PDE receptors via introduction of said sequence. To this end, we selected seven variants, consisting of the intact PCMs (PAS-GAF-PHY) of homologous BphPs and the *Hs*PDE2A effector module (see Fig. 2b), and stepwise altered their linker segments toward the GERL motif by exchanging between two and four residues (Figs. 2d, S2 and S5). BCECF activity measurements revealed that this approach indeed succeeded in converting five out of the seven BphP-PDEs into light-activated receptors. Although these light-regulated variants generally showed BCECF activity lower than LAPD, they exhibited similar factors of activation upon red-light exposure.

Notably, in certain of these variants, light responsiveness was only achieved when retaining the terminal residue of the original PCM rather than altering it to leucine. For example, in the *Rs-Hs*PDE2A receptor, comprising the PCM of *Rhodobacter sphaeroides* BphP, red light prompted an activity increase when the corresponding residue was the original threonine (GER**T**) but not when it was leucine. Perplexingly, in LAPD the replacement of leucine in this position for threonine abrogated light responsiveness (see Fig. 3).

Modular exchange of Phosphodiesterase effector modules

The above experiments compellingly illustrate that the engineering of derivative red-light-regulated PDEs via modification of the BphP photosensor module is challenging. In a parallel approach, we substituted the effector unit of LAPD for the catalytic domains from five vertebrate PDE2A enzymes (Fig. 1d), an approach that benefits from high levels of sequence homology between 81% and 98%. With the original LAPD as template, we constructed fusions between the *Dr*BphP PCM and the homologous PDE2A effectors, expressed the resultant receptors (Fig. S2) and assessed cGMP hydrolysis in bacterial lysate (Fig. S6). Whereas two of these receptors showed low activity and no significant response to illumination, the variants *Dr-Bt*PDE2A, *Dr-Pc*PDE2A, and *Dr-Xt*PDE2A, based on the PDE2A enzymes from *Bos taurus*, *Phascolarctos cinereus* and *Xenopus tropicalis*, respectively, exhibited light-stimulated activity. Notably, the *Dr-Bt*PDE2A receptor displayed reduced activity in darkness relative to LAPD, but increased activity upon red-light exposure, translating into a much more pronounced regulation by light. Compared to the above efforts at derivatizing LAPD that centered on the BphP photosensor module, the exchange of the effector module proved strikingly more successful and yielded PDE variants with stringent light regulation.

To better characterize cNMP hydrolysis and response to light, we expressed and purified *Dr-Bt*PDE2A, *Dr-Pc*PDE2A, and *Dr-Xt*PDE2A, as well as the above variants *Dd*GERL-*Hs*PDE2A and *DdDr-Hs*PDE2A (see Fig. 2c, d). UV/vis spectroscopy indicated that in darkness, all these BphP-PDEs predominantly assume their Pr state, which maximally absorbs around 700 nm (Fig. 4). In case of *DdDr-Hs*PDE2A, partial population of the Pfr state, maximally absorbing around 750 nm, was evident even in darkness. Red light (670 nm) drove the Pr → Pfr transition in the PDE variants to similar but slightly lower extent relative to LAPD. As an exception, the degree of Pr → Pfr photoconversion in *DdDr-Hs*PDE2A was markedly reduced, and both the Soret and the Q bands, at around 400 and 700 nm, respectively, exhibited shoulders. These observations point toward impaired photochemistry, which presumably results from the recombination of the PAS-GAF domains from one BphP with the PHY domain from another in this variant. Subsequent illumination with far-red light (780 nm) reverted the spectra to their dark-adapted states in all cases.

We went on and quantified cGMP hydrolysis at 1 mM substrate concentration by the BphP-PDE variants in darkness and following red-light application via high-performance liquid chromatography

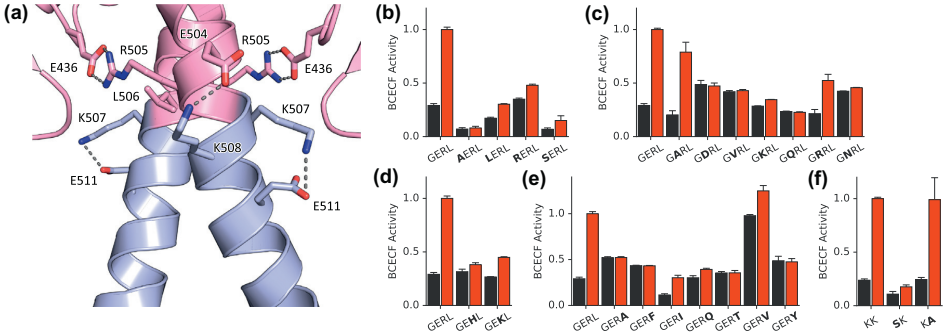

Fig. 3. Probing the linker region in LAPD. (a) Close-up of the linker region in the LAPD structural model (see Fig. 1b). Residues around the seam between photosensor and effector are shown in stick representation. Salt bridges observed in the structures of PagC [28] and *Hs*PDE2A [17] or inferred from the model are indicated. (b–e) Individual residues within the ^{503}GERL^{506} motif of LAPD at the C-terminal end of the photosensor unit were exchanged for residues observed at the corresponding position in the homologous bacteriophytochromes (see Fig. 1d). Activity of the resultant LAPD variants in their dark-adapted states (dark) or upon red-light exposure (red) was assessed by BCECF fluorescence. All data represent mean ± s.d. of four biological replicates. (f) Exchanges of the residues K507 and K508 within the PDE fragment of the linker region.

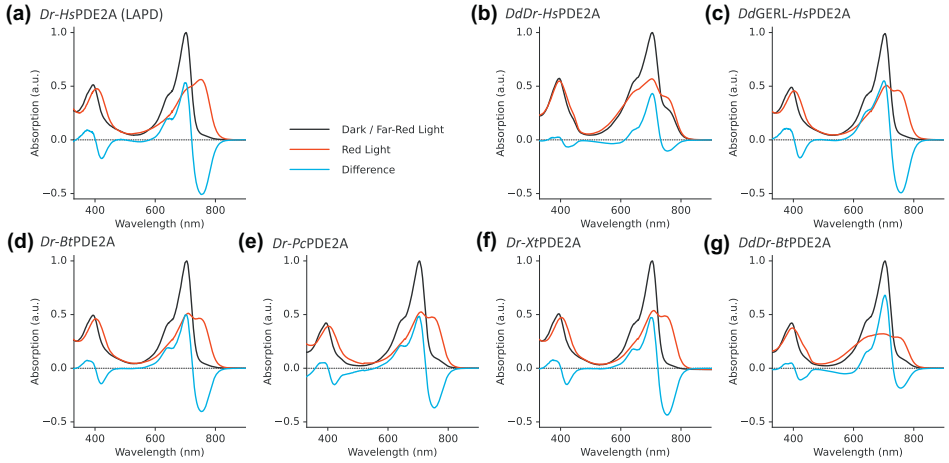

Fig. 4. UV/vis-absorption spectra of BphP-PDE variants in their dark-adapted states (black) and after red-light exposure (red). The cyan curves show dark–light difference spectra. Spectra were normalized to the peak maximum of the Q band in the dark-adapted state. (a) LAPD. (b) *DdDr-Hs*PDE2A. (c) *Dd*GERL-*Hs*PDE2A. (d) *Dr-Bt*PDE2A. (e) *Dr-Pc*PDE2A. (f) *Dr-Xt*PDE2A. (g) *DdDr-Bt*PDE2A.

(Fig. 5). At 29 °C, LAPD displayed specific cGMP hydrolysis activities of (2.0 ± 0.1) µmol (nmol enzyme min)$^{-1}$ in darkness and (11.0 ± 0.3) µmol (nmol enzyme min)$^{-1}$ under red light, similar to our previous findings [36]. Compared to LAPD, most variants had lower specific activities in both darkness and red light, and somewhat reduced degrees of light stimulation between 2.9-fold and 5.5-fold. However, *Dr-Bt*PDE2A exhibited higher activation of around 8.0-fold and maximal specific activity of (13.5 ± 0.1) µmol (nmol enzyme min)$^{-1}$ under red light. We next probed the reversibility of activation in the BphP-PDEs by exposing them successively to red and far-red light, followed by enzymatic assays. As observed previously [36], LAPD could not be fully switched off by far-red light and hydrolyzed cGMP with a turnover of (4.3 ± 0.1) µmol (nmol enzyme min)$^{-1}$. Notably, the above spectroscopic measurements used the same illumination protocol and showed that LAPD fully assumes the Pr configuration of its chromophore under these conditions, pointing to at least partial uncoupling of photochemical events and catalytic activity. Although two BphP-PDE variants, *Dr-Pc*PDE2A and *Dd*GERL-*Hs*PDE2A, shared with LAPD an incomplete or even absent reversal of hydrolysis activity under far-red light, the other variants showed markedly enhanced properties. In *Dr-Bt*PDE2A, far-red light returned hydrolysis activity to (2.3 ± 0.1) µmol (nmol enzyme min)$^{-1}$, almost the same value as in darkness. In the remaining variants, *Dr-Xt*PDE2A and *DdDr-Hs*PDE2A, far-red light completely reverted prior activation by red light. Thus, the extent of far-red-light-driven activity reversal in (engineered) bacteriophytochromes is apparently determined by both the photosensor and effector modules: whereas the *Dr*BphP PCM supported complete reversal when connected to *Xt*PDE2A, it failed to do so in the context of other effectors [29,36]. We also assessed cAMP hydrolysis in the PDE variants and found overall similar specific activities and degrees of light activation (Figs. S7 and 5i). As an exception, the specific cAMP hydrolysis activity of LAPD under red light amounted to (5.7 ± 0.1) µmol (nmol enzyme min)$^{-1}$, somewhat lower than observed for cGMP hydrolysis but consistent with our previous measurements [36]. By recombining the chimeric *DdDr*-PCM and the *Bt*PDE, we also produced the variant *DdDr-Bt*PDE2A, which, however, did not lead to an improvement of catalytic properties over *DdDr-Hs*PDE2A. As optogenetic actuators are often deployed in living animals, we also determined the cGMP and cAMP hydrolysis activities of LAPD and *Dr-Bt*PDE2A at 37 °C (Fig. S8). At this temperature, the cGMP and cAMP hydrolysis activities under red light were around 40% higher than at 29 °C. Interestingly, the activities of LAPD in darkness or under far-red light were slightly reduced at the higher temperature, thus improving its regulatory efficiency.

Optogenetic application of light-regulated Phosphodiesterases in mammalian cells

Having engineered a set of red-light-responsive BphP-PDEs, we next addressed whether they allow to regulate signaling in mammalian cells. We transfected HEK-TM cells, stably expressing a

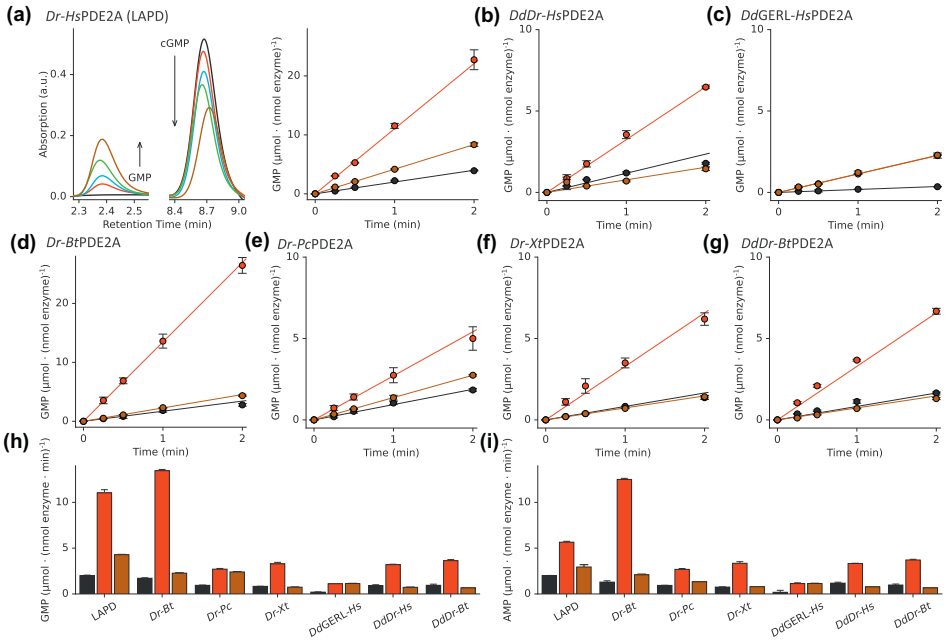

Fig. 5. Analysis by high-performance liquid chromatography of cNMP hydrolysis in light-regulated PDE variants. (a) (Left) As exemplarily shown for a hydrolysis reaction catalyzed by red-light-exposed LAPD, the amount of substrate cGMP decreases over time and that of the product GMP increases over time. (reaction times of 0, 0.25, 0.5, 1 and 2 min, as indicated by the arrows). (Right) Hydrolysis of 1 mM cGMP was assessed for dark-adapted (black) and for red-light-exposed LAPD (red; 670 nm), as well as for LAPD exposed first to red light and then to far-red light (brown; 780 nm). All data represent mean ± s.d. of three biological replicates. (b–g) cGMP hydrolysis data for the PDE variants *DdDr-Hs*PDE2A, *Dd*GERL-*Hs*PDE2A, *Dr-Bt*PDE2A, *Dr-Pc*PDE2A, *Dr-Xt*PDE2A and *DdDr-Bt*PDE2A. (h) Overview of cGMP turnover in the different PDE variants in their dark-adapted forms (black), following red-light illumination (red), and after successive exposure to red and far-red light (brown). (i) Overview of cAMP turnover in the different PDE variants (see Fig. S7).

variant of the cyclic nucleotide-gated ion channel CNGA2, denoted CNGA2-TM [59], with the genes for LAPD, *Dr-Bt*PDE2A, *Dr-Pc*PDE2A and *Dr-Xt*PDE2A. To readily monitor expression and facilitate the generation of stable cell lines, an mCherry tag was fused to the C terminus of these PDEs. Using antibiotics selection, we isolated cell clones that stably express the different BphP-PDEs and the CNG channel, as confirmed by fluorescence microscopy and Western blot (Fig. 6a, b). We then analyzed catalytic activity and response to illumination of these PDEs in the HEK-TM cells at 29 and 37 °C using a coupled reporter assay similar to our previous studies (Fig. 6c) [36]. To this end, the cells were loaded with a calcium (Ca^{2+})-sensitive fluorophore and treated with the water-soluble forskolin derivative NKH477 to stimulate endogenous adenylyl cyclase activity. The resultant increase in intracellular cAMP prompts opening of the CNG channel, prompting Ca^{2+} influx from the exterior and fluorescence increase. Upon reaching a steady-state, the PDEs were activated by red light, thus reducing intracellular cAMP and, in turn, attenuating Ca^{2+} influx and fluorescence. For normalization of the fluorescence signals, the Ca^{2+} ionophore ionomycin was added at the end of each experiment. In the non-transfected HEK-TM cells, NKH477 addition caused fluorescence to gradually increase to a plateau of around half-maximal normalized fluorescence (Figs. 6d and S9a). In the stable LAPD cell line, NKH477 also triggered a fluorescence increase to a constant, albeit lower level of around 0.13 (Fig. 6d). The lower fluorescence amplitude is likely due to basal PDE activity in darkness, consistent with the above BCECF and HPLC experiments and earlier measurements [36]. Illumination with red light resulted in a decrease of the fluorescence signal to baseline, indicative of light-activated PDE activity. Notably, in these experiments, no exogenous biliverdin was added, demonstrating that the endogenous supply

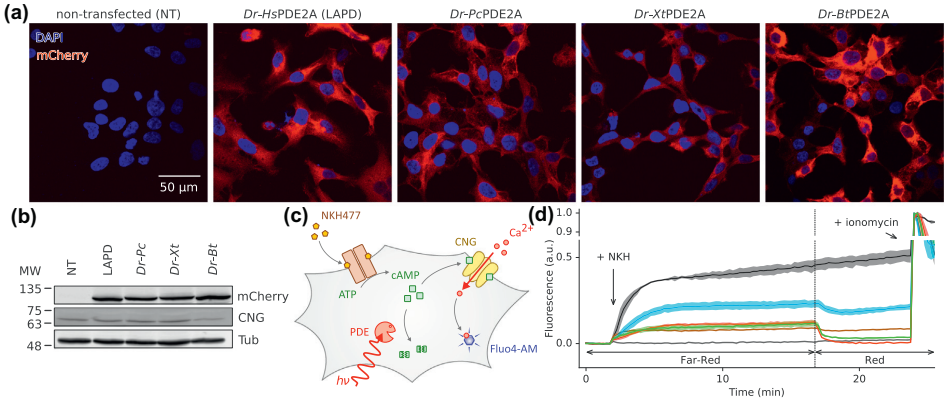

Fig. 6. Optogenetic control of cyclic adenosine monophosphate (cAMP) in mammalian cells. (a) HEK-TM cells, stably expressing a cyclic nucleotide-gated (CNG) ion channel, were stably transfected with mCherry-tagged LAPD, *Dr-Bt*PDE2A, *Dr-Pc*PDE2A or *Dr-Xt*PDE2A and observed by fluorescence microscopy. The elevated mCherry signal relative to a non-transfected control (NT) indicates PDE expression. (b) Cells from panel a were analyzed by Western blot, stained with antibodies directed against mCherry, the CNGA2 channel, and β tubulin. Sizes of a molecular weight (MW) marker are indicated in units of kDa. (c) Schematic of the coupled PDE reporter assay in the HEK-TM cells. Treatment with 100 µM NKH477 stimulates endogenous adenylyl cyclase activity and leads to a build-up of intracellular cAMP. In turn, the CNG channels open, thus resulting in Ca^{2+} influx and elevated fluorescence of the Ca^{2+}-sensitive dye Fluo4-AM. (d) Cell lines were initially incubated under far-red light at 37 °C, and NKH477 was added after 2 min. At 17 min, the cells were illuminated with red light (690 nm), and after another 6 min, the cell-permeabilizing ionophore ionomycin was added. Fluo4-AM fluorescence was monitored throughout the experiment and normalized to its maximum value reached after ionomycin addition. Lines and shaded areas represent mean normalized fluorescence ± s.d. of four biological replicates for the PDE lines and of two for the positive and negative controls. Non-transfected HEK-TM cells are shown in black, the LAPD cell line in red, *Dr-Bt*PDE2A in brown, *Dr-Pc*PDE2A in green and *Dr-Xt*PDE2A in blue; the bottom gray trace shows results from non-transfected HEK-TM cells that were not stimulated with NKH477.

suffices to evoke light responses, in line with previous observations [27,28,36]. We observed similar responses to NKH477 addition and illumination in the stable cell lines expressing *Dr-Pc*PDE2A and *Dr-Xt*PDE2A. For the latter, the fluorescence signal reached altogether higher levels in darkness, but the amplitude of reduction under red light was comparable (Fig. 6d). The on average higher fluorescence readings for *Dr-Xt*PDE2A may reflect different expression levels and a lower specific hydrolysis activity in this variant (see Fig. 5). By contrast, several stable *Dr-Bt*PDE2A cell lines that we tested all exhibited suppressed responses to NKH477 addition and were not stimulated by red-light exposure. As a possible reason, the expression levels and the specific activity of this PDE in the current cellular setting might have been too high, thus suspending significant cAMP accumulation upon NKH477 addition even under non-activating conditions. To test this hypothesis, we transiently transfected HEK-TM cells with *Dr-Bt*PDE2A, which leads to heterogenous and overall lower expression. As a corollary, NKH477 addition induced a stronger fluorescence increase in these cells than in the stable LAPD cell line; subsequent exposure to red light prompted a fluorescence decrease albeit of lower amplitude (Fig. S9b). These experiments demonstrate the principal functionality of *Dr-Bt*PDE2A in mammalian cells, but also indicate that, as for other optogenetic tools [35], the cellular expression level needs to be properly adjusted.

Discussion

Optogenetic control of cyclic mononucleotides

Through the recombination of bacteriophytochrome photosensor and vertebrate PDE effector modules, we engineered receptors that catalyze cAMP/cGMP hydrolysis and can be activated by red light. Compared to the LAPD blueprint [36], certain of the present BphP-PDE variants exhibit improved switching in that illumination with far-red light fully undoes prior activation with red light. Of particular note, the *Dr-Bt*PDE2A variant displays not only enhanced reversibility but also higher and more strongly light-regulated hydrolysis activity. Thus, this PDE variant represents an improvement over

LAPD and appears as a tool-of-choice for red-/far-red-light-regulated cNMP hydrolysis. As we demonstrate (see Fig. 6), LAPD, *Dr-Bt*PDE2A and several other PDE variants can be deployed optogenetically in mammalian cells to regulate by light cNMP-dependent physiological processes, for example, the ion flux through CNG channels. These studies also pinpoint a frequent challenge [20,35] associated with optogenetic applications: the desired light-induced physiological effects may only manifest to full extent (or even at all) if the cellular expression level and activity of the optogenetic actuator employed fall within appropriate intervals, and the ideal tool may hence depend on cellular context. For a given application scenario, these parameters may be demanding to gauge upfront, let alone adjust, especially when the degree of light regulation in the underlying photoreceptor is altogether limited. Against this backdrop, we deem it an advantage to now have at disposal a suite of several red-light-regulated PDEs with varying cellular activity and performance. By the same token, a recently characterized rhodopsin-based light-activated PDE from a flagellate expands and diversifies the optogenetic toolkit [43–45]. Compared to LAPD, this PDE is membrane-integral, is sensitive to other light colors, and primarily responds to illumination with changes in substrate affinity rather than maximal turnover.

cNMP-specific PDEs sensitive to red/far-red light are well suited for multiplexing with photoactivated nucleotidyl cyclases that mostly respond to light of shorter wavelengths [23,24,39–41]. The combination of individually addressable nucleotidyl cyclases and PDEs affords bimodal control by light of intracellular cyclic mononucleotides. Moreover, by optogenetically regulating both the making and breaking of cNMPs, a net regulatory effect much surpassing those of the light-regulated cyclase or PDE alone might be achieved [35]. This aspect is borne out in certain photoreceptors, which act as both histidine kinases and phosphatases and exhibit very stringent light responses [53]. Nucleotidyl cyclases and PDEs may also be paired with genetically encoded, fluorescent cNMP biosensors to enable all-optical experiments [60,61], in which acute cNMP levels inside cells are continuously read out to allow optogenetic feedback control of the light-sensitive actuators. As covered in the introduction, cyclic mononucleotides are integral to manifold physiological pathways, thus offering diverse toeholds for optogenetic intervention. As a case in point, the so-called two-component optogenetics strategy [62] combines photoreceptors, which generate primary responses, with secondary, light-inert components that latch onto these first responses and alter them in modality, time, space and amplitude. In a recent manifestation of this concept, a bacterial K^+-selective CNG channel was used in conjunction with a blue-light-sensitive PAC to trigger light-induced potassium currents and concomitant neuronal silencing [63]. Arguably, the sensitivity of the modular two-component approach may be extended to the red/far-red spectral region through combination with one of the BphP-PDE variants engineered presently. As of now, the *Dr-Bt*PDE2A variant appears best-suited for this approach.

Bacteriophytochrome engineering and signal transduction

Whereas three of the parallel design strategies pursued here eventually yielded novel light-activated PDEs, the exchange of the catalytic effector module clearly emerges as the simplest and at the same time, most successful strategy. Directly modeled on the LAPD template, the substitution of the effector unit for homologous modules readily yielded functional PDE variants, which in certain cases exhibited enhanced regulatory traits compared to LAPD. Arguably, this design strategy benefitted from high sequence homology among vertebrate PDE2A enzymes, including within the coiled-coil linker region (see Fig. 1d). Strikingly, the converse and equally obvious approach of replacing the entire PAS-GAF-PHY PCM of LAPD for the photosensors of other BphPs failed, despite pronounced, if somewhat lower, levels of sequence homology among the various PCMs. In marked contrast, the recent redesign of a red-light-sensitive PAC [28] via modular exchange of its *Dr*BphP unit, that it shares with LAPD, for PCMs from other BphPs proved straightforward [29]. Beyond effector identity, this design also differed in employing a somewhat more C-terminal junction site within the *Dr*BphP coiled-coil linker (see Fig. S4). Evidently, LAPD represents a local optimum in BphP-PDE design space, as most alterations, be they extensive (see Fig. 2b), be they small (see Fig. 3), are detrimental. These observations are surprising given that LAPD employs the *Dr*BphP PCM, yet its construction was based on the PCM structure of *Pa*BphP [36]; put another way, the original LAPD design does not stipulate the use of any particular BphP (other than *Pa*BphP), let alone of *Dr*BphP. Although a full molecular understanding is lacking, we concluded that the junction between the PCM and PDE modules, as configured in the original LAPD, is particularly conducive to signal transduction and should hence be preserved. In a first, rather coarse approach, we retained the *Dr*PHY domain thus leaving the junction intact, albeit at the cost of introducing a new seam between the GAF and PHY domains within the PCM. That notwithstanding, the strategy yielded light-activated PDEs, which, however, exhibited impaired photochemical properties (see Fig. 4). In a similar vein, by pursuing a more limited exchange of the PHY tongue region between PCMs, the regulatory response of an

engineered BphP has recently been greatly boosted [64], a rationale that may be transferrable to LAPD. In a second, more subtle approach, we altered the linker region of intact homologous PCMs near the junction site toward the GERL motif present in LAPD. Although not successful in all cases, most BphP-PDEs could be endowed with light responsiveness in this manner. Taken together, the above strategies pave the way toward the generation of additional BphP-PDEs, ideally with low dark activity, strong activation by red and/or far-red light, and full reversibility.

Given the above pitfalls and our ultimately incomplete molecular understanding, it is challenging to much extrapolate, let alone infer fail-safe design recipes. Nonetheless, several general aspects inform future efforts directed at engineering BphP photoreceptors. First, in combination with previous work [28,29,64,65], our study reveals that to a certain extent BphP photosensor modules (or constituent fragments) are mutually interchangeable. By extension, this observation implies shared, if not necessarily universal, signal-transduction mechanisms among and potentially even transcending BphPs. Second, additional molecular determinants, beyond the sheer (re)combination of protein domains, govern activity and regulation in composite (photo)receptors. Specifically, the inter-domain junctions mediate efficient communication between photosensor and effector entities. Although not probed here, previous work pinpointed the length of these, often α-helical, linkers as important parameters [27,28,36,53,54]; as we show presently, the sequence and specific molecular interactions of these linkers can be crucial factors as well. Third, effector identity determines the difficulty of a particular protein engineering task, and by extension, its ultimate success or failure. As a case in point, the derivatization of BphP-based PACs proved efficient [29] but that of BphP-PDEs, such as LAPD, did not, although some of the same BphP modules were used. Not only the sensor module but also the effector can profoundly affect receptor traits, as exemplified by the exchange of the PDE effector unit in LAPD (see Figs. 4 and 5). Specific receptor properties may not even be associated with a given photosensor or effector per se but rather a particular combination thereof. Hence, the characteristics of a receptor are often hard to exactly recapitulate a posteriori, and even harder to predict or plan a priori. Fourth, the engineering of actuators for optogenetics often strives to attain several desiderata in parallel, for example, optimization of diverse photochemical and catalytic aspects [35], which may be difficult to simultaneously realize in a single receptor variant, thus further complicating the design process. Against this backdrop, functional and genuinely light-regulated receptors, be they of natural origin, be they engineered, serve as valuable starting points for further, often iterative engineering efforts. The present and related previous studies [27–29,36,65] showcase a range of principal design strategies, which may be pursued to this end. That notwithstanding, the key to eventual success will likely often be the ability to construct and readily assess for light-regulated function many design variants in parallel.

Materials and Methods

Molecular biology

The LAPD gene, encoding the PCM of *D. radiodurans* BphP (Uniprot BPHY_DEIRA, residues 1–506) fused to the catalytic effector domain of *H. sapiens* PDE 2A (PDE2A_HUMAN, residues 555–941) and a C-terminal hexahistidine tag, was amplified by PCR from a previous pASK43 expression vector [36] and subcloned into a pCDFDuet plasmid (Novagen, Merck, Darmstadt, Germany) by Gibson assembly [66]. The gene encoding *Synechocystis* sp. heme oxygenase 1 (*Ss*HO) was PCR-amplified from plasmid pKT270 [51] and cloned by Gibson assembly into the pCDFDuet vector as well, such that within the resultant pCDF-LAPD-HO plasmid, expression of both LAPD and *Ss*HO is under control of T7-lacO promoters. Residue substitutions in LAPD were introduced by site-directed mutagenesis in the pCDF-LAPD-HO background. LAPD variants were generated by Gibson assembly in the same background via replacement of either the BphP PCM, the PDE unit, or both for homologous modules from BphPs and PDEs, respectively. Specifically, the PCM of *P. aeruginosa* BphP (BPHY_PSEAE, 1–497) was derived from a previous pET-24a vector [47]; genes for the BphP PCMs from *Azorhizobium caulinodans* (GenBank WP_012169446.1, 1–502), *Acaryochloris* sp. CCMEE 5410 (WP_010479127.1, 1–531), *A. tumefaciens* P1 (WP_010971984.1, 1–493), *A. tumefaciens* P2 (WP_004430460.1, 1–500), *Agrobacterium vitis* (WP_015916920.1, 1–499), *D. deserti* (WP_012695070.1, 1–520), *Hymenobacter swuensis* (AHJ98859.1, 1–515), *Idiomarina* sp. A28L (WP_007419415.1, 1–507), *Janthinobacterium* sp. CG23_2 (WP_054263721.1, 1–518), *Pleurocapsa* sp. PCC7319 (WP_019503487.1, 1–523), *Rhizobium etli* (WP_004673045.1, 1–502), *Rhizobium leguminosarum* (WP_077988302.1, 1–502), *R. palustris* P5 (WP_119019282.1, 1–500), *R. sphaeroides* (AMJ49789.1, 1–502), and *Xanthomonas campestris* (WP_011270102.1, 1–512) were synthesized with *E. coli*-adapted codon usage (GeneArt, Regensburg, Germany). The PCM of *P. syringae* BphP (RMN66899.1, 1–626) was obtained by PCR amplification from genomic DNA. In case of the effector module, genes with *E. coli*-adapted codon

usage were synthesized for the PDE2A homologs from *Alligator mississippiensis* (KYO25631.1, 538–925), *B. taurus* (XP_024830786.1, 636–1022), *P. cinereus* (XP_020845306.1, 566–953), *Rattus norvegicus* (NP_112341.1, 543–928), and *X. tropicalis* (NP_001072607.1, 558–951). For the PAS-GAF exchange variants, the N-terminal part of LAPD (residues 1–323) was replaced by corresponding parts from homologous BphPs as follows: *P. aeruginosa* (1–310), *A. caulinodans* (1–312), *Acaryochloris* sp. CCMEE 5410 (1–339), *A. tumefaciens* P1 (1–304), *A. tumefaciens* P2 (1–311), *D. deserti* (1–321), *Janthinobacterium* sp. CG23_2 (1–320), *P. syringae* (1–324), *R. sphaeroides* (1–362), and *X. campestris* (1–321). For expression in eukaryotic cells, select LAPD variants were subcloned into the pCDNA3.1+ vector (Invitrogen, ThermoFisher Scientific) with C-terminal mCherry and HA tags. To facilitate eukaryotic expression, genes for *D. radiodurans* and *D. deserti* BphP, as well as *H. sapiens* and *B. taurus* PDE2A with human-adapted codon usage were synthesized and used in place of the genes with bacterial codon adaptation. The identity of all constructs was confirmed by Sanger DNA sequencing (GATC, Konstanz, Germany; or, Microsynth Seqlab, Göttingen, Germany).

Protein expression and purification

pCDFDuet plasmids encoding individual PDE variants and *Ss*HO were transformed into BL21 (DE3) or LOBSTR BL21(DE3) cells [67]. Resultant transformants were used to inoculate two baffled flasks with 800 mL lysogeny broth (LB) medium supplemented with 100 µg mL^{-1} streptomycin (Strep). Bacterial cultures were grown at 37 °C and 225 rpm until an optical density at 600 nm (OD_{600}) of around 0.6 was reached, at which point the temperature was lowered to 16 °C and 0.5 mM δ-amino levulinic acid (δ-ALA) was added. Expression of the PDE variant and *Ss*HO was induced by addition of 1 mM isopropyl β-D-1-thiogalactopyranoside (IPTG), and cultivation continued at 16 °C and 225 rpm for 16 h. Purification of LAPD variants was conducted similar to previous protocols [36]. Briefly, cells were harvested by centrifugation, resuspended in buffer [50 mM Tris/HCl (pH 8.0), 20 mM NaCl, 20 mM imidazole] and supplemented with protease inhibitors (cOmplete Ultra, Roche Diagnostics, Mannheim, Germany). After lysis by ultrasound or microfluidizer and centrifugation, the supernatant was incubated for 1 h at 4 °C with 100 µM biliverdin hydrochloride (Livchem Logistics GmbH, Frankfurt, Germany) and 5 mM Tris-(2-carboxyethyl)-phosphine. The lysate was then applied to Co^{2+}- or Ni^{2+}-nitrilotriacetic acid affinity resin (HisPur Cobalt Resin, ThermoFisher Scientific, Dreieich, Germany, or, Protino Ni-NTA, Macherey & Nagel GmbH, Düren, Germany). Following washing and elution with 200 mM imidazole, the protein was dialyzed into buffer [50 mM Tris/HCl (pH 8.0, 20 mM NaCl] and purified by anion-exchange chromatography (HiTrap Q HP, GE Healthcare, Munich, Germany). Purity was analyzed by denaturing polyacrylamide gel electrophoresis (PAGE) and Coomassie staining; covalent chromophore incorporation was assessed by Zn^{2+}-induced bilin fluorescence [52]. Fractions containing pure protein were pooled, dialyzed into storage buffer [50 mM Tris/HCl (pH 8.0), 20 mM NaCl, 20% (w/v) glycerol] and concentrated by spin filtration (Vivaspin 6, 10-kDa cutoff, GE Healthcare). Sample concentration was determined by absorption measurements (8453 UV–vis, Agilent Technologies, Waldbronn, Germany) using a molar extinction coefficient of 45,700 M^{-1} cm^{-1} at the isosbestic point (724 nm) [68]. For storage, protein aliquots were flash-frozen in liquid nitrogen and stored at −80 °C.

Western blot analysis of bacterial expression

To verify bacterial expression of the BphP-PDE variants, bacterial clones harboring pCDFDuet expression plasmids (see above) were grown in 5 mL LB/Strep liquid culture in darkness at 37 °C until an OD_{600} between 0.6 and 0.8 was reached. PDE expression was induced by addition of 1 mM IPTG and 0.5 mM δ-ALA, the temperature lowered to 16 °C, and incubation continued for 20 h. To verify protein expression, the bacterial cells were pelleted by centrifugation and resuspended in 500 µL Laemmli loading buffer [62.5 mM Tris/HCl (pH 6.8), 2.5% (w/v) SDS, 0.002% (w/v) bromophenol blue, 5% (v/v) 2-mercaptoethanol, 10% (w/v) glycerol]. Samples were denatured at 95 °C, cleared by centrifugation and separated via denaturing PAGE. The resulting gels were transferred onto a PVDF membrane by semi-dry blotting (Bio-Rad Laboratories GmbH, München, Germany). The membrane was washed with TBS-Tween buffer [20 mM Tris/HCl (pH 7.5), 150 mM NaCl, 0.1% (v/v) Tween 20] and blocked with TBS-Tween plus 3% (w/v) bovine serum albumin (BSA), followed by incubation at 4 °C over night with the primary mouse anti-His antibody (MA1-21315 Pierce 5x-His Epitope Tag Antibody His.H8, ThermoFisher Scientific) in TBS-Tween/BSA. After extensive washing with TBS-Tween, the secondary anti-mouse antibody (A3562 anti-mouse IgG-alkaline phosphatase; Sigma-Aldrich) was added for 4 h at 22 °C. After renewed washing with TBS-Tween, the membranes were incubated in development buffer for 2 min at 22 °C [100 mM/Tris–HCl (pH 9.5), 100 mM NaCl, 5 mM $MgCl_2$, 30 µg L^{-1} nitroblue tetrazolium, 15 µg L^{-1} 5-bromo-4-chloro-3-indolyl phosphate]. The reaction was stopped by rinsing the membranes thoroughly with water, and the membranes were dried and photographed with a digital camera.

PDE activity measurements

For the determination of PDE activity in crude lysate [49], bacterial clones harboring pCDFDuet expression plasmids were grown in 5-mL scale as described above. After induction and overnight expression at 16 °C, 2 mL of each culture were centrifuged, the supernatant discarded, and the pellet resuspended in buffer AB I [2 mM potassium phosphate (pH 7.6), 5 mM $MgCl_2$, 100 mM KCl, 10 mM dithiothreitol, 0.04% (w/v) bovine serum albumin]. Lysis was accomplished by three cycles of freezing in liquid nitrogen and thawing. Lysate (10 µL) was transferred to a clear 96-well microtiter plate (MTP) and 60 µL buffer AB II [0.5 µM 2′,7′-bis-(2-carboxyethyl)-(5-and-6)-carboxyfluorescein (BCECF [50], ThermoFisher Scientific) in buffer AB I] were added. Following equilibration at 29 °C in darkness, the samples were either kept in darkness or illuminated with red light [(670 ± 15) nm, 500 µW cm^{-2}, 10 s] or far-red light [(780 ± 15) nm, 500 µW cm^{-2}, 10 s]. The PDE reaction was initiated via addition of 2 mM cGMP (Sigma-Aldrich, Darmstadt, Germany). Using a CLARIOstar multimode MTP reader (BMG Labtech GmbH, Ortenberg, Germany), BCECF fluorescence intensities F_{440} and F_{500} were measured over time at excitation wavelengths of (440 ± 5) and (500 ± 5) nm, respectively, and a joint emission wavelength of (560 ± 30) nm. The ratio of F_{500} over F_{440} was corrected for buffer background and plotted as a function of time. The early time course was fitted to a linear function to determine initial reaction velocities. All measurements were performed in biological triplicates. Unless stated otherwise, data were evaluated and plotted with the Fit-o-mat program [69].

The catalytic activity of purified PDE variants was addressed by high-performance liquid chromatography (HPLC). Enzyme (20 nM) was incubated at 29 °C or 37 °C in 700 µL reaction buffer [20 mM Tris/HCl (pH 8.0), 20 mM NaCl] in darkness, under red light [(670 ± 15) nm, 80 µW cm^{-2}, 60 s], or under red light followed by far-red light [(780 ± 15) nm, 80 µW cm^{-2}, 60 s]. Reactions were started by addition of 1 mM substrate cGMP or cAMP (Merck), and 50 µL aliquots were drawn at discrete timepoints and rapidly inactivated by incubation at 95 °C for 1 min. Samples were cleared by centrifugation for 5 min at 20,000*g* and filtered (Chromafil, 0.2-µm pore size, Macherey & Nagel GmbH), followed by HPLC analysis on reversed-phase (RP) C18 columns using isocratic elution with 97% (v/v) 100 mM potassium phosphate pH 5.5 and 3% (v/v) acetonitrile. In case of cGMP, the samples were analyzed on a Eurospher II C18 RP column (Knauer, Berlin, Germany) using a Smartline HPLC system (Knauer). cAMP hydrolysis reactions were assessed on a Kinetex 5 µ EVO C18 RP column (Phenomenex, Torrance, USA) and an Acquity UPLC (Waters GmbH, Eschborn, Germany). Peak areas for the cGMP and cAMP hydrolysis reactions were integrated with the OpenLAB (Agilent) or Empower (Waters) programs and calibrated against cAMP, cGMP, AMP, and GMP standards. All measurements were performed in triplicate.

Eukaryotic cell culture

Cell culture experiments were conducted with HEK-TM cells, derived from HEK293 ATCC cells, which stably express a variant of the cyclic nucleotide-gated ion channel CNGA2 [59]. Cells were incubated at 37 °C and 5% (v/v) CO_2 (HERAcell 240, ThermoFisher Scientific). DMEM medium was obtained from Gibco (ThermoFisher Scientific) and supplemented with 10% (v/v) fetal calf serum (Biochrom, Berlin, Germany) and 100 µg mL^{-1} hygromycin. The HEK-TM cell line stably expressing LAPD was maintained in medium containing 50 µg mL^{-1} hygromycin and 5 µg mL^{-1} blasticidin (Invitrogen). Cells were transfected using Lipofectamine 2000 (Life Technologies, Carlsbad, USA) according to the manufacturer's protocol. Stable HEK-TM cell lines were established for the LAPD variants *Dr-Bt*PDE, *Dr-Pc*PDE and *Dr-Xt*PDE and maintained in medium containing 100 µg mL^{-1} hygromycin and 0.8 mg mL^{-1} G418 (Geneticin, Gibco, ThermoFisher Scientific).

Western blot analysis and immunocytochemistry

The expression of the PDE variants in HEK-TM cells was ascertained by immunochemical approaches. For Western blot analysis, HEK-TM cells were lysed [10 mM Tris/HCl (pH 7.6), 140 mM NaCl, 1 mM EDTA, 1.0% (v/v) Triton-X 100, protease inhibitor cocktail (Sigma-Aldrich, no. P8340)] on ice for 30 min, followed by centrifugation (10 min, 10,000 *g*, 4 °C). The protein concentration of the supernatant was determined in a bicinchoninic acid assay, and samples were analyzed by denaturing PAGE followed by semi-dry blotting (Carl Roth, Karlsruhe, Germany) on a PVDF membrane (Immobilon-FL, Merck). The blots were stained using primary antibodies against mCherry (0.22 µg mL^{-1}, rabbit polyclonal, Rockland Immunochemicals Inc., Limerick, USA, no. 600-401-379); β tubulin (31.3 µg mL^{-1}, mouse monoclonal, Sigma, no. T4026); and the CNGA2 channel (3B10, [70]). The following secondary antibodies were used: donkey anti-rabbit IRDye680LT (LI-COR Biosciences, Bad Homburg, Germany, no. 925-68023); donkey anti-mouse IRDye680LT (LI-COR Biosciences, no. 926–68022); and donkey anti-mouse IRDye800CW (LI-COR Biosciences, no. 926-32212). Fluorescence was detected with an Odyssey imaging system (LI-COR Biosciences).

For immunocytochemical analysis, 10^5 cells each were seeded into wells containing a poly-L-lysine (PLL)-coated 13-mm coverslip. After one day incubation, the cells were washed with PBS [10 mM Na_2HPO_4,

1.8 mM KH_2PO_4, 137 mM NaCl, 2.7 mM KCl (pH 7.4)] and fixed in 4% (v/v) paraformaldehyde. After washing with PBS, the cells were blocked by addition of 300 µL blocking buffer [5% (v/v) ChemieBlocker (Millipore, Merck), 0.5% (v/v) Triton-X 100, in PBS] for 30 min. Cells were then incubated for 60 min with anti-mCherry primary antibody (1.83 µg ml^{-1}) in blocking buffer. After washing with PBS, 150 µL blocking buffer containing fluorescently labeled secondary antibody [4 µg mL^{-1}, goat anti-rabbit Alexa Fluor 488 (AF488), Life Technologies, no. A-11034] and 0.5 mg mL^{-1} 2-(4-amidinophenyl)-1H-indole-6-carboxamidine (DAPI, ThermoFisher Scientific) were added. Following incubation for 60 min in darkness and washing, the coverslips were mounted in Aqua-Poly/Mount (Polysciences, Warrington, USA). The slides were then analyzed on a fluorescence microscope (Eclipse Ti, Nikon) using excitation and emission wavelengths of 408/417–477 nm for DAPI, 561/570–1000 nm for mCherry and 488/500–550 nm for AF488.

Phosphodiesterase activity measurements in HEK-TM cells

For PDE activity assays in eukaryotic cells, stable cell lines were seeded on a PLL-coated 96-well MTP at 3×10^4 cells per well and incubated over night at 37 °C and 5% (v/v) CO_2 in darkness. All following steps were conducted under dim green light. Medium was removed, and cells were washed with 50 µL ES buffer [120 mM NaCl, 5 mM KCl, 2 mM $CaCl_2$, 2 mM $MgCl_2$, 10 mM glucose, 10 mM HEPES (pH 7.4)]. Cells were loaded with 2 µM Fluo4-AM and 3 mM probenecid in 50 µL ES buffer and incubated for 30 min at 29 or 37 °C. Afterward, the buffer was replaced with 90 µL ES containing 3 mM probenecid, and the MTP was incubated at 29 or 37 °C for 30 min inside a multimode MTP reader (FLUOstar omega, BMG Labtech). Fluorescence was measured with excitation and emission wavelengths of (485 ± 6) and (530 ± 15) nm, respectively, and the gain was adjusted for the stable LAPD cell line. After 2 min, 100 µM NKH477 (Sigma-Aldrich) in ES buffer was added, and measurements continued for 15 min. In controls, ES buffer was added rather than the NKH477 solution. During the measurement, the plate was first illuminated with an 850-nm LED mounted inside the MTP reader. At a set point, the illumination switched to a 690-nm LED for activation of the LAPD variants. After an additional 6 min, 2 µM ionomycin was added, and fluorescence was recorded until a maximal response was observed. For the transiently transfected HEK-TM cells (see Fig. S9b), the experiment was conducted at 29 °C and the timing of the illumination was different, but other than that, the experiments were conducted in the same manner.

Supplementary data to this article can be found online at https://doi.org/10.1016/j.jmb.2019.07.011.

Acknowledgments

We thank past and present members of the Möglich and Wachten laboratories for support and comments, and Thessa Jacob for assistance with HPLC analysis. Funding through the Deutsche Forschungsgemeinschaft (grant MO2192/4-1 to A. M.; SPP1926 grant WA3382/2-1, SPP1726 grant WA3382/3-1, and under Germany's Excellence Strategy: EXC2151-390873048 to D.W.), the Alexander von Humboldt Foundation (Sofja-Kovalevskaya Award to A.M.), and the Boehringer Ingelheim Fonds (to J.N.H.) is gratefully appreciated.

Declaration of Competing Interest

None.

Received 26 February 2019;
Received in revised form 22 June 2019;
Accepted 2 July 2019
Available online 10 July 2019

Keywords:
bacteriophytochrome;
cyclic mononucleotide;
optogenetics;
phosphodiesterase;
sensory photoreceptor

Abbreviations used:
cAMP and cGMP, 3′, 5′-cyclic adenosine and guanosine monophosphate; CNG, cyclic nucleotide-gated; cNMP, cyclic nucleoside monophosphate; PDE, phosphodiesterase; PAC, photoactivated adenylyl cyclase; PCM, photosensory core module; BphP, bacterial phytochrome.

References

[1] Gerhard. Krauss, Biochemistry of Signal Transduction and Regulation., Wiley-VCH, 2014.
[2] T.W. Rall, E.W. Sutherland, Formation of a cyclic adenine ribonucleotide by tissue particles, J. Biol. Chem. 232 (1958) 1065–1076.

[3] D.F. Ashman, R. Lipton, M.M. Melicow, T.D. Price, Isolation of adenosine 3′, 5′-monophosphate and guanosine 3′, 5′-monophosphate from rat urine, Biochem. Biophys. Res. Commun. 11 (1963) 330–334.
[4] T.W. Rall, E.W. Sutherland, J. Berthet, The relationship of epinephrine and glucagon to liver phosphorylase. IV. Effect of epinephrine and glucagon on the reactivation of phosphorylase in liver homogenates, J. Biol. Chem 224 (1957) 463–475.
[5] J.F. Kuo, P. Greengard, Cyclic nucleotide-dependent protein kinases. VI. Isolation and partial purification of a protein kinase activated by guanosine 3′,5′-monophosphate, J. Biol. Chem. 245 (1970) 2493–2498.
[6] D.A. Walsh, J.P. Perkins, E.G. Krebs, An adenosine 3′,5′-monophosphate-dependent protein kinase from rabbit skeletal muscle, J. Biol. Chem. 243 (1968) 3763–3765.
[7] E.E. Fesenko, S.S. Kolesnikov, A.L. Lyubarsky, Induction by cyclic GMP of cationic conductance in plasma membrane of retinal rod outer segment, Nature. 313 (1985) 310–313, https://doi.org/10.1038/313310a0.
[8] J. de Rooij, F.J.T. Zwartkruis, M.H.G. Verheijen, R.H. Cool, S.M.B. Nijman, A. Wittinghofer, J.L. Bos, Epac is a Rap1 guanine-nucleotide-exchange factor directly activated by cyclic AMP, Nature. 396 (1998) 474–477, https://doi.org/10.1038/24884.
[9] B. Andrée, T. Hillemann, G. Kessler-Icekson, T. Schmitt-John, H. Jockusch, H.-H. Arnold, T. Brand, Isolation and characterization of the novel Popeye gene family expressed in skeletal muscle and heart, Dev. Biol. 223 (2000) 371–382, https://doi.org/10.1006/dbio.2000.9751.
[10] J.N. Marden, Q. Dong, S. Roychowdhury, J.E. Berleman, C. E. Bauer, Cyclic GMP controls Rhodospirillum centenum cyst development, Mol. Microbiol. 79 (2011) 600–615, https://doi.org/10.1111/j.1365-2958.2010.07513.x.
[11] M. Gomelsky, cAMP, c-di-GMP, c-di-AMP and now cGMP: bacteria use them all! Mol. Microbiol. 79 (2011) 562–565, https://doi.org/10.1111/j.1365-2958.2010.07514.x.
[12] T. Shimada, N. Fujita, K. Yamamoto, A. Ishihama, Novel roles of cAMP receptor protein (CRP) in regulation of transport and metabolism of carbon sources, PLoS One 6 (2011), e20081. https://doi.org/10.1371/journal.pone.0020081.
[13] B. Görke, J. Stülke, Carbon catabolite repression in bacteria: many ways to make the most out of nutrients, Nat. Rev. Microbiol. 6 (2008) 613–624, https://doi.org/10.1038/nrmicro1932.
[15] M. Conti, J. Beavo, Biochemistry and physiology of cyclic nucleotide phosphodiesterases: essential components in cyclic nucleotide signaling, Annu. Rev. Biochem. 76 (2007) 481–511, https://doi.org/10.1146/annurev.biochem.76.060305.150444.
[16] S.H. Francis, M.A. Blount, J.D. Corbin, Mammalian cyclic nucleotide phosphodiesterases: molecular mechanisms and physiological functions, Physiol. Rev. 91 (2011) 651–690, https://doi.org/10.1152/physrev.00030.2010.
[17] J. Pandit, M.D. Forman, K.F. Fennell, K.S. Dillman, F.S. Menniti, Mechanism for the allosteric regulation of phosphodiesterase 2A deduced from the x-ray structure of a near full-length construct, Proc. Natl. Acad. Sci. U. S. A. 106 (2009) 18225–18230, https://doi.org/10.1073/pnas.0907635106.
[18] K. Deisseroth, G. Feng, A.K. Majewska, G. Miesenböck, A. Ting, M.J. Schnitzer, Next-generation optical technologies for illuminating genetically targeted brain circuits, J. Neurosci. 26 (2006) 10380–10386, https://doi.org/10.1523/JNEUROSCI.3863-06.2006.
[19] V. Jansen, J.F. Jikeli, D. Wachten, How to control cyclic nucleotide signaling by light, Curr. Opin. Biotechnol. 48 (2017) 15–20, https://doi.org/10.1016/j.copbio.2017.02.014.
[20] A. Losi, K.H. Gardner, A. Möglich, Blue-light receptors for optogenetics, Chem. Rev. 118 (2018) 10659–10709, https://doi.org/10.1021/acs.chemrev.8b00163.
[21] M. Iseki, S. Matsunaga, A. Murakami, K. Ohno, K. Shiga, K. Yoshida, M. Sugai, T. Takahashi, T. Hori, M. Watanabe, A blue-light-activated adenylyl cyclase mediates photoavoidance in *Euglena gracilis*, Nature. 415 (2002) 1047–1051, https://doi.org/10.1038/4151047a.
[22] S. Schröder-Lang, M. Schwärzel, R. Seifert, T. Strünker, S. Kateriya, J. Looser, M. Watanabe, U.B. Kaupp, P. Hegemann, G. Nagel, Fast manipulation of cellular cAMP level by light in vivo, Nat. Methods 4 (2007) 39–42, https://doi.org/10.1038/nmeth975.
[23] M. Stierl, P. Stumpf, D. Udwari, R. Gueta, R. Hagedorn, A. Losi, W. Gärtner, L. Petereit, M. Efetova, M. Schwarzel, T.G. Oertner, G. Nagel, P. Hegemann, Light-modulation of cellular cAMP by a small bacterial photoactivated adenylyl cyclase, bPAC, of the soil bacterium beggiatoa, J. Biol. Chem. 286 (2011) 1181–1188, https://doi.org/10.1074/jbc.M110.185496.
[24] M.-H. Ryu, O.V. Moskvin, J. Siltberg-Liberles, M. Gomelsky, Natural and engineered photoactivated nucleotidyl cyclases for optogenetic applications, J. Biol. Chem. 285 (2010) 41501–41508, https://doi.org/10.1074/jbc.M110.177600.
[25] S. Raffelberg, L. Wang, S. Gao, A. Losi, W. Gärtner, G. Nagel, A LOV-domain-mediated blue-light-activated adenylate (adenylyl) cyclase from the cyanobacterium *Microcoleus chthonoplastes* PCC 7420, Biochem. J. 455 (2013) 359–365, https://doi.org/10.1042/BJ20130637.
[26] M. Blain-Hartung, N.C. Rockwell, M.V. Moreno, S.S. Martin, F. Gan, D.A. Bryant, J.C. Lagarias, Cyanobacteriochrome-based photoswitchable adenylyl cyclases (cPACs) for broad spectrum light regulation of cAMP levels in cells, J. Biol. Chem. 293 (2018) 8473–8483, https://doi.org/10.1074/jbc.RA118.002258.
[27] M.-H. Ryu, I.-H. Kang, M.D. Nelson, T.M. Jensen, A.I. Lyuksyutova, J. Siltberg-Liberles, D.M. Raizen, M. Gomelsky, Engineering adenylate cyclases regulated by near-infrared window light, Proc. Natl. Acad. Sci. U. S. A. 111 (2014) 10167–10172, https://doi.org/10.1073/pnas.1324301111.
[28] S. Etzl, R. Lindner, M.D. Nelson, A. Winkler, Structure-guided design and functional characterization of an artificial red light-regulated guanylate/adenylate cyclase for optogenetic applications, J. Biol. Chem. 293 (2018) 9078–9089, https://doi.org/10.1074/jbc.RA118.003069.
[29] B. Stüven, R. Stabel, R. Ohlendorf, J. Beck, R. Schubert, A. Möglich, Characterization and engineering of photoactivated adenylyl cyclases, Biol. Chem. 400 (2019) 429–441, https://doi.org/10.1515/hsz-2018-0375.
[30] G. Gourinchas, S. Etzl, A. Winkler, Bacteriophytochromes — from informative model systems of phytochrome function to powerful tools in cell biology, Curr. Opin. Struct. Biol. 57 (2019) 72–83, https://doi.org/10.1016/j.sbi.2019.02.005.
[31] N.C. Rockwell, J.C. Lagarias, A brief history of phytochromes, Chemphyschem. 11 (2010) 1172–1180, https://doi.org/10.1002/cphc.200900894.
[32] H. Takala, A. Björling, O. Berntsson, H. Lehtivuori, S. Niebling, M. Hoernke, I. Kosheleva, R. Henning, A. Menzel, J.A. Ihalainen, S. Westenhoff, Signal amplification and

transduction in phytochrome photosensors, Nature. 509 (2014) 245–248, https://doi.org/10.1038/nature13310.
[33] E.S. Burgie, J. Zhang, R.D. Vierstra, Crystal structure of deinococcus phytochrome in the photoactivated state reveals a cascade of structural rearrangements during photoconversion, Structure. 24 (2016) 448–457, https://doi.org/10.1016/j.str.2016.01.001.
[34] R. Weissleder, A clearer vision for *in vivo* imaging, Nat. Biotechnol. 19 (2001) 316–317, https://doi.org/10.1038/86684.
[35] T. Ziegler, A. Möglich, Photoreceptor engineering, Front. Mol. Biosci. 2 (2015) 30, https://doi.org/10.3389/fmolb.2015.00030.
[36] C. Gasser, S. Taiber, C.-M. Yeh, C.H. Wittig, P. Hegemann, S. Ryu, F. Wunder, A. Möglich, Engineering of a red-light-activated human cAMP/cGMP-specific phosphodiesterase, Proc. Natl. Acad. Sci. U. S. A. 111 (2014) 8803–8808, https://doi.org/10.1073/pnas.1321600111.
[37] G.S. Filonov, K.D. Piatkevich, L.-M. Ting, J. Zhang, K. Kim, V. V. Verkhusha, Bright and stable near-infrared fluorescent protein for in vivo imaging, Nat. Biotechnol. 29 (2011) 757–761, https://doi.org/10.1038/nbt.1918.
[38] T. Kim, M. Folcher, M.D.-E. Baba, M. Fussenegger, A synthetic erectile optogenetic stimulator enabling blue-light-inducible penile erection, Angew. Chem. Int. Ed. 54 (2015) 5933–5938, https://doi.org/10.1002/anie.201412204.
[39] G.M. Avelar, R.I. Schumacher, P.A. Zaini, G. Leonard, T.A. Richards, S.L. Gomes, A rhodopsin-guanylyl cyclase gene fusion functions in visual perception in a fungus, Curr. Biol. 24 (2014) 1234–1240, https://doi.org/10.1016/j.cub.2014.04.009.
[40] U. Scheib, K. Stehfest, C.E. Gee, H.G. Körschen, R. Fudim, T.G. Oertner, P. Hegemann, The rhodopsin–guanylyl cyclase of the aquatic fungus Blastocladiella emersonii enables fast optical control of cGMP signaling, Sci. Signal. 8 (2015) rs8-rs8, https://doi.org/10.1126/scisignal.aab0611.
[41] S. Gao, J. Nagpal, M.W. Schneider, V. Kozjak-Pavlovic, G. Nagel, A. Gottschalk, Optogenetic manipulation of cGMP in cells and animals by the tightly light-regulated guanylyl-cyclase opsin CyclOp, Nat. Commun. 6 (2015) 8046, https://doi.org/10.1038/ncomms9046.
[42] Y. Tian, S. Gao, E.L. von der Heyde, A. Hallmann, G. Nagel, Two-component cyclase opsins of green algae are ATP-dependent and light-inhibited guanylyl cyclases, BMC Biol. 16 (2018) 144, https://doi.org/10.1186/s12915-018-0613-5.
[43] K. Yoshida, S.P. Tsunoda, L.S. Brown, H. Kandori, A unique choanoflagellate enzyme rhodopsin exhibits light-dependent cyclic nucleotide phosphodiesterase activity, J. Biol. Chem. 292 (2017) 7531–7541, https://doi.org/10.1074/jbc.M117.775569.
[44] L.B. Lamarche, R.P. Kumar, M.M. Trieu, E.L. Devine, L.E. Cohen-Abeles, D.L. Theobald, D.D. Oprian, Purification and characterization of RhoPDE, a retinylidene/phosphodiesterase fusion protein and potential optogenetic tool from the choanoflagellate *Salpingoeca rosetta*, Biochemistry. 56 (2017) 5812–5822, https://doi.org/10.1021/acs.biochem.7b00519.
[45] Y. Tian, S. Gao, S. Yang, G. Nagel, A novel rhodopsin phosphodiesterase from *Salpingoeca rosetta* shows light-enhanced substrate affinity, Biochem. J. 475 (2018) 1121–1128, https://doi.org/10.1042/BCJ20180010.
[46] V. Jansen, L. Alvarez, M. Balbach, T. Strünker, P. Hegemann, U.B. Kaupp, D. Wachten, Controlling fertilization and cAMP signaling in sperm by optogenetics, ELife. 4 (2015)https://doi.org/10.7554/eLife.05161.
[47] X. Yang, J. Kuk, K. Moffat, Crystal structure of *Pseudomonas aeruginosa* bacteriophytochrome: photoconversion and signal transduction, Proc. Natl. Acad Sci. U A. 105 (2008) 14715–14720.
[48] G. Rottwinkel, I. Oberpichler, T. Lamparter, Bathy phytochromes in rhizobial soil bacteria, J. Bacteriol. 192 (2010) 5124–5133, https://doi.org/10.1128/JB.00672-10.
[49] C.H. Schumacher, H.G. Körschen, C. Nicol, C. Gasser, R. Seifert, M. Schwärzel, A. Möglich, A fluorometric activity assay for light-regulated cyclic-nucleotide-monophosphate actuators, Methods Mol. Biol. Clifton NJ. 1408 (2016) 93–105, https://doi.org/10.1007/978-1-4939-3512-3_7.
[50] T.J. Rink, R.Y. Tsien, T. Pozzan, Cytoplasmic pH and free Mg^{2+} in lymphocytes, J. Cell Biol. 95 (1982) 189–196.
[51] K. Mukougawa, H. Kanamoto, T. Kobayashi, A. Yokota, T. Kohchi, Metabolic engineering to produce phytochromes with phytochromobilin, phycocyanobilin, or phycoerythrobilin chromophore in *Escherichia coli*, FEBS Lett. 580 (2006) 1333–1338, https://doi.org/10.1016/j.febslet.2006.01.051.
[52] T.R. Berkelman, J.C. Lagarias, Visualization of bilin-linked peptides and proteins in polyacrylamide gels, Anal. Biochem. 156 (1986) 194–201.
[53] A. Möglich, R.A. Ayers, K. Moffat, Design and signaling mechanism of light-regulated histidine kinases, J. Mol. Biol. 385 (2009) 1433–1444, https://doi.org/10.1016/j.jmb.2008.12.017.
[54] R. Ohlendorf, C.H. Schumacher, F. Richter, A. Möglich, Library-aided probing of linker determinants in hybrid photoreceptors, ACS Synth. Biol. 5 (2016) 1117–1126, https://doi.org/10.1021/acssynbio.6b00028.
[56] G. Gourinchas, S. Etzl, C. Göbl, U. Vide, T. Madl, A. Winkler, Long-range allosteric signaling in red light-regulated diguanylyl cyclases, Sci. Adv. 3 (2017), e1602498. https://doi.org/10.1126/sciadv.1602498.
[57] D. Bellini, M.Z. Papiz, Structure of a bacteriophytochrome and light-stimulated protomer swapping with a gene repressor, Structure. 20 (2012) 1436–1446, https://doi.org/10.1016/j.str.2012.06.002.
[58] L.H. Otero, S. Klinke, J. Rinaldi, F. Velázquez-Escobar, M.A. Mroginski, M. Fernández López, F. Malamud, A.A. Vojnov, P. Hildebrandt, F.A. Goldbaum, H.R. Bonomi, Structure of the full-length bacteriophytochrome from the plant pathogen *Xanthomonas campestris* provides clues to its long-range signaling mechanism, J. Mol. Biol. 428 (2016) 3702–3720, https://doi.org/10.1016/j.jmb.2016.04.012.
[59] S. Wachten, J. Schlenstedt, R. Gauss, A. Baumann, Molecular identification and functional characterization of an adenylyl cyclase from the honeybee, J. Neurochem. 96 (2006) 1580–1590, https://doi.org/10.1111/j.1471-4159.2006.03666.x.
[60] J.A. Kaczmarski, J.A. Mitchell, M.A. Spence, V. Vongsouthi, C.J. Jackson, Structural and evolutionary approaches to the design and optimization of fluorescence-based small molecule biosensors, Curr. Opin. Struct. Biol. 57 (2019) 31–38, https://doi.org/10.1016/j.sbi.2019.01.013.
[61] S. Mukherjee, V. Jansen, J.F. Jikeli, H. Hamzeh, L. Alvarez, M. Dombrowski, M. Balbach, T. Strünker, R. Seifert, U.B. Kaupp, D. Wachten, A novel biosensor to study cAMP dynamics in cilia and flagella, ELife. 5 (2016), e14052. https://doi.org/10.7554/eLife.14052.
[62] E.A. Ferenczi, J. Vierock, K. Atsuta-Tsunoda, S.P. Tsunoda, C. Ramakrishnan, C. Gorini, K. Thompson, S.Y. Lee, A. Berndt, C. Perry, S. Minniberger, A. Vogt, J. Mattis, R. Prakash, S. Delp, K. Deisseroth, P. Hegemann, Optogenetic

approaches addressing extracellular modulation of neural excitability, Sci. Rep. 6 (2016) 23947, https://doi.org/10.1038/srep23947.

[63] Y.A.B. Sierra, B.R. Rost, M. Pofahl, A.M. Fernandes, R.A. Kopton, S. Moser, D. Holtkamp, N. Masala, P. Beed, J.J. Tukker, S. Oldani, W. Bönigk, P. Kohl, H. Baier, F. Schneider-Warme, P. Hegemann, H. Beck, R. Seifert, D. Schmitz, Potassium channel-based optogenetic silencing, Nat. Commun. 9 (2018) 4611, https://doi.org/10.1038/s41467-018-07038-8.

[64] G. Gourinchas, U. Vide, A. Winkler, Influence of the N-terminal segment and the PHY-tongue element on light-regulation in bacteriophytochromes, J. Biol. Chem. 294 (2019) 4498–4510, https://doi.org/10.1074/jbc.RA118.007260.

[65] M.-H. Ryu, M. Gomelsky, Near-infrared light responsive synthetic c-di-GMP module for optogenetic applications, ACS Synth. Biol. 3 (2014) 802–810, https://doi.org/10.1021/sb400182x.

[66] D.G. Gibson, L. Young, R.-Y. Chuang, J.C. Venter, C.A. Hutchison, H.O. Smith, Enzymatic assembly of DNA molecules up to several hundred kilobases, Nat. Methods 6 (2009) 343–345, https://doi.org/10.1038/nmeth.1318.

[67] K.R. Andersen, N.C. Leksa, T.U. Schwartz, Optimized *E. coli* expression strain LOBSTR eliminates common contaminants from His-tag purification, Proteins Struct. Funct. Bioinforma. 81 (2013) 1857–1861. doi:https://doi.org/10.1002/prot.24364.

[68] J.R. Wagner, J. Zhang, D. von Stetten, M. Günther, D.H. Murgida, M.A. Mroginski, J.M. Walker, K.T. Forest, P. Hildebrandt, R.D. Vierstra, Mutational analysis of *Deinococcus radiodurans* bacteriophytochrome reveals key amino acids necessary for the photochromicity and proton exchange cycle of phytochromes, J. Biol. Chem. 283 (2008) 12212–12226.

[69] A. Möglich, An open-source, cross-platform resource for nonlinear least-squares curve fitting, J. Chem. Educ. 95 (2018) 2273–2278, https://doi.org/10.1021/acs.jchemed.8b00649.

[70] M.R. Meyer, A. Angele, E. Kremmer, U.B. Kaupp, F. Müller, A cGMP-signaling pathway in a subset of olfactory sensory neurons, Proc. Natl. Acad. Sci. 97 (2000) 10595–10600, https://doi.org/10.1073/pnas.97.19.10595.

7.5. Manuskript V

Stabel, R.; Möglich, A.; BIOspektrum (2017) „Die Kontrolle zyklischer Nukleotide mittels Licht“

Sensorische Photorezeptoren

Die Kontrolle zyklischer Nukleotide mittels Licht

ROBERT STABEL, ANDREAS MÖGLICH
LEHRSTUHL FÜR BIOCHEMIE, FORSCHUNGSZENTRUM FÜR BIO-MAKROMOLEKÜLE BIOMAC, UNIVERSITÄT BAYREUTH

Sensory photoreceptors underpin diverse adaptive responses in nature and serve as genetically encoded, light-gated actuators in optogenetics. Photoactivated nucleotide cyclases (PACs) enable light-dependent control over the formation of cyclic nucleotides (cNMPs). Conversely, the engineered, red-light-activated phosphodiesterase LAPD mediates the hydrolytic breakdown of cNMPs. In combination, PACs and LAPD hence unlock precise and graded control over intracellular cNMPs and associated processes.

DOI: 10.1007/s12268-017-0813-5

■ Sensorische Photorezeptoren sind in der Natur weit verbreitet und vermitteln vielfältige lichtabhängige Anpassungen in zahlreichen Organismen. Einfallendes Licht wird hierbei von einem im Photosensormodul des Photorezeptors eingebetteten Chromophor absorbiert, prozessiert und letztlich in Aktivitätsänderungen eines Effektormoduls umgesetzt. Basierend auf Identität des Chromophors und der nach Lichtabsorption ausgelösten photochemischen Prozesse unterteilen sich Photorezeptoren in etwa zehn verschiedene Klassen, die sich durch unterschiedliche Lichtempfindlichkeit im UV-/sichtbaren Bereich des elektromagnetischen Spektrums auszeichnen [1]. Bekannte Vertreter der Photorezeptoren sind die Rhodopsine, die unter anderem für den Sehprozess in Säugern verantwortlich zeichnen, und die Phytochrome (Phy), die beispielsweise in Pflanzen verschiedene lichtabhängige Antworten vermitteln. Bei aller Vielfalt zeichnen sich Photorezeptoren durchweg durch die räumlich-zeitliche Präzision und die Reversibilität der von ihnen ausgelösten physiologischen Antworten aus. Just diese Vorzüge bedingen den regen Einsatz von Photorezeptoren als licht-

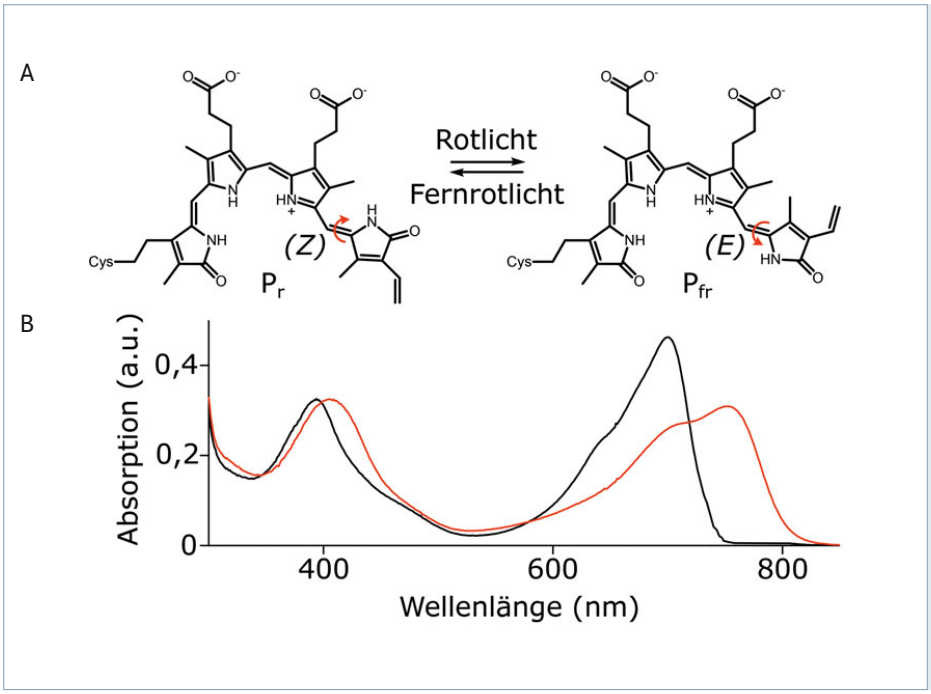

◀ **Abb. 1:** Photochemischer Mechanismus eines bakteriellen Phytochroms (BPhy). **A**, *Z*/*E*-Photoisomerisierung der C15=C16-Doppelbindung im Biliverdin-Chromophor. **B**, Im dunkeladaptierten 15*Z*-Zustand absorbiert das BPhy maximal bei 700 nm (schwarze Kurve). Rotlichtbestrahlung führt zu partieller Population des 15*E*-Zustands, welcher maximal bei 750 nm absorbiert (rote Kurve).

gesteuerte molekulare Schalter in der Optogenetik [2]: Durch genetische Methoden in Zielzellen verbracht, erlauben Photorezeptoren, dort über Licht (das heißt optische Signale) gewünschte Prozesse reversibel, räumlich-zeitlich exakt und nicht-invasiv zu manipulieren. Frühe optogenetische Ansätze bedienten sich vornehmlich des lichtgesteuerten Kationenkanals Kanalrhodopsin aus Mikroalgen, um mittels Lichteinstrahlung Kanalöffnung und Aktionspotenziale auszulösen [2]. Seitdem gelangen auch andere in der Natur vorkommende Photorezeptoren zum optogenetischen Einsatz; zu nennen sind hier insbesondere die PACs (photoaktivierte Adenylatzyklase) [3–5], die lichtstimuliert die Bildung der Botenstoffe (*second messenger*) 5',3'-zyklisches Adenosin- bzw. Guanosinmonophosphat (cAMP und cGMP) katalysieren. Noch einmal deutlich erweitert wird das Repertoire der Optogenetik durch den gezielten Bau neuartiger Photorezeptoren [6], welcher auch zentraler Gegenstand dieses Artikels ist.

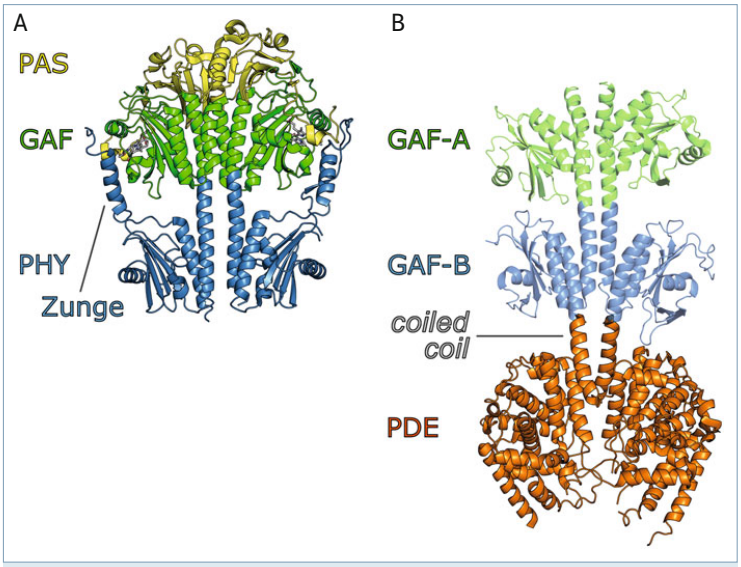

▲ **Abb. 2:** Bakteriophytochrome (BPhy) [8] (**A**) und die humane Phosphodiesterase 2A (*Hs*PDE2A) [9] (**B**) weisen als Gemeinsamkeit eine parallele homodimere Struktur, ein α-helikales Rückgrat und lateral angefügte PAS-, GAF- bzw. PHY-Domänen auf. Bei der lichtabhängigen Signaltransduktion in BPhys spielt eine als PHY-Zunge bezeichnete Schleife der PHY-Domäne eine zentrale Rolle [15]. Für die Konstruktion einer lichtaktivierten Phospodiesterase (LAPD) [12] wurden der PAS-GAF-PHY-Photosensor aus einem BPhy und der PDE-Effektor aus der humanen PDE2A miteinander fusioniert. Dadurch konnte die katalytische Aktivität der PDE-Domäne in LAPD einer Kontrolle durch Rotlicht unterworfen werden.

Phytochrom-Rotlichtrezeptoren

Für eine optogenetische Verwendung in Zellen oder Tiermodellen sind Photorezeptoren interessant, die langwelliges Licht absorbieren, welches lebendes Gewebe tiefer durchdringt als Licht kürzerer Wellenlänge. In besonderer Hinsicht gilt dies für bakterielle Phytochrome [7], im Folgenden als Bakteriophytochrome (BPhy) bezeichnet, welche auf Licht im roten bis fernroten (bzw. nahinfraroten) Wellenlängenbereich ansprechen. Wie pflanzliche Phytochrome weisen BPhys einen modularen Aufbau auf, bestehend aus einem konservierten N-terminalen Photosensormodul und einem variablen C-terminalen Effektormodul, häufig eine Histidinkinase oder Diguanylatzyklase. Der Photosensor umfasst ein Tandem von PAS(Per-ARNT-Sim)-, GAF(*cGMP phosphodiesterase/adenylyl cyclase/*FhlA)- und PHY(Phytochrom)-Domänen und bindet lineare Tetrapyrrole (Biline) als Chromophor, Phytochromobilin bei pflanzlichen Phytochromen und Biliverdin IXα (BV) bei bakteriellen (**Abb. 1A**). Lichtbestrahlung löst eine *Z/E*-Photoisomerisierung der C15=C16-Doppelbindung des Bilins aus, wobei der 15*Z*-Zustand maximal im roten (für BPhys ungefähr 660–710 nm) und der 15*E*-Zustand maximal im fernroten Bereich (ungefähr 730–760 nm) absorbiert (**Abb. 1B**); folglich werden die 15*Z*- und 15*E*-Isomere auch als P_r- und P_{fr}-Formen bezeichnet. Bei kanonischen Phytochromen bildet P_r den thermodynamisch stabileren, im Dunklen vorherrschenden Zustand; im Falle der Bathyphytochrome ist es P_{fr}. Lichtgetriebene Isomerisierung führt zur Population des jeweilig anderen Zustands, der thermisch in den Dunkelzustand relaxiert oder lichtgetrieben in diesen zurückgeführt werden kann. Die erste Kristallstruktur eines vollständigen Phy-Photosensormoduls wurde für das *Pseudomonas aeruginosa*-Bathyphytochrom gelöst [8] (**Abb. 2A**). Es handelt sich um ein paralleles Homodimer, dessen C_2-Achse von einem zentralen α-helikalen Bündel durchzogen wird, an dem seitlich die PAS-GAF-PHY-Domänen aufgereiht sind. Obschon der BV-Chromophor in die GAF-Domäne eingebettet ist, weist er auch direkte Kontakte zu den PAS- und PHY-Domänen auf, im letzteren Fall über eine lange Proteinschleife, die PHY-Zunge.

cNMP-spezifische Zyklasen und Phosphodiesterasen

Die molekulare Architektur der Phytochrome offenbart erstaunliche Ähnlichkeiten zu der mehrerer am Stoffwechsel zyklischer Nukleotide (cNMPs) in Säugern beteiligter Enzyme. So weisen einige Zyklasen und Phosphodiesterasen (PDE), die die Bildung bzw. den hydrolytischen Abbau von cNMPs vermitteln, ebenso wie Phytochrome einen homodimeren Aufbau, ein α-helikales Rückgrat und laterale GAF-Domänen auf. Klar ersichtlich wird dies an der Kristallstruktur der homodimeren, humanen PDE2A [9] (**Abb. 2B**), in der zwei GAF-Domänen (GAF-A und GAF-B) als Sensormodul fungieren und über einen *coiled-coil*-Linker an katalytische PDE-Domänen gekoppelt sind. Die Struktur repräsentiert hierbei einen katalytisch inaktiven Zustand, in dem die beiden PDE-Module einen unproduktiven dimeren Komplex ausbilden; die Bindung von cGMP an GAF-B löst allosterisch eine etwa vierfache Steigerung der katalytischen Aktivität aus, mutmaßlich durch Dissoziation der beiden PDE-Domänen bedingt [9].

Konstruktion lichtregulierter cNMP-spezifischer Phosphodiesterasen

Angespornt durch diese frappante strukturelle Ähnlichkeit ergründeten wir, ob das PAS-GAF-PHY-Photosensormodul bakterieller Phytochrome auch in der Lage ist, die katalytische Aktivität humaner PDEs zu steuern.

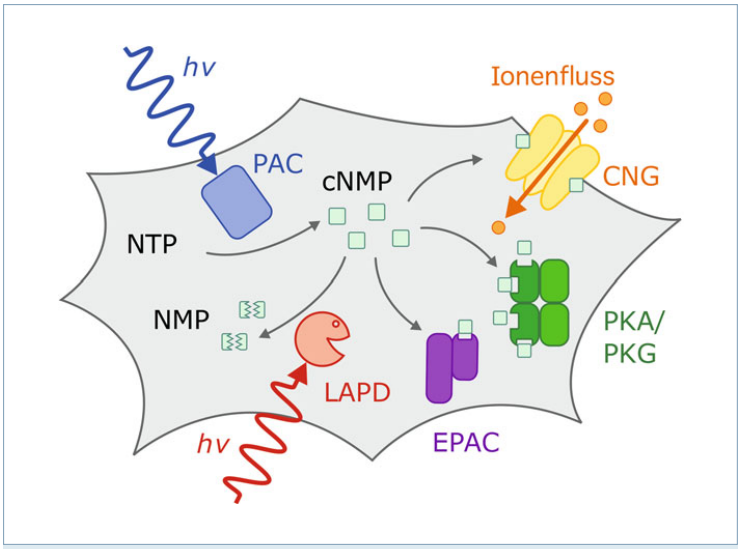

▲ **Abb. 3:** Lichtabhängige Kontrolle der cNMP-Konzentration in Eukaryoten mittels lichtaktivierter Phospodiesterase (LAPD) und photoaktivierter Adenylatzyklase (PAC). Zyklische Nukleotide (cNMPs) vermitteln durch Bindung an verschiedene Zielproteine eine Vielzahl an physiologischen Prozessen. So binden PKA bzw. PKG (cAMP/cGMP-abhängige Proteinkinase, grün) zyklische Nukleotide, was ihre Aktivierung zur Folge hat. Anschließend werden durch Phosphorylierung von Enzymen und Transkriptionsfaktoren verschiedene zelluläre Ereignisse vermittelt. Die Proteinfamilie der EPACs (*exchange protein directly mediated by cAMP*, violett) ist ebenfalls in einer Vielzahl von zellulären Prozessen wie Differenzierung, Proliferation, Genexpression und Apoptose involviert. Zudem transportieren CNG-Kanäle (*cyclic nucleotide-gated ion channels*, gelb) Kationen abhängig von der cNMP-Konzentration und spielen z. B. eine Rolle in der Reizwahrnehmung.

Außer durch die Erbringung grundlegender Einblicke in Mechanismen der Signaltransduktion ist dieser Ansatz auch motiviert durch die Möglichkeit, neuartige optogenetische Werkzeuge zu kreieren. Wie eingangs erwähnt, kommen in der Natur mehrere durch Licht aktivierte cNMP-spezifische Nukleotidzyklasen – die PACs – vor, die direkt in der Optogenetik eingesetzt werden können und dort Kontrolle über die intrazelluläre Synthese zyklischer Nukleotide erschließen. Durch Verwendung von PACs, die meist auf Blaulicht ansprechen, konnte z. B. der Flagellenschlag von Mausspermien einer optogenetischen Kontrolle unterworfen werden [10]. Hingegen sind in der Natur vorkommende, für cNMPs spezifische und direkt durch Licht kontrollierte PDEs nicht beschrieben worden. (Die im Sehprozess zentral wichtige PDE6 wird in ihrer Aktivität nicht direkt durch Licht, sondern indirekt über visuelles Rhodopsin reguliert. Eine erst kürzlich beschriebene, direkt an ein mikrobielles Rhodopsin gekoppelte PDE weist nur eine minimale Antwort auf Licht auf [11].) Eine durch Licht, vorzugsweise roter Farbe, regulierte PDE erweitert daher den Werkzeugsatz der Optogenetik beträchtlich.

Die Erzeugung dieses Werkzeugs gelang uns mit der Konstruktion von LAPD (lichtaktivierte Phosphodiesterase), die sich aus dem PAS-GAF-PHY-Tandem von *Deinococcus radiodurans*-BPhy und der katalytischen Domäne der humanen PDE2A zusammensetzt [12]. Obgleich dieses Unterfangen auf die erwähnten strukturellen Informationen zu BPhys und PDEs zurückgreifen konnte, wiesen erste chimäre Konstrukte keine katalytische Aktivität auf, geschweige denn eine durch Licht regulierte. Erst die Deletion zweier Reste in dem Photosensor und Effektor verbindenden *coiled coil* erbrachte eine LAPD mit der gewünschten Eigenschaft lichtabhängiger Aktivität: Die Hydrolyse von cAMP und cGMP wurde nach Rotlichtbestrahlung etwa sechs- bis siebenfach hoch- und nach Bestrahlung mit Fernrotlicht wieder herabreguliert. Die enzymatische Charakterisierung zeigte, dass LAPD beide cNMPs mit ähnlichen Raten und Affinitäten umsetzt und somit die duale Selektivität der PDE2A beibehält. Allerdings zeigt LAPD eine nur unzureichend reversible $P_r \leftrightarrow P_{fr}$-Photochemie, was deren optogenetischen Einsatz erschwert. Ein Hauptaugenmerk unserer aktuellen Arbeit gilt folglich der Verbesserung der photochemischen und katalytischen Eigenschaften der LAPD und abgeleiteter Licht-regulierter PDEs. Befördert wird dieses Vorgehen ungemein durch die zwischenzeitliche Etablierung effizienter PDE-Aktivitätstests [13]. Der Ansatz, der der Erzeugung von LAPD zugrunde liegt, ist modular und auf verwandte Proteine ausdehnbar, wie an der durch Rotlicht regulierten Zyklase IlaC deutlich wird [14]. IlaC basiert auf dem Photosensor von *Rhodobacter sphaeroides*-BPhy und der katalytischen Domäne der Zyklase CyaB aus *Nostoc* spec. Obschon die spezifische Aktivität von IlaC deutlich hinter der von CyaB zurückbleibt, konnte eine etwa sechsfache Steigerung durch Rotlicht erzielt werden.

Optogenetische Anwendung von PACs und LAPD

Der optogenetische Einsatz von PACs und LAPD wurde unlängst in einem gelungenen Übersichtsartikel dargestellt [10], weswegen wir uns auf ausgewählte Aspekte beschränken. Die erste optogenetische Anwendung derartiger Photorezeptoren beruhte auf der durch Blaulicht regulierten euPAC aus dem Protisten *Euglena gracilis* [3]. Besonders hervorzuheben ist bei dieser Studie, dass die lichtvermittelte Bildung von cAMP zur Kontrolle des Verhaltens transgener, euPAC-exprimierender *Drosophila*-Fliegen verwandt wurde. Die beträchtliche Größe von euPAC, gepaart mit relativ hoher Basalaktivität im Dunkeln erschweren allerdings deren weiten Einsatz. Die Entdeckung der kompakter gebauten und leistungsstärkeren, ebenfalls Blaulicht-regulierten bPACs in einem Bakterium adressierte diese Einschränkungen [4]. Die cAMP-bildende bPAC und abgeleitete Varianten, die cGMP produzieren, haben seitdem breite Anwendung gefunden, da sie die Schwächen von euPAC überwinden [10]. Sehr vielversprechend scheint auch die Rhodopsin-gekoppelte Zyklase RhoGC [5], die auf Grünlicht anspricht, spezifisch cGMP bildet und eine sehr niedrige Basalaktivität aufweist. Da LAPD durch Rotlicht reguliert wird, eignet das Enzym sich prinzipiell gut, um mit den vorgenannten lichtaktivierten Zyklasen kombiniert zu werden. Wie in **Abbildung 3** ausgeführt, verheißt die simultane Anwendung lichtgesteuerter Nukleotidzyklasen und -phosphodiesterasen eine präzisere Kontrolle und letztlich Homöostase intrazellulärer cNMP-Konzentrationen. Auf diese Weise kann

eine Reihe nachgelagerter, cNMP-vermittelter physiologischer Prozesse einer optogenetischen Kontrolle unterworfen werden. Bislang haben wir den optogenetischen Einsatz von LAPD in Säugerzellkulturen, Zebrafisch und *Drosophila* demonstriert [12, 13]. Hierbei ist anzumerken, dass der notwendige Kofaktor Biliverdin in allen bislang getesteten Systemen in ausreichender Menge vorlag.

Mechanismus der Signaltransduktion

Der erfolgreichen Konstruktion von LAPD ungeachtet, bleibt unser Verständnis des molekularen Mechanismus der zugrunde liegenden lichtabhängigen Signaltransduktion lückenhaft. Biochemische Untersuchungen legten zwar nahe, dass Länge und Identität des *coiled-coil*-Linkers entscheidende Bedeutung besitzen, doch atomare Details bleiben unklar. Seither haben insbesondere zwei neuere Arbeiten bahnbrechende Einblicke geliefert, die die Weiterentwicklung von LAPD ungemein begünstigen. So konnte die Struktur des PAS-GAF-PHY-Photosensors des *D. radiodurans*-BPhy in den P_r- und P_{fr}-Zuständen bestimmt werden [15]. Rotlicht vermittelt demnach eine reversible Umfaltung der PHY-Zunge zwischen α-Helix- und β-Faltblatt-Konformation, einhergehend mit einer Aufspreizung der PHY-Domänen im dimeren Rezeptor. Über den *coiled coil* ist diese Änderung der Quartärstruktur in LAPD an das PDE-Modul gekoppelt, wobei die molekularen Zusammenhänge noch einer genaueren experimentellen Untersuchung bedürfen. In einer kürzlichen Arbeit konnte erstmalig atomar aufgelöst werden, wie ein BPhy-Photosensormodul an ein katalytisch aktives Effektormodul gekoppelt ist [16]. Es ist anzunehmen, dass sich in LAPD ähnliche Prinzipien verwirklicht finden und die Erkenntnisse dieser Arbeit somit direkt relevant sind.

Fazit

Wie wir am Beispiel der LAPD illustrieren, können neuartige Photorezeptoren durch Kombination von Photosensor- und Effektormodulen erschaffen werden und als zuvor nicht verfügbare optogenetische Werkzeuge dienen [6]. Die Kontrolle zyklischer Nukleotide über PACs und LAPD ermöglicht neue Einblicke in zelluläre cNMP-abhängige Prozesse. Die Erzeugung neuartiger Photorezeptoren und ihre gezielte Optimierung gründen auf molekularem Verständnis der Struktur, der photochemischen Eigenschaften und des Signalmechanismus sensorischer Photorezeptoren. Insbesondere die Anwendung dieser Grundlagen befördern die Erzeugung effizienter Licht-gesteuerter Schalter, die im optogenetischen Einsatz eine hohe räumliche und zeitliche Auflösung sowie Reversibilität der Methode erbringen. ■

Literatur

[1] Möglich A, Yang X, Ayers RA et al. (2010) Structure and function of plant photoreceptors. Annu Rev Plant Biol 61:21–47
[2] Deisseroth K (2011) Optogenetics. Nat Methods 8:26–29
[3] Schröder-Lang S, Schwärzel M, Seifert R et al. (2007) Fast manipulation of cellular cAMP level by light *in vivo*. Nat Methods 4:39–42
[4] Stierl M, Stumpf P, Udwari D et al. (2011) Light-modulation of cellular cAMP by a small bacterial photoactivated adenylyl cyclase, bPAC, of the soil bacterium *Beggiatoa*. J Biol Chem 286:1181–1188
[5] Avelar GM, Schumacher RI, Zaini PA et al. (2014) A rhodopsin-guanylyl cyclase gene fusion functions in visual perception in a fungus. Curr Biol 24:1234–1240
[6] Ziegler T, Möglich A (2015) Photoreceptor engineering. Front Mol Biosci 2:30
[7] Rockwell NC, Lagarias JC (2010) A brief history of phytochromes. Chem Phys Phys Chem 11:1172–1180
[8] Yang X, Kuk J, Moffat K (2008) Crystal structure of *Pseudomonas aeruginosa* bacteriophytochrome: photoconversion and signal transduction. Proc Natl Acad Sci USA 105:14715–14720
[9] Pandit J, Forman MD, Fennell KF et al. (2009) Mechanism for the allosteric regulation of phosphodiesterase 2A deduced from the X-ray structure of a near full-length construct. Proc Natl Acad Sci USA 106:18225–18230
[10] Jansen V, Jikeli JF, Wachten D (2017) How to control cyclic nucleotide signaling by light. Curr Opin Biotechnol 48:15–20
[11] Yoshida K, Tsunoda SP, Brown LS et al. (2017) A unique choanoflagellate enzyme rhodopsin with cyclic nucleotide phosphodiesterase activity. J Biol Chem 292:7531–7541
[12] Gasser C, Taiber S, Yeh C-M et al. (2014) Engineering of a red-light-activated human cAMP/cGMP-specific phosphodiesterase. Proc Natl Acad Sci USA 111:8803–8808
[13] Schumacher CH, Körschen HG, Nicol C et al. (2016) A fluorometric activity assay for light-regulated cyclic-nucleotide-monophosphate actuators. Methods Mol Biol 1408:93–105
[14] Ryu M-H, Gomelsky M (2014) Near-infrared light responsive synthetic c-di-GMP module for optogenetic applications. ACS Synth Biol 3:802–810
[15] Takala H, Björling A, Berntsson O et al. (2014) Signal amplification and transduction in phytochrome photosensors. Nature 509:245–248
[16] Gourinchas G, Etzl S, Göbl C et al. (2017) Long-range allosteric signaling in red light-regulated diguanylyl cyclases. Sci Adv 3:e1602498

Korrespondenzadresse:
Prof. Dr. Andreas Möglich
Lehrstuhl für Biochemie
Forschungszentrum für Bio-Makromoleküle
BIOmac
Universität Bayreuth
Universitätsstraße 30
NW III, Room 1.05
D-95440 Bayreuth
Tel.: 0921-55-7835
andreas.moeglich@uni-bayreuth.de

AUTOREN

Robert Stabel
Jahrgang **1987**. **2009–2014** M. Sc. in Biochemie an der Universität Düsseldorf. Seit **2015** Promotion am Lehrstuhl für Biochemie der Universität Bayreuth.

Andreas Möglich
Jahrgang **1975**. **1996–2001** Biochemie-Diplom an der Universität Regensburg. **2002–2005** Promotion am Biozentrum der Universität Basel, Schweiz. **2006–2010** Postdoc an der University of Chicago, IL, USA. **2010–2015** Professor (W2) Biophysikalische Chemie an der HU Berlin. Seit **2015** Professor (W3) Biochemie an der Universität Bayreuth.

8. Publikationsliste

Tang, K.; Knipp, M.; Liu B.; Cox, N.; Stabel, R.; He, Q.; Zhou, M.; Scheer, H.; Zhao, K.; Gärtner, W.; *Biological Chemistry* (2015) "*Redox-dependent Ligand Switching in a Sensory Heme-binding GAF Domain of the Cyanobacterium Nostoc sp. PCC7120*", vol. 290, issue 31, pp. 19067-19080
https://doi.org/10.1074/jbc.M115.654087

Stabel, R.; Stüven, B.; Ohlendorf, R.; Möglich, A.; *Methods in Molecular Biology* (2017) "*Primer- Aided Truncation for the Creation of Hybrid Proteins*" vol. 1596 pp. 287-304
https://doi.org/10.1007/978-1-4939-6940-1_18

Stüven, B.*; Stabel, R.*; Ohlendorf, R.; Beck, J.; Schubert, R.; Möglich, A.; *Biological Chemistry* (2019) "*Characterization and engineering of photoactivated adenylyl cyclases*", vol 400, issue 3, pp. 429–441
https://doi.org/10.1515/hsz-2018-0375

Dietler, J.; Stabel, R.; Möglich, A.; *Methods in Enzymology* (2019) "*Pulsatile Illumination for Photobiology and Optogenetics*"
https://doi.org/10.1016/bs.mie.2019.04.005

Stabel, R.*; Stüven, B.*; Hansen, J.N.; Körschen, H.G.; Wachten D.; Möglich, A.; *Journal of Molecular Biology* (2019) " *Revisiting and Redesigning Light-activated Cyclic-Mononucleotide Phosphodiesterases*", vol. 431, issue 17, pp. 3029-3045
https://doi.org/10.1016/j.jmb.2019.07.011

Stabel, R.; Möglich, A.; BIOspektrum (2017) „Die Kontrolle zyklischer Nukleotide mittels Licht", vol. 23, issue 4, pp.384-387
https://doi.org/10.1007/s12268-017-0813-5

*gleichberechtige Erstautoren

9. Danksagung

An dieser Stelle möchte ich mich bei allen bedanken, die mich während meiner Promotion unterstützt haben.

Als erstes möchte ich mich bei meinem Doktorvater Prof. Dr. Andreas Möglich für die gemeinsame Zeit bedanken. Besonders dafür, mich gerade in den schwierigen Phasen der Promotion immer wieder motiviert und aufs Neue begeistert zu haben. Dank seiner fachlichen Expertise, der immer offenen Tür und dem sehr guten Austausch habe ich mich während meiner Zeit als Doktorand sowohl fachlich, als auch persönlich weiterentwickeln können.

Zudem geht ein großer Dank an die ganze AG Möglich für eine tolle Zeit und angenehme Zusammenarbeit. Besonders an Birthe, für ihren Einsatz während ihrer Masterarbeit und den gemeinsamen Erfolgen.

Bei den Mitarbeitern der Arbeitsgruppen von Prof. Dr. Birte Höcker und Prof. Dr. Clemens Steegborn möchte ich mich für das angenehme Arbeitsklima, den regen Austausch und gemeinsamen Sport bedanken.

Mein Dank gilt auch den Sekretärinnen für ihre tatkräftige Unterstützung im Hintergrund.

Ich möchte auch Charlotte, Anna und Thimo danken, die mich während meines Studiums und darüber hinaus begleitet haben.

An letzter Stelle möchte ich mich bei Vanessa, meinen Eltern und der ganzen Familie bedanken, die mich immer in meinem Tun bestärken.

10. (Eidesstattliche) Versicherungen und Erklärungen

(§ 8 Satz 2 Nr. 3 PromO Fakultät)
Hiermit versichere ich eidesstattlich, dass ich die Arbeit selbstständig verfasst und keine anderen als die von mir angegebenen Quellen und Hilfsmittel benutzt habe (vgl. Art. 64 Abs. 1 Satz 6 BayHSchG).

(§ 8 Satz 2 Nr. 3 PromO Fakultät)
Hiermit erkläre ich, dass ich die Dissertation nicht bereits zur Erlangung eines akademischen Grades eingereicht habe und dass ich nicht bereits diese oder eine gleichartige Doktorprüfung endgültig nicht bestanden habe.

(§ 8 Satz 2 Nr. 4 PromO Fakultät)
Hiermit erkläre ich, dass ich Hilfe von gewerblichen Promotionsberatern bzw. –vermittlern oder ähnlichen Dienstleistern weder bisher in Anspruch genommen habe noch künftig in Anspruch nehmen werde.

(§ 8 Satz 2 Nr. 7 PromO Fakultät)
Hiermit erkläre ich mein Einverständnis, dass die elektronische Fassung der Dissertation unter Wahrung meiner Urheberrechte und des Datenschutzes einer gesonderten Überprüfung unterzogen werden kann.

(§ 8 Satz 2 Nr. 8 PromO Fakultät)
Hiermit erkläre ich mein Einverständnis, dass bei Verdacht wissenschaftlichen Fehlverhaltens Ermittlungen durch universitätsinterne Organe der wissenschaftlichen Selbstkontrolle stattfinden können.

…….
Ort, Datum, Unterschrift